DETECTION OF NEUROTRANSMITTERS USING METALLOPHTHALOCYANINES AS ELECTROCATALYSTS

THESIS

Submitted to Rhodes University

in fulfilment of the requirements

for the degree of

DOCTOR OF PHILOSOPHY

BY

JOSHUA IDOWU ONI

CHEMISTRY DEPARTMENT

RHODES UNIVERSITY; GRAHAMSTOWN

SOUTH AFRICA

NOVEMBER 2001

DEDICATION

To the Glory of God

and the prosperity of mankind

ACKNOWLEDGEMENTS

My unreserved gratitude and appreciation goes to my supervisor, Professor Tebello Nyokong for lavishly sharing her wealth of knowledge and experience through her tenacious, second-to-none supervision, guidance, timely and constructive criticism and her unflinching support and encouragement every inch of the journey through the research exercise. **"'Me, kea leboha"**.

My parents, brothers and sisters and their families also deserve my thanks for their support in all ways always during the course of this programme. You had so little, yet you gladly gave all. **"E se pupo"**.

Too numerous to mention one by one are **friends** and **colleagues** who "kept me sane" all through this programme. **I will forever be indebted to you in gratitude**.

To Dr. Philippe Westbroek, **"Dank U"**.

This page will be largely incomplete without thanking the academic and technical members of staff of chemistry department, not only for making things "run" smoothly but also for providing an informal, yet effective working environment. Thanks a bunch!

The National Research Foundation (South Africa) was most generous with a graduate bursary towards this study. Thanks indeed.

Above all, I ascribe all glory, honour and majesty to God for His faithfulness never comes to an end!

ABSTRACT

Some metallophthalocyanine complexes were synthesized and their catalytic activities towards the detection and quantification of the neurotransmitters dopamine, serotonin and histamine were investigated. The study of the possible interaction between these transmitter substances and the metallophthalocyanine complexes was undertaken.

Dopamine, serotonin and histamine formed complexes with iron (II) tetrasulfophthalocyanine. The rate and equilibrium constants obtained for the coordination are in the range of values reported in the literature for ligand coordination to iron phthalocyanine complexes.

Carbon paste electrodes of millimetric diameters modified with iron (II) tetrasulfophthalocyanine exhibited good electrocatalytic activity towards the detection and analysis of dopamine and serotonin while at the same time eliminated the problem of interference posed by ascorbic acid in the electrochemical analysis of neurotransmitters. A detection limit of the order of 10^{-6} mol dm^{-3} was obtained for both dopamine and serotonin at the modified electrodes.

Carbon paste ultra microelectrodes modified with iron (II) tetrasulfophthalocyanine were also used for the detection of dopamine and serotonin as well as the simultaneous determination of dopamine and ascorbic acid in a mixture. The detection limit obtained for dopamine at the ultra microelectrode was 4.2×10^{-7} mol dm^{-3}.

The electrode kinetics of vitamin B_1 as well as the stability of the electrode towards its determination was improved upon by modifying carbon paste electrodes with manganese phthalocyanine. The modified electrodes were used for the analysis of vitamin B_1 in tablets.

TABLE OF CONTENTS

LIST OF ABBREVIATIONS

^{1}HNMR	proton nuclear magnetic resonance
5-HT	serotonin
AA	ascorbic acid
AFM	atomic force microscopy
Ag|AgCl	silver|silver chloride reference electrode
c_{AA}	concentration of ascorbic acid
c_{DA}	concentration of dopamine
CME	chemically modified electrode
CNS	central nervous system
$[Co^{II}TSPc]^{4-}$	cobalt (II) tetrasulfophthalocyanine
CoPc	cobalt phthalocyanine
CPE	carbon paste electrode
CPUMBE	carbon paste ultra micro band electrode
CPUMDE	carbon paste ultra micro disk electrode
Ct	catalyst
CT	charge transfer
CV	cyclic voltammetry
DA	dopamine
D_{AA}	diffusion coefficient of ascorbic acid
D_{DA}	diffusion coefficient of dopamine
DMA	dimethyl acetamide
DMF	dimethyl formamide

DMSO	dimethyl sulfoxide
ECF	extracellular fluid
$[Fe^{III}TSPc]^{3-}$	iron (III) tetrasulfophthalocyanine
$Fe^{II}Pc(t\text{-}Bu)_4$	iron (II) tetratertiarybutylphthalocyanine
$[Fe^{II}TSPc]^{4-}$	iron (II) tetrasulfophthalocyanine
FePc	iron phthalocyanine
FePc-CPE	iron phthalocyanine modified carbon paste electrode
FeTSPc-CPE	iron tetrasulfophthalocyanine modified carbon paste electrode
FeTSPc-CPUMDE	iron tetrasulfophthalocyanine modified carbon paste ultra micro disc electrode
FSCV	fast scan cyclic voltammetry
FTIR	Fourier transform infrared
GABA	γ-amino butyric acid
GCE	glassy carbon electrode
HIS	histamine
HIV	human immunodeficiency virus
HOMO	highest occupied molecular orbital
IHP	inner Helmholtz plane
im	imidazole
IR	infrared
ITO	indium tin oxide
LMCT	ligand to metal charge transfer
LUMO	lowest unoccupied molecular orbital

MLCT	metal to ligand charge transfer
MnPc	manganese phthalocyanine
MnPc-CPE	manganese phthalocyanine modified carbon paste electrode
MPc	metallophthalocyanine
$[MTSPc]^{4-}$	metallotetrasulfophthalocyanine
$[Ni^{II}TSPc]^{4-}$	nickel (II) tetrasulphophthalocyanine
NLO	non-linear optics
NMR	nuclear magnetic resonance
NO	nitric oxide
OHP	outer Helmholtz plane
OSWV	Osteryoung square wave voltammetry
OTE	optically transparent electrode
OTTLE	optically transparent thin-layer electrode
Pc	phthalocyanine
PDT	photodynamic therapy
PET	polyethylene
PP	polypropylene
ppm	parts per million
PTFE	polytetrafluoroethylene
PVC	polyvinyl chloride
py	pyridine
QCM	quartz crystal microbalance
SAM	self-assembled monolayer

SCE	saturated calomel electrode
SECM	scanning electrochemical microscopy
SWV	square wave voltammetry
Tris	Tris[hydroxymethyl]aminomethane hydrochloride
UME	ultra microelectrode
UV	ultraviolet
vis	visible

LIST OF SYMBOLS

π	bonding orbital
ψ	quasi-reversible current function
Γ	surface coverage
α	transfer coefficient
π^*	antibonding orbital
∇^2	laplacian diffusion operator
ΔE_p	separation between peak potentials
ΔE_s	step height
ε	extinction coefficient
A	amps
A	area of electrode surface
A_∞	final absorbance
A_0	initial absorbance
A_{eq}	equilibrium absorbance
c	concentration
c_0	concentration of oxidized species
c_R	concentration of reduced species
D	diffusion coefficient
E	potential
E^0	standard potential
$E_{1/2}$	half-wave potential
E_f	final potential

E_i	initial potential
E_p	peak potential
E_{pa}	anodic peak potential
E_{pc}	cathodic peal potential
F	Faraday's constant
f	frequency
Hz	hertz
i_L	limiting current
i_{pa}	anodic peak current
i_{pc}	cathodic peak current
K	equilibrium constant
K	Kelvin
k^0	standard rate constant
k_f	rate of forward reaction
k_{obs}	observed rate constant
k_r	rate of reverse reaction
n	number of electrons
O	oxidized form of an analyte
Q	charge
R	reduced form of an analyte
R	universal gas constant
r_0	radius of electrode
T	temperature in Kelvin

v	scan rate
V	volts
V	volume

LIST OF FIGURES

LIST OF SCHEMES

LIST OF TABLES

CHAPTER 1

INTRODUCTION

1.1 ELECTROANALYTICAL TECHNIQUES: A BRIEF OVERVIEW

Electroanalytical techniques are very useful for the measurement of electrical quantities such as current, potential and charge, and their relationship to chemical parameters. The use of these electrical measurements for analytical purposes has found a wide range of applications in industrial quality control, environmental monitoring and biomedical analysis.[1]

Electrochemical processes take place at the highly non-homogeneous electrode-solution interphase; unlike most other chemical measurements that involve homogeneous bulk solutions. Placing an electrode in contact with a solution creates a phase boundary that differentiates otherwise identical solute molecules: those at a distance from the electrode, and those close enough to participate in the electron transfer process at the surface of the electrode.[2]

In this thesis, electrochemical techniques are employed for the analysis of neurotransmitters and pharmaceutical preparations using electrodes modified with metallophthalocyanines complexes. A closer look at electrode processes and the two electrochemical techniques used (cyclic and square wave voltammetry) follows:

1.1.1 The electrode-solution interphase

The currently widely accepted model[2,3,4] of the electrode-solution interphase is depicted by Figure 1.1. This is called the electrical double layer. This model was developed from

the Helmholtz model, which considers the interphase as a simple capacitor and the Gouy-Chapman model, which explains the interphase as a Boltzman distribution of ions.

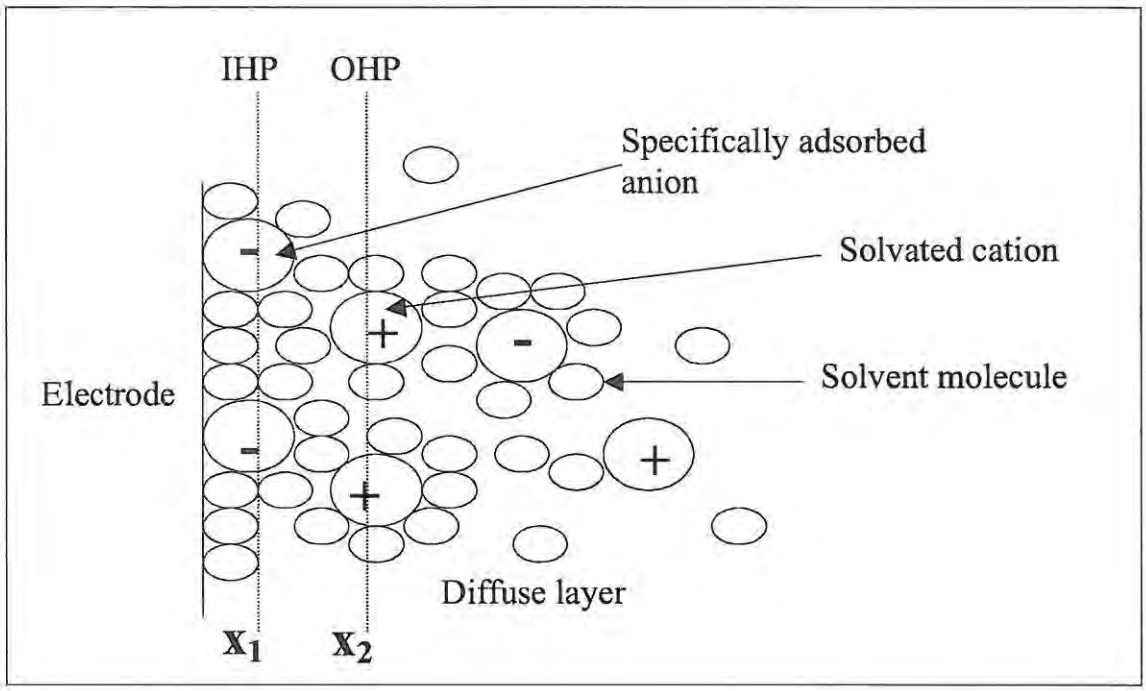

Figure 1.1: model of the electrode-solution double layer region[3]

The solution side of the double layer is thought to be made up of several layers. The layer closest to the electrode contains solvent molecules and molecules or ions that are said to be specifically adsorbed. The locus of the electrical centers of the specifically adsorbed ions, which is at a distance x_1 from the electrode, is called the inner Helmholtz plane (IHP). Solvated ions said to be nonspecifically adsorbed can only approach the electrode to a distance x_2, which is the locus of the centers of these solvated ions, called the outer Helmholtz plane (OHP).

The layer that extends from the OHP contains nonspecifically adsorbed ions, which are distributed in a three-dimensional region, is called the diffuse layer.[3] In this region, thermal motion tends to distribute the ions evenly throughout the solution while at the same time, there is electrostatic force of attraction and repulsion from the surface of the electrode. These two forces counterbalance each other, resulting in a non-uniform distribution of ions near the electrode surface. Beyond the diffuse layer, ions in the homogeneous bulk solution cannot "feel"[2] the presence of the electrode.

The existence of the double-layer capacitance or the presence of a charging current in electrochemical experiments deserves a careful consideration. During electrode reactions involving very low concentrations of electroactive species, the charging current may be larger[3] than the faradaic current arising from the oxidation or reduction reaction; making the species undetectable.

1.1.2 Classification of electroanalytical techniques

Electroanalytical techniques are easily classified into two broad groups: static and dynamic.[5] In static methods, a potential difference is measured at zero current such that the electrode-solution interphase is not disturbed and Nernstian equilibrium is maintained; whereas in dynamic techniques, the system is intentionally disturbed from equilibrium by excitation signals consisting of a wide variety of potential and current programs and a response signal is monitored.[5] Individual techniques are best recognized

by their excitation-response characteristics. Most electroanalytical techniques are based on the dynamic techniques.

The electroanalytical experiments carried out in this research work are based on controlled-potential techniques. The advantages[1] of controlled-potential techniques include high sensitivity, selectivity towards electroactive species, a wide linear range, portable and low cost instrumentation, speciation capability and a wide range of electrodes that allow assays in unusual environments.

1.1.3 The Faradaic process

In controlled potential electroanalytical or voltammetric experiments, a current response corresponding to the concentration of the analyte oxidized or reduced at the electrode surface is obtained. This is achieved by monitoring the transfer of electrons during the redox process of the analyte as represented by equation 1.1.

$$O + ne \equiv R \qquad 1.1$$

Where O = oxidized form of the analyte

n = number of electrons transferred

R = reduced form of the analyte

The current resulting from the oxidation or reduction of the analyte is called faradaic current because it obeys Faraday's law.

Equation 1.2, also called the Nernst equation, applies to thermodynamically controlled reversible systems.

$$E = E^{o} + \frac{2.303RT}{nF}\log\frac{c_O}{c_R} \qquad \textbf{1.2}$$

Where E = the potential applied,

T = temperature (K)

E^{o} = standard potential of the redox couple,

R = universal gas constant

F = Faraday's constant,

c_o = concentration of oxidized species

c_R = concentration of oxidized species,

n = number of electrons

1.1.4 The electrochemical cell

Dynamic electrochemical experiments are usually carried out in a three-electrode electrochemical cell, shown schematically in Figure 1.2.

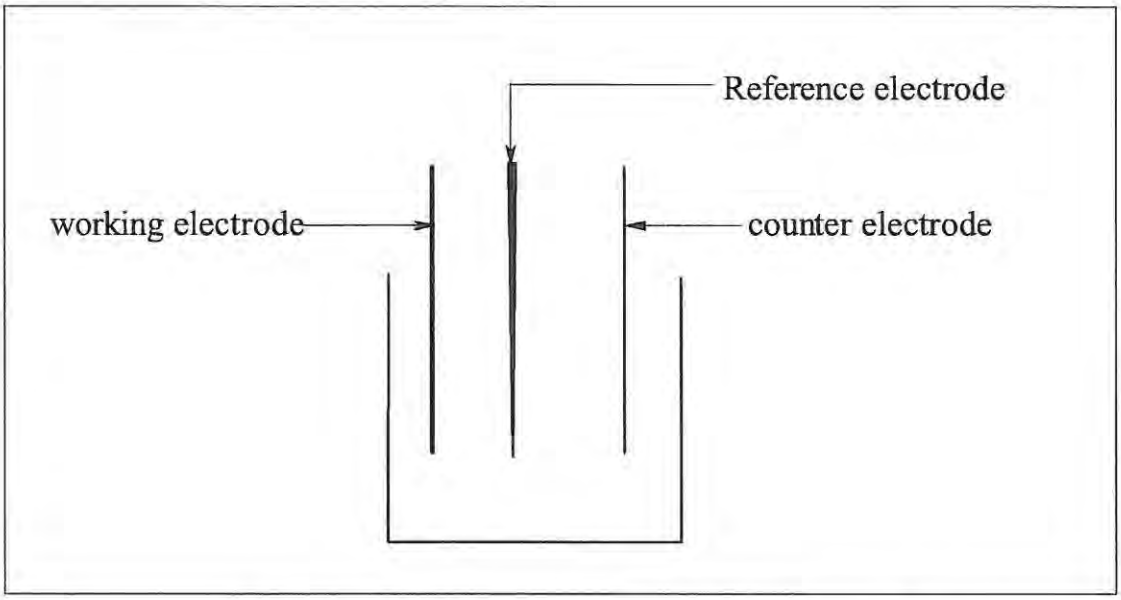

Figure 1.2: A schematic representation of the three- electrode cell

The three electrodes are called the working, reference and counter electrodes respectively.[3,4] The electron transfer process takes place at the surface of the working electrode. Current passes from the working electrode to the counter electrode which completes the circuit. Current does not pass through the reference electrode, its potential is constant and it monitors the changes taking place at the surface of the working electrode.

Counter electrodes are most commonly made from platinum foil, wire, gauze or loop. Several reference electrodes are in use for electroanalytical experiments; Silver|silver chloride (Ag|AgCl) reference electrode is a very popular one. It consists of a piece of silver wire anodized with silver chloride in a glass tube. The wire is in contact with concentrated KCl or NaCl solution. The electrode is usually protected from the bulk of analyte solution by a semi-permeable salt bridge.[6]

Materials that have found important use as working electrodes in electroanalysis include mercury, carbon, and "inert" metals particularly, platinum and gold. Carbon-based electrodes were employed as working electrodes in this study, they are discussed in detail below.

1.1.5 Carbon paste electrode

Carbon materials in the form of graphite, glassy carbon, pyrrolytic graphite and carbon fibers have been important players in solid electrode development for a number of reasons: [7]

(i) they are available in a variety of forms and are generally inexpensive,

(ii) the slow kinetics of carbon oxidation leads to a wide useful potential range,

(iii) carbon has a rich surface chemistry which can be exploited to influence reactivity by a wide variety of chemical derivatizations on the surface,

(iv) controlled variation of electron transfer kinetics and adsorption on carbon

surfaces can be used to enhance analytical utility.

These properties of carbon can be exploited to an advantage if the user is familiar with the relationship between the properties of carbon materials, surface preparation and electroanalytical behavior.

Carbon paste electrode (CPE) was introduced in 1958.[8] Carbon paste is a mixture of ground carbon and a mulling liquid. Practical considerations require that the mulling liquid should be electroinactive and pure with respect to electroactive impurities, chemically inert, have very low solubility or immiscible with the analyte solution, should have low volatility, and should ensure low residual currents in the investigated potential range.[9,10] Different types of mulling liquids or binders have been used for the preparation of CPE. Among these are: liquid petrolactum, paraffin or Nujol®,[11] silicone lubricants, alkanes,[12] polychlorotrifluoroethylene oils[13] and α-bromonaphthalene. Nujol® is more commonly used.

The required properties[10] of the particulate component (graphite) of the paste are:

(i) uniform particle size distribution

(ii) high chemical purity

(iii) low adsorption capability for oxygen and electroactive impurities

(iv) right level of porosity.[14] Materials such as carbon black, animal charcoal or similar products, which are extremely porous, are not suitable for the preparation of carbon pastes.

Typically, pastes for CPEs may be prepared by thoroughly mixing Nujol® and graphite powder until the mixture is uniformly wetted.[9,15] The usual particle size of graphite materials ranges between 2 and 5μm,[16] larger particles produce a rough texture and unfavourable mechanical and electrochemical properties.[17] Graphites of smaller particle size (e.g. 0.2μm) can be suitable for the preparation of carbon paste microelectrodes.[18] The resultant paste should have a consistency similar to that of peanut butter. The optimum formulation seems to consist of 3g of graphite powder and 2ml of oil,[9] but the ratio between the pasting liquid and graphite powder usually varies between 0.3 to 0.5ml per gram of graphite powder (dry pastes), and 0.5 to 0.9ml per gram of graphite powder (wet pastes).[9] After thorough mixing, the paste is packed into an inert holder such as Teflon or glass tubes. Electrical contact with the paste is maintained using a piece of conducting wire. The surface could be "polished" using weighing paper, it is important that the face of the holder is flat and smooth so as to obtain a flat, reproducible carbon paste surface.

To prevent the separation of graphite and the mulling liquid, it is important, when packing the paste into the holder to avoid too much pressure. Separation of the liquid from graphite results in high-resistance contact between paste and metal.[9]

CPEs have rather low background currents compared to solid graphite or noble metal electrodes,[14,19] but the magnitude increases with an increasing quantity of pasting liquid, which invariably decreases the sensitivity of the electrode.[16] CPEs can be polarized

within a wide potential window of –1.0 to 1.3V vs saturated calomel electrode (SCE) in acidic media and from –1.5 to 1.0V versus (vs) SCE in neutral and alkaline solutions. With the use of tricresyl phosphate as a pasting liquid, a very wide range of –2.0 to 2.0V vs Ag|AgCl in ammonia buffer can be obtained.[10, 16]

Simply pushing a small column of electrode material out of the holder and cutting it off with a scalpel or the edge of very clean paper easily regenerates the surfaces of CPEs[20,21]

The nature of the CPE is amenable to chemical modification by a variety of methods. CPEs may be advantageously modified in order to improve selectivity, sensitivity and to promote an otherwise slow redox reaction.[16,22] In fact, a major motivation for developing carbon paste electrodes was the ease of modification, surface renewal and reproducibility.[7] To prepare a modified CPE, a modifying agent is either dissolved in the pasting liquid or physically mixed with graphite or the paste. In some cases, the modifier and pasting liquid are dissolved in a common solvent such as hexane, which is later evaporated. However, it is important to ensure uniform dispersion of the modifier in the electrode in order to achieve good reproducibility.

The major setbacks of the use of CPEs in electroanalysis have to do with reproducibility, use in nonaqueous media and presence of entrapped oxygen in the paste.[10] The reproducibility of CPEs is a bit worse than that of mercury electrodes or sensors made of compact materials such as the noble metals and glassy carbon. The order of magnitude of

the relative standard deviation for measurements with CPEs is about 5%.[19] CPEs suffer substantially from the presence of oxygen entrapped in the paste, brought in by carbon particles or introduced by the preparation procedure of the paste.[23] In voltammetric measurements, oxygen seriously interferes when employing CPEs in the negative potential range. The heterogeneous nature of CPEs is disadvantageous with respect to applications in nonaqueous media because the electrode material obviously disintegrates, due to the solubility of the mulling liquid in organic solvents.

1.1.6 Mass transport to the electrode

Electrochemical oxidation or reduction of an analyte takes place at the electrode-solution interphase. The transport of analyte molecules from the bulk of the solution in the electrochemical cell to the electrode-solution interphase is of absolute necessity for the electrode process to occur.[2] Diffusion, convection and migration are the three possible modes of mass transport to the electrode surface.[1,2,4]

Diffusion is the spontaneous movement of analyte molecules from regions of high concentration to regions of lower concentration in order to minimize concentration differences.

A concentration gradient develops in solution in the vicinity of the electrode due to the reaction occurring at the electrode which gives rise to a diffusion flux. The total diffusion

limited current is made up of the planar flux and the radial flux diffusion components as expressed by equation 1.3.

$$i_{total} = i_{planar} + i_{radial} \qquad \textbf{1.3}$$

Fick's second law, equation 1.4, generally gives the rate of change of concentration in solution induced by this diffusional flux.

$$\frac{\delta c}{\delta t} = D\nabla^2 c \qquad \textbf{1.4}$$

Where c = concentration of diffusing species

t = time

D = diffusion coefficient

∇^2 = Laplacian diffusion operator.

The Laplacian operator takes a different form for each diffusion geometry.[3] Fick's second law thus has a unique solution for different electrode geometry.

Mass transport by convection is effected by the gross physical movement of solution by stirring, rotating or vibrating the electrode or flowing the solution in a cell.

Migration occurs as a result of movement of charged particles due to their interaction with an electric field. Cations will normally be attracted by negatively charged electrode and vice-versa. Since migration is complicated, its effect is minimized by the addition of supporting electrolytes.

The dynamic electroanalytical techniques employed in this work are cyclic voltammetry and square-wave voltammetry. An overview of these techniques is provided in the following sections, as well as a brief description of spectroelectrochemistry.

1.1.7 Cyclic voltammetry

Cyclic voltammetry (CV) is a technique most widely used for obtaining qualitative information about electrochemical reactions; it offers a rapid location of redox potentials of the electroactive species and an evaluation of the effect of media upon the process.[1]

In this technique, the potential of a stationary working electrode in a quiescent solution is scanned linearly using a triangular potential waveform, and the current resulting from the applied potential measured.[1,3,4,24] The resulting plot of current versus potential is termed a cyclic voltammogram. A representative cyclic voltammogram is shown in Figure 1.3.

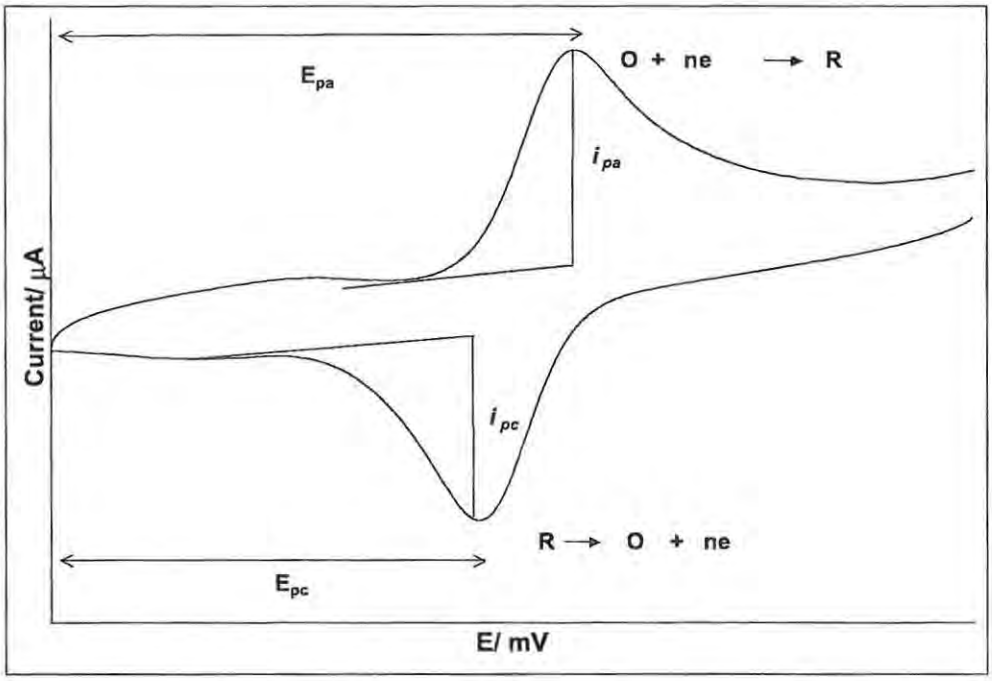

Figure 1.3: A typical cyclic voltammogram

The important parameters[4] for recording a cyclic voltammogram are the initial potential, E_i, direction of sweep, the sweep rate, and the final potential, E_f.

The information that could be obtained from a cyclic voltammogram includes the magnitude of the anodic (i_{pa}) and cathodic (i_{pc}) peak currents, the anodic (E_{pa}) and cathodic (E_{pc}) peak potentials.

Cyclic voltammetric processes could be reversible, quasi-reversible or irreversible depending on the nature of the reaction.

1.1.7.1 Reversible process

A reversible electrochemical system is one in which the species oxidized or reduced in the forward scan are reduced or oxidized respectively during the reverse scan. Reversibility implies that the system is at equilibrium at all potentials, which means that the Nernst equation is valid at these potentials. Also, the kinetics of electron transfer at the electrode is fast such that mass transport is the rate determining parameter, even at small overpotentials. The peak current for a reversible system, at 298K, is given by equation 1.5, called the Randles-Sevcik equation.

$$i_P = (2.69x10^5)n^{3/2}AcD^{1/2}v^{1/2} \qquad 1.5$$

Where i_p = peak current (A)

n = number of electrons transferred

A = electrode area (cm^2)

D = diffusion coefficient ($cm^2\ s^{-1}$)

c = concentration ($mol\ cm^{-3}$)

v = scan rate (Vs^{-1})

The peak current is directly proportional to the concentration and it increases with an increase in the square root of the scan rate, $v^{1/2}$. For a simple reversible couple, the magnitude of i_{pa} is equal to that of i_{pc}.

The half-wave potential ($E_{1/2}$) is the potential where the current is half of its limiting value. $E_{1/2}$ is related to the formal potential (E^0) according to equation 1.6.

$$E_{1/2} = E^0 + \frac{RT}{nF}\log\left(\frac{D_R}{D_0}\right)^{1/2} \qquad \textbf{1.6}$$

Since the ratio of diffusion coefficients is nearly unity, $E_{1/2}$ is usually a very good approximation of E^0 for a reversible couple. Thus E^0 for a reversible couple is centered between E_{pa} and E_{pc} as shown in equation 1.7

$$E^0 = \frac{E_{pa} + E_{pc}}{2} \qquad \textbf{1.7}$$

While the separation between the peak potentials, ΔE_p, for a reversible couple is given by equation 1.8, and can be used to determine the number of electrons transferred. ΔE_p is independent of the scan rate employed.

$$\Delta E_P = E_{Pa} - E_{Pc} = \frac{RT}{nF} \qquad \textbf{1.8}$$

At 298K, equation 1.8 can further be simplified to equation 1.9

$$\Delta E_P = \frac{RT}{nF} = \frac{0.059V}{n} \qquad \textbf{1.9}$$

For a reversible one-electron redox process, $\Delta E_p = 0.059V$.

1.1.7.2 Irreversible process

The cyclic voltammograms of irreversible processes often show a single oxidation or reduction peak with no reverse wave, in some cases a weak reverse wave is observed.

Where the reverse wave is present, it is widely separated from the forward wave. Irreversibility is caused by a slow exchange of redox species with the working electrode.[24] Electrochemical irreversibility is characterized by a separation of peak potentials (ΔE_p), which is greater than 0.059V/n. The Nernst equation is not valid for irreversible systems because of the slow kinetics of the forward and/or reverse reaction. The peak potentials of totally irreversible systems shift with scan rate as described by equation 1.10. With increasing scan rates, the peak potential separation (ΔE_p) becomes greater, the electron transfer rate (α) and the rate constant (k^o) decrease.

$$\Delta E_P = E^O - \frac{RT}{\alpha nF}\left[0.78 - \ln\frac{k^O}{D^{1/2}} + \ln\left(\frac{\alpha nF\nu}{RT}\right)^{1/2}\right] \qquad \textbf{1.10}$$

Where α = transfer coefficient

k^o = standard rate constant

other constants are as defined in equation 1.5.

Equation 1.10 reveals that E_p occurs at a potential higher than E^0. The overpotential is related to k^o and α. Independent of the value of k^o, such peak displacement can be compensated by an appropriate change of the scan rate. At 298K, the peak potential (E_p) and the half-peak potential ($E_{p1/2}$) will differ by $0.048/\alpha n$ V; the voltammogram becomes more drawn out as αn decreases.

The peak current (i_p) for irreversible processes given by equation 1.11 is still proportional to the bulk concentration of the analyte in the solution and the scan rate.

$$i_P = (2.99x10^5)n(\alpha n)^{1/2} AcD^{1/2}v^{1/2} \qquad \textbf{1.11}$$

1.1.7.3 Quasi-reversible process

Quasi-reversible processes show electron transfer kinetic limitations where the reverse reaction has to be considered.[3] As a general conclusion, the extent of irreversibility increases with increase in scan rate.[4] For quasi-reversible systems, the current, given by equation 1.12, is controlled by both charge transfer and mass transport.[1]

$$i_P = nFACD^{1/2}\left(\frac{nF}{RT}\right)^{1/2}\psi v^{1/2} \qquad \textbf{1.12}$$

Where ψ is the quasi-reversible current function with given values of $n\Delta E$.

1.1.7.4 Electrocatalysis using cyclic voltammetry

In the cyclic voltammetry mode, electrocatalysis is observed with either the absence of a reverse peak, the enhancement of the cathodic or anodic currents, or both, and a shift in redox potentials to lower values. Hypothetical cyclic voltammetry curves showing the scheme of electrocatalytic behavior of a catalyst (Ct) towards the oxidation of an analyte A are shown in Figure 1.4.

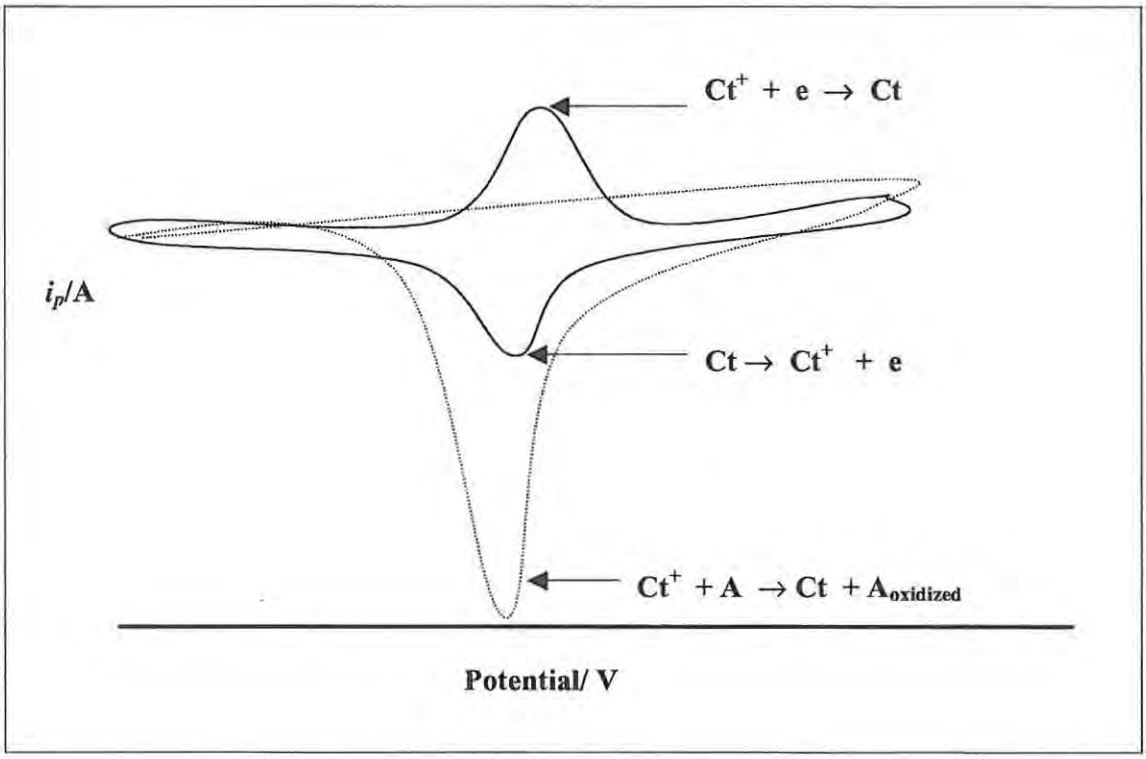

Figure 1.4: Cyclic voltammogram showing electrocatalytic behavior

1.1.8 Square-wave voltammetry

Square-wave voltammetry (SWV) was developed in the early 1950s by Barker and Jenkins.[25] It is a large amplitude differential technique in which a waveform composed of a symmetrical square-wave that is superimposed on a base staircase potential is applied to the working electrode.[1,26] During each square-wave cycle, the current is sampled twice. Once at the end of the forward pulse and once at the end of the reverse pulse. The reverse pulse causes the reversion of the reaction of the forward pulse.

Plotting the difference between the two measured current signals versus the base staircase potential results in peak-shaped voltammograms that are symmetrical about the half-wave potentials of the oxidation or reduction of the electroactive species at the electrode surface. The peak current is proportional to the concentration of the electroactive species in solution.

The advantages of square-wave voltammetry are optimal peak separation and excellent sensitivity. Very low detection limits of $1x10^{-8}$ mol dm^{-3} can be obtained, and using double step SWV[27,28] detection limits of 10^{-11} mol dm^{-3} can be obtained.

For SWV, the effective scan rate, v, is given by equation 1.13.

$$v = f\Delta E_s \qquad \textbf{1.13}$$

Where f = square-wave frequency (Hz)

ΔE_s = step height

In the SWV mode, electrocatalysis is also observed with an increase in cathodic or anodic currents as well as shift of redox potentials to lower values.

1.1.9 Spectroelectrochemistry

The development of optically transparent electrodes (OTEs),[29,30] enable spectral observations to be made simultaneously with electrochemical perturbations. This technique is termed spectroelectrochemistry.[5] The technique is extremely useful for the elucidation of reaction mechanisms and for the delineation of kinetic and thermodynamic parameters.[1]

There are several types of OTEs.[29,30] They may be thin films of semiconductors such as doped tin oxide or a conductive material such as gold, platinum or carbon deposited on a glass, quartz or plastic substrate as well as fine wire mesh minigrids. The cells that incorporate these electrodes are called optically transparent thin-layer electrode (OTTLE) cells. Typical volumes of OTTLE cells range between 30-50 μl[1,3,4] which makes the complete electrolysis of the solute possible in a few seconds and at the same time allowing for transmission experiments. Transmission experiments may involve the study of absorbance with time as the electrode potential is scanned or as the wavelength is scanned to obtain spectra of electrogenerated species. This is the primary advantage of spectroelectrochemistry.

A careful treatment of the absorbance-time curve during electrochemical generation or consumption of an optically active species can yield extremely useful information on reaction mechanisms and kinetics. Thin layer spectroelectrochemistry is also useful for measuring the number of electrons exchanged in a redox process. Faraday's law, given by equation 1.14, gives the amount of charge passed during electrolysis.

$$Q = nFVc \qquad \textbf{1.14}$$

where Q = amount of charge passed

V = volume of the cell

other constants are as defined previously

1.2 CHEMICALLY MODIFIED ELECTRODES

In this thesis, chemically modified electrodes (CMEs) were employed in electroanalysis, hence a discussion on CMEs follow:

A chemically modified electrode (CME) is an electrode made of a conducting or semiconducting material that is coated with a film of a chemical modifier. By means of faradaic (charge transfer) reactions or interfacial potential differences (no net charge transfer) the CME exhibits chemical, electrochemical and/or optical properties of the modifier film.[31]

The art of modifying electrodes by attaching specific molecules to the surfaces of "inert" electrodes to yield CMEs was first introduced by Lane and Hubbard.[32] The distinguishing feature of a CME is that a thin film of a selected chemical is bonded to or coated on the electrode surface to endow the electrode with the chemical, electrochemical or other desirable properties of the film in a rational, chemically designed manner.[31,33]

1.2.1. Methods of modifying electrode surfaces

Various methods have been demonstrated for the preparation of CMEs. Some of these approaches[31,34] are described below:

1.2.1.1 Chemisorption

This is an adsorptive interaction between the electrode surface and a molecule in which electron density is shared by the adsorbed molecule and the electrode surface. The forces

involved are the valence forces of the same kind as those operating in the formation of chemical compounds.[31,34] The coverage achievable on the electrode surface using this approach is usually a monolayer or less[31,34,35] (this is about $1x10^{-10}$ mol cm^{-2}, or 6×10^{13} molecules cm^{-2} [35]) because direct contact between the modifier and the electrode surface is required.

Chemisorption is rarely completely irreversible; this places a limitation on modifying electrodes through this approach since there is the possibility of the adsorbed molecules slowly leaching into the contacting solution phase.[33] The use of thiols, sulfides and disulfides as chemisorption agents to form self-assembled monolayers (SAMs) for the derivatization of gold electrode surfaces is another way through which chemisorption is generally applied. The electrode is simply immersed into a dilute solution of the thiol for a length of time.[34,36] A densely packed and highly ordered monolayer film is formed on the electrode surface.

1.2.1.2 Composite

In this method, the chemical modifier is simply mixed with an electrode matrix material. The combination of the modifier with the carbon particles of carbon based electrodes[37,38,39] utilizes this approach of modifying electrodes.

1.2.1.3 Polymer film coating

Polymer film coating on the electrode as modifying agent is perhaps the most popular method of electrode modification for a number of reasons:[31,34]

(i) there are many ways of depositing a polymer film onto the electrode surface,

(ii) it is easy to prepare multilayer films using the polymer route,

(iii) the thickness of the film can be reliably and reproducibly varied,

(iv) there is no loss of the polymer on the electrode surface since the polymer films have tremendous chemical stability and can be made completely insoluble in the contacting solution phase,

(v) other functional groups can be added as additional coats on the polymer.[40]

Some of the methods that have been used to deposit polymer films on electrode surfaces are[31] :

(a) **Dip–dry coating:** the electrode material is simply immersed in a solution of the polymer for a period sufficient for spontaneous film formation to occur by adsorption. The electrode is withdrawn from the solution and the solvent is then allowed to dry off.

(b) **Drop-dry coating:** a few drops of a solution of the polymer is applied to the electrode surface and the solvent is allowed to evaporate.

(c) **Spin coating:** a droplet of a solution of the modifier is applied to the surface of a rotating electrode; excess solution is spun off the surface and the thin film

layer is allowed to dry. Multiple layers may be applied this way until the desired thickness is obtained.

(d) **Electropolymerization:** This is a clean and efficient route to polymer synthesis; an electrode is immersed in a concentrated solution ($\approx 10^{-3}$ mol l^{-1}) of the desired modifier followed by repetitive voltammetric scanning within a specified potential range.[40,41,42] The rate and extent of the polymerization process as well as the chemical and physical properties of the resulting polymer can be carefully controlled.[42] Repetitive scanning of the monomer at the electrode produces a gradual increase in both anodic and cathodic peak currents with successive cycles, which is indicative of electropolymerization of the monomeric form onto the electrode. Normally, the first CV cycle is different from subsequent scans showing that a different species (polymer) is adsorbed onto the electrode as opposed to simple electrodeposition. Electropolymerization is complete when there is no further increase in the peak height (hence the film thickness) showing that the surface of the electrode is fully covered. Reproducible coating can be achieved by controlling the number of cycles.

1.2.1.4 Covalent bonding

This method makes use of linking agents to covalently attach one to several monomolecular layers to the surface functionalities of the electrode.[43,44] The attachment

of organosilanes to the hydroxyl groups on carbon electrodes,[4,34] shown schematically in Figure 1.5, serves as an example of this mode of electrode modification.

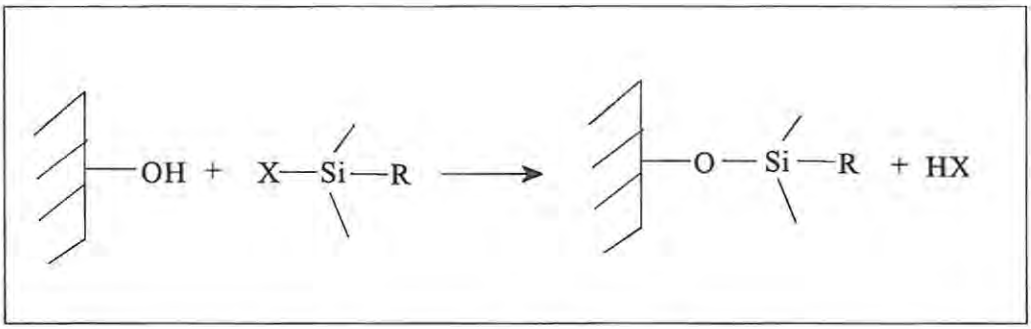

Figure 1.5: Schematic representation of a silane derivatised surface[4].

1.2.1.5 Coating electrode surface with inorganic materials

Inorganic microcrystalline-structured materials such as clays, zeolites and alumina have been used to modify electrode surfaces.[34,45] These materials are of interest because they are ion exchangers that can withstand high temperatures and highly oxidizing solution environments. In this respect, a microporus alumina membrane[46] prepared by anodizing metallic alumina in an acidic electrolyte has been used to prepare inorganic membrane modified electrodes.

1.2.1.6 Electrodeposition

Electrodeposition involves the same procedure as electropolymerization, but the oxidized or reduced form of the modifier is less soluble and is adsorbed onto the electrode without polymer formation. The first CV scan is the same as subsequent scans.

1.2.2 Characterization of chemically modified electrodes

Once an electrode surface has been successfully modified, it is desirable to characterize such a modified surface. A number of techniques are actively in use for characterizing modified electrode surfaces.

Electrochemical methods, particularly cyclic voltammetry, provide an effective way of determining the amount of the modifier deposited on the electrode.[35] The amount of modifier deposited on the electrode surface (termed "surface coverage") may be obtained by cycling the electrode within an appropriate potential window in a solution that contains a supporting electrolyte, the voltammetric characteristics of the immobilized species can then be observed. The area under the oxidation or reduction wave gives the charge associated with the species coated on the electrode,[3,34] expressed by equation 1.15.

$$Q = nFA\Gamma \qquad \textbf{1.15}$$

where A = area of the surface of the electrode, cm^2

Γ = surface coverage, mol cm^{-2}

other parameters are as defined in equation 1.14

Optical methods such as ultraviolet/visible transmission and reflection spectroscopy are also routinely used for characterizing modified electrode surfaces. In cases where the substrate electrode is transparent as in indium tin oxide (ITO) electrodes[47] and if the modifying layer contains visible-range chromophores, the examination of the potential induced chemical changes in the film is possible. Reflectance methods are employed

where the electrode material is not transparent. Other optical methods commonly employed for the characterization of modified electrode surfaces include infrared reflectance spectroscopy,[48] raman spectroscopy and ellipsometry.[49]

Methods based on x-ray,[50] scanning tunneling microscopy,[51,52] atomic force microscopy (AFM) and quartz crystal microbalance (QCM)[53] are widely used for characterizing modified electrode surfaces.

1.2.3 Applications of chemically modified electrodes

Applications of chemically modified electrodes vary considerably from catalysis of organic and inorganic reactions to electron transfer from and to biological molecules.[4] The wide spectrum of application as well as the vast amounts of information that could be obtained at modified surfaces have attracted considerable research interest into CMEs. For example, fundamental information about the mechanism of electron transfer[32] at the modified electrode surfaces can be obtained.

Modifying an electrode surface imparts to the surface some chemical specificity not available at the unmodified electrode[33,43,54] thus increasing the selectivity of the electrode. Carbon paste electrode modified with stearic acid has been used for the determination of dopamine in the presence a large excess of ascorbic acid,[38] which is a major source of interference in the analysis of dopamine. The negative charge of the stearate in the matrix of the electrode caused a repulsion of the negatively charged ascorbate in solution away

from the electrode surface thereby making the electrode selective for the determination of dopamine in the presence of ascorbic acid.

The investigation of the electrochemistry of proteins, enzymes and other biological molecules of interest is hindered strongly because of the strong attraction of these compounds to the electrode surface causing poisoning.[4] Also, many compounds form radicals that readily polymerize at the electrode surface and deactivate it. Examples are the cresols and phenolic compounds. There have been reports on the use of CMEs to prevent the deactivation of the electrode by the oxidation products[55,56,57,58] causing the electrode to be stable towards the analysis of these species.

Many reactions do not occur readily at unmodified electrode materials, which make it imperative to catalyze such reactions by introducing suitable and stable modifiers to the electrode surface.[35] The modified electrode decreases the overpotential required for the reaction to take place. Examples of reactions in this category include the electroreduction of oxygen,[59,60] the oxidation of propan-2-ol to acetone[61] and the electroreduction and oxidation of nitric oxide[62,63] where CMEs have been successfully applied.

The use of CMEs is desirable for the analysis of amino acids, proteins and small biological molecules, as many of these molecules have slow electron transfer kinetics and high overpotentials at unmodified electrodes.[64] The development of CMEs for the sensitive and selective determination of biological molecules is an active area of

research.[45,62,63] Much attention and emphasis is placed on identifying and characterizing modifiers that will enhance selectivity and sensitivity. This constitutes the core of this research work.

Lastly CMEs have found application in display devices where modified electrodes in electrochemical cells change colours or emit light when excited electrically[35] and in photoelectrochemical devices for preventing photocorrossion in semiconductor electrodes used in photoelectrochemical cells for solar energy conversion.[35]

Considerable interest has been generated in the study of CMEs worldwide as evidenced by the large number of records on this subject matter in the literature. Many new types of surface structures are being prepared and electrochemical studies are leading to a better understanding of the way charge is transported and exchanged through surface species and the molecules in solution.[35]

Aim of thesis

One of the aims of this thesis is to identify and characterize metallophthalocyanine complexes that could be used to modify electrode surfaces so as to improve on the selectivity and sensitivity of such electrodes for the detection and quantitation of biomolecules such as the neurotransmitters and pharmaceuticals. The practical considerations in this respect include the optimum method of attachment of the modifier

to the electrode surface, the chemical state and identity of the modifier, the possible interaction of the modifier with the analyte, solvents, electrolytes and buffers.

1.3 ULTRA MICROELECTRODES

Ultra microelectrodes (UMEs) are defined as electrodes which have small dimensions, usually ranging from a few tens of micrometer to about 100Å,[4,65,66] compared to "regular" electrodes of millimetric dimensions.[66] Common geometries of UMEs include spherical, hemispherical, disk, cylinder, ring, line, and bands.[4,65]

The fabrication of most UME geometries is technically demanding because of the fragile nature of the very thin metal wires used.[1] For example, a 5-μm-radius platinum wire at times seems to break just by looking at it![65] and getting to pack carbon paste into holders of μm dimensions is an up-hill task.

Array of UMEs, Figure 1.6, also called composite UMEs consists of ensembles of UMEs that may be dispersed in a regular or random manner within a continuous insulating matrix.

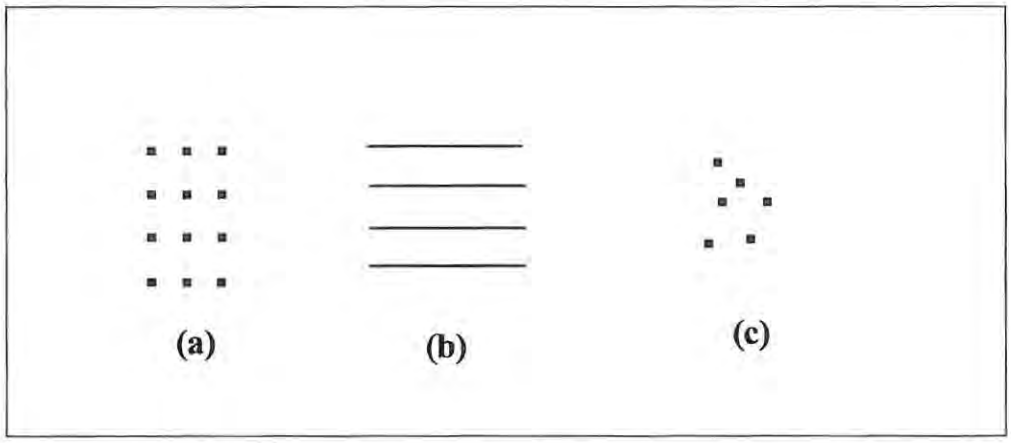

Figure 1.6: Schematic examples of arrays of UMEs: (a) regular arrangement of electrodes of identical shape and size, (b) arrays of parallel band electrodes, (c) random array of UMEs.[66]

Ensembles of electrodes with identical shape but uneven dimensions or statistical arrangements of irregular shaped electrodes are also possible.[66] Provided there is negligible overlap of the diffusion layers from adjacent sites, the current of composite electrodes is the sum of currents of individual sites.[1] In order to isolate the diffusional field of each microelectrode from neighboring ones, larger separations and smaller dimensions are preferred.

The small size of UMEs offers many analytical advantages. These include:[1,4,65]

(i) the total currents at UMEs are small which makes it possible to work in highly resistive solution such as systems with little or no deliberate addition of a supporting electrolyte, work with two-electrode systems and in non-aqueous media,

(ii) UMEs have greatly reduced double-layer capacitance because of their small size. This results in electrochemical cells with small time constants and voltammetric experiments can be carried out at very fast scan rates.[67,68,69,70] High speed voltammetric experiments can be used to probe the kinetics of very fast electron-transfer and coupling chemical reactions,[71]

(iii) UMEs posses excellent signal-to-background ratio because of higher current densities that arise as a result of increased mass transport to the electrode and reduced charging currents. Thus lower detection limits are generally obtained at UMEs compared to their "larger" counterparts,[72,73,74,75]

(iv) the percentage electrolysis at UMEs is small. This allows the rapid attainment of time independent steady-state or quasi-steady-state currents and the contribution of convective transport is negligible.[76,77,78]

For the description of the diffusion of analytes at UME geometries, the planar, cylindrical and spherical forms of Fick's law (see section 1.1.5.1) and a combination of these forms are sufficient.[66] For a non-planar UME of radius r_o, the limiting current is given by equation 1.16.

$$i_t = nFADc\left[\frac{1}{\sqrt{\pi Dt}} + \frac{1}{r_0}\right] \qquad \textbf{1.16}$$

At long experimental times, the current behaviour approaches a non-zero steady state value given by equation 1.17.

$$i_{t=\infty} = 2\pi nFr_0Dc \qquad \textbf{1.17}$$

Applications of ultra microelectrodes

UMEs are used for measurements in very small volumes, particularly as end-column detectors in liquid chromatography, where low concentrations in small volumes are routinely handled.[79]

UMEs mounted on piezoelectric micropositioners are being used to map the local concentrations of electroactive substances in two dimensions via a technique called scanning electrochemical microscopy (SECM).[80,81] UMEs have been developed for probing chemical events within single biological cells,[82] and for use inside the living brain[83] in order to gather information on the dynamic concentrations of neurotransmitters.

Aim of thesis

This thesis seeks to contribute modest improvements by developing chemically modified ultra microelectrodes capable of spatial and temporal resolution of signals arising from the oxidation of neurotransmitters, particularly dopamine and serotonin, and at the same time eliminate interference from other electroactive components of the extracellular fluid (ECF).

1.4 NEUROTRANSMITTERS

The understanding of the chemistry of the brain, its structure, functions and neurotransmission in particular, has been a longtime goal.[84,85] The main function of the brain is as an information storage and processing system. Neurotransmission is the process of exchange and use of this information; it occurs within a discrete group of highly specialized cells called neurons.[86] Neurotransmission consists of two distinct but related events: the passage of an electrical impulse along neurons and the release of molecules, called neurotransmitters, from small packages or vesicles between two neurons.[86] Neurotransmitters are substances that aid in transmitting impulses between nerve cells or between a nerve and a muscle.[87] Figure 1.7 shows the structures of some neurotransmitters. On release from nerve terminals, they act on receptor sites at postsynaptic membranes to produce either excitation or inhibition.[88,89]

1.4.1 Discovery of neurotransmitters

Early in the 20th century, the search for chemical agents that can transmit the activity of peripheral nerves onto target organs began. Acetylcholine (Figure 1.7) was the first substance to be unequivocally demonstrated as a neurotransmitter, acting at voluntary motor nerve terminals to initiate muscle contraction.[90] Norepinephrine (Figure 1.7) and its immediate precursor, dopamine, (Figure 1.7) were shown to be neurotransmitters after a long accumulation of evidence in the 1950s.[91] The neurotransmitter function of serotonin (Figure 1.7) was also clearly established in the 1950s.[91]

During the same period, five amino acids – glutamate, aspartate, γ-aminobutyric acid (GABA, Figure 1.7), glycine and taurine – were considered as neurotransmitters. The neural peptides were detected, isolated and characterized and were added to the list of chemical substances that could be operating as neurotransmitters in various regions of the animal nervous system. Histamine (Figure 1.7) is one of the neurotransmitters whose neuroregulatory role was recognised very late due to its low concentration in the brain. Among the roles attributed to histamine in the brain are arousal, regulation of biological rythms, thermoregulation and various vegetative and neuroendocrine functions.[88]

Today, more than thirty potent compounds, which are water soluble and electrically charged including such unexpected agents as adenosine and adenosine triphosphate, have been found to be acting independently or in concert to control communication between neurons through their points of intimate contact, the chemical synapses, and at their junctions with their various target organs.[91]

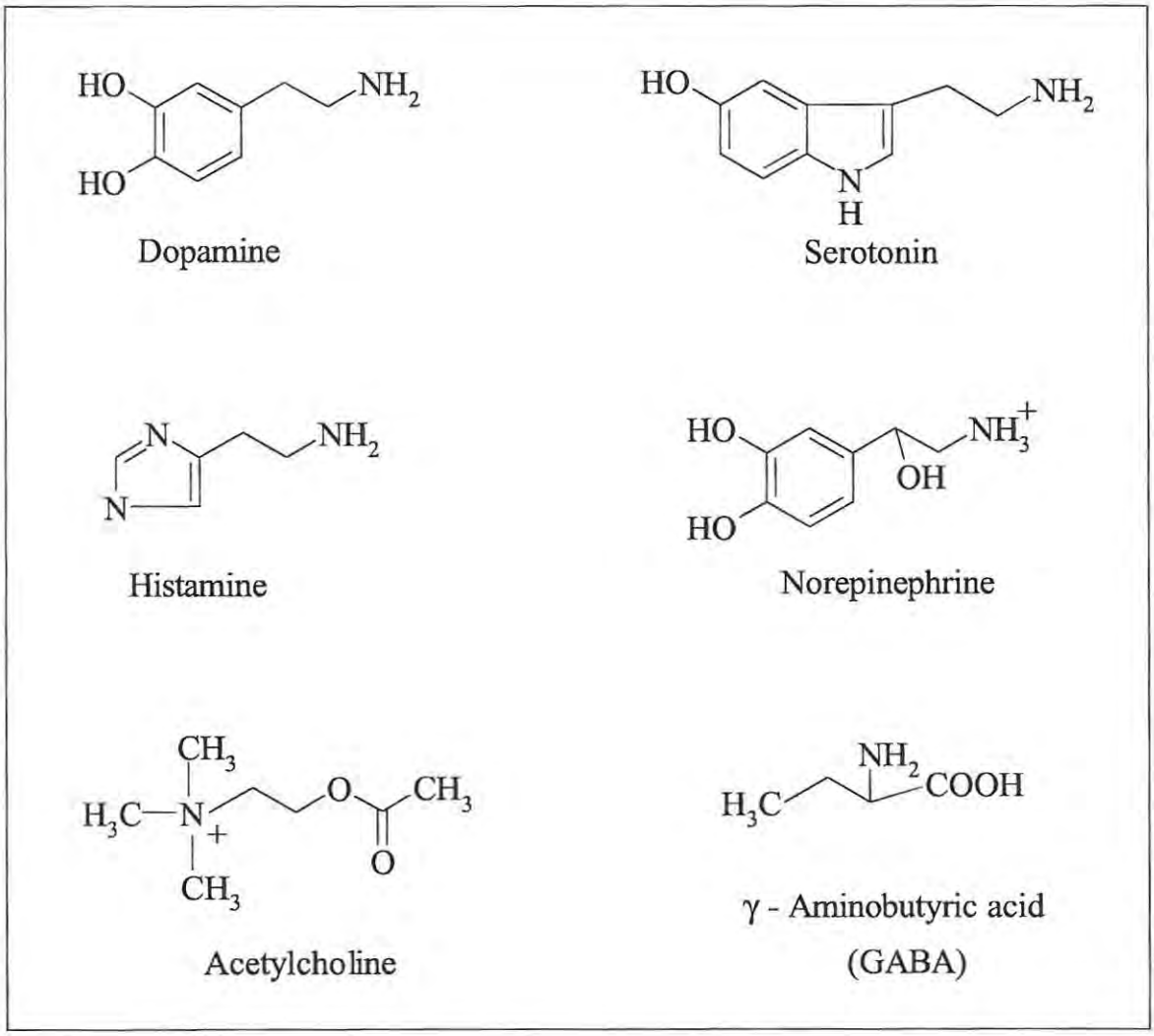

Figure 1.7: molecular structure of some neurotransmitters

1.4.2 Identification criteria of neurotransmitters

Several chemical substances that act as neurotransmitters have been identified; but not all substances that are found associated with nerves and are able to alter nervous activities are neurotransmitters. There is a set of criteria[88,89,91,92] which must be satisfied before a substance could be considered as a neurotransmitter. Where most of the requirements are met but not all, the substance is given the status of putative neurotransmitter. The criteria which must be satisfied before a substance is considered a neurotransmitter are:

(i) the substance must be synthesized within the neuron from which it is released,

(ii) enzymes capable of synthesizing the substance are demonstrated in those same neurons,

(iii) precursors and any compound forming part of a biosynthetic route are present in the neurons,

(iv) calcium-dependent release of the substance to extracellular fluids is shown to occur during action potential or during depolarization of its axon terminals,

(v) the tissue close to the neuron in question must possess mechanisms for the inactivation of the proposed neurotransmitter once released,

(vi) the substance mimics exactly the postsynaptic action of the synaptically released neurotransmitter when added to the region of the synapse. This means that it must duplicate the effect of stimulating the nerve pathway in question,

(vii) pharmacological agents, such as antagonists, that interact with the synaptically released neurotransmitter also interact, in an identical manner, with the added substance,

(viii) Specific receptors for the substance must be present in the tissue region containing the synapse.

1.4.3 Significance and fluctuations of neurotransmitters

The highly sophisticated and controlled mechanism of communication between populations of neurons is largely kept operational by neurotransmitters. The delicate balance of pre- and postsynaptic mechanisms within defined fibre projections can be upset by a failure or reduction in the formation of a neurotransmitter or a malfunction of its receptors. Similarly, exaggerated release of neurotransmitters or changed sensitivity of its receptor will lead to similar derangement of function. This derangement of functions manifests itself as distortions of neuronal performance leading to neurological and psychiatric diseases.[91,93,94] The distinction between these two classes of diseases is now largely artificial and reflects the mode of treatment rather than any intrinsic differences. The term "neuropsychiatric" probably provides a better description of the whole spectrum of nervous system disorders.[93] A number of diseases associated with neurotransmitter fluctuations are enumerated below:

1.4.3.1 Parkinson's disease and dyskinesias

Dr. James Parkinson first described Parkinson's disease in detail in 1817; it is primarily due to the deficiency of dopamine.[86,93] The salient features of parkinsonism are tremor, muscular rigidity, relatively little limb movement and a pattern of walking with small slow steps.[86,93] At an advanced stage, the secondary symptoms include depression, senility, postural deformity and loss of speech.[86,94] On the other hand, dyskinesias is characterized by excessive, exaggerated and bizarre muscle or limb movement or postures.[91] These abnormal movements occur either spontaneously at rest or are superimposed on voluntary movements causing distortions and apparent lack of control. Dyskinesia is believed to result from excessive dopaminergic stimulations.[91]

1.4.3.2 Huntington's Chorea

This degenerative disease process is largely believed to result from the depletion of the level of γ-aminobutyric acid (GABA),[94] based on the information provided through studies of the neurotransmitter-system profiles of postmortem brains.

1.4.3.3 Schizophrenia

Schizophrenia is a widespread psychotic disorder characterized by withdrawal, confused thinking, delusions, paranoia and hallucinations. Reports have appeared of increases of dopamine in postmortem schizophrenic brains suggesting that increased dopamine release may be at the root of schizophrenia.[95]

1.4.3.4 Depression

The group of conditions collectively known as depression is characterized by a severe and chronic change in emotional state with prominent subjective feelings of sadness, withdrawal, apathy, lowered ego and a negative self assessment.[91] The two neurotransmitters predominantly implicated by current findings on the etiology of depression and mania are serotonin and norepinephrine. Lowered levels of serotonin or its metabolites in the brains of depressive suicides[96] have been reported.

1.4.3.5 Alzheimer's disease

The clinical features of Alzheimer's disease include profound deterioration of most aspects of mental function, including memory, intellect and judgment. There may be speech disorders, inability to perform voluntary movements and impairment of recognition.[86,91,97] Lowered level of acetylcholine[98] in the brain is believed to be the major cause of Alzheimer's disease.

1.4.3.6 Excitotoxicity

The acidic amino acids such as L-glutamate and L-aspartate are important excitatory transmitters in the mammalian central nervous system (CNS).[99] Excessive stimulation of excitatory amino acid receptors can lead to a distinctive pattern of seizures and neurodegeneration which is termed Excitotoxicity.[100,101,102] Excitotoxic process may contribute to the neuropathology resulting from stroke, cardiac arrest, perinatal asphixia and hyperglycaemia.[102] It is possible that excitotoxicity might be involved in other

neurodegerative diseases such as Huntington's disease, Alzheimer's disease, seizure-related brain damage, sulfite oxidase deficiency and olivo-ponto cerebellar atrophy.[101,102] Recent studies show that hypofunction of the excitatory amino acids may result in psychotic and/or memory disturbances.[101]

In view of the grave consequences posed by either an excess or insufficient quantities of neurotransmitters in the CNS, the design of sensors for monitoring their concentrations becomes imperative. One of the aim of this thesis is to design sensors (electrodes) for the analysis of neurotransmitters.

1.4.4 Methods of neurotransmitter analysis.

1.4.4.1 Non-electrochemical methods

A variety of analytical techniques have been employed in the quest to completely understand the mechanism of action or inaction of neurotransmitters, their concentrations in living systems and the effects of concentration changes on their mode of action. Of particular interest has been the study of the effects of concentration changes on biological systems. The methods most often applied in the laboratory for neurotransmitter studies before the "intrusion"[84,103] of electrochemical techniques involve the use of fluorimetric,[104,105,106,107,108] radioenzymatic,[109] chromatographic,[110,111,112,113,114,115] spectrometric[105,116] and chemiluminescence[117,118] techniques.

Chromatographic techniques have been the most widely used of the techniques listed above. They offer a means of separating the neurotransmitters from the complex matrix in which they exist in biological/physiological systems. For improved selectivity and sensitivity, chromatographic techniques have been coupled to other techniques such as luminescence,[119] mass spectrometry,[120,121] electron capture,[122] and very recently, electrochemical techniques[123, 124, 125, 126, 127] for detection.

All the methods enumerated above are only applicable to cases where samples of tissues, neurons, glia, cytoplasm, vessicles and extracellular fluid (ECF) have been withdrawn from the subject. They cannot be used for real-time *in vivo* monitoring of neurotransmitter levels. A direct implication of this limitation is that these methods

cannot be used as diagnostic tools for assessing the neurotransmitter imbalance in subjects. In fact, the majority of the evidence available to date for the role of neurotransmitter imbalance in some diseases were obtained only during the post mortem analysis of the patients.[91] Furthermore, only one point data could be obtained from a subject using these methods; information about the compartmentation of the neurotransmitters among the various structures of the brain such as neurons, glia, cytoplasm vessicles and ECF cannot be obtained. Since communication is achieved via chemicals released by one cell to stimulate receptors on the surface of another cell, it is primarily the compartments outside the cells where observations are desired, in particular, on the release and removal of neurotransmitters.[85]

1.4.4.2 Electrochemical techniques

Many of the transmitter substances in the brain are easily oxidized at conventional electrodes which allows the use of electrochemical techniques for their analysis. This list of easily oxidizable transmitters include dopamine, serotonin, norepinephrine, epinephrine (collectively called the catecholamines), histamine and insulin. The use of electrochemical techniques for the *in vivo* analysis of neurotransmitters was introduced by Adams[103] and his coworkers who were "crazy"[84] enough to put an electrode in the brain but "smart" enough to recognize its huge potential. Since the introduction of electrochemical techniques, various techniques such as differential normal pulse voltammetry,[128] fast scan cyclic voltammetry,[129,130,131] differential pulse voltammetry,[132,133] square wave voltammetry,[134,135] adsorptive potential stripping

voltammetry,[45] alternating current voltammetry,[38] and cyclic voltammetry[136,137,138,139] have been employed for the analysis of neurotransmitters. The list of references given above is illustrative and in no way exhaustive, given the vast records of the use of electrochemical techniques that abound in the literature for the analysis of neurotransmitters.

The major problem associated with the use of electrochemical techniques for the analysis of neurotransmitters is the presence of other easily oxidized molecules in the ECF, most especially ascorbic acid. Ascorbic acid is present at concentrations $10^2 - 10^3$ times higher than the catecholamines and gets oxidized at similar oxidation potentials[40,84,85,130,138,140] which results in overlapped voltammetric response, thereby posing the problem of interference.

There have been many approaches towards overcoming this problem of selectivity. These include the use of a specific procedure for electrode pretreatment, particularly for carbon-based electrodes, which result in the separation of oxidation signals for the analyte of interest and the interfering molecule. Among the methods used in this category of selectivity improvement are electrochemical pretreatment,[141,142,143,144] laser activation[145] and heat treatment.[146]

Another approach was based on precoating the surface of the electrode with a permselective layer, such as Nafion®, which incorporates positively charged

neurotransmitters such as dopamine and serotonin and repels ascorbic acid and other negatively charged species due to its ion exchange properties.[147,148] Closely related to this approach is the modification of carbon paste electrodes with stearic acid[38] where the stearate on the electrode repels ascorbic acid and other negatively charged ions.

A number of electroactive materials such as nickel phthalocyanine,[40] ruthenium oxide perchlorate[149] and nickel hexacyanoferrate[150] have been found to exhibit catalytic activity towards the detection of some neurotransmitters. Electrodes have been modified by covering their surfaces with these electroactive species and then applying a second layer of Nafion®. The combination of the electrocatalytic function of the underlying electroactive coat and the charge exclusion/preconcentration property of the outer Nafion® layer has helped to achieve desired sensitivity and selectivity at the modified electrodes. Electrosynthesized polymeric films of 3-methylthiophene, aniline and pyrrole[132,135,151,152] onto electrode surfaces are also reported as being useful in the selective detection of neurotransmitters in the presence of an excess of ascorbic acid.

Enzyme extracts[153] or enzymes in vegetal tissues[154,155] have been used to develop biosensors for the analysis of neurotransmitters in the presence of interfering molecules. Graphite reinforced carbon electrodes[134] and highly boron-doped diamond electrodes[139] have also been demonstrated to be capable of selectively detecting neurotransmitters in the presence of interfering molecules.

In sharp contrast to the other methods of neurotransmitter analysis, electrochemical techniques can be used for real-time *in vivo* measurements[85,130,142] of neurotransmitters in biological systems because of the speed of measurement and the size of electrode[142,156,157] which allows for good temporal and chemical resolution.[85,157] Electrodes for voltammetry can be made quite small for them to be placed in the ECF and used to measure neurotransmitter release and/or uptake with little or no damage to surrounding tissue.[147,158] For example, fast scan cyclic voltammetry (FSCV) takes only a few microseconds to record and is made at a carbon fiber electrode of diameters of between 1.0 to 8.0 μm.[156,157,158] These measurements can be repeated many times per second and thus give near real-time detections of transmitter substances in biological systems.[85,156,158] In this thesis, electrodes modified with metallophthalocyanines are used in the electroanalysis of neurotransmitters and pharmaceutical preparations.

1.5 VITAMIN B_1

The pharmaceutical product whose electrocatalytic determination at MPc modified electrodes was investigated in this work is Vitamin B_1.

Vitamin B_1 (also called thiamine, aneurin, torulin) is an important pharmaceutical substance and it constitutes an important component of man's diet. The molecular structure is shown in Figure 1.8.

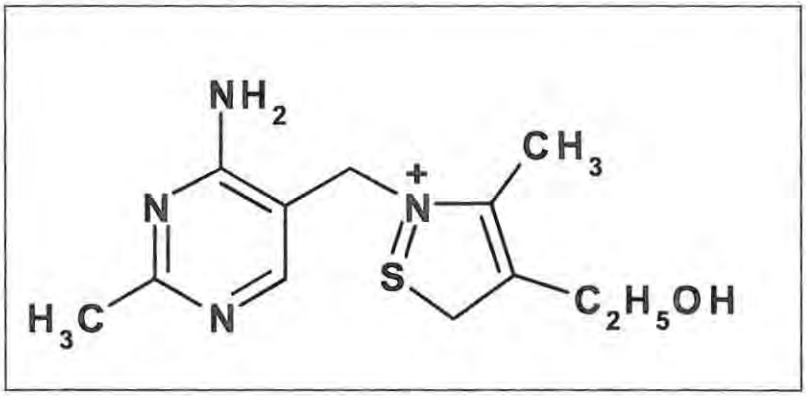

Figure 1.8: Molecular structure of Vitamin B_1

The chief natural source of vitamin B_1 is rice husk. It exists in variable amounts in milk, yeast, green leaves, roots and tubers.[159,160] A deficiency of vitamin B_1 leads to beriberi,[161] a nutritional disease characterized by degenerative changes in the nervous system, including multiple peripheral neuritis; accompanied by generalized oodema and serous effusions, with a tendency to cardiac hypertrophy and dilation.[161]

Several analytical techniques have been devised for the determination of vitamin B_1. These include chromatographic,[162,163,164] spectrophotometric,[165,166] spectrofluorime-

tric,[167,168] chemiluminescence[169] and reaction rates[170] methods. Both the United States [171] and the British[172] Pharmacopoeia prescribe a method based on liquid chromatography for the assay of vitamin B_1. However, these methods involve tedious, time consuming and complicated procedures, and require the use of expensive instrumentation or dangerous and undesirable reagents.[168,173,174] This necessitates the need to develop faster, easier and cleaner methods, such as the use of electrochemical techniques, for the determination of Vitamin B_1. Polarographic and potentiometric methods have been used for the determination of Vitamin B_1; records of the use of voltammetric methods for the determination of this product were not found in the literature. In this work, the use of voltammetric method employing modified electrodes for the determination of Vitamin B_1 was carried out.

1.6 METALLOPHTHALOCYANINES

1.6.1 History of Metallophthalocyanines

Metallophthalocyanines (MPcs) form an important class of organic functional materials. They were discovered by accident in 1928 during the large-scale preparation of phthalimide from phthalic anhydride at the Grangemouth plant of Scotish Dyes.[175] The process involved the passing of ammonia into molten phthalic anhydride in iron vessels. It was found that during certain preparations, traces of a dark-blue substance were formed in the molten amide. This dark-blue product was later shown to be ferrous phthalocyanine.

1.6.2 Structure of Metallophthalocyanines

The geometric structure of metallophthalocyanines, Figure 1.9, has been elucidated[176] using x-ray diffraction analysis.

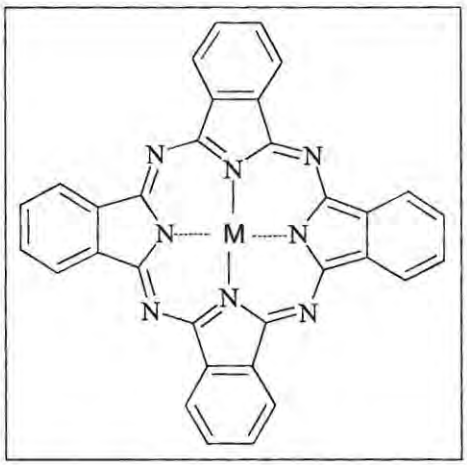

Figure 1.9: The geometric structure of metallophthalocyanines, M represents the metal in the center of the macrocyle

The MPc molecule is a 18-π–electron aromatic macrocycle made up of four isoindole units linked together by aza nitrogen atoms.[176] This structure is closely related to that of naturally occurring porphyrin; Figure 1.10.

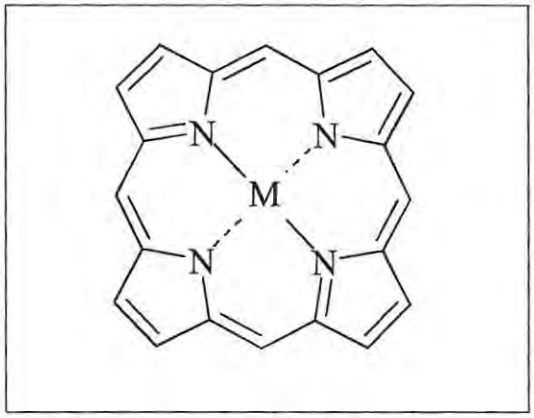

Figure 1.10: The structure of metalloporphyrins

There are only a few basic differences in the two structures. These differences are:

(i) Porphyrin ring is made up of pyrrole units instead of isoindole units of the phthalocyanines (Pcs)

(ii) The pyrrole units are linked by carbon atoms in place of the nitrogen atoms in the phthalocyanines.

The central cavity of Figure 1.9 can play host to a wide range of metal cations, which can include group 1 and 2 metals[177] transition metals,[178] lanthanides and actinides[179] and main group metals and metalloids.[180] More than seventy different metal phthalocyanine derivatives are known[181] whose unique physical and chemical properties have been exploited from both the practical as well as the theoretical point of view.

1.6.3 Synthesis of Metallophthalocyanines

There are a number of different methods for preparing MPcs.[182] The commonly used routes for MPc synthesis are:

The reaction of phthalic anhydride/urea with metal salt in a refluxing solvent in the presence of a catalyst, Scheme 1.1.

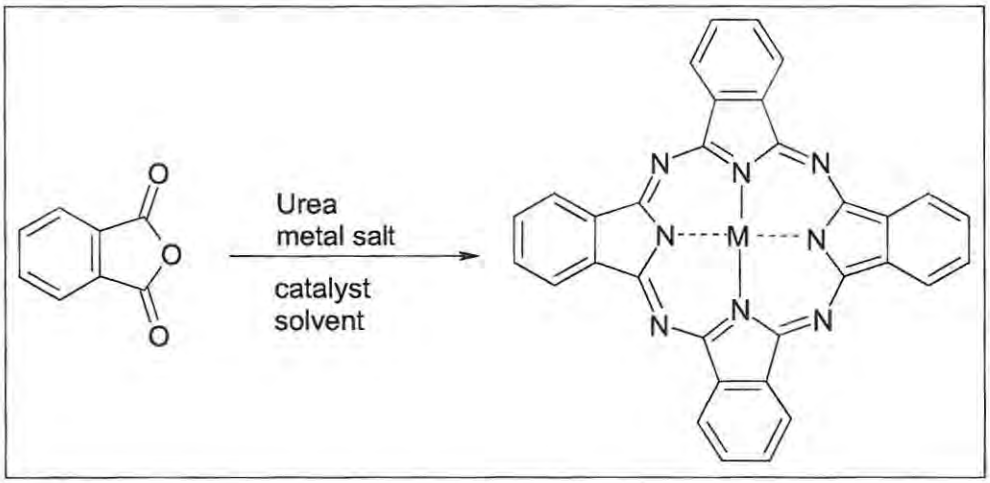

Scheme 1.1: Synthesis of MPcs from phthalic anhydride.

This is the route used in the large-scale production of MPcs since it utilizes inexpensive starting materials.[183]

The phthalonitrile route (Scheme 1.2) gives a higher purity product. This route is normally used for Pcs used in high technology application where quality, not cost, is the main consideration; since phthalonitrile is a more expensive starting material.

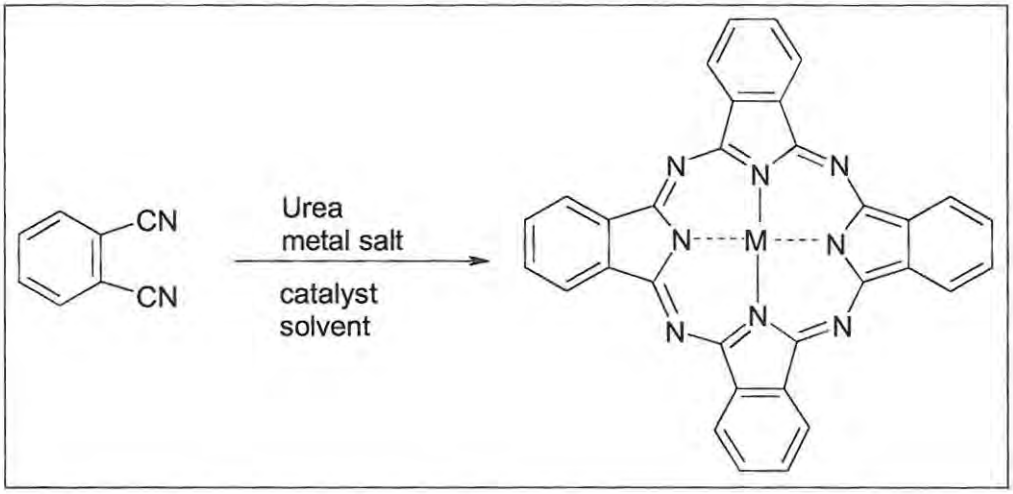

Scheme 1.2: Synthesis of MPcs from phthalonitrile

Metallophthalocyanines can also be synthesized by the reaction of o-cyanobenzamide, Scheme 1.3, with metal salts in high boiling solvents.[184]

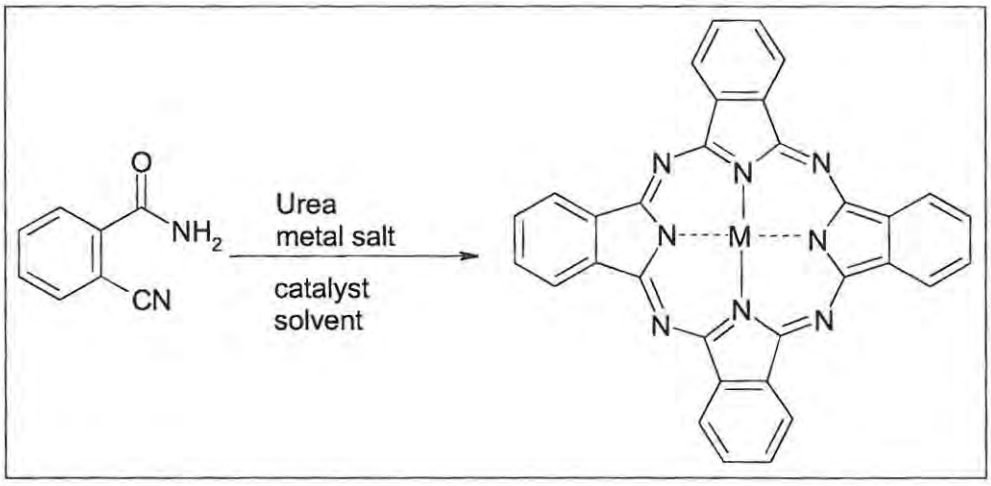

Scheme 1.3: Synthesis of MPcs from o-cyanobenzamide

Recent advances in research have led to the use of microwave irradiation for the synthesis of MPcs.[185,186] This eliminates the use of solvents therefore enhancing the synthesis of purer products. Also the reaction time is dramatically reduced; it takes anything between three to six minutes to synthesize MPcs by microwave method as opposed to minimum of six hours of refluxing in high boiling solvents.[186]

The presence of substituents on the Pc macrocycle can dramatically modify the basic properties of the Pc ring system. Most unsubstituted Pcs are characterized by strong intermolecular cohesion that makes them non-melting and insoluble solids. However, the introduction of substituents into the Pc ring system makes them to melt easily and to be soluble in a number of organic solvents to an extent depending on the nature of substituents used.[187]

Most substituted Pcs are derived from the cyclotetramerization of the appropriate phthalonitrile or phthalic anhydride derivative, thereby allowing for the introduction of up to four substituents into each of the four benzo subunits.[7] For example, soluble octasubstituted MPc complexes are normally synthesized from the substituted phthalonitriles and the metal salt,[188] Scheme 1.4.

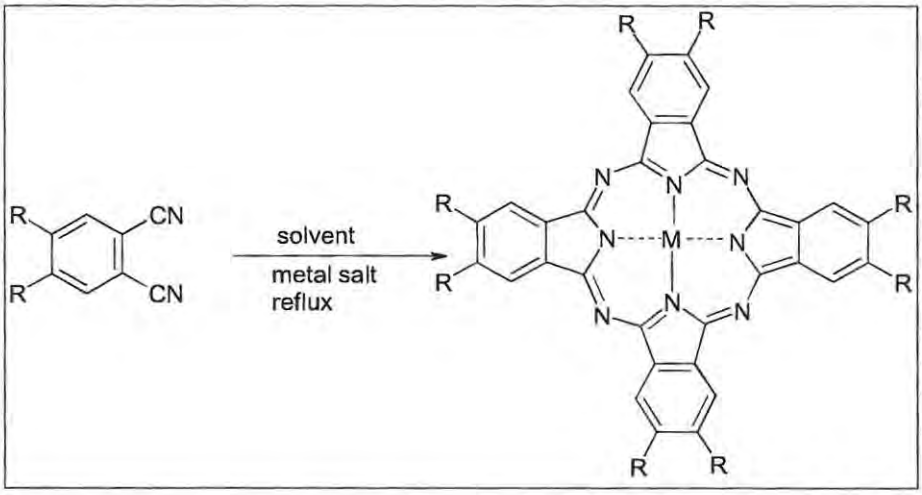

Scheme 1.4: Simplified route to the synthesis of octasubstituted MPc from substituted phthalonitrile

Tetrasufonated MPcs are known to be soluble in water.[189] They are normally synthesized, Scheme 1.5, by refluxing the appropriate divalent metal salt and the monosodium salt of 4-sulfophthalic acid in nitrobenzene in the presence of a catalyst.

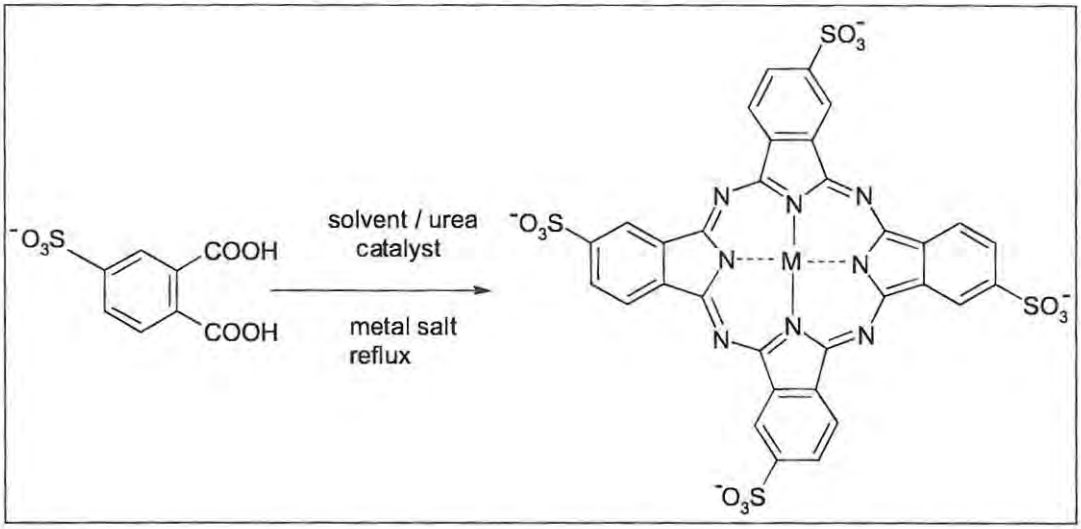

Scheme 1.5: Synthesis of water soluble tetrasulfophthalocyanine

It is also possible to introduce axial substituents into the appropriate cation held within the central cavity of the Pc macrocycle. The resulting complexes are referred to as axially coordinated MPc complexes. Axial ligands are normally introduced by refluxing the unligated MPc in a coordinating solvent or other axial ligands,[190,191] Scheme 1.6. For example, several axial ligands have been introduced into SiPc by microwave irradiation.[186]

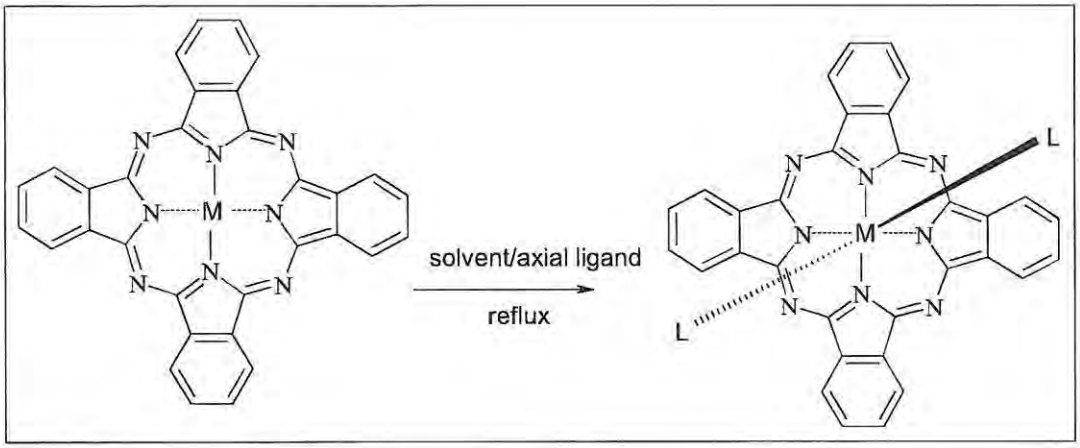

Scheme 1.6: Synthesis of axially ligated MPc complex

1.6.4 Electronic absorption spectra of metallophthalocyanines

Metallophthalocyanine complexes show a number of strong characteristic absorptions in the visible and ultraviolet regions. The electronic absorption spectra arise primarily from the π to π^* transitions within the delocalised phthalocyanine ring system.[192] Figure 1.11 shows the ultraviolet/visible (UV/vis) absorption spectrum of a typical metallophthalocyanine.

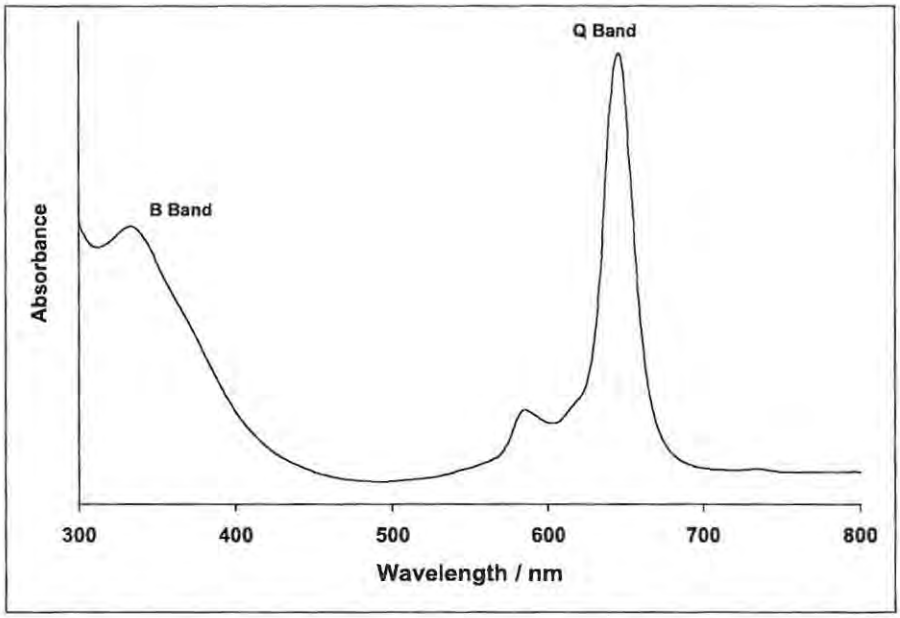

Figure 1.11: UV/vis spectrum of a typical MPc

The purity and depth of the colour of MPcs arise from the unique property of having an isolated, single band located in the far red end of the visible spectrum with a molar absorptivity often exceeding 10^5 L mole^{-1} cm^{-1}.[193] This isolated band is called the Q band. The next most energetic set of transitions is generally much less intense, lying just to the blue of the visual region near 340nm[193,182] called the B or Soret band. The Q band in the metallophthalocyanines is reasonably constant in energy irrespective of the central metal ion,[192,193] but is shifted by the substituents.

The origin of the absorption of the first two π to π^* transitions (the Q and the B bands) is shown in Figure 1.12.

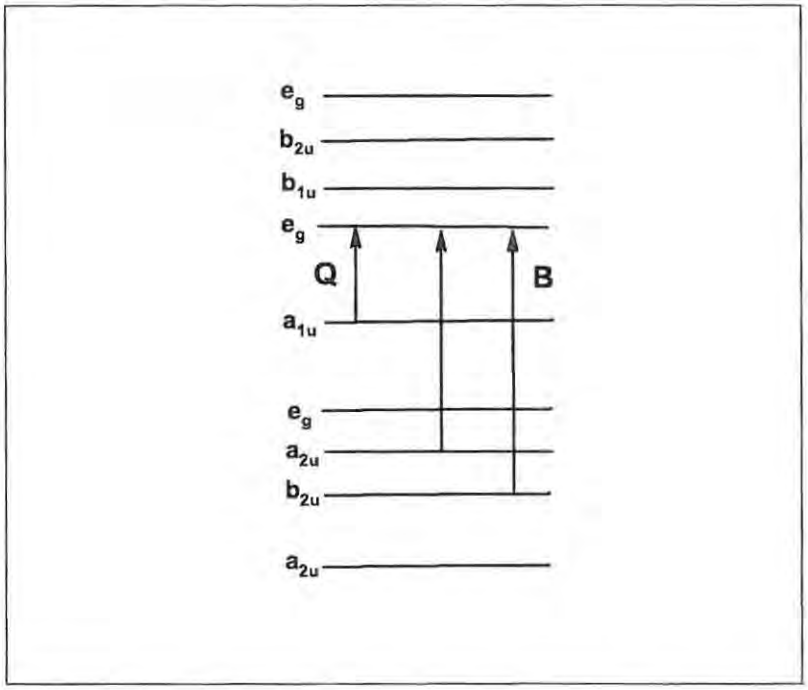

Fig. 1.12: The origin of the Q and B absorption bands of phthalocyanines.

Using the four-orbital model proposed by Gouterman[194] based on the two top occupied molecular orbital and the lowest unoccupied orbital, the spectra of MPcs arise from transition of electrons from the highest occupied molecular orbital (HOMO) of π nature to the lowest unoccupied molecular orbital (LUMO) of π^* nature. The first two allowed $\pi \rightarrow \pi^*$ bands arise from transitions from an a_{1u} and a_{2u} into the same e_g orbital.[193]

Additional absorptions that are seen in the spectra of MPc complexes have been assigned to charge transfer (CT) transitions. With the exception of d^0 and d^{10} metals, CT transitions, either metal to ligand (MLCT) or ligand to metal (LMCT), can be expected in

the 200 to 1000nm spectral window.[178,193,195] As an illustration, Figure 1.13 is a diagram that shows the possible symmetry allowed transitions for a low spin d^6 metal complex.[193] Transitions in the 500nm region of the spectra of MPcs are typically assigned to charge transfer.

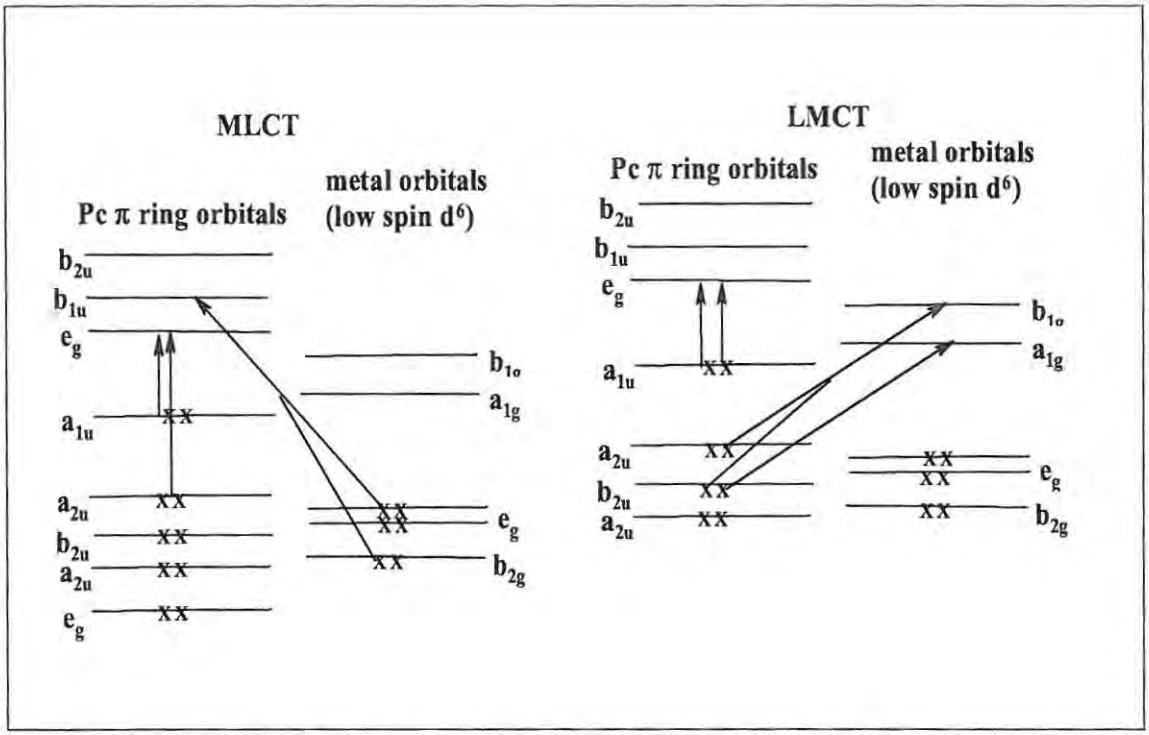

Fig. 1.13: Charge transfer transitions between the metal and the Pc ring.

A nomenclature proposed by Platt[196] and his co-workers is generally used to describe the bands in the UV/vis region of MPc spectra. Additional bands (N, L and C) have been identified in the UV region of the absorption spectra of MPcs.

1.6.4.1 Methods of recording UV/vis spectra of metallophthalocyanines

A large number of techniques have been used to gather information about the electronic absorption properties of MPcs. UV/vis spectra have been recorded for MPcs as solutions in UV transparent solvents such as dimethyl acetamide (DMA), dimethyl formamide (DMF), and dimethyl sulfoxide (DMSO) as well as in concentrated acids and aromatic solvents like α-chloronaphthalene and pyridine. Also vapour phase spectra have been reported for many MPcs.[193] Lastly, spectra have been obtained from MPcs in the solid state as thin films and from crystals. Many MPcs sublime readily near 623K in a high vacuum and can be laid down as thin polymorphic films on a substrate, usually quartz.[197] Crystals are either too optically dense or too small for study by transmission techniques because of intense absorptivity. However, reflectance spectra have been reported.[198]

The most resolved spectra were obtained in the vapour phase at temperatures of about 773K. The absence of solvents allows bands to be measured to the cut-off of the spectrometer near 200nm. A common feature, but not unexpected is the broadness of all the bands.[199] Solid state spectra, especially from thin films, are also complicated by the broadening that arises from Davydov effect, the spectral envelopes obtained are in no way similar to the envelopes observed for either vapour or solution phase.[197]

1.6.4.2 Comparison of the electronic absorption spectra of porphyrins and phthalocyanines

Metallophthalocyanine complexes in general have richer electronic spectra than the porphyrins for a number of reasons:

There is a greater delocalisation of metal orbitals in MPc complexes which enhances the intensity of charge transfer transitions. Additional number of low-lying empty π^* orbitals in MPcs give a greater number of allowed transitions.

The smaller hole size in the Pcs gives rise to greater covalent interaction between the metal and the Pc ring.

The most important difference in the characteristic spectral features of the phthalocyanines and the porphyrins is that the intense band in the spectra of the phthalocyanines is the Q band near 630 nm while the Soret band of the porphyrins located near 410 nm is the intense band. The difference in the intensities of these bands could be understood by considering Gouterman's four orbital model.[194] This is represented diagrammatically in Figure 1.14.

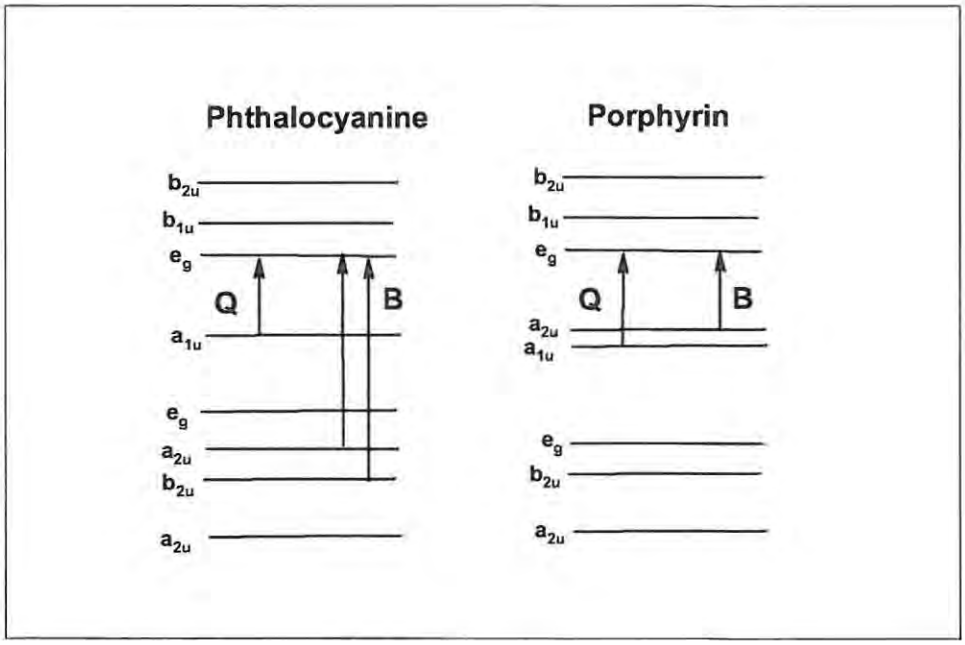

Figure 1.14: Origin of Q and B bands of Phthalocyanines and Porphyrins[193]

The first two allowed $\pi \rightarrow \pi^*$ bands arise from transitions out of a_{1u} and a_{2u} into the same e_g orbital. For the phthalocyanines, the HOMOs are widely separated (a_{1u} lies well above a_{2u}), whereas for the porphyrins, the HOMOs are accidentally degenerate (a_{1u} and a_{2u} are close enough together). This leads to extensive configuration interaction for transitions to the same e_g (LUMO)[193,194] in porhyrins. Thus Pcs generally exhibit a significant red shift in energy and intensification of the Q band relative to the B band compared to porphyrins.

1.6.4.3 Effects of aggregation on the spectra of MPcs

MPcs form aggregated species in solution. There are four major ways[193] by which MPcs may form dimeric (or polymeric species):

(i) direct linkage or bridge between two or more Pc rings whose rings are close enough in space to allow intramolecular association.[200]

(ii) covalent bonding involving the metal as μ oxo links, especially for Fe and Si containing Pcs.[201]

(iii) sandwich-type complex formation, whereby two Pc rings share one central metal.[202,203,204]

(iv) weak association in which peripheral substituents hold two rings adjacent in space.[205]

Aggregation results in spectral effects such as broadening of bands, blue shift of the Q band and the splitting of the Q band. The extent of the effect of association on spectral features depends on the closeness of approach of the rings; the overlap position, the tilt angle that the MPc rings adopt, the bulkiness of the peripheral group and the extinction coefficients of the electronic bands involved.[193]

1.6.4.4 Importance of spectral studies of Metallophthalocyanines.

The spectral properties of MPcs are central to studies of their chemical and electronic properties. The variety of spectra that are found for transition metal Pcs also attracted interest in the search for model compounds that mimic complex biological systems. There have been records in the literature where UV/vis spectroscopy was used to monitor the interaction of MPcs with biologically and environmentally significant molecules as nitrite,[206] cysteine, histidine[207] and nitric oxide.[62,63]

The study of the spectral properties of MPcs resulted in the use of peripherally substituted MPcs as replacements for hematoporphyrin derivatives in the photodynamic therapy (PDT) of cancer because of their higher absorbance in the 650-670nm window which is the region where the skin is most transparent to light. Another important reason for the study of the spectral properties of MPcs is that it allows the solid-state chemistry of MPcs to be explored with the use of absorption or reflectance spectroscopy. Lastly, the spectral properties of MPcs can be used as a guide to the accuracy of the theoretical treatments of their electronic structures.[193]

1.6.5 Redox properties of Metallophthalocyanines

The MPc ring is an 18π electron aromatic system. In its common oxidation state, it carries two negative charges designated as Pc(-2).[208] The ring is capable of oxidation or reduction.[208,209,210,211] Oxidation by the loss of one or two electrons yields Pc(-1) and Pc(0) respectively. The ring may be reduced to give a series of negative ions by successive addition of one to four electrons to vacant or partially filled orbitals of the metal complex to yield Pc(-3), Pc(-4), Pc(-5) and Pc(-6).[212, 213 ,214]

The central metal ion may be capable or incapable of a redox process in the usual electrochemical regime. Cyclic voltammetry provides a rapid assessment of the electrochemical properties of MPc species, such as establishing whether the electron transfer process is electrochemically reversible or not and whether there are coupled chemical reactions involved. On a broad scale, ring reduction processes are often electrochemically reversible, while ring oxidation processes, especially that associated with Pc(0)/Pc(-1), are often irreversible.[212]

1.6.5.1 Main group MPcs

The low solubility of most main group MPcs has limited the availability of acceptable quality electrochemical data. Most studies on this class of MPcs are on magnesium and zinc phthalocyanine for which six redox processes corresponding to $[M^{II}Pc(0)]^{2+}$ to $[M^{II}Pc(-6)]^{4-}$ have been reported.[215,216,217,218,219] The effects of axial ligation on redox potentials has been studied for some main group MPcs especially magnesium

phthalocyanine. It was observed that axial ligation does not affect the magnitude of redox potentials significantly.[220,221] Ring substitution with electron withdrawing groups such as cyanide and chloride on zinc phthalocyanine has been reported to shift the reduction potential to more positive values compared to the non-substituted counterparts.[216, 222]

The redox processes in the main group phthalocyanines are expected to occur exclusively on the Pc ring. The first ring oxidation is separated from the first ring reduction by approximately 1.5V; which corresponds to the magnitude of the difference between the HOMO and LUMO.[215] The polarizing power of the central metal ion, expressed as charge per radius, ze/r, remarkably affects the individual potentials for the first ring reduction and the first ring oxidation process. Generally, the more polarizing the central metal ion, the easier it is to reduce and the more difficult it is to oxidize the ring.[214]

Main group Pcs are said to be redox inactive with respect to the metal centre since they do not contain accessible d-orbitals.

1.6.5.2 Transition metal Pcs

Transition metal Pcs can be classified as redox active and redox inactive MPcs; if the transition metal ion concerned has no accessible d-orbital levels lying within the HOMO-LUMO gap of a Pc ring, then its redox chemistry will appear like that of the main group Pc.[214] Metallophthalocyanines containing Ni, Cu, Pt and Pd as the metal center are examples of redox inactive MPcs whose redox properties are similar to those of main

group MPcs in which all redox processes are expected to occur exclusively on the ring.[211,223,224,225,226]

Redox active transition metal Pcs have the d-orbitals of the central metal lying within the HOMO-LUMO gap. The redox processes for these species occur both on the Pc ring and on the central metal depending on the factors within the environment of the MPc such as the nature of the axial ligand, solvent, electrolyte and ring substituents.[178]

Many MPcs form aggregates influenced by pH, ionic strength, temperature, amount electrolyte in solution, net charge on the MPc unit and the presence of axial ligands both in aqueous and organic solvents.[182,227] Care must then be taken in distinguishing redox potentials arising from mononuclear MPcs species and aggregated species.[214] Many MPcs bind one or two axial ligands and the presence of different axial ligands attached to the metal center can have a major effect upon the observed redox activity of the MPc. [220,178,228] Supporting electrolyte anions and the solvent employed can also affect the observed redox properties of MPcs if they axially coordinate.[214] This can lead to marked differences in the redox chemistry of the same MPc in a donor, potentially binding solvent and in a non-donor solvent such as dichloromethane.

1.6.6 Uses of Metallophthalocyanines

MPcs are remarkably stable, have beautiful bright blue to green colours, high tinctorial strength and an excellent fastness to light. These properties have helped establish MPcs as useful colorants. Thousands of tons of MPcs are produced all over the world to satisfy the increasing demand for blue and green colorants in printing inks, photographic materials, textiles, automotive coatings, plastics and paints.[181,183]

MPcs are being used in electronic sensors for the detection of toxic, oxidizing gases such as nitrogen dioxide at concentrations as low as parts per billion. This is based on the increase in conductivity of MPcs when they form charge-transfer complexes. The increase in photoconductivity of MPcs when illuminated with light is currently being used commercially in devices such as photocopiers and laser printers.[181,183]
The active layer of the latest generation of re-writable compact discs is made of uniform films of suitable MPcs. It is predicted that discs made with MPcs could store data for up to 100 years.

MPcs constitute a promising class of catalysts and they present some advantages over metals and metal oxides because of their lower cost. The catalytic action of MPcs can be described more definitely in terms of their chemical structure, chemical and physical properties, and their reactive centres can be identified.[229] MPcs that contain redox active transition metals have been used to catalyse a number of useful processes (see section

1.6.7). Prominent examples of these systems are the Merox process, fuel cell and solar energy conversion devices.[229,230]

MPcs have found use in non-linear optics (NLO) to manipulate optical signals in optical communication and optical signal processing application in the form of electro-optical or optical switches and modulators, high density data storage, phase conjugation holography, spatial light modulators and laser frequency conversion devices.[231]

Photodynamic therapy (PDT) of cancer is a major photocatalytic application of MPcs in medicine. MPcs are preferentially retained by tumour cells and can cause localized cellular damage on excitation by visible light.[232] Zn, Al and Si Pcs are already in clinical trials for the treatment of cancer. Apart from the treatment of cancer, MPc mediated PDT has been used to cause inactivation of viral pathogens such as found in hepatitis and human immunodeficiency viruses (HIV), in blood and blood products, and to produce antibiotic and antifungal effects.[233] Radio-labelled MPcs are being used for imaging and therapy.[234]

There are a wide variety of ways in which MPcs have been employed in modern technology. The applications mentioned above are rather illustrative and not in any way exhaustive. The search for more plausible ways of putting MPcs to use in biomedical application constitutes one of the aims of this thesis. The main thrust is to develop electrodes suitably modified with MPcs for the detection and analysis of neurotransmitters and the active components of pharmaceutical preparations.

1.6.7 Electrocatalytic properties of metallophthalocyanines

Metallophthalocyanines have the ability to add and subtract many electrons and still retain their molecular structure and stability[235] due to their dual donor π-acceptor function. This property makes them to exhibit electrocatalytic activity towards various technologically important redox reactions from use in organic synthesis, removal of waste from water, to detection of low concentrations of compounds.[236] MPc complexes have thus been used as both homogeneous and heterogeneous redox catalysts in a wide range of chemical reactions. The electrocatalytic activity is believed to be mediated by the metal and/or the ring[41,55,192,235,236,237] because electrocatalytic activities are generally observed at potentials close to those of the oxidation of the metal center and/or the ring.[238] The catalytic activity of the MPc complex largely depends on the particular central metal and the total oxidation state of the complex as well as presence of substituents on the MPc backbone.[192]

The generally accepted mechanism[41,207,229,239,240,241] of electrocatalysis by MPcs is believed to be a two-step process initiated by the electrochemical oxidation of the central metal or the ring, followed by the transfer of electrons from the species being oxidized to the metal or ring regenerating the initial catalyst. Equations 1.18 and 1.19 show the mechanism for metal-based electrocatalytic oxidation of an analyte.

$$M^{II}Pc(-2) \rightarrow M^{III}Pc(-2) + e \qquad \textbf{1.18}$$

$$M^{III}Pc(-2) + A \rightarrow M^{II}Pc(-2) + A_{ox} \qquad \textbf{1.19}$$

where A is the analyte of interest and A_{ox} is the oxidation product of A.

Similarly, equations 1.20 to 1.22 describe the mechanism for ring-mediated electrocatalysis.[242]

$$MPc(-2) \rightarrow [MPc(-1)]^{+} + e \qquad \textbf{1.20}$$

$$2[MPc(-1)]^{+} \rightarrow ([MPc(-1)]^{+})_2 \qquad \textbf{1.21}$$

$$([MPc(-1)])_2^{+} + 2A \rightarrow 2MPc(-2) + 2A_{ox} \qquad \textbf{1.22}$$

Table 1.1 gives a list of some molecules whose oxidation process have been electrocatalysed by MPc complexes, while Table 1.2 gives a list of molecules that have been electroreduced with MPcs as catalysts. The types of electrodes used are also given.

Table 1.1: List of some selected MPc mediated electrooxidized molecules

Molecules	**MPc complex**	**Electrode material**	**Reference**
Nitric oxide	CoPc, NiPc	Glassy carbon	63, 243
Cysteine	CoPc, OMoPc	Glassy carbon, carbon paste	237, 241, 244
Dopamine	NiPc	Glassy carbon	40
2-mercaptoethanol	CoPc, ZnPc, CuPc	Vitreous carbon disk	41, 245, 246
Nitrite	CoPc, RuPc	Glassy carbon	206, 235, 239
Hydrazine	FePc, CoPc, NiPc, ZnPc	Graphite	236, 247
Sulfur dioxide	CoPc	pyrographite	236
Glucose and carbohydrates	CoPc, MnPc, FePc	Glassy carbon, carbon paste	236, 248

Table 1.2: List of selected MPC mediated electroreduced molecules

Molecules	MPc complex	Electrode material	Reference
Carbon dioxide	NiPc, CoPc, FePc, InPc, SnPc, MgPc, MnPc,TiPc	Almagamated platinum, carbon-based gas diffusion	229, 236, 249, 250
Oxygen	CoPc, FePc, CuPc, NiPc, MnPc, RuPc, ZnPc	Graphite, Glassy carbon, Carbon black	229, 240, 251
Hydrogen peroxide	RuPc, PtPc,	Graphite, Glassy carbon	235, 252
Cystine	CoPc, MnPc, NiPc, FePc	Graphite	253, 254
Nitric oxide	CoPc	Glassy carbon	62, 255
Thionyl chloride	FePc, NiPc, CuPc, CoPc(polymer)	Carbon, solution	236, 256, 257
Sulfur dioxide	FePc, CoPc	Carbon black	236
Chlorate	FePc, CoPc	Carbon	236
Nitrogen	FePc	Porous carbon	236

1.6.7.1 Metallophthalocyanine catalyzed analysis of neurotransmitters

Despite the popularity of the MPcs as electrocatalysts for the detection and analysis of a wide range of molecules, they still remain largely unexplored for the analysis of neurotransmitter substances. Records in the literature reveal that it is only nitric oxide and dopamine whose MPc electrocatalysed determination have received some cursory attention. The extension of the electrocatalytic property of the MPcs to the determination of a wider range of neurotransmitters is one of the aims of this thesis.

Glassy carbon electrodes modified with CoPc[62,255] and electropolymerized tetraamino phthalocyanine of cobalt ($CoPc(NH_2)_4$), nickel ($NiPc(NH_2)_4$) and copper ($CuPc(NH_2)_4$) have been used for the analysis of nitric oxide.[258,259] A detection limit of $1x10^{-8}$ mol dm^{-3} was obtained.[259]

Nickel tetraaminophthalocyanine, electropolymerized on glassy carbon electrode, has been used by Kang et al.[40] for the determination of dopamine. The modified electrode showed good electrocatalytic behavior towards the detection of dopamine in that the oxidation current per unit concentration was enhanced about three times as well as a decrease in the overpotential of dopamine by shifting the peak potential value negatively by 180mV compared to the peak potential on an unmodified electrode. The interference from ascorbic acid was eliminated by additionally covering the modified electrode with a layer of Nafion®. A detection limit of $9x10^{-8}$ mol dm^{-3} was obtained with this electrode.

The mechanism proposed by Kang et al.,[40] shown in equations 1.23 and 1.24, for the electrocatalytic oxidation of dopamine at the modified electrode is in agreement with the

general mechanism described by equations 1.18 and 1.19 (section 1.6.7). The first process that took place was the oxidation of the central metal in the polymeric film, followed by the transfer of electron from dopamine in solution to the metal.

$$(Ni^{II}TAPc) \rightarrow (Ni^{III}TAPc) + e \qquad \textbf{1.23}$$

$$(Ni^{III}TAPc) + DA_{(aq)} \rightarrow (Ni^{II}TAPc) + DA_{ox(aq)} \qquad \textbf{1.24}$$

The electrocatalytic oxidation of dopamine is related to the catalytic circulation of Ni^{III}/Ni^{II} couple in the polymeric film. The electrocatalytic activity observed with NiPc is surprising since NiPc complexes are known to be redox inactive at the metal center.

Glassy carbon electrodes modified with meso-(tetrapyridyl)porphirinate cobalt(III) [bis(-bipyridine)(chloro)ruthenium(II)] complex has been employed in the amperometric detection of dopamine in flow injection analysis by Agnes et al.[260] A detection limit in the range of μgl^{-1} was obtained.

1.6.7.2 Interaction of metallophthalocyanines with neurotransmitters

Records in the literature show that nitric oxide is the only transmitter substance whose interaction with MPc complexes has been reported. Axial ligation of nitric oxide to FePc,[261,262] CoPc,[62] CoTSPc[63] and NiTSPc[263] has been reported. $Fe^{II}Pc$ has been shown to reversibly bind nitric oxide in dimethyl sulfoxide (DMSO) according to equation 1.25 resulting in the formation of a complex, $Fe^{III}Pc(NO)$.

$$(DMSO)_2Fe^{II}Pc + NO \equiv (DMSO)Fe^{III}Pc + DMSO \qquad \textbf{1.25}$$

The coordination of nitric oxide to the MPcs involved the transfer of an electron from the metal center of the MPc macrocycle to nitric oxide. The metal is in the higher oxidation state in the complex formed.

Kinetics and equilibrium data were obtained for the ligation of nitric oxide to the MPcs listed above. Table 1.3 gives a summary of these data.

Table 1.3: Summary of kinetic and equilibrium data for the ligation of nitric oxide to MPcs

Complex	Solvent	K($dm^3\ mol^{-1}$)	k_f($dm^3\ mol^{-1}s^{-1}$)	Reference
FePc	DMSO	$1.1x10^6$	$2.2x10^4$	261
CoPc	DMF	$5.4x10^4$	15	62
CoTSPc	H_2O	$3.0x10^5$	142	63

where k_f is the rate constant of the forward reaction and K is the equilibrium constant. These quantities are given by the equations which follow shortly.

Axial ligand substitution reactions in MPc complexes are known to be stepwise with the formation of a highly reactive five-coordinate intermediate.[191,261,264] MPcs are generally coordinated to solvent molecules in solution as $(L)_2MPc$, representing leaving solvent molecules as L. If the entering axial ligand is represented as E, the axial ligand substitution in $(L)_2MPc$ may then be represented by equations 1.26 and 1.27.

$$(L)_2MPc \underset{k_{-1}}{\overset{k_1}{\equiv}} (L)MPc + L \qquad \textbf{1.26}$$

$$(L)MPc + E \underset{k_{-2}}{\overset{k_2}{\equiv}} (L)(E)MPc \qquad \textbf{1.27}$$

The rate law[265] for axial ligand exchange reactions in MPc complexes (equations 1.26 and 1.27) is generally given by equation 1.28.

$$k_{obs} = \frac{k_1 k_2[E] + k_{-1}k_{-2}[L]}{k_{-1}[L] + k_2[E]} \qquad \textbf{1.28}$$

Since L is a solvent, its concentration is large hence $k_{-1}[L] >> k_2[E]$. Equation 1.28 may then be rewritten as equation 1.29

$$k_{obs} = \frac{k_1 k_2[E] + k_{-1}k_{-2}[L]}{k_{-1}[L]} \qquad \textbf{1.29}$$

which can further be simplified to equation 1.30

$$k_{obs} = \frac{k_1 k_2[E]}{k_{-1}[L]} + k_{-2} \qquad \textbf{1.30}$$

if $\frac{k_1 k_2}{k_{-1}[L]}$ is represented by k_f and k_{-2} by k_r, equation 1.30 may be written as

$$k_{obs} = k_f[E] + k_r \qquad 1.31$$

The study of the mechanism of the interaction of MPcs with neurotransmitters is of premium biological importance since MPcs could be used as important biological models because of their close relation to the metalloporphyrins. In this thesis, the study of the interaction of some selected neurotransmitters with MPc complexes has been carried out.

Equilibrium data were determined using the standard spectroscopic expression shown in equation 1.32.

$$Log\left[\frac{(A_{eq} - A_0)}{(A_\infty - A_{eq})}\right] = LogK_{eq} + nLog[E] \qquad 1.32$$

where A_{eq} = equilibrium absorbance

A_∞ = the final absorbance

A_0 = the initial absorbance

K_{eq} = equilibrium constant

n = number of moles of ligand exchanged

[E] = concentration of the ligand

1.6.7.3 Metallophthalocyanines in pharmaceutical analysis

The use of MPcs complexes as electrocatalysts in the analysis of pharmaceutical products has not received the desired attention. The general use of electrochemical techniques for the analysis of pharmaceutical preparations has also been largely neglected.[266] Electroanalytical techniques ironically are exceptional, particularly with electrodes modified with suitable electrocatalysts such as the MPcs, for the analysis of pharmaceutical products because of the ease of sample preparation, lack of interference from incipients in the dosage form and the availability of highly sensitive commercial instrumentation, which yields easily interpretable data for quantitation at low levels.

To the knowledge of the author, records of the use of MPcs for the electrocatalytic determination of pharmaceuticals are not available in the literature at the moment. However, Chen et al.[267] have used iron (III) tetrasufonatophthalocyanine $[Fe^{III}TSPc]^{3-}$ as a mimetic enzyme in conjunction with hydrogen peroxide as a catalyst for the spectrofluorimetric determination of thiamine. $[Fe^{III}TSPc]^{3-}$ considerably increased the yield of thiochrome which is the fluorescent marker for the determination of thiamine. It is therefore one of the aims of this thesis to explore the possibility of the use of MPc complexes as electrocatalysts towards the electrocatalytic analysis of pharmaceutical products.

1.7 Summary of aims of the thesis

The aims of the thesis are summarized as follows:

- the study of the interaction of metallophthalocyanines with some neurotransmitters,
- the development of MPc modified electrodes that will be sensitive and selective for the electrocatalytic analysis of selected neurotransmitters (dopamine, serotonin and histamine),
- the miniaturization of the modified electrode developed to ultra micro dimensions that could be used for the for the analysis of neurotransmitters *in vivo*,
- the development of MPc modified electrodes for use in the electrocatalytic analysis of pharmaceutical preparations.

CHAPTER 2

EXPERIMENTAL

2.1 Materials

Dopamine (4-(2-aminoethyl)benzene-1,2-diol) hydrochloride, serotonin (5-hydroxytryptamine) creatinine sulfate monohydrate, histamine dihydrochloride, thiamine hydrochloride and tris(hydroxymethyl)aminomethane (Tris) buffer were purchased from Sigma. Cobalt acetate, ammonium chloride, ammonium molybdate, urea, nitrobenzene, sodium chloride, silver nitrate, sodium hydroxide, iron (II) chloride tetrahydrate, nickel sulphate, potassium ferrocyanide, potassium chloride, potassium nitrate, ascorbic acid, ethanol, methanol, sodium sulfite nonahydrate, phthalimide, sulfuric acid, nitric acid, and trimelitic anhydride were purchased from SAARCHEM. Graphite powder was purchased from UNITEK, mineral oil and tetrachlorophthalic anhydride were purchased from Fluka. Nitrogen gas was supplied by MG Fed gas.

Metallophthalocyanine complexes of iron (FePc) and cobalt (CoPc) were purchased from Aldrich. Manganese phthalocyanine was purchased from Eastman. Monosodium salt of 4-sulfophthalic acid was purchased from Aldrich when possible. Otherwise it was synthesized as described below.

Monosodium salt of 4-sulfophthalic acid was prepared as described by Rollman and Iwamoto[211] in which sodium hydroxide was reacted with aqueous 30% of 4-sulfophthalic acid in a 1:1 mole ratio. The mixture was left overnight to allow the product to crystallize out of solution. The pale pink crystals obtained were filtered off under reduced pressure, washed with water and left to dry in the open.

2.2 Synthesis of metallophthalocyanines complexes

All the complexes presented in this work have been reported before in the literature. The complexes were thus synthesized and characterized following the literature methods (as shown) and gave spectral characterizations that closely agree with those reported in the literature.

The only complex that has not been fully characterized is the iron tetrasulfophthalocyanine species. Different authors have reported different complexes for the same synthesis method. Hence a close look at the nature of iron tetrasulfophthalocyanine is presented later in this thesis.

2.2.1 Synthesis of tetrasodium salt of iron (II) tetrasulfophthalocyanine, Na_4[FeTSPc] (2) Scheme 2.1.

The tetrasodium salt of iron (II) tetrasulfophthalocyanine, **2**, was synthesized following the procedure reported by Weber and Busch.[189] The simplified synthetic route is shown in Scheme 2.1. 4.32g (16mmol) monosodium salt of 4-sulfophthalic acid, **1**, 0.47g (9mmol) ammonium chloride, 5.80g (97mmol) urea, 0.068g (0.06mmol) ammonium molybdate and 0.95g (4.8mmol) iron (II) chloride tetrahydrate were ground together in a mortar until homogeneous. 4ml nitrobenzene was placed in a three-necked round-bottomed flask fitted with a thermometer and a condenser, and was heated to 463K. The solid mixture was added to the heated nitrobenzene slowly with stirring; keeping the temperature between 440 and 463K. The mixture was heated for 6 hours at 453K. The solid product

obtained was finely ground and washed with methanol until the smell of nitrobenzene could no longer be detected. The resulting powder was dissolved in 110ml of 1mol dm^{-3} hydrochloric acid saturated with sodium chloride and heated to boiling. The mixture was cooled to room temperature and filtered. The product obtained was dissolved in 70ml of 0.1mol dm^{-3} sodium hydroxide, heated to 353K and the insoluble impurities filtered off. 27.0g sodium chloride was added to the filtrate and heated at 353K with stirring until the evolution of ammonia ceased. The product, which crystallized out at this stage, was obtained by filtration and was washed with 80% ethanol until it was chloride free on testing with 1mol dm^{-3} silver nitrate. The washed product was refluxed in 20ml absolute ethanol for 4 hours, cooled to room temperature and filtered. The dark-blue product obtained was dried overnight in vacuo over phosphorous pentoxide. Yield 60%.

Elemental analysis calculated for $C_{32}H_{15}N_8O_{14}S_4Na_4Fe.3H_2O$; C, 38.56; H, 2.12; N, 11.24; S, 12.87; Fe, 5.60. Found C, 38.10; H, 1.95; N, 11.22; S, 12.84, Fe, 5.32.

IR (KBr disc, cm^{-1}) 3419, 1733, 1603, 1363, 1184, 1104, 1028, 830, 742, 697, 628, 594.

UV/vis spectrum was recorded in water, pH≈ 6.8 (λ_{max}, nm (log ε)) 665 (4.68), 633, 327.

^{1}HNMR peaks, recorded in D_2O, were observed as two weak and broad multiplets at 8.2 and 11.6 ppm, typical of the α and β protons of the phthalocyanine macrocycle.

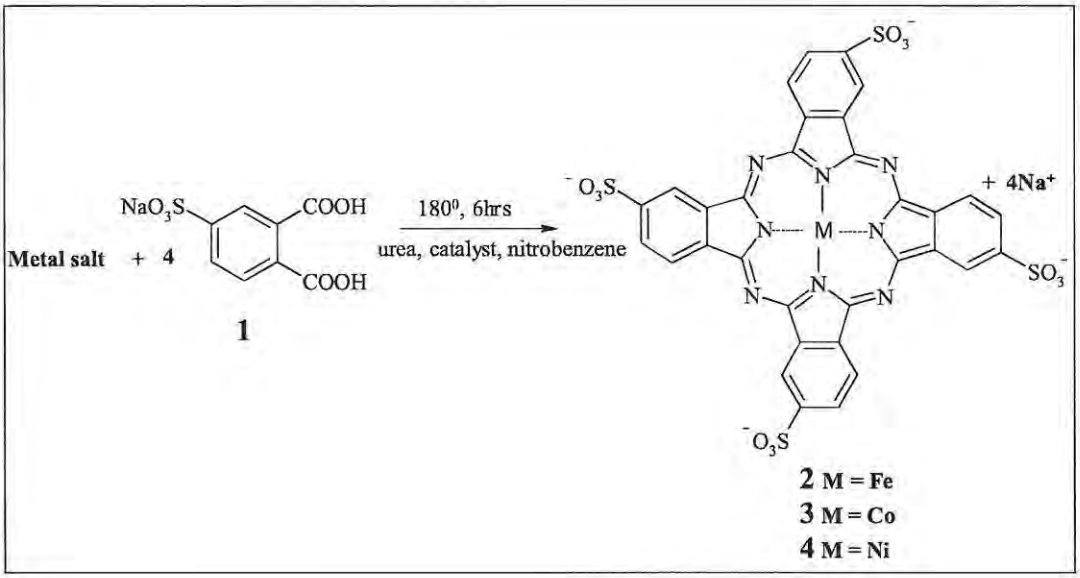

Scheme 2.1: Simplified synthetic route to $[MTSPc]^{4-}$

2.2.2 Synthesis of tetrasulfophthalocyanines of other metals

2.2.2.1 Synthesis of tetrasodium salt of cobalt (II) tetrasulfophthalocyanine, $Na_4[Co^{II}TSPc]$ (3) Scheme 2.1

Tetrasodium salt of cobalt tetrasulfophthalocyanine, $Na_4[Co^{II}TSPc]$, **3**, was synthesized in the same manner as described in Section 2.2.1 (Scheme 2.1)[189] except that 1.36g (48mmol) cobalt (II) sulfate heptahydrate was used in place of the iron salt. Yield 80%

IR (KBr disc, cm^{-1}) 2370,1622, 1379, 1256, 1098, 1029, 805, 697, 632, 381.

UV/vis in water, pH≈ 6.8 (λ_{max}, nm (log ε)) 657, 627 (4.76), 322.

2.2.2.2 Synthesis of tetrasodium salt of nickel (II) tetrasulfophthalocyanine, $Na_4[Ni^{II}TSPc]$ (4) Scheme 2.1

Tetrasodium salt of nickel (II) tetrasulfophthalocyanine, **4**, was synthesized in the same manner as described in Section 2.2.1 (Scheme 2.1)[189] except that 1.19g (48mmol) cobalt (II) acetate was used in place of the iron salt. Yield 74%.

IR (KBr disc, cm^{-1}) 3443, 1630, 1405, 1189, 1028, 830, 746, 697.

UV/vis in water, pH ≈ 6.8 (λ_{max}, nm (log ε)) 660, 624 (4.62), 330.

2.2.3 Synthesis of hexadecachlorophthalocyanino iron (II), $FePc(Cl)_{16}$ (5) Scheme 2.2

Hexadecachlorophthalocyanino iron (II), $FePc(Cl)_{16}$, **5**, was prepared according to the method of Metz et al.[190] and Golovin et al.[268] (Scheme 2.2). 3.5g (50mmol) urea, 4.8g (17mmol) tetrachlorophthalic anhydride **6**, 0.85g (4mmol) iron (II) chloride tetrahydrate and 0.02g (0.02mmol) ammonium molybdate were finely ground and stirred into 15ml of nitrobenzene. The suspension was heated to 453-463K, then this temperature was maintained for 4 hours or until the evolution of ammonia ceased. The reaction mixture was then cooled to 363K, diluted with 15ml ethanol and filtered hot. The product obtained was washed with boiling water. Further purification was effected by boiling the product for ten minutes each in 1% HCl and 1% NaOH; it was then washed with water until the washings were neutral. The product was then treated with acetone and ether. The olive-green scaly powdery product obtained was extracted for 3 days with chlorobenzene.

Yield 46%. IR (KBr disc, cm^{-1}). 3106, 1720, 1495, 1388, 1298, 1270, 1270, 1211, 1152 (ν C-Cl), 1089 (ν C-Cl), 951, 765, 750, 505.

UV/vis in DMF (λ_{max}, nm) 662, 601, 434, 312. The molar extinction coefficient of this complex was not obtained because of its poor solubility in almost all solvents.

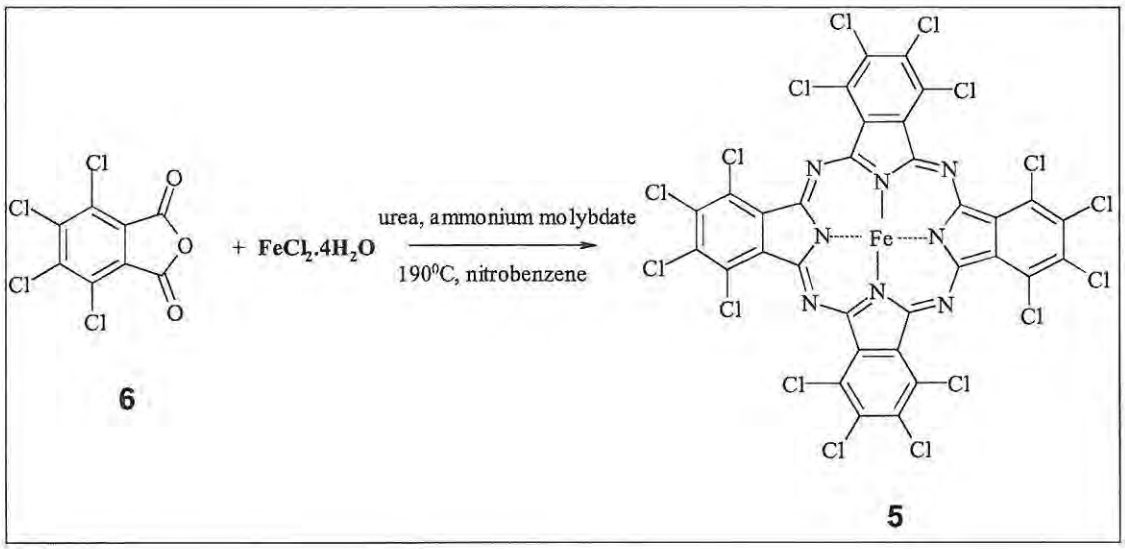

Scheme 2.2: Synthetic route to $FePc(Cl)_{16}$

2.2.4 Synthesis of iron (II) tetranitrophthalocyanine, $FePc(NO_2)_4$ (8) Scheme 2.3

$FePc(NO_2)_4$, **8**, was synthesized according to the method described by Achar et al.[269] and Metz et al.[190] (Scheme 2.3). 1.81g (9.45mmol) 4-nitrophthalimide, **7**, (synthesis described below in section 2.2.4.1), 0.51g (2.59mmol) iron (II) chloride tetrahydrate, 0.25g (4.63mmol) ammonium chloride, 0.03g (0.02mmol) ammonium molybdate and excess urea (≈ 3.00g) were finely ground and added to 10ml nitrobenzene in a three-necked round-bottomed flask. The temperature of the mixture was gradually raised to 463K

within 30 minutes and maintained at this temperature for 5 hours. The solid product obtained was washed with methanol until nitrobenzene was completely removed. The product was then dispersed in 30ml (1mol dm^{-3}) hydrochloric acid saturated with sodium chloride, boiled for 5 minutes and filtered after cooling. It was then dispersed in 30ml (1mol dm^{-3}) sodium hydroxide saturated with sodium chloride, heated at 363K for 30 minutes cooled and filtered. The alternate acid and base treatment was repeated twice more. The product obtained was washed with water and dried overnight at 400K. Yield 42%.

IR (KBr disc, cm^{-1}) 3527, 3473, 3404, 3083, 1721, 1607, 1508 (ν-NO_2), 1350, 1401, 1325, 1249, 1139, 1092, 906, 796, 758, 727. UV/vis in DMF (λ_{max}, nm) 697, 634, 340.

Cobalt (II) and nickel (II) analogues of iron tetranitrophthalocyanine were as described above, replacing iron (II) chloride tetrahydrate with the appropriate metal salt.

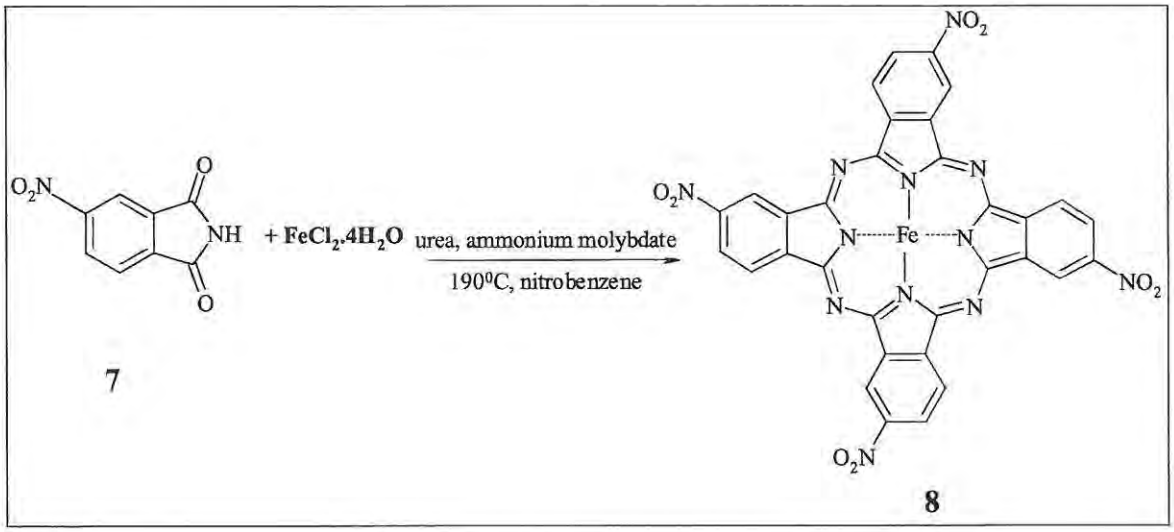

Scheme 2.3: Synthetic route to $FePc(NO_2)_4$

2.2.4.1 Synthesis of 4-nitrophthalimide (7)

4-nitrophthalimide, **7,** was synthesized following the method reported by Huntress and Shriner.[270] 15ml fuming nitric acid was slowly added to 90ml concentrated sulfuric acid and the mixture cooled to 285K in an ice bath. 25.0g phthalimide was quickly stirred into the cooled acid mixture; keeping the temperature below 288K. The mixture was allowed to attain room temperature and left to stand overnight. The yellow solution obtained was poured into 500g ice with rapid stirring to give a suspension of 4-nitrophthalimide which was filtered off under reduced pressure, washed with ice-cold water and dried. Yield 50% IR (KBr disc, cm^{-1}) 1780, 1720, 1536, 1349.

2.2.5 Synthesis of iron (II) tetraamino phthalocyanine, $FePc(NH_2)_4$ (9) Scheme 2.4

$FePc(NH_2)_4$, **9**, was synthesized following literature methods[269] (scheme 2.4). 0.74g (0.98mmol) $FePc(NO_2)_4$, **8**, was finely ground and dispersed in 20ml water after which 3.7g (15.41mmol) sodium sulfite nonahydrate was added. The mixture was stirred at 323K for 5 hours. The product was separated using a centrifuge and treated with 60ml (1mol dm^{-3}) hydrochloric acid. The solid was then stirred in 40ml (1mol dm^{-3}) sodium hydroxide for 1 hour. The product obtained was washed with water and dried overnight at 410K. Yield 85%. IR (KBr disc, cm^{-1}) 3340 (N-H stretch), 1714, 1607 (ν-NH_2), 1512, 1318, 1250, 1141, 1094, 758, 732. UV/vis in DMF (λ_{max}, nm) 756, 550, 299.

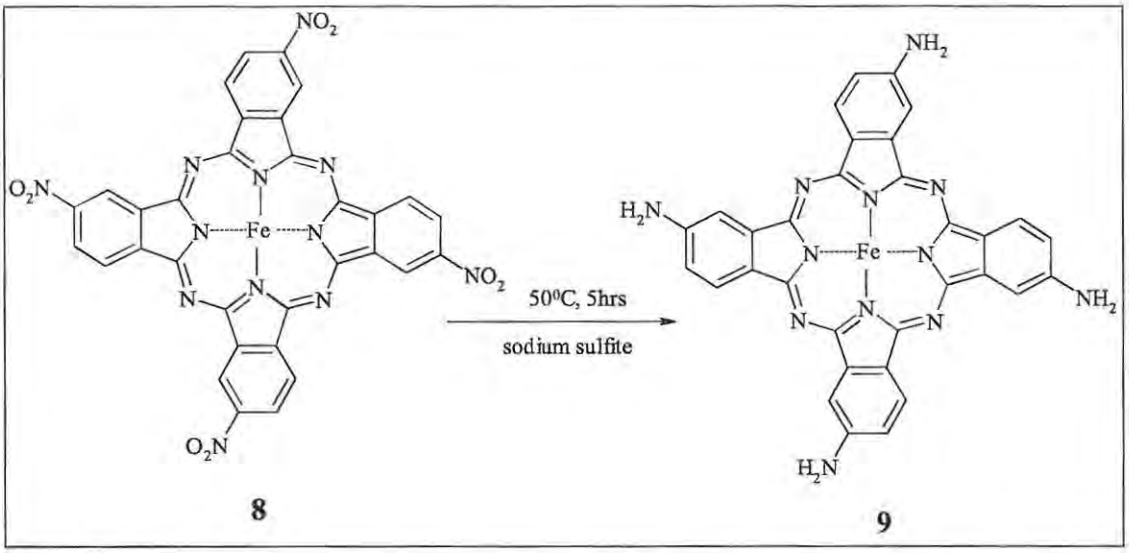

Scheme 2.4: simplified synthetic route to $FePc(NH_2)_4$

Cobalt (II) and nickel (II) analogues of $FePc(NH_2)_4$ were prepared in the same way as $FePc(NH_2)_4$, starting with the appropriate metallotetranitro phthalocyanine.

2.2.6 Synthesis of iron (II) tetratertiarybutyl phthalocyanine, $Fe^{II}Pc(t\text{-}Bu)_4$ (10)

Scheme 2.5

Following literature methods,[190] Fe^{II}(t-Bu)Pc, **10**, was synthesized (Scheme 2.5). 1.84g (10mmol) 4-tertiarybutyl phthalodinitrile, **11**, was dissolved in 4ml 1,2,4-trichlorobenzene and heated to 488K, 0.49g (25mmol) iron pentacarbonyl dissolved in 8ml 1,2,4-trichlorobenzene was added dropwise over a period of 1 hour. The solution was then refluxed for 1 hour, cooled to room temperature and diluted with an equal volume of methanol. The precipitate formed was filtered under reduced pressure and washed with methanol. A dark-blue product was obtained which was dried at 333K. Yield 35%.

IR (KBr disk, cm^{-1}) 3427, 3068, 2954, 2900, 2854, 2358, 1725, 1641, 1478, 1360, 1280, 1192, 1078, 921, 819, 746, 693.

UV/vis in DMF (λ_{max}, nm) 700, 667, 328.

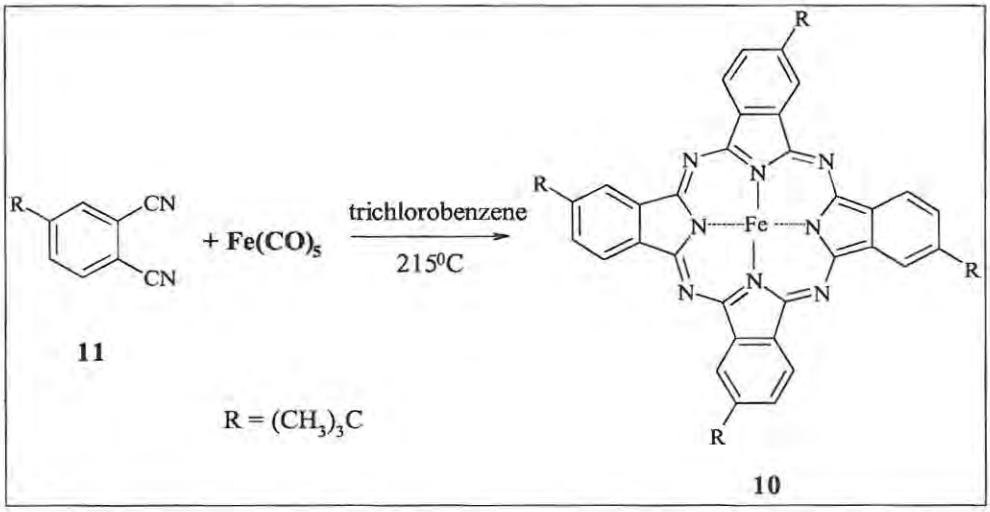

Scheme 2.5: Synthesis of $Fe^{II}Pc(t\text{-}Bu)_4$

2.2.7 Synthesis of iron (II) tetracarboxy phthalocyanine, $FePc(COOH)_4$ (12) Scheme 2.6

The method reported by Kobayashi et al.[271] (scheme 2.6) was adopted for the synthesis of $FePc(COOH)_4$, **12**. 1.0g (5mmol) trimellitic anhydride, **13**, 3.0g (0.5mmol) urea, 0.72g (3mmol) cobalt (II) chloride and 0.1g (0.1mmol) ammonium molybdate were finely ground and added to 15ml nitrobenzene. The mixture was refluxed for 3 hours at 438K. A dark-blue solid resulted which was filtered off and washed with methanol until the smell of nitrobenzene could no longer be detected. 10% potassium hydroxide (5ml) was

added to the solid and the mixture was refluxed for 5 hours, allowed to cool to room temperature and the insoluble impurities separated using a centrifuge. The liquid obtained was acidified with cold, concentrated hydrochloric acid to precipitate the carboxylic acid, **12,** which was filtered and washed with water and dried overnight at 383K. Yield 33%

IR (KBr disc, cm^{-1}) 3348 (OH stretch), 1722 (C=O stretch), 1602, 1352, 1220, 1036, 981, 745, 688. UV/vis in 0.1 mol dm^{-3} sodium hydroxide (λ_{max}, nm) 676, 622, 330.

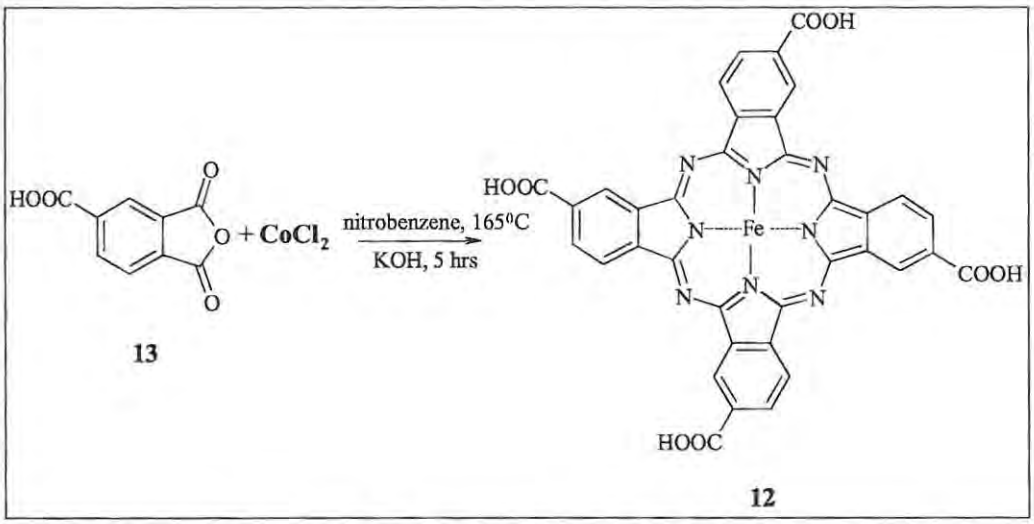

Scheme 2.6: synthesis of $FePc(COOH)_4$

2.2.8 Synthesis of bis(axial pyridine) iron (II) phthalocyanine, $(py)_2FePc$.

$(py)_2FePc$ was synthesized[190] by refluxing iron (II) phthalocyanine with excess pyridine at 363K for 3 hours. The product was isolated by filtration. IR (KBr disc, cm^{-1}) 3183, 1516, 1420, 1321, 1283, 1154, 1120, 1085, 910, 723. UV/vis in DMF (λ_{max}, nm) 660, 599, 431, 356.

2.2.9 Synthesis of bis(axial imidazole)iron (II) phthalocyanine, $(im)_2FePc$.

$(im)_2FePc$ was synthesized[191,272] treating iron (II) phthalocyanine with an excess of imidazole in refluxing dimethyl formamide (DMF) for 3 hours. The product obtained after evaporating off DMF was washed with water, then acetone and dried. IR (KBr disk, cm^{-1}) 3419, 1657, 1500, 1417, 1321, 1280, 1170, 1111, 1093, 1062, 714. UV/vis in DMF (λ_{max}, nm) 658, 597, 428, 346.

2.2.10 Synthesis of bis(axial cyano) iron (II) phthalocyanine, $(CN)_2FePc$.

$(CN)_2FePc$ was synthesized[191,272] as described in Section 2.2.8 above except that an excess of potassium cyanide was used in the place of imidazole. IR (KBr disc, cm^{-1}): 3240, 2120 (ν C≡N) , 1609, 1502, 1460, 1421, 1324, 1290, 1164, 1120, 1075, 910, 759. UV/vis in DMF (λ_{max}, nm) 663, 599, 431, 356.

2.2.11 Synthesis of complex between $[FeTSPc]^{4-}$ and dopamine

The solid complex formed between $[FeTSPc]^{4-}$ and dopamine was prepared by dissolving 0.1094g (0.1 mmol) $[FeTSPc]^{4-}$ and 0.019g (0.1 mmol) dopamine in 5ml water. After a colour change from blue to green, the water was evaporated off.

IR (KBr disc, cm^{-1}) 3240, 3054, 2763, 1714, 1622, 1364, 1189, 1024, 819, 754, 693, 636. UV/vis in water, pH ≈ 6.8 (λ_{max}, nm (log ε)) 659 (3.77). Elemental analysis (Calculated for $C_{40}H_{24}N_9S_4O_{19}ClNa_4Fe$: C, 38.55; H, 1.93; N, 10.12%. Found. C, 38.46; H, 3.56; N, 10.31%). ^{1}HNMR (D_2O, δ ppm) 2.80, 3.20, 6.70, 8.40, 11.50.

2.2.12 Synthesis of complex between $[FeTSPc]^{4-}$ and serotonin

The complex formed between $[FeTSPc]^{4-}$ and serotonin was synthesized by dissolving 0.109g (0.1 mmol) $[FeTSPc]^{4-}$ and 0.405g (0.1mmol) serotonin in 5ml water. After a colour change from blue to green, the water was evaporated off.

IR (KBr disc, cm^{-1}) 3367, 2930, 1707, 1637, 1545, 1456, 1414, 1344, 1102, 1028, 701, 601. UV/vis in water, pH ≈ 6.8 (λ_{max}, nm (log ε)) 663 (3.58). Elemental analysis (calculated for $C_{46}H_{37}N_{13}S_5O_{24}Na_4Fe$: C, 37.73; H, 2.55, N, 13.27%. Found: C, 37.79, H, 4.69, N, 15.29%). ^{1}HNMR (D_2O, δ ppm) 2.20, 3.50, 4.30, 6.78, 7.20, 7.45, 8.40, 11.50.

2.2.13 Synthesis of complex between $[FeTSPc]^{4-}$ and histamine

The complex formed between $[FeTSPc]^{4-}$ and histamine was obtained by evaporating water off a solution containing 0.109g (0.1mmol) $[FeTSPc]^{4-}$ and 0.201g (0.1 mmol) histamine. IR (KBr disc, cm^{-1}) 3219, 3114, 3022, 2870, 1718, 1622, 1489, 1405, 1184, 1028, 807, 754, 601. UV/vis in water, pH ≈ 6.8 (λ_{max}, nm (log ε)) 673 (5.01), 420, 327. Elemental analysis (Calculated for $C_{37}H_{23}N_{11}S_4O_{12}Cl_2Na_3Fe.10\ H_2O$: C, 33.71 H, 3.26. Found: C, 32.35; H, 3.06). ^{1}HNMR (D_2O, δ ppm) 0.50, 3.40, 7.30, 8.30, 8.50, 11.60.

2.3 Preparation of electrodes

2.3.1 Preparation of unmodified carbon paste electrodes (CPEs)

Unmodified carbon paste electrodes were prepared[9,15] by intimately mixing 0.5g of finely ground graphite powder with 0.3ml of mineral oil. The resulting paste was packed into a fused silica capillary whose internal diameter is 0.92mm. Electrical contact was maintained with the electrode material in the capillary tube by inserting a piece of copper wire through the open end of the tube. A schematic representation of a typical carbon paste electrode prepared is shown in Figure 2.1.

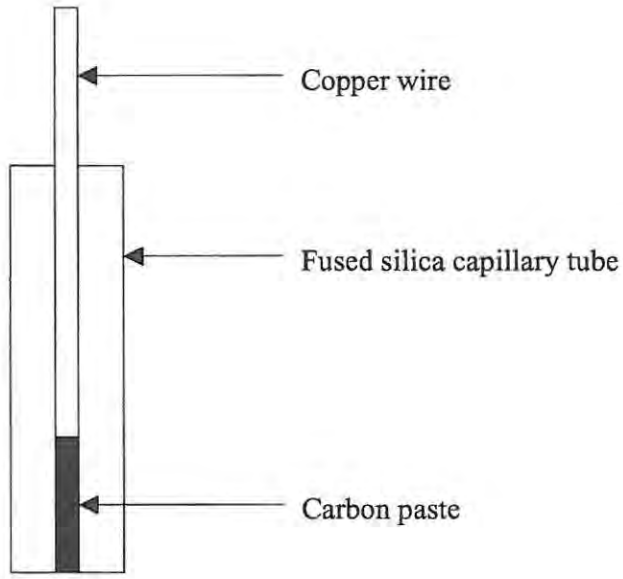

Figure 2.1: Schematic representation of carbon paste electrode

2.3.2 Preparation of modified carbon paste electrodes

Modified carbon paste electrodes were prepared in a similar way described for unmodified electrodes in Section 2.3.1 above except that the desired amount of the metallophthalocyanines used to modify the electrode was first ground with graphite powder in order to ensure an even dispersion of the modifier in the electrode matrix before the addition of mineral oil.

2.3.3 Preparation of carbon paste ultra micro disc electrodes (CPUMDEs)

The paste used for preparing CPUMDEs was prepared as described in Section 2.3.1 or 2.3.2 for the electrodes. The paste was packed into fine fused silica capillaries of 75μm internal diameter. A small piece of the fused capillary was cut and positioned in a micropipette tip that had earlier been filled with carbon paste. In order to prevent the creeping of the test solution into the pipette tip, the point of contact between the fine glass capillary and the pipette tip was covered with epoxy glue. Electrical contact was maintained by the use of a piece of copper wire. A schematic representation of the CPUMDE is shown in Figure 2.2.

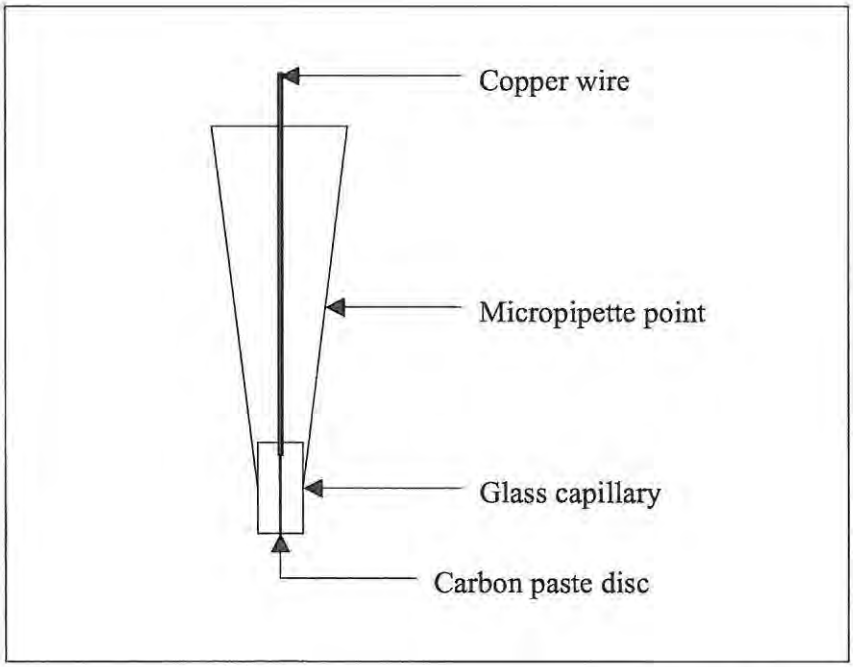

Figure 2.2: Schematic representation of carbon paste ultra micro disc electrode

2.3.4 Preparation of carbon paste ultra micro band electrodes (CPUMBEs)

To prepare carbon paste ultra micro band electrodes, fine grooves (≈ 150μm in diameter) were made in a polycarbonate plastic body with a penknife. The grooves were then filled with carbon paste prepared as described in Section 2.3.1, followed by polishing the surface with smooth paper. The polishing process also removed the excess paste present on the surface of the plastic plate. Electrical contact with the carbon paste in the grooves was established by filling a small hole at the top of the grooves with carbon paste and a piece of copper wire positioned in the filled hole. In order to define the length of the CPUMBE and to protect the electrical contacts, a small amount of epoxy glue was deposited on the surface. Each CPUMBE consisted of five individually accessible

electrodes. The individual electrode in the band was 3mm from its neighbours. Figure 2.3 shows a schematic representation of the CPUMBE.

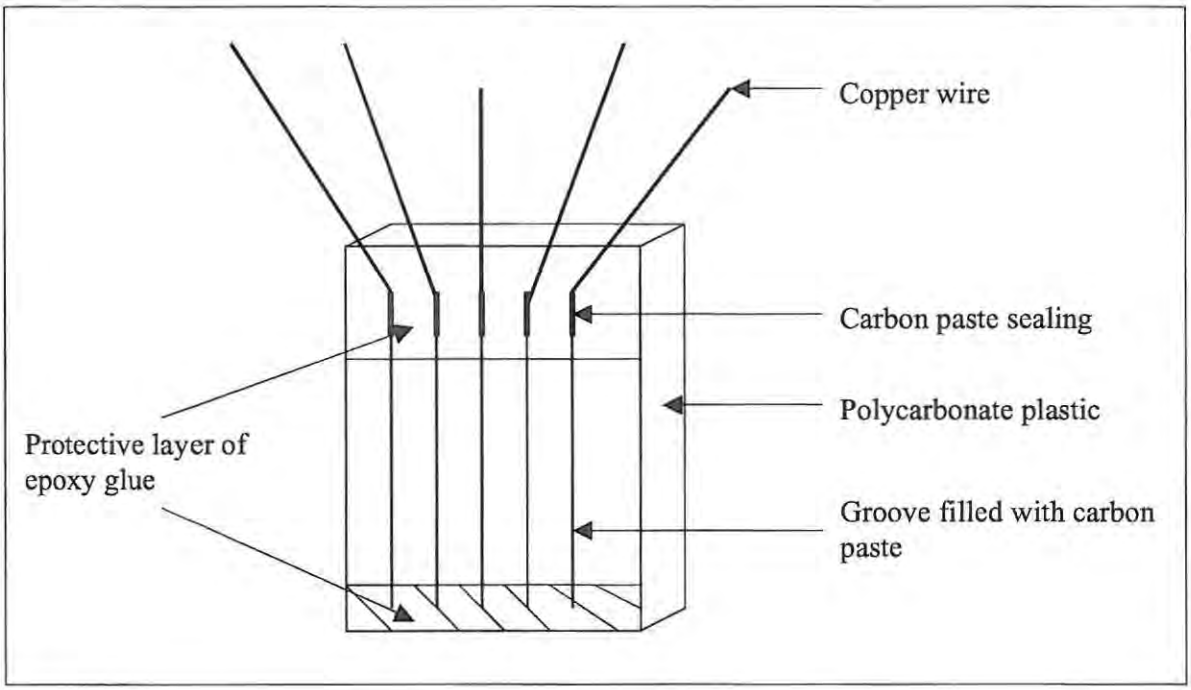

Figure 2.3: Schematic representation of carbon paste ultra micro band electrode

The cyclic voltammetry of the redox couple of potassium ferrocyanide was used to characterize these electrodes at scan rates of 100 mV s^{-1}. The electrolyte used was 0.5 mol dm^{-3} KNO_3.

2.4 Kinetics and equilibria

Kinetics and equilibria studies were carried out at constant temperatures and monitored with a Cary 500 UV/vis/NIR spectrophotometer. Typically, a known volume of aqueous

solution of $[MTSPc]^{4-}$ was added to a 1cm path-length spectrophotometric cell and deaerated using nitrogen. Then a known volume of aqueous solution of dopamine, serotonin or histamine was added to the cell and the changes in spectral features monitored with time. The concentration of $[MTSPc]^{4-}$ was kept constant ($\approx 10^{-5}$ mol dm^{-3}) while the concentrations of dopamine, serotonin and histamine were varied and made larger by at least a factor of ten, thereby maintaining a pseudo-first order reaction condition. The spectrophtometric cell was fitted with a stopper to prevent the interference of oxygen with the reaction mixture. The volume of the cell used was 3ml.

2.5 Electrochemical methods

Voltammetric measurements were carried out in a three-electrode electrochemical cell consisting of Ag|AgCl reference and platinum wire counter electrode. (The three-electrode cell has been discussed earlier in Section 1.1.4, Figure 1.2.) The working electrodes employed in this study were glassy carbon, unmodified carbon paste, modified carbon paste, carbon paste ultra micro band and carbon paste ultra micro disk electrodes. Cyclic (CV) and Osteryoung square wave voltammetry (OSWV) were performed with a Bioanalytical Systems model BAS 100B electrochemical analyzer. Parameters for OSWV were: step potential 4mV, square wave amplitude 25mV and frequency 15Hz. All cyclic voltammograms were recorded at a scan rate of 100mV per second except otherwise indicated. The electrolyte employed for all electrochemical experiments involving dopamine, serotonin and histamine was 0.1 mol dm^{-3} Tris buffer. The pH was

adjusted to 7.4 with 0.1 mol dm^{-3} NaOH. All electrochemical experiments were carried out under an atmosphere of high purity nitrogen.

Nitrogen was purified by passing it through a Drierite self-indicating mesh 8 containing anhydrous calcium sulfate from SAARCHEM.

Glassy carbon electrode was cleaned by polishing to a shining finish with 0.05μm alumina on a Buehler pad followed by washing thoroughly with distilled water.

Glassy carbon electrode was modified by both dip-dry and drop-dry methods. Using the dip-dry method, the electrode was immersed in a solution ($\approx 10^{-3}$ mol dm^{-3}) of the phthalocyanine for five minutes for spontaneous film formation by adsorption to occur. The electrode was then withdrawn from the solution and the solvent allowed to dry off. While with drop-dry method, two or three drops of the solution of the phthalocyanine were applied to the electrode surface and the solvent was evaporated off.

Spectroelectrochemical technique was used to characterize $[Fe^{II}TSPc]^{4-}$ and the complex formed between $[Fe^{II}TSPc]^{4-}$ and histamine. The optically transparent thin-layer electrode cell used was constructed as described by Hartl et al.[273] The working and counter electrodes of the cell were platinum grits; a piece of silver wire served as the pseudo-reference electrode. The cell was connected to a BAS CV 27 voltammograph. Solutions of both $[Fe^{II}TSPc]^{4-}$ and the complex formed with histamine prepared in pH 7.4 Tris buffer were introduced into the OTTLE cell and electrolysis was performed at the

appropriate potentials. Changes in spectral features were monitored with a UV/vis/NIR spectrophotometer.

2.6 Preparation of vitamin B_1 tablets for analysis

Vitamin B_1 tablets were carefully pulverized and dissolved in 0.1 mol dm^{-3} pH 10.0 Tris buffer. The solution was filtered into a 100ml standard flask and was made up to the mark with buffer solution. This stock solution was diluted as appropriate for analysis.

2.7 Instrumentation

A Bioanalytical Systems (BAS) model BAS 100 electrochemical analyzer was used for the collection of electrochemical data. For accurate measurements, the very small current responses obtained when ultra micro electrodes were employed as working electrodes were amplified using a Bioanalytical Systems PreAmplifier model BAS PA-1. Fourier transform infrared (FTIR) spectra were recorded with a Perkin Elmer Spectrrum 2000IR spectrometer. Samples were dispersed in potassium bromide discs. Electronic absorption spectra data were obtained using a Cary 500 UV/vis/NIR spectrophotometer. Spectroelectrochemical experiments were carried out with the OTTLE cell connected to a Bioanalytical Systems model BAS CV 27 voltammograph. The Bruker EMX 400 NMR spectrometer was used to acquire nuclear magnetic resonance (NMR) data.

CHAPTER 3

CHARACTERIZATION AND INTERACTION WITH NEUROTRANSMITTERS*

* Part of the research work presented in this chapter resulted in the publication cited below and it is not referenced further in this thesis. J. Oni, T. Nyokong, Polyhedron, 2000, 19, 1355.

3.1 Spectroscopic characterization of metallophthalocyanines

3.1.1 Metallotetrasulfophthalocyanine complexes, $[MTSPc]^{4-}$

Metallotetrasulfophthalocyanines $[MTSPc]^{4-}$ are known to exist as dimers in equilibrium with monomers in aqueous solutions. The relative concentrations of monomer and dimer are dependent on a number of factors such as pH, ionic strength and temperature.[182,211,274,275,276] Their UV/vis spectra thus consist of two peaks in the Q band region. The lower energy absorption band near 670 nm is associated with the monomeric species, while the high energy absorption band near 620 nm is due to the dimeric species.[274]

Like all $[MTSPc]^{4-}$ complexes, UV/vis spectrum of iron (II) tetrasulfophthalocyanine, $[FeTSPc]^{4-}$, in aqueous solution shows that it exists in an equilibrium between monomeric and dimeric species, Figure 3.1a. The dimeric peak in water was observed at 633 nm and the monomeric peak at 665nm. The Soret band was observed at 327 nm. The nature of the $[FeTSPc]^{4-}$ has been a subject of several investigations.[277] The nature of $[FeTSPc]^{4-}$ prepared according to the method of Weber and Busch[189] has been found to vary from batch to batch[278] with some authors reporting on the formation of μ-oxo complexes, while some authors found no evidence for dimeric μ-oxo species. In buffered medium, the dimeric species predominates, Figure 3.1b.

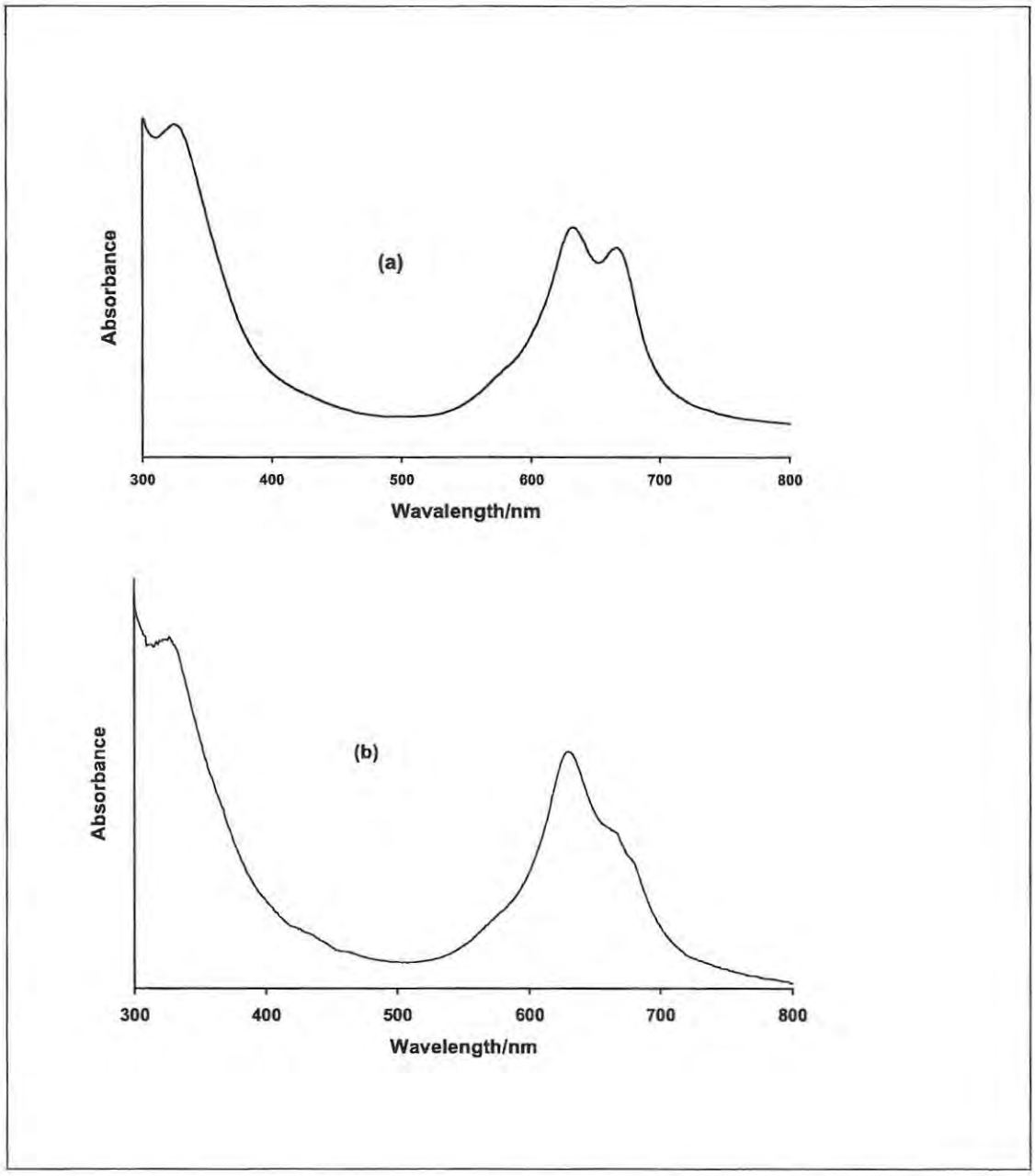

Figure 3.1: UV/vis spectra of $FeTSPc]^{4-}$ in (a) water (b) pH 7.4 buffer.

The UV/vis spectrum of cobalt (II) tetrasulfophthalocyanine, Figure 3.2, showed the monomer/dimer peaks at 657 and 627 nm, respectively. The B band was observed at 322 nm. The UV/vis spectrum of nickel (II) tetrasufophthalocyanine showed the monomer/dimer peaks at 640 and 624 nm, and a B band at 330 nm.

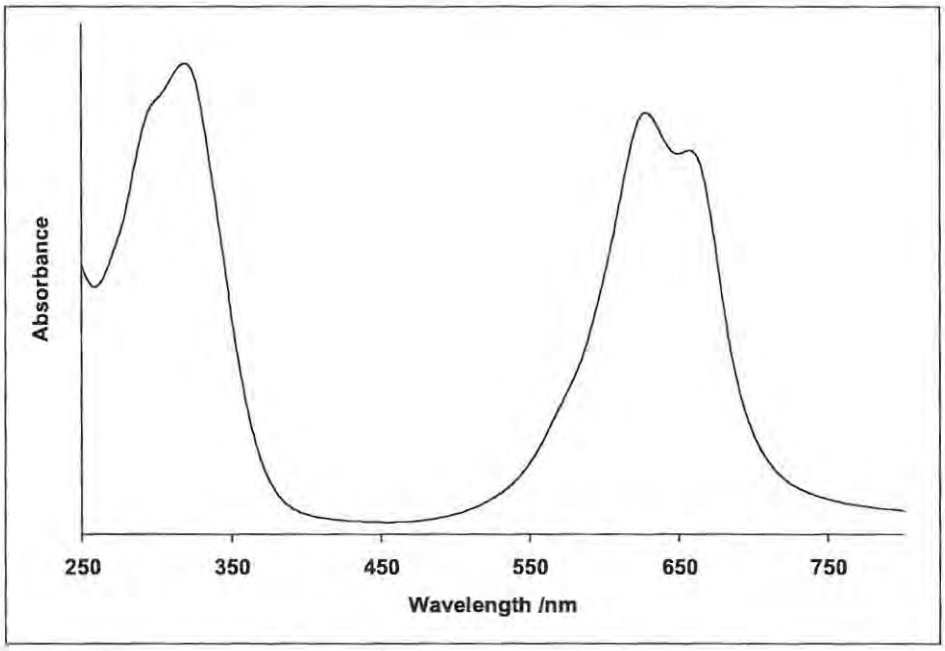

Figure 3.2: UV/vis spectrum of $[Co^{II}TSPc]^{4-}$ in water, pH ≈ 6.8

The IR spectra of all the tetrasufophthalocyanines were very similar and correlates well with the values recorded in the literature.

3.1.2 Other ring substituted metallophthalocyanines

All other ring substituted metallophthalocyanines synthesized in this work were also duly characterized using spectroscopic methods. With the exception of $FePc(COOH)_4$ which is soluble in alkaline media, all the UV/vis spectra were recorded in DMF.

The UV/vis spectrum of $FePc(t\text{-}Bu)_4$ showed absorption bands at 700, 667 and 328 nm. The synthesis of $FePc(t\text{-}Bu)_4$ has been reported to always yield aggregated products.[190] The Q band was broad; typical of aggregated metallophthalocyanines. The IR spectrum correlates well with literature values.

$FePc(NH_2)_4$ showed UV/vis absorption bands at 756, 550, and 299 nm. –NH vibrations at 3340 cm^{-1} and intense $-NH_2$ in-plane bending vibrations at 1607 cm^{-1} as well as the Pc skeletal vibrations[269] were observed in the IR spectrum of this complex.

$FePc(Cl)_{16}$ is highly insoluble in almost all solvents. Its UV/vis spectrum showed absorption bands at 662 601, 434 and 312 nm, Figure 3.3. Aromatic C-Cl vibrations were observed at 1152 and 1089 cm^{-1} in addition to the Pc skeletal vibrations.

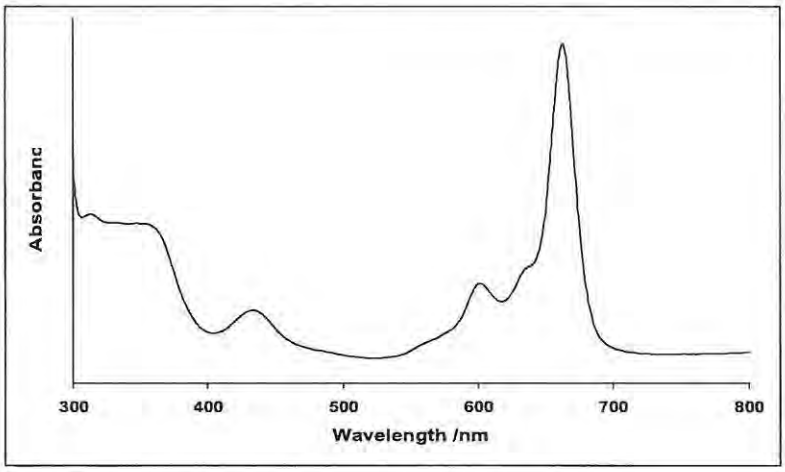

Figure 3.3: UV/vis spectrum of $FePc(Cl)_{16}$ in DMF

The UV/vis spectrum of $FePc(COOH)_4$ was recorded in 0.1 ml dm^{-1} NaOH and has a very broad Q band characteristic of aggregated metallophthalocyanine complexes. UV/vis absorption bands were noted at 676, 622, and 322 nm. C=O and C-O vibrations were seen at 1720 and 12220 cm^{-1} in the IR spectrum of the complex.

3.1.3 Axially substituted metallophthalocyanines

The axial ligands introduced into iron phthalocyanine were cyanide ($(CN)_2FePc$), imidazole ($(im)_2FePc$) and pyridine ($(py)_2FePc$). All the axially substituted complexes were monomeric as indicated by the sharp Q band in their UV/vis spectra.

The UV/vis spectrum of $(CN)_2FePc$ showed a sharp Q band at 667 nm and a split B band at 425 and 394 nm. The split B band is a characteristic feature of dicyano-substituted MPc complexes.[191] C≡N vibration was observed at 2120 cm^{-1} in the IR spectrum of the complex in addition to the Pc skeletal vibrations.

Absorption bands in the UV/vis spectrum of $(im)_2FePc$ were observed at 658, 597, 428 and 341 nm. IR spectrum showed imidazole ring double bond vibrations at 1622 to 1426 cm^{-1} as well as the Pc skeletal vibrations.

$(py)_2FePc$ also has a sharp Q band centered on 660nm and a B band at 356 nm. Other absorption bands were at 599 and 431 nm. IR spectrum recorded from KBr disc also correlates well with the literature values.[190]

A summary of the spectroscopic properties of the MPc complexes synthesized in this work is presented in Table 3.1.

Table 3.1: Summary of the spectroscopic characteristics of some MPc complexes

MPc	UV/vis data (nm)	Solvent	IR (KBr disc) cm^{-1}
$[FeTSPc]^{4-}$	665, 633, 327	water	1028, aromatic S=O vibration
$[NiTSPc]^{4-}$	660, 624, 330	water	1029, aromatic S=O vibration
$[CoTSPc]^{4-}$	662, 626, 317	water	1028, aromatic S=O vibration
$FePc(NO_2)_4$	697, 634, 340	DMF	1350, 1508, $-NH_2$ str vibration
$FePc(NH_2)_4$	756, 550, 299	DMF	1607, 3340, $-NH_2$ str vibration
$FePc(t\text{-}Bu)_4$	700, 667, 328	DMF	2900-3000, C-H t-Bu
$FePc(COOH)_4$	676, 622, 330	0.1 mol dm^{-3} NaOH	1722, C=O str 1220, C-O str vibrations
$FePc(Cl)_{16}$	662, 601, 434, 312	DMF	1089, 1152,- C-Cl vibrations
$(im)_2FePc$	658, 597, 428, 346	DMF	1426-1622, imidaz-ole ring double bond vibrations
$(CN)_2FePc$	667, 602, 425, 394	DMF	2120, C≡N vibrations
$(py)_2FePc$	660, 622, 330	DMF	910, Fe-N 1321, C-N aromatic ring vibrations

3.1.4 Electrochemical characterization of iron tetrasulfophthalocyanine

The $[FeTSPc]^{4-}$ species is the main electrocatalyst employed in this thesis, hence a further characterization by electrochemical techniques follows:

The nature of the iron tetrasulfophthalocyanine synthesized was studied using cyclic voltammetry and spectroelectrochemistry. A wide range of iron phthalocyanine complexes have been obtained with different preparation batches,[278] with some authors reporting on the formation of μ-oxo complexes, while some authors found no evidence for dimeric μ-oxo species. The formation of $[Fe^{III}TSPc]^{3-}$ is common in many preparations.[189,278] In order to confirm the nature of the iron tetrasulfophthalocyanine complex synthesized, its cyclic voltammogram in pH 7.4 solution was recorded and spectroelectrochemistry was used to characterize the oxidation products. Figure 3.4 shows the cyclic voltammogram of the iron tetrasulfophthalocyanine species in pH 7.4 buffer, using a glassy carbon electrode (GCE). Several authors have reported the difficulty of obtaining CV peaks for $[FeTSPc]^{4-}$. Thus the observation of weak and irreversible oxidation peaks in Figure 3.4 is not surprising.

Two irreversible oxidation peaks (processes **I** and **II**) were observed near 0.45 and 0.8 V vs Ag|AgCl, respectively. A large reduction peak (**III**) was observed at -0.87 V vs Ag|AgCl. Very weak return peaks were observed in the vicinity of process **III**. The potential for the reduction peak is in the range reported (0.85 V)[214] for metal reduction ($Fe^{II}(-2)/Fe^{I}$ Pc(-2), couple **III**). The first oxidation process in $[Fe^{II}TSPc]^{4-}$ would be expected to occur on the central metal. However, if the starting complex is the

$[Fe^{III}TSPc]^{3-}$ species, the first oxidation would occur on the ring. It has been shown that aggregated MPc species may show two closely spaced peaks clearly observable only when differential pulse voltammetry is employed, due to the aggregation-disaggregation equilibrium.[214] Only one peak was observed for each process (**I** to **III**) when either differential pulse or square wave voltammetry was employed for the solution used for Figure 3.4.

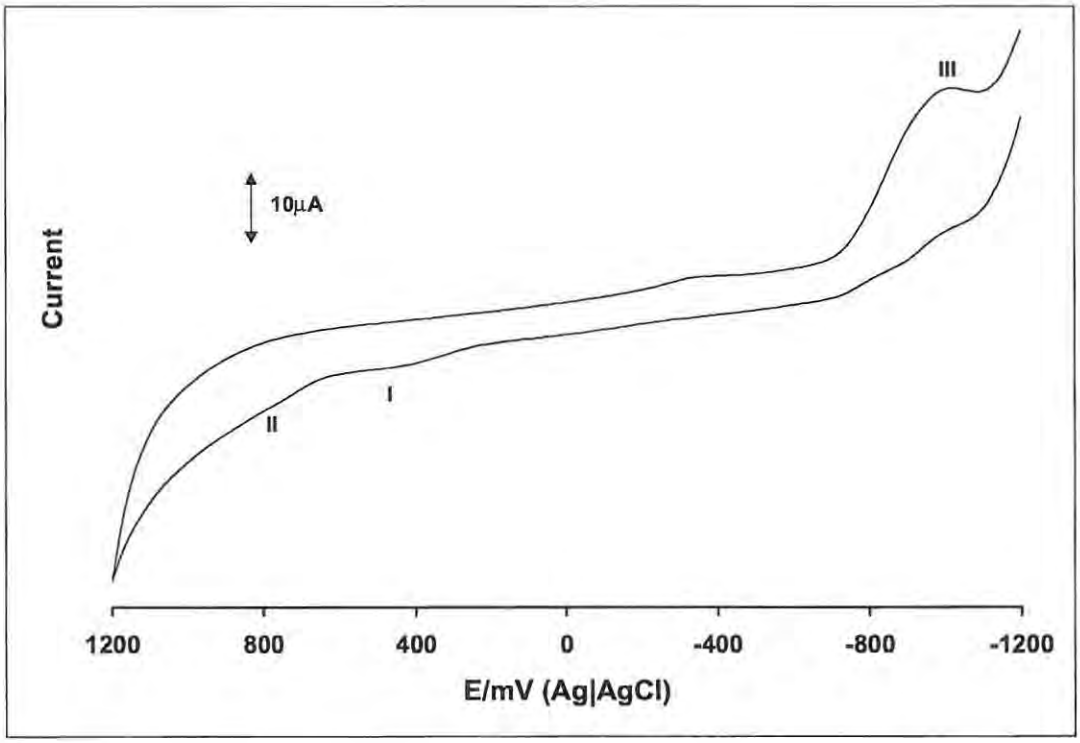

Figure 3.4: Cyclic voltammogram of $[Fe^{II}TSPc]^{4-}$ in pH 7.4 buffer, scan rate = 100 mV s^{-1}

In order to confirm that the complex synthesized in this work is $[Fe^{II}TSPc]^{4-}$ and not $[Fe^{III}TSPc]^{3-}$, spectroelectrochemistry was employed. Spectroelectrochemistry in an OTTLE cell of the solution containing iron tetrasulfophthalocyanine complex at the potential of the first oxidation (process I), 0.6 V, resulted in spectral changes shown in Figure 3.5. The solution turned from blue to green. The spectral changes shown in Figure 3.5 consisted of the decrease in the dimeric peak with an increase in the monomer peak. The monomer peak shifted from 665 nm to 673 nm as it increased in intensity. The peak at 434 nm intensified with time. This peak has been observed for low spin Fe^{III} phthalocyanine complexes.[193] Spectral changes in Figure 3.5 are typical of the spectra for the oxidation at the central metal in metallophthalocyanine complexes.

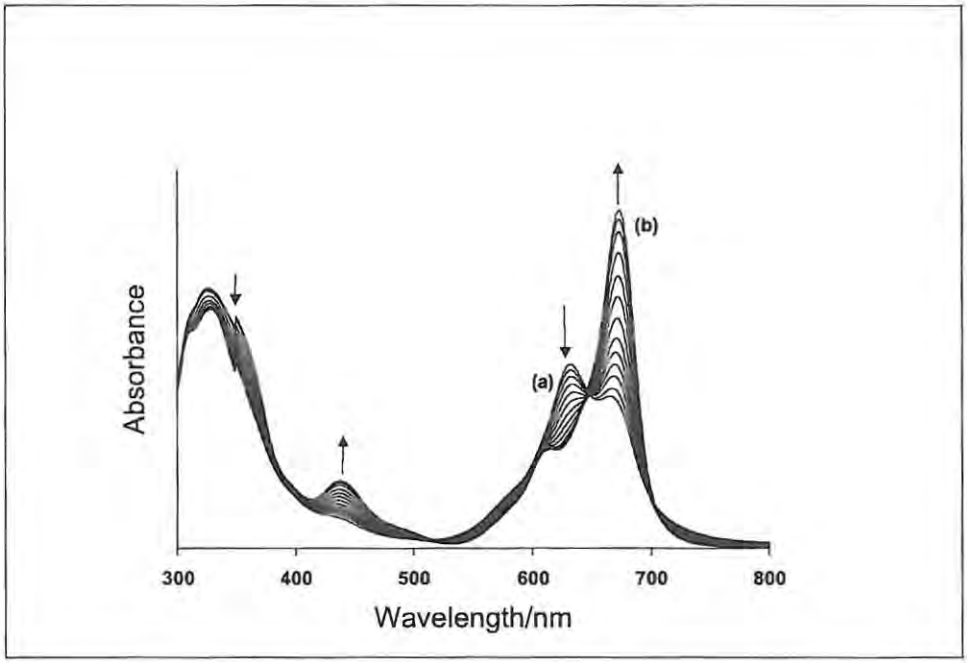

Figure 3.5: Changes in spectral features observed on electrolysis of $[Fe^{II}TSPc]^{4-}$ in an OTTLE cell at the potential of process I, pH = 7.4

Oxidation based on the phthalocyanine ring would be accompanied by a loss in the intensity of the Q band with the formation of weak broad bands near 500 nm and 700 nm,[279] as shown in Figure 3.6. Metal oxidation in $Fe^{II}Pc$ complexes is accompanied by a shift in the Q band to higher wavelengths.[193] Thus the spectral changes shown in Figure 3.5 are assigned to the oxidation of $[Fe^{II}TSPc]^{4-}$ and the formation of the $[Fe^{III}TSPc]^{3-}$ species, this confirms that the complex synthesized in this work contains an Fe^{II} species (i.e.$[Fe^{II}TSPc]^{4-}$) before oxidation. The number of electrons transferred following the electrolysis in Figure 3.5 was found to be near unity. Further oxidation of the species generated in Figure 3.5 at potentials of the second oxidation couple generated spectra typical of the ring oxidized species, Figure 3.6 curve b, with a broad band near 500 nm.

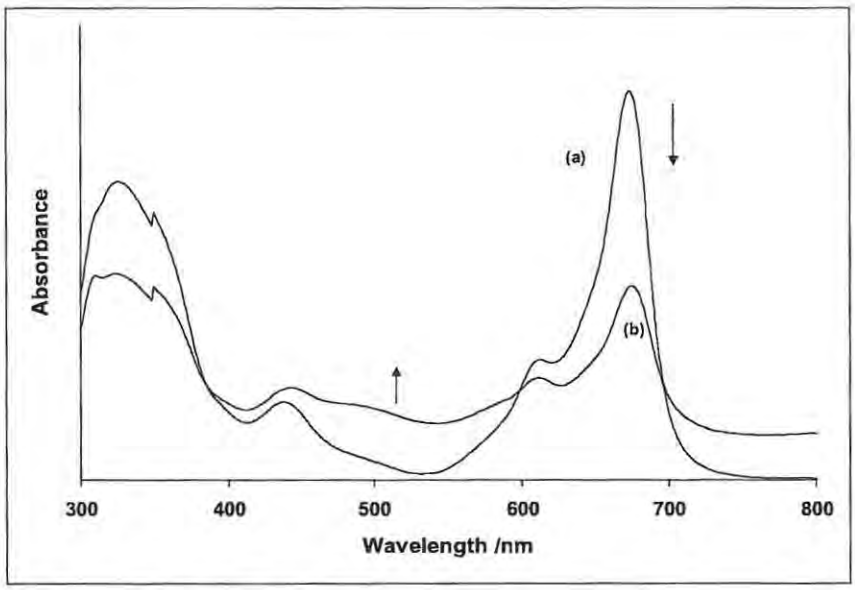

Figure 3.6: UV/vis absorption spectrum of (a) $[Fe^{III}TSPc]^{3-}$ in an OTTLE cell (same as (b) in Figure 3.5), (b) spectrum generated by oxidation of (a) at the potential of process II, pH = 7.4

The spectroelectrochemistry studies thus confirm that process I in Figure 3.4 is due to the oxidation of $[Fe^{II}TSPc]^{4-}$ to the $[Fe^{III}TSPc]^{3-}$ species. Spectral changes in Figure 3.5 confirm that the oxidized species is monomeric. Reduction of the oxidized species at zero volts did not result in the regeneration of the original spectra in Figure 3.5 showing that the oxidation of $[Fe^{II}TSPc]^{4-}$ to the $[Fe^{III}TSPc]^{3-}$ is not reversible, confirming the cyclic voltammetry data. The lack of reversibility of the oxidation of $[Fe^{II}TSPc]^{4-}$ may be explained by the fact that the dimeric species oxidized is irreversibly converted to the monomer. It has been reported that one-electron oxidation of aggregated $[MTSPc]^{4-}$ species, results in disaggregation.[280] Also Figure 3.5 confirms that a monomeric species is formed during oxidation.

3.2 Spectroscopic characterization of the interaction of neurotransmitters with iron (II) tetrasulfophthalocyanine

3.2.1 Dopamine

The changes in spectral features observed on addition of dopamine (DA) to solution of $[FeTSPc]^{4-}$ in unbuffered water (pH ≈ 6.8) are shown in Figure 3.7. Similar spectral changes were observed at pH 7.4, except that the starting spectrum is mainly the dimer in the latter. The peak due to the monomeric species at 665 nm is enhanced greatly with a small shift in wavelength to 667 nm, whereas the peak due to the dimeric species at 633 nm disappeared. The peak at 428 nm was enhanced.

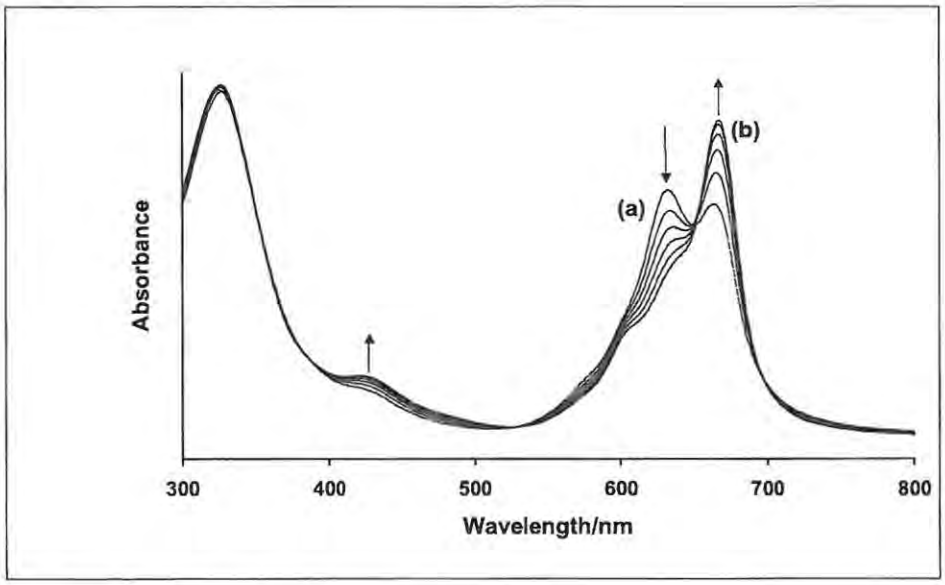

Figure 3.7: Electronic absorption spectra of $[FeTSPc]^{4-}$ (a) before and (b) 5 minutes after the addition of $3.3x10^{-5}$ mol dm^{-3} DA in water (pH ≈ 6.8).

The changes shown in Figure 3.7 were only observed at concentrations of dopamine less than $1.0x10^{-4}$ mol dm^{-3}. The increase in the monomeric peak, Figure 3.7 occurred with

clear isosbestic points at 651, 529 and 389 nm. With higher concentrations of DA, the increase in the peak due to the monomeric species was not gradual as observed in Figure 3.7, but instantaneous. The enhancement in the peak due to the monomeric species on addition of DA to $[FeTSPc]^{4-}$ shows that the dimer/monomer equilibrium for the $[FeTSPc]^{4-}$ species is shifted towards the monomeric side. The dimer-monomer equilibrium in $[MTSPc]^{4-}$ complexes can be affected by ionic strength[275] and by axial ligation.[206,207] The changes in spectral features in Figure 3.7 suggest the ligation of DA to $[FeTSPc]^{4-}$.

Figure 3.8 shows the changes in spectral features when concentrations of DA larger than $1x10^{-4}$ mol dm^{-3} were added to solutions of $[FeTSPc]^{4-}$.

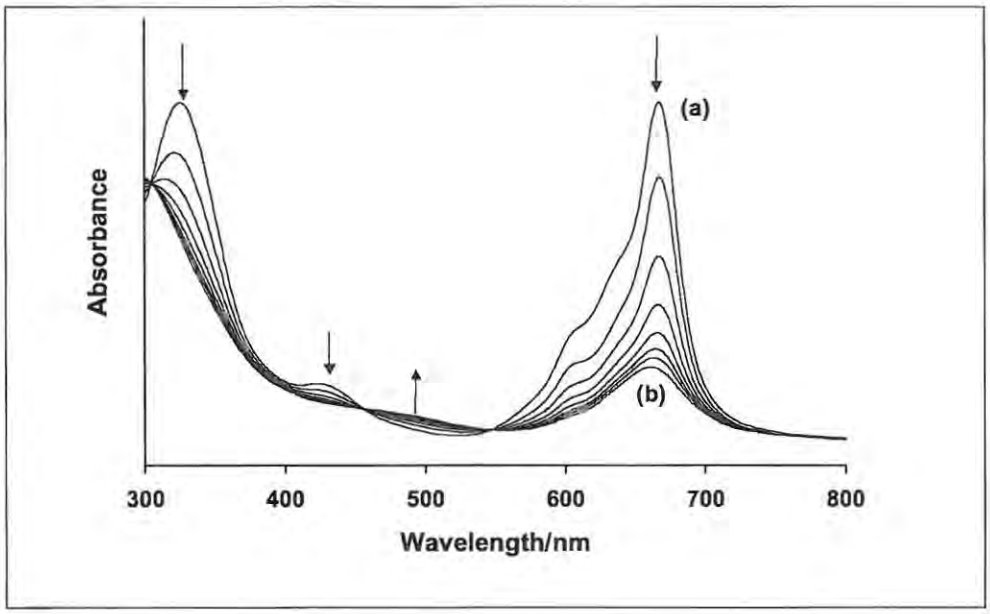

Figure 3.8: Electronic absorption spectra changes observed 2 minutes (a) and 20 minutes (b) after the addition of $3.3x10^{-4}$ mol dm^{-3} DA to solution of $[FeTSPc]^{4-}$ in water, pH ≈ 6.8.

The changes in spectral features shown in Figure 3.8 consisted of the decrease in the intensity of the peak due to the monomeric species at 667 nm up to a point where no further decrease in intensity was observed, accompanied by a shift to 659 nm. These spectral changes occurred with isosbestic points at 545, 454 and 305 nm. The peak at 428 nm decreased in intensity and a new broad feature developed near 500 nm. The Soret band shifted to higher energies. Alongside the spectral changes shown in Figure 3.8 was a change in the colour of the solution from blue to green. The final spectrum in Figure 3.8 and the colour change are similar to those observed on reduction of the $[Fe^{II}TSPc]^{4-}$ species to $[Fe^{I}TSPc]^{4-}$ using sodium borohydride. Thus the final spectrum in Figure 3.8 could be said to be due to the reduction of the central metal in $[Fe^{II}TSPc]^{4-}$ with the formation of the $Fe^{I}TSPc$ species, as a result of the electron transfer from DA.

Ligation of species such as NO_2^- or cysteine to $[CoTSPc]^{4-}$ has been shown to be accompanied by oxidation of $[Co^{II}TSPc]^{4-}$ to the $[Co^{III}TSPc]^{4-}$ species.[206,207] Axial ligation followed by electron transfer has also been suggested for the interaction of nitric oxide (NO) with iron Porphyrins.[281] El-Uyaan et al.[282] have shown that coordination of DA to Fe^{III} results in the formation of an Fe^{III}(DA) complex involving the use of both oxygen atoms in DA. This is followed by internal electron transfer forming Fe^{II} and a semiquinone, hence the dissociation of the complex.[282] It is suggested in this work that axial ligation of DA to $[FeTSPc]^{4-}$ occurs prior to internal electron transfer resulting in the formation of $(DA^+)Fe^{I}TSPc$ species.

IR spectra of the solid complex formed following evaporation of water from a solution containing $[FeTSPc]^{4-}$ and DA showed a new peak at 819 cm^{-1} which could not be identified with either DA or $[FeTSPc]^{4-}$. Fe-O vibrations are observed in the 800 to 830 cm^{-1} region for oxoiron porphyrin complexes.[283] The vibration at 819 cm^{-1} is thus in the range for Fe-O vibration suggesting the presence of an Fe-O bond in the complex between $[FeTSPc]^{4-}$ and DA. Also a new vibration at 3419 cm^{-1} was observed for the complex between DA and $[FeTSPc]^{4-}$. This band is due to indole N-H vibrations and gives evidence of cyclization in DA following its oxidation. Prominent vibrations due to DA at 1931 and 1500 cm^{-1} and between 800 and 1000 cm^{-1} disappeared on formation of a complex between $[FeTSPc]^{4-}$ and DA.

Proton nuclear magnetic resonance (^{1}HNMR) spectra of unsubstituted MPc complexes are characterized by weak multiplets near 9.30 and 8.60 ppm due to the α and β protons of the phthalocyanine ring.[222,284,285] These were observed at 11.6 and 8.2 ppm for $[FeTSPc]^{4-}$. The ^{1}HNMR spectra of dopamine showed a multiplet at 6.95 ppm due to the aromatic protons of the ring, and two sets of triplets due to side chain protons at 3.30 and 2.90 ppm. The ^{1}HNMR spectra observed following interaction between $[FeTSPc]^{4-}$ and DA showed no changes in the 3.30 and 2.90 resonances of DA, but showed a small shift in the resonances of the aromatic protons (6.95 to 6.80 ppm). This shift is probably a result of changes in the electronic effects of the ring following cyclization of DA. There was also an improvement in the resolution of the resonances due to the phthalocyanine ring following the interaction between DA and $[FeTSPc]^{4-}$. This could be due to improved solubility of the axially ligated $Fe^{I}TSPc$ species.

Elemental analysis also to confirmed the coordination of DA to $[FeTSPc]^{4-}$ as noted from the close agreement between the calculated values and the experimental values of the percentage composition. The UV/vis spectrum of the $(DA^{+})Fe^{I}TSPc$ complex well defined peak at 659 nm (log ε =3.77) and broad bands at 500 and 310 nm, Figure 3.8.

3.2.2 Serotonin

Spectral changes observed on addition of serotonin (5-HT) to solutions of $[FeTSPc]^{4-}$ are shown in Figures 3.9 and 3.10.

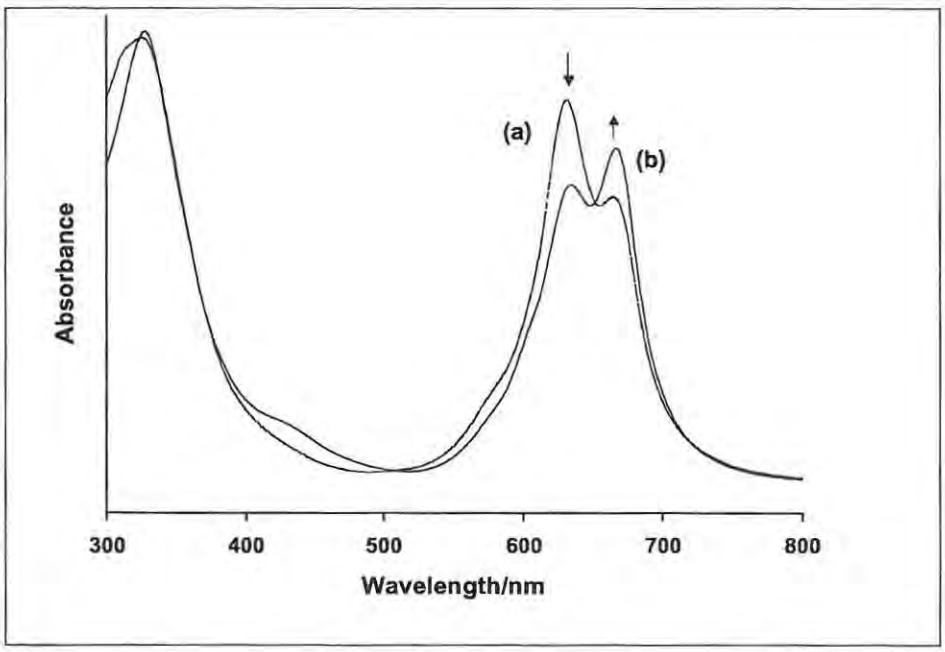

Figure 3.9: Absorption spectra of $[FeTSPc]^{4-}$ (a) before (b) 1minute after the addition of $2.7x10^{-4}$ mol dm^{-3} 5-HT in water, pH ≈ 6.8.

Contrary to the observation above for dopamine, the disappearance of the peak due to the dimeric species was not complete on addition of 5-HT to $[FeTSPc]^{4-}$, the peaks due to

both the monomeric and dimeric species were observed regardless of the concentration of serotonin added. There was however, a decrease in the intensity of the peak due to the dimeric species and an increase in the monomeric peak on initial addition of serotonin to $[FeTSPc]^{4-}$, Figure 3.9. Also the increase in the intensity of the monomeric peak occurred without any measurable shift in the wavelength. The peak due to the monomeric species did not show an increase with time that was observed for DA (Figure 3.7) regardless of the concentration of 5-HT added. The enhancement in the peak due to the monomeric species on addition of 5-HT to $[FeTSPc]^{4-}$ also shows that the dimer/monomer equilibrium for the $[FeTSPc]^{4-}$ species is shifted towards the monomeric side.

The spectral changes observed with time, on addition of 5-HT to $[FeTSPc]^{4-}$ solution in unbuffered water are shown in Figure 3.10. Similar changes in spectral features were observed in pH 7.4 buffered medium. The spectral changes in this case involved the decrease in both the dimeric and monomeric peaks and the formation of a broad peak at 663 nm. The new peak was formed with isosbestic points at 521 and 374 nm. As is the case with DA discussed above, it is suggested in this work that axial ligation of 5-HT to $[FeTSPc]^{4-}$ occurs prior to internal electron transfer resulting in the formation of $(5\text{-}HT^{+})Fe^{I}TSPc$ species.

The fact that the final spectrum following addition of DA or 5-HT to $[Fe^{II}TSPc]^{4-}$ is observed at different wavelengths shows that the final $Fe^{I}TSPc$ species formed are slightly different. This can be explained by differences in the complexes formed due to

ligation of DA or 5-HT, with the formation of $[(DA^{+})Fe^{I}TSPc]^{4-}$ and $[(5\text{-}HT^{+})Fe^{I}TSPc]^{4-}$, respectively.

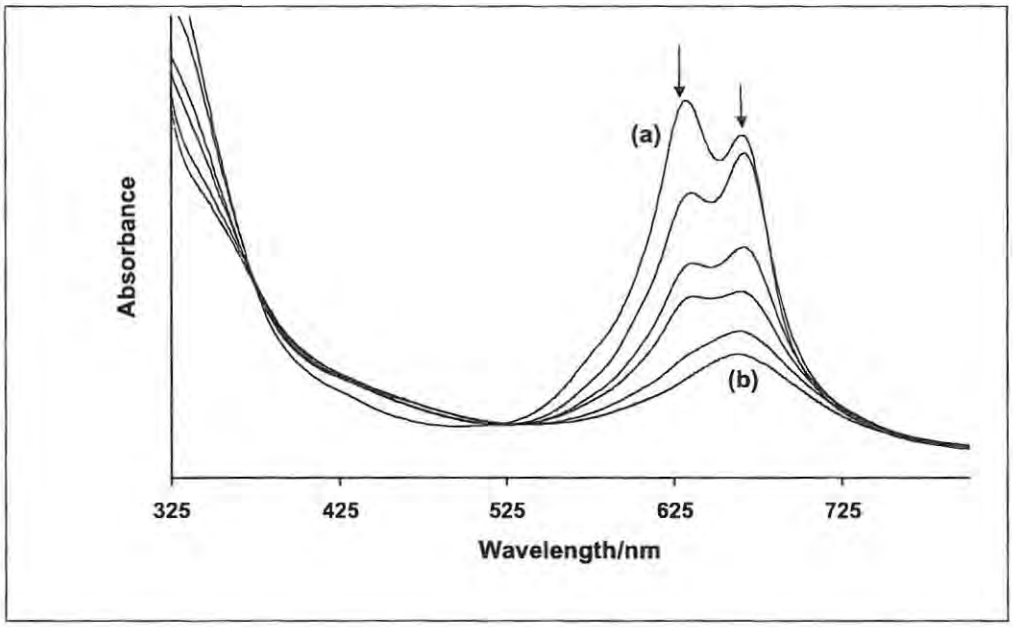

Figure 3.10: Electronic absorption spectra changes observed (a) 1 min and (b) 20 min after the addition of $2.7x10^{-4}$ mol dm^{-3} 5-HT to solution of $[FeTSPc]^{4-}$ in water, pH = 6.8.

No new peaks were evident in the IR spectrum of the complex between $[FeTSPc]^{4-}$ and 5-HT in the 800 to 830 cm^{-1} region where Fe-O vibrations are expected, this could be due to overlap with serotonin vibrations. The indole N-H vibration is observed at 3475 cm^{-1} for serotonin. Upon interaction between serotonin and $[FeTSPc]^{4-}$, this band disappeared and a sharp new band was observed at 2927 cm^{-1}.

The ^{1}HNMR resonances for the protons of the fused aromatic rings of serotonin were observed at different positions (6.85, 7.06, 7.25 and 7.38 ppm) due to their different environments. The side chain protons gave resonances at 3.29 and 4.19 ppm, while the

protons due to the creatinine unit were observed at δ = 3.08 ppm. Upon interaction between 5-HT and $[FeTSPc]^{4-}$, significant changes in the ^{1}HNMR spectra were observed. The spectra broadened and in general, the resonances due to the protons of the fused rings shifted upfield except for the resonance at 7.38 ppm that shifted downfield to 7.45 ppm. The resonances due to the side chain protons and due to creatinine unit remained unchanged. The shifting and broadening of the 5-HT resonances may be a result both of its coordination to $[FeTSPc]^{4-}$ and its oxidation.

The UV/vis spectrum of the complex formed between 5-HT and $[FeTSPc]^{4-}$ has an absorption peak at 663nm (log ε = 3.58) and broad features in the Soret region. Elemental analysis showed good agreement between the calculated and experimental values of percentage composition further confirming the coordination of 5-HT to $[FeTSPc]^{4-}$.

3.2.3 Histamine

The spectral changes observed with time upon the addition of histamine to solution of $[Fe^{II}TSPc]^{4-}$ in pH 7.4 buffer, are shown in Figure 3.11. The solution went from blue to green with time. The peak due to the monomeric species at 665nm was enhanced, accompanied by a shift to 673 nm while the peak due to the dimeric species at 633nm decreased considerably in intensity. The decrease in the absorbance of the peak due to the dimeric species and an increase in the peak of the monomeric species indicates that it is the monomeric form of $[Fe^{II}TSPc]^{4-}$ that forms a complex with histamine.

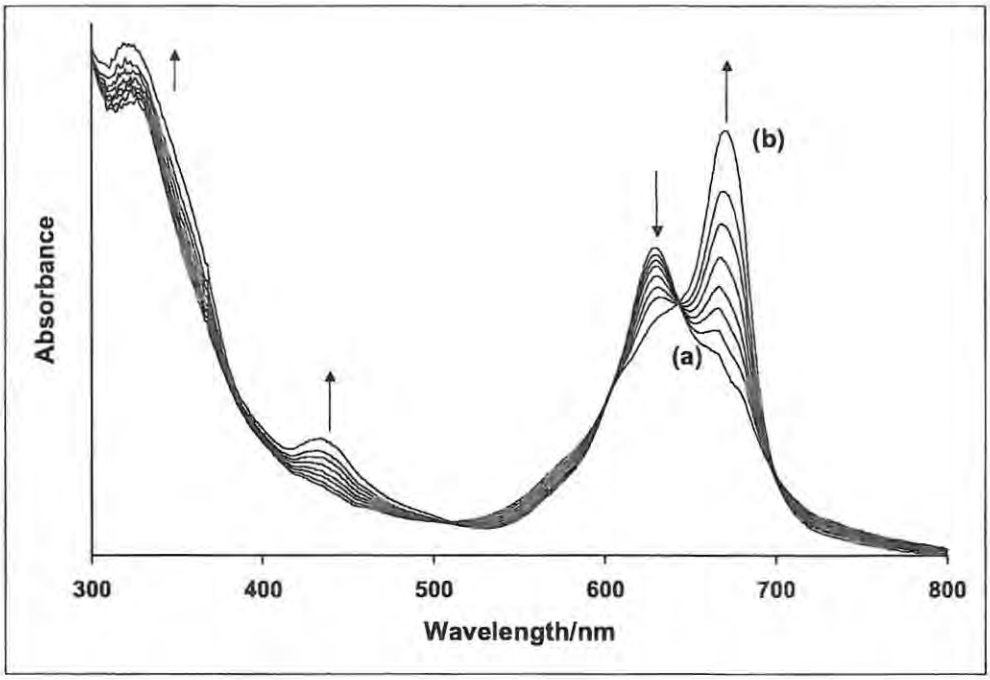

Figure 3.11: Changes in absrption spectra observed (a) before and (b) 3 hours after the addition of $1.82x10^{-2}$ mol dm^{-3} histamine to solution of $[FeTSPc]^{4-}$ in pH 7.4 buffer.

The spectral changes shown in Figure 3.11 are similar to those observed when $[FeTSPc]^{4-}$ was oxidized suggesting that oxidation of the $[Fe^{II}TSPc]^{4-}$ species to the $[Fe^{III}TSPc]^{3-}$ complex accompanies the interaction of the species with histamine. The changes in spectral features gave rise to isosbestic points at 695, 645, and 499 nm. The spectral changes shown in Figure 3.11 were obtained in pH 7.4 buffer. Similar changes were also obtained in unbuffered water and at pH 10.0, whereas at pH 4.0, there was no noticeable change in the spectrum of solution of $[Fe^{II}TSPc]^{4-}$ upon the addition of histamine. It is expected that histamine is deprotonated at pH values greater than 6 (pK_a = 5.97). The observation that spectral changes occurred on addition of histamine to $[Fe^{II}TSPc]^{4-}$ only

at higher pH values, suggests that it is the deprotonated form of histamine that interacts with the $[Fe^{II}TSPc]^{4-}$ species. Studies[286] on the related complex, $[Co^{II}TSPc]^{4-}$, have shown that the rate of autooxidation of this species to $[Co^{III}TSPc]^{3-}$ depends strongly on the axial ligands, with the oxidation being favoured by strong δ donor ligands.[193] Thus, the differences in the ability of histamine to influence the oxidation of $[Fe^{II}TSPc]^{4-}$ at different pH values could also be attributed to the differences in the electron donor ability of histamine at various pH values.

Substituted imidazole ligands are known to facilitate the oxidation of $[Co^{II}TSPc]^{4-}$ to $[Co^{III}TSPc]^{3-}$ by atmospheric oxygen.[287] There have also been suggestions that electron transfer in the Fe^{II} cytochrome species is mediated by oxygen oxidation of both histidine (the precursor of histamine) and Fe^{II} cytochrome, with a subsequent phosphorylation of the oxidized histidine molecule.[288] The oxygen mediated oxidation of both $[Fe^{II}TSPc]^{4-}$ and histamine is suggested in this work. The residual oxygen present in water is thus enough to effect the oxidation. Briefly bubbling nitrogen through the solution containing $[Fe^{II}TSPc]^{4-}$ and histamine, resulted in slower transformation of the $[Fe^{II}TSPc]^{4-}$ species hence confirming that oxygen is involved as an oxidant.

There were no changes observed in the spectra with time for the oxygenated or non-oxygenated solutions of $[Fe^{II}TSPc]^{4-}$ in buffer in the absence of histamine, showing that oxygen alone does not oxidize the $[Fe^{II}TSPc]^{4-}$ species.

In order to confirm the coordination of histamine to the $[Fe^{III}TSPc]^{3-}$ species, ^{1}HNMR and IR spectroscopic studies were employed. The ^{1}HNMR spectrum of $[Fe^{II}TSPc]^{4-}$ showed two weak and broad multiplets at 8.2 and 11.6 ppm typical[222,284,285] of the α and β protons of the phthalocyanine ring in MPc complexes while the ^{1}HNMR of histamine showed two singlets at 7.5 and 8.8 ppm due to the isolated protons on the aromatic ring. The peaks due to the protons on the side chain were observed at 3.3 and 3.5 ppm. The ^{1}HNMR spectrum of the complex formed between histamine and $[FeTSPc]^{4-}$ broadened considerably and resonances of the protons in the aromatic region of $[FeTSPc]^{4-}$ shifted downfield by at least 0.2 ppm and were observed at 8.5 and 11.8 ppm. The ^{1}HNMR peaks for histamine were greatly reduced in intensity and broadened, and the ring protons were shifted upfield to 7.3 and 8.3 ppm. The ring protons of histamine were shifted to a larger extent than the side chain protons, suggesting that coordination of histamine to $[FeTSPc]^{4-}$ may occur via one of the ring N atoms. The two distinct singlets due to the protons on the side chain in histamine were also reduced to a broad doublet centered at 3.4 ppm in the presence of $[FeTSPc]^{4-}$. The shift in δ suggests the formation of a complex between $[FeTSPc]^{4-}$ and histamine. The broadening of the ^{1}HNMR signals is as a result of the oxidation of $[Fe^{II}TSPc]^{4-}$ to the $[Fe^{III}TSPc]^{3-}$ complex upon interaction with histamine. The iron (III) central metal in $[Fe^{III}TSPc]^{3-}$ (d^5) would contain unpaired electrons in either low or high spin, hence resulting in the broadening of the NMR peaks. The IR spectrum of the complex is more or less the sum of the spectra of $[FeTSPc]^{4-}$ and histamine in the 2400 to 3600 cm^{-1} region. The several bands due to the double bonds of the imidazole ring from 1436 to 1622 cm^{-1} were greatly modified on coordination, again

suggesting the possible involvement of ring N atom in the coordination. Elemental analysis also confirmed the formation of a complex between $[FeTSPc]^{4-}$ and histamine.

3.2.4 Interaction of dopamine, serotonin and histamine with other metallotetra-sulfophthalocyanine complexes.

The possibility of the interaction of dopamine, serotonin and histamine with other tetrasulfophthalocyanines ($[CoTSPc]^{4-}$ and $[NiTSPc]^{4-}$) was investigated. Addition of DA or 5-HT to solutions of $[CoTSPc]^{4-}$ or $[NiTSPc]^{4-}$ resulted in a small change in the spectra of $[MTSPc]^{4-}$ species. A small increase in the peak due to the monomer peak and a small decrease in the dimer peak were observed. There was no evidence for the formation of the reduced $[CoTSPc]^{4-}$ or $[NiTSPc]^{4-}$ species. The differences in the behaviour of $[NiTSPc]^{4-}$ in the presence of DA or 5-HT when compared to $[FeTSPc]^{4-}$ may be explained by the fact that for the $[NiTSPc]^{4-}$ complex reduction or oxidation occurs at the phthalocyanine ring and not at the central metal.[214] Also NiPc complexes are square planar and do not favour axial ligation. For $[Co^{II}TSPc]^{4-}$ complexes, reduction occurs at the central metal forming $[Co^{I}TSPc]^{4-}$, and hence this complex would be expected to behave in a manner similar to $[FeTSPc]^{4-}$ on interaction with DA or 5-HT. However reduction of the $[Co^{II}TSPc]^{4-}$ to $[Co^{I}TSPc]^{4-}$ was not observed in the presence of DA or 5-HT.

When histamine was added to a solution of $[CoTSPc]^{4-}$ in water, the changes in spectral features are shown in Figure 3.12. The first step was the decrease in the peak due to the

monomeric species at 656 nm upon the addition of histamine. With time, a new peak was generated at 666 nm, accompanied by a decrease in the absorbance of the peak due to the dimeric species at 629 nm. The changes in spectral features gave rise to an isosbestic point at 641nm. The kinetic and equilibrium studies of this interaction were not followed up because the changes observed were extremely slow in taking place. The spectral changes shown in Figure 3.12 were monitored over 5 days. However, these changes suggest that a complex is slowly formed between $[CoTSPc]^{4-}$ and histamine, the rate being much slower than observed above for $[FeTSPc]^{4-}$. Axial ligand reactions are known to occur faster for FePc complexes than for CoPc complexes.[289]

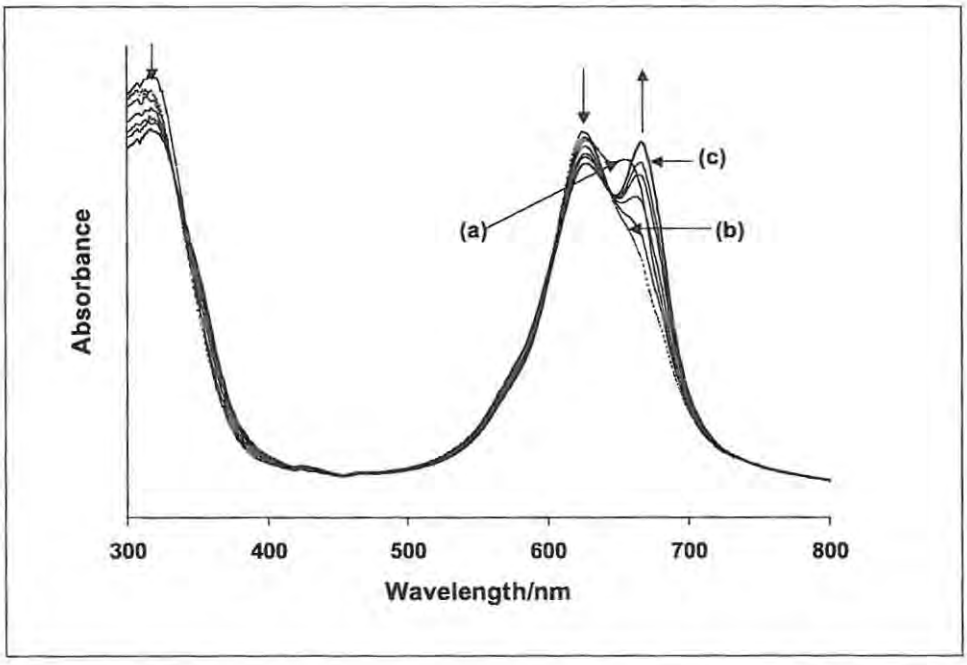

Figure 3.12: Electronic absorption spectra changes observed for $[CoTSPc]^{4-}$ in water, (a) before and (b) immediately after the addition of 1.82×10^{-2} mol dm^{-3} histamine (c) 5 days after the addition of histamine

There were no changes observed in the UV/vis spectrum of $[NiTSPc]^{4-}$ when histamine was added to the solution. This is expected because nickel phthalocyanine complexes do not normally coordinate axial ligands due to their square planar geometry as explained above.

3.3 Kinetic and equilibrium studies of the interaction of neurotransmitters with iron (II) tetrasulfophthalocyanine

3.3.1 Dopamine

Kinetic data for the coordination of DA to $[FeTSPc]^{4-}$ were obtained by monitoring the formation of the peak due to $[(DA^{+})Fe^{I}TSPc]^{4-}$ complexes with Q bands at 659 nm, under conditions of Figure 3.8. The formation of the $[(DA^{+})Fe^{I}TSPc]^{4-}$ species was monitored following the complete shift to the monomeric side, hence the starting spectra in Figure 3.8 is that of the monomeric species, thus avoiding influences due to the dimeric species. The concentration of $[FeTSPc]^{4-}$ was kept constant at 2.0×10^{-5} mol dm^{-3} while the concentration of dopamine was varied from 1.7×10^{-4} to 8.3×10^{-4} mol dm^{-3}. Under these conditions, a pseudo first order reaction condition was assumed for kinetic studies since the concentration of dopamine was much larger than that of $[FeTSPc]^{4-}$.

Plots of $\log(A_\infty - A_t)$ against time were linear (where A_∞ is the final absorbance at the end of the reaction and A_t is the absorbance at time t) for the coordination of dopamine to $[FeTSPc]^{4-}$ as shown in Figure 3.13. The linearity of the plots confirms that the reaction between $[FeTSPc]^{4-}$ and dopamine is first order with respect to $[FeTSPc]^{4-}$. The observed rate constant (k_{obs}) is given by the slope of the plot of absorbance versus time (slope of

Figure 3.13 for different concentrations of dopamine). A plot of the observed rate constant vs concentration of dopamine was linear, Figure 3.14 indicating that the axial ligand exchange reaction is first order with respect to DA.

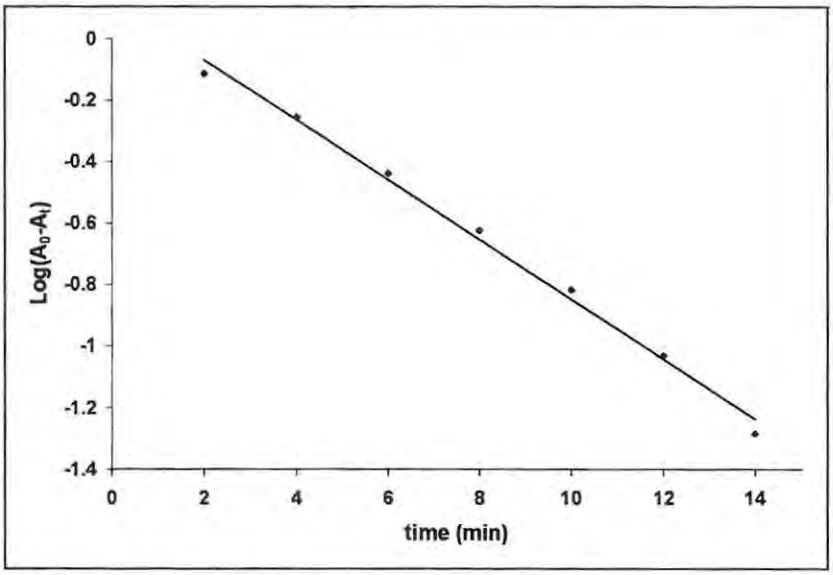

Figure 3.13: Plot of log of absorbance against time for the coordination of DA to $[FeTSPc]^{4-}$.

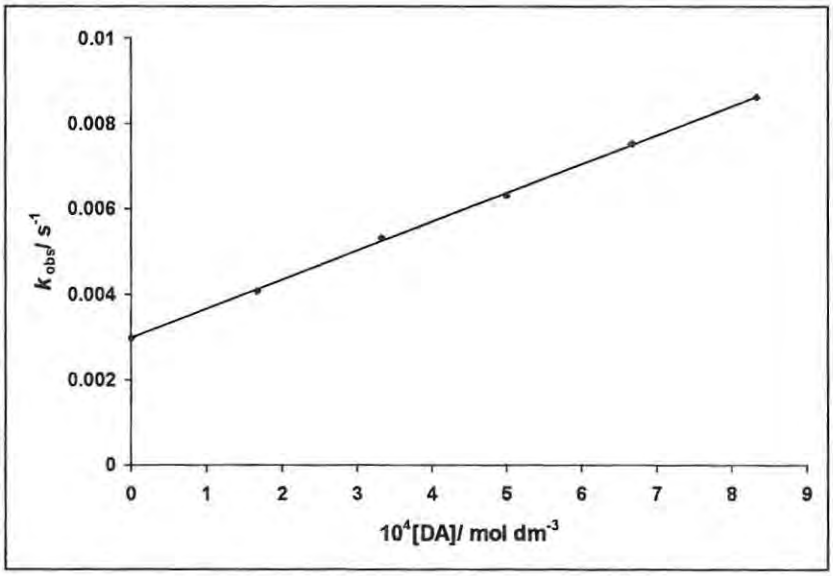

Figure 3.14: Plot of observed rate constant vs concentration for the coordination of DA to $[FeTSPc]^{4-}$.

As mentioned in Section 1.6.7.2, axial ligand substitution reactions in MPCs are dissociative and the formation of a highly reactive five-coordinate intermediate.[191,261,264] It is expected that the monomeric form of $[FeTSPc]^{4-}$ is coordinated to water molecules in aqueous solutions forming the $[(H_2O)_2FeTSPc]^{4-}$ species.[277] The coordination of DA to $[(H_2O)_2FeTSPc]^{4-}$ may then be represented by equations 3.1 and 3.2:

$$(H_2O)_2Fe^{II}TSPc \underset{k_{-1}}{\overset{k_1}{\equiv}} (H_2O)Fe^{II}TSPc + H_2O \qquad \textbf{3.1}$$

$$(H_2O)Fe^{II}TSPc + DA \underset{k_{-2}}{\overset{k_2}{\equiv}} (H_2O)(DA^{+})Fe^{I}TSPc \qquad \textbf{3.2}$$

The rate law for axial ligand exchange reactions in MPc complexes shown by equations 3.1 and 3.2 is generally given by equation 3.3 and was derived as outlined in Section 1.6.7.2, substituting E with DA, in equation 1.31.

$$k_{obs} = k_f[DA] + k_r \qquad \textbf{3.3}$$

Where k_f, the rate constant for the forward reaction is given by $k_1k_2/(k_{-1}[H_2O])$ and k_r is the rate constant for the reverse reaction. Least square analysis of the data presented in Figure 3.9 gave $k_f = 6.8 \forall 0.2$ dm^3 mol^{-1} s^{-1} from the slope and $k_r = 3.0 \forall 0.1 \times 10^{-3}$ s^{-1} from the intercept for the coordination of DA.

Using these values of rate constants, the value of the equilibrium constant for DA coordination to $[FeTSPc]^{4-}$ was estimated to be $K = 2.3 \times 10^3$ dm^3 mol^{-1} from the relationship, $K = k_f/k_r$.

Similar to the kinetic studies for DA coordination, the equilibrium data were determined following complete shifting of the equilibrium to the monomeric side, and the spectral changes for the decrease in the peak due to the monomeric species were followed, Figure 3.8. For the interaction between DA and $[FeTSPc]^{4-}$, the equilibrium constant for the formation of the $[(DA^+)Fe^{I}TSPc]^{4-}$ was obtained by monitoring the decrease in the peak due to the monomeric species at 667 nm, using equation 3.4.

$$Log\left[\frac{(A_{eq} - A_0)}{(A_\infty - A_{eq})}\right] = LogK_{eq} + nLog[DA] \qquad \textbf{3.4}$$

where A_{eq} is the equilibrium absorbance at 667 nm and A_0 is the starting absorbance at 667 nm of the monomeric, $[FeTSPc]^{4-}$ species. A_4, is the absorbance after complete formation of the $[(DA^+)Fe^{I}TSPc]^{4-}$ complex. This parameter was determined from the final absorbance at 659 nm. Figure 3.15 shows the plot of $\log[(A_{eq} - A_0)/(A_4 - A_{eq})]$ versus log[DA].

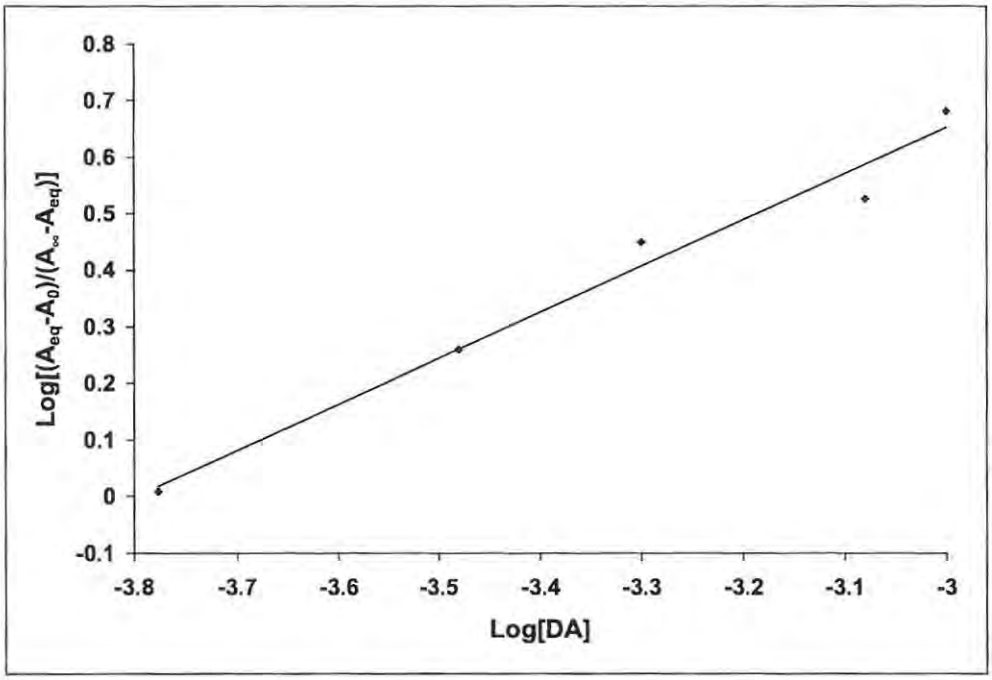

Figure 3.15: Plot of Log[$(A_{eq}-A_0)/(A_\infty-A_{eq})$] vs Log[DA] for the coordination of DA to $[FeTSPc]^{4-}$.

A linear plot with a slope near unity (n = 0.9 ∀ 0.2) was obtained, showing that only one mole of DA was coordinated to the $[FeTSPc]^{4-}$ species. The linearity of the plot confirms the coordination of DA to the $[FeTSPc]^{4-}$ complex. Least square analysis gave an equilibrium constant of, K = 2.2 ∀ 0.1 x 10^3 dm^3 mol^{-1}, in agreement within experimental error with the value of $2.3x10^3$ dm^3 mol^{-1} calculated from the kinetic data. The values of the equilibrium and rate constants obtained for the coordination of dopamine to $[FeTSPc]^{4-}$ are in the range reported for axial ligand exchange reactions in FePc complexes.[191] (see summary in Table 3.2)

3.3.2 Serotonin

Kinetic and equilibrium data for the coordination of 5-HT to $[FeTSPc]^{4-}$ were obtained by monitoring the formation of the peak due to $[(5\text{-}HT^{+})Fe^{I}TSPc]^{4-}$ complex with Q band at 663 nm under conditions of Figure 3.10. The concentration of 5-HT was varied from $6.7x10^{-5}$ to $4.7x10^{-4}$ mol dm^{-3} while the concentration of $[FeTSPc]^{4-}$ was kept constant at $2.5x10^{-5}$ mol dm^{-3}. A pseudo first order reaction condition was assumed for kinetic studies as the concentration of 5-HT was larger than that of $[FeTSPc]^{4-}$.

Plots of Log (A_∞ - A_t) against time for the formation of $[(5\text{-}HT^{+})Fe^{I}TSPc]^{4-}$ complex were linear for the various concentrations used as shown in Figure 3.16 from which the k_{obs} were obtained. A plot of the k_{obs} against the concentration of 5-HT was linear (Figure 3.17) showing that the coordination of 5-HT to $[FeTSPc]^{4-}$ was first order in 5-HT.

Kinetic and equilibrium data were obtained using equations 3.3 and 3.4 above. Least square analysis of the data presented in Figure 3.16 gave $k_f = 9.3 \pm 0.3$ dm^3 $mol^{-1}s^{-1}$ from the slope and $k_r = 5.6 \pm 0.1 \times 10^{-3}$ s^{-1} from the intercept were obtained. The value of the equilibrium constant was estimated to be $K = 1.7 \times 10^3$ dm^3 mol^{-1} from the relationship $K=k_f / k_r$.

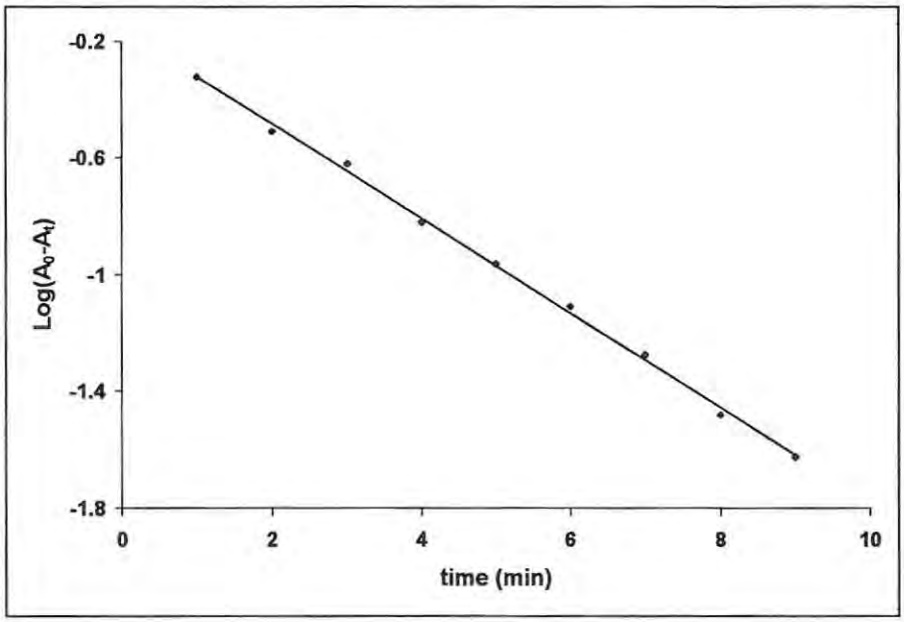

Figure 3.16: Plot of Log of absorbance vs time for the coordination of 5-HT to $[FeTSPc]^{4-}$.

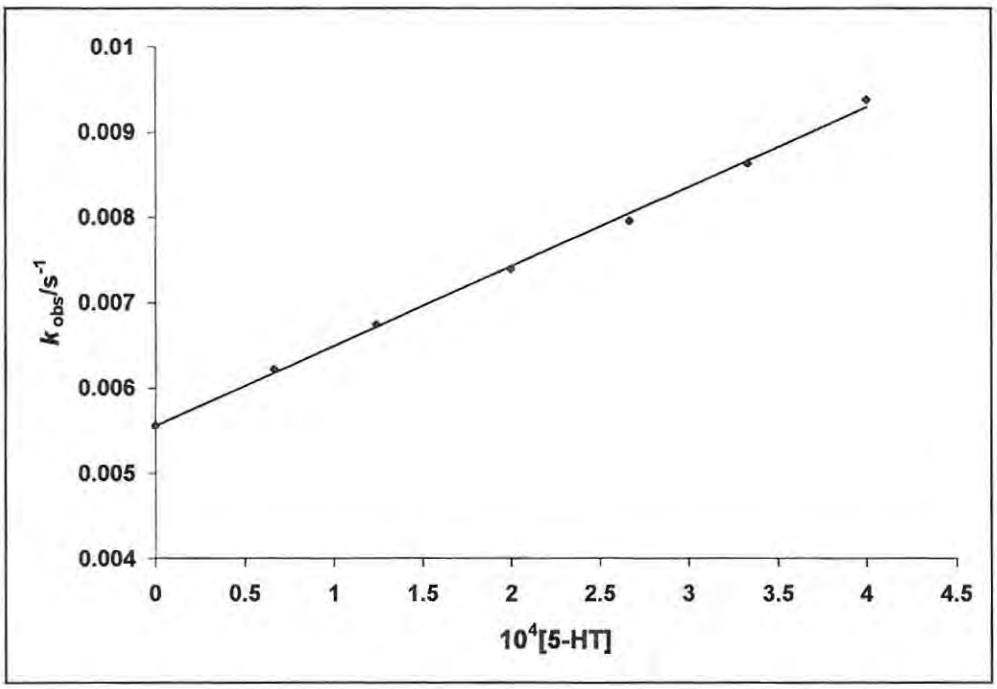

Figure 3.17: Plot of observed rate constant vs concentration for the coordination of 5-HT to $[FeTSPc]^{4-}$.

The equilibrium data for the coordination of 5-HT to $[FeTSPc]^{4-}$ was determined by using the spectra due to the formation of the reduced $[(5\text{-}HT^{+})Fe^{I}TSPc]^{4-}$ species and equation 3.4. Thus in this case, A_{eq} is the equilibrium absorbance at 665 nm, A_0 is the absorbance at 665 nm before addition of 5-HT and A_∞, the absorbance after complete formation of the $[(5\text{-}HT^{+})Fe^{I}TSPc]^{4}$ complex, was determined from the final absorbance at 663 nm. The plot of $\log[(A_{eq} - A_0)/(A_\infty - A_{eq})]$ versus log[5-HT] is shown in Figure 3.18. A linear plot with a slope $n = 0.9 \pm 0.1$ was obtained and the value of K was determined to be $K = 1.5 \pm 0.2 \times 10^3$ dm^3 mol^{-3}, in agreement with the value determined using k_f/k_r. These values are also within the range of constants for axial ligand exchange in FePc complexes.[191] (see summary in Table 3.2)

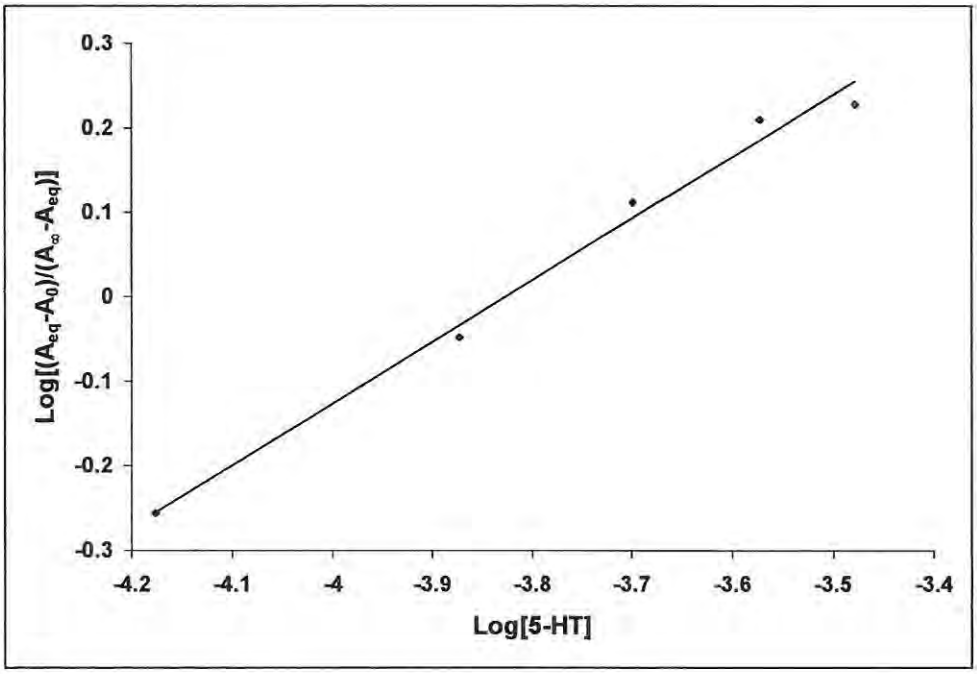

Figure 3.18: Plot of $Log[(A_{eq}-A_0)/(A_\infty-A_{eq})]$ vs Log [5-HT] for coordination to $[FeTSPc]^{4-}$.

3.3.3 Histamine

Kinetic data for the coordination of histamine to $[Fe^{II}TSPc]^{4-}$ were obtained by monitoring the increase in the absorbance of the monomeric species at 672 nm following the addition of histamine to solutions of $[Fe^{II}TSPc]^{4-}$ in pH 7.4 Tris buffer as shown in Figure 3.11. The concentration of $[FeTSPc]^{4-}$ was kept constant at 1.7×10^{-5} mol dm^{-3} while the concentration of histamine was varied from 9.1×10^{-3} to 4.5×10^{-2} mol dm^{-3}. Pseudo first order conditions were assumed for kinetic studies since the concentration of histamine was much higher than that of $[FeTSPc]^{4-}$.

The plots of the logarithm of absorbance versus time were linear confirming the assumption of a first order reaction with respect to $[Fe^{II}TSPc]^{4-}$. The observed rate constants, k_{obs}, were obtained from the slopes of these plots at different concentrations of histamine. The plot of k_{obs} versus the concentration of histamine was linear, Figure 3.19, showing that the reaction was first order in histamine.

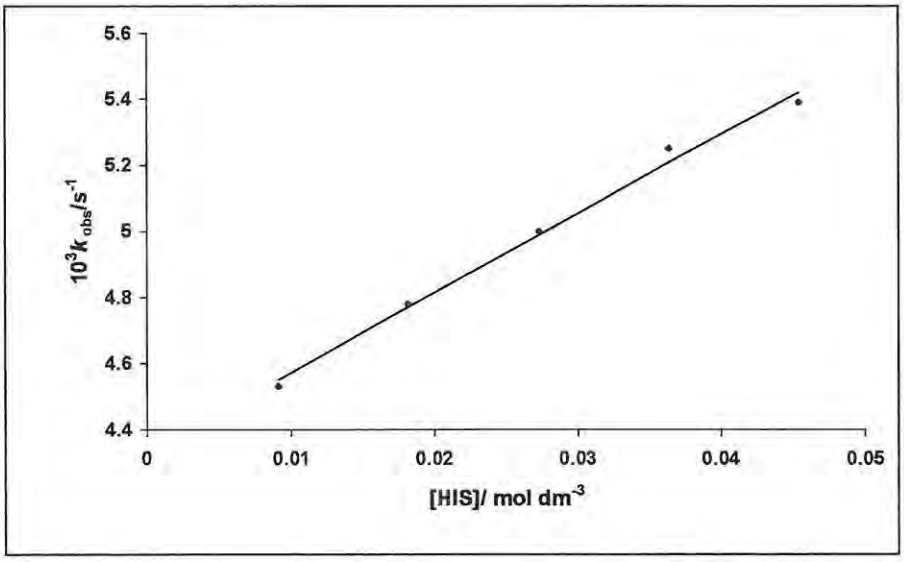

Figure 3.19: Plot of observed rate constant vs concentration for the coordination of histamine to $[FeTSPc]^{4-}$

The axial ligand exchange reaction between $[Fe^{II}TSPc]^{4-}$ and histamine can be represented by equations 3.5 and 3.6:

$$(H_2O)_2Fe^{II}TSPc \underset{k_{-1}}{\overset{k_1}{\equiv}} (H_2O)Fe^{II}TSPc + H_2O \qquad \textbf{3.5}$$

$$(H_2O)Fe^{II}TSPc + HIS \underset{k_{-2}}{\overset{k_2\ [O_2]}{\equiv}} (H_2O)(HIS^{+})Fe^{III}TSPc \qquad \textbf{3.6}$$

Equations 3.3 and 3.4 also hold true for the coordination of histamine to $[Fe^{II}TSPc]^{4-}$. Kinetic and equilibrium data for the coordination of histamine to $[FeTSPc]^{4-}$ were thus determined using equations 3.3 and 3.4. Least square analysis of the data in Figure 3.19 gave $k_f = 2.41 \pm 0.01 \times 10^{-2}$ dm^3 mol^{-1} s^{-1} from the slope and $k_r = 4.33 \pm 0.03 \times 10^{-3}$ s^{-1} from the intercept. The value of the equilibrium constant for the coordination of histamine to $[FeTSPc]^{4-}$ was then found to be $K = 5.6 \pm 0.3$ dm^3 mol^{-1} from the expression $K = k_f / k_r$.

Equation 3.4 was used to obtain equilibria data. In this situation, A_{eq} is the equilibrium absorbance of the monomeric species at 673 nm, A_0 is the absorbance before the addition of histamine and A_∞ is the final absorbance at 673nm. Figure 3.20 shows the plot of $\text{Log}[(A_{eq} - A_0)/(A_4 - A_{eq})]$ versus Log[HIS]. (HIS stands for histamine)

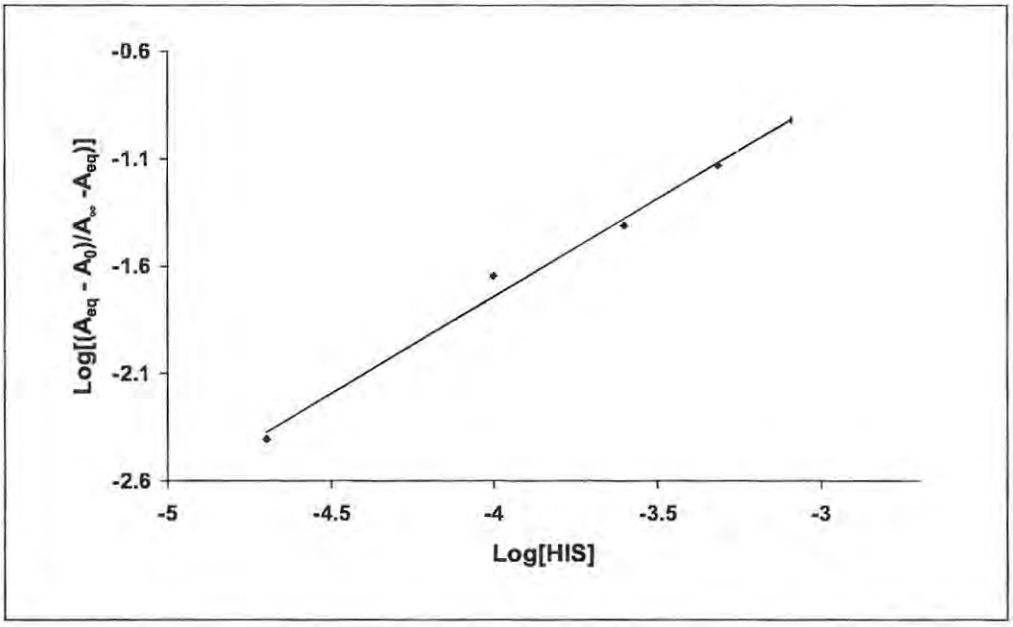

Figure 3.20: Plot of Log[(A_{eq}-A_0)/(A_∞-A_{eq})] versus Log[histamine] for coordination to $[FeTSPc]^{4-}$.

A linear plot was obtained with a slope near unity (n = 0.9 ∀ 0.1), confirming the coordination of histamine to $[Fe^{II}TSPc]^{4-}$, and showing that only one mole of histamine is coordinated to $[Fe^{II}TSPc]^{4-}$. Least square analysis gave an equilibrium constant K = 6.3 ∀ 0.8 dm^3 mol^{-1} in agreement within experimental error with the value determined using k_f/k_r.

The equilibrium and rate constants for the coordination of histamine to $[Fe^{II}TSPc]^{4-}$ are lower than those reported for the interaction between $[Fe^{II}TSPc]^{4-}$, dopamine and serotonin above, Table 3.2, but are higher than those reported for the coordination of nitrite to the $[Co^{II}TSPc]^{4-}$ species.[206] The coordination of dopamine or serotonin to the $[Fe^{II}TSPc]^{4-}$ species was accompanied by the reduction of the latter, whereas oxidation of

this species is observed on interaction with histamine, hence different rate constants are obtained.

Table 3.2 summarizes the kinetic and equilibrium constants obtained for the coordination of dopamine, serotonin and histamine to $[FeTSPc]^{4-}$ and compares the values with those obtained from other axial ligand exchange reactions involving iron phthalocyanine complexes.

Table 3.2: Summary of kinetic and equilibrium data for the coordination of some ligands to $[FeTSPc]^{4-}$

MPc	Ligand	k_f ($dm^3\ mol^{-1}\ s^{-1}$)	k_r (s^{-1})	K ($dm^3\ mol^{-1}$)	Reference
$Fe^{II}TSPc$	Dopamine	6.8	$3.0x10^{-3}$	$2.2x10^{3}$	this work
$Fe^{II}TSPc$	Serotonin	9.3	$5.6x10^{-3}$	$1.5x10^{3}$	this work
$Fe^{II}TSPc$	Histamine	$2.4x10^{-2}$	$4.3x10^{-3}$	6.3	this work
FePc	Cyanide	0.2	$3.5x10^{-4}$	$5.7x10^{2}$	191
$FePc(Cl)_{16}$	Cyanide	$4.2x10^{-3}$	$2.3x10^{-6}$	$1.6x10^{3}$	290
FePc	Pyridine	$7.5x10^{-3}$	$2.5x10^{-6}$	$3.0x10^{2}$	261
FePc	Imidazole	$1.2x10^{-2}$	$1.6x10^{-6}$	$7.4x10^{3}$	261

In conclusion, the coordination of DA, 5-HT and HIS to $[FeTSPc]^{4-}$, which is accompanied by electron transfer reactions has been reported in this chapter. The ability

of $[FeTSPc]^{4-}$ to coordinate these molecules is important for the study of the electrocatalytic properties of $[FeTSPc]^{4-}$ towards the detection of DA, 5-HT and HIS which follows in the next chapter.

CHAPTER 4

ELECTROCATALYTIC DETECTION OF NEUROTRANSMITTERS*

* The following publication resulted from part of the research work presented in this chapter and it is not refereced further in this thesis: J. Oni, T. Nyokong, Anal. Chim. Acta, 2001, 434, 9.

4.1 Characterization of modified carbon paste electrode

4.1.1 Determination of optimum phthalocyanine content of the electrode

Dopamine was employed for characterization studies and the parameters developed were used for the other analytes.

In order to obtain the optimum MPc composition of the modified electrode that gives the highest current response per unit concentration of DA, the MPc content of the modified electrode was varied from 0 to 10% the highest current response for the same concentration of DA was obtained at an MPc content of 4% as shown in Figure 4.1. A percentage MPc composition of the electrode more than 4% gave rise to large background currents which swamped the current arising from the oxidation of DA. Thus an MPc content of 4% based on the weight of graphite used in the preparation of modified electrodes was employed for the electrocatalytic studies.

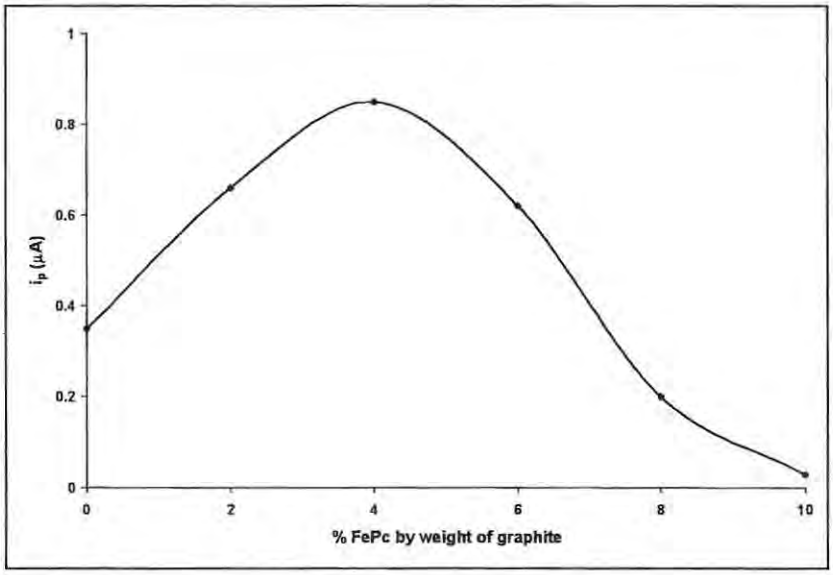

Figure 4.1: Variation of peak current with % composition of FePc in modified electrode

4.1.2 Characterization of the modified electrodes

4.1.2.1 Iron (II) tetrasulfophthalocyanine modified carbon paste electrode

The Osteryoung square wave voltammogram (OSWV) of iron (II) tetrasulfophthalocyanine modified carbon paste electrode (FeTSPc-CPE) in buffer alone in the absence of DA, Figure 4.2, gave peaks at 0.40 (peak **I**) and 0.70 V (peak **II**), assigned respectively to the oxidation of the central metal and the ring in $[FeTSPc]^{4-}$. These peaks however disappeared with scan number and were not observed after 7 scans. Thus for all studies involving $[FeTSPc]^{4-}$, OSW voltammograms were carried out for 10 cycles to establish background conditions for the electrode before use in electrocatalytic studies. The decrease and the eventual disappearance of the peaks could be attributed to the depletion of $[Fe^{II}TSPc]^{4-}$ at the surface of the electrode forming $[Fe^{III}TSPc]^{3-}$ irreversibly.

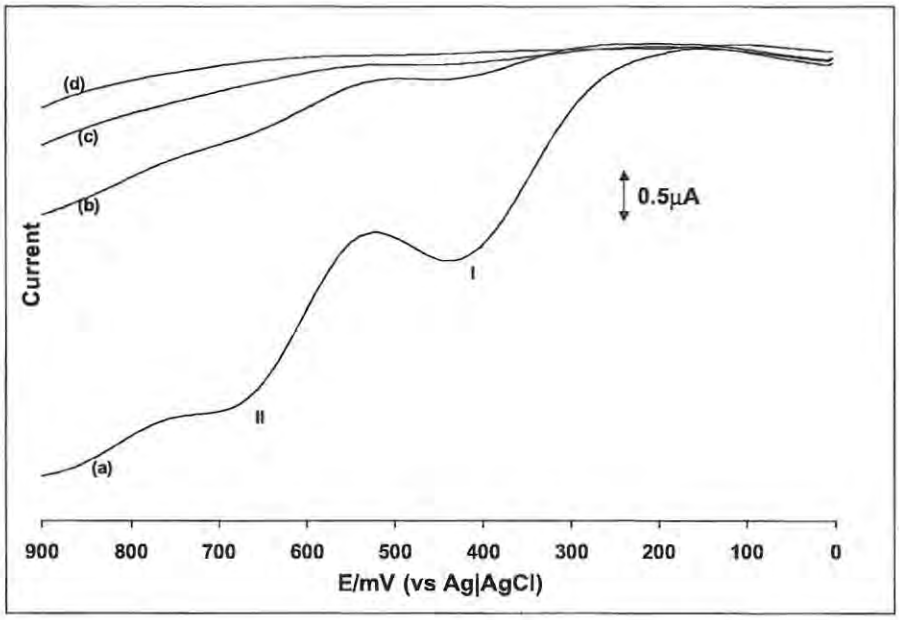

Figure 4.2: OSWV of FeTSPc-CPE in pH 7.4 buffer (a) 1st (b) 5th (c) 7th (d) 10th scan

4.1.2.2 Iron (II) phthalocyanine modified carbon paste electrode

The cyclic voltammetry (CV) as well as the SWV of iron (II) phthalocyanine modified carbon paste electrode (FePc-CPE) in buffer alone did not show any significant peaks. The electrodes were nevertheless cycled ten times in blank buffer solutions to establish stable background currents before being used for analysis.

4.2 Electrocatalytic oxidation of neurotransmitters

4.2.1 Dopamine

The electrochemical behaviour of DA on conventional electrodes has been described.[154,291,292] Oxidation of dopamine is dependent on pH. In acidic media, it is a two-electron process that is accompanied by the transfer of two protons, forming dopamine *o*-quinone, Scheme 4.1.

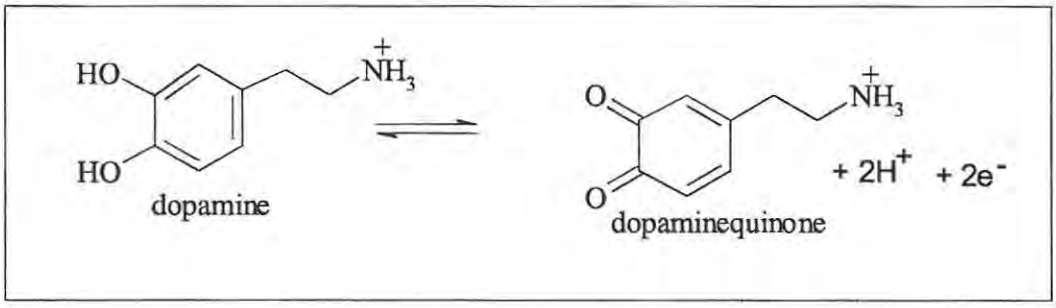

Scheme 4.1: Scheme of the oxidation of dopamine in acidic media

One wave is observed on the cathodic scan due to the reduction of the dopamine *o*-quinone. In basic media, Scheme 4.2, when a small quantity of the unprotonated quinone is formed, an intermolecular nucleophilic attack can occur resulting in leucochrome as a

product of 1,4-Michael addition reaction. A second cathodic peak is observed due to a two-electron reduction of leucochrome to aminochrome.

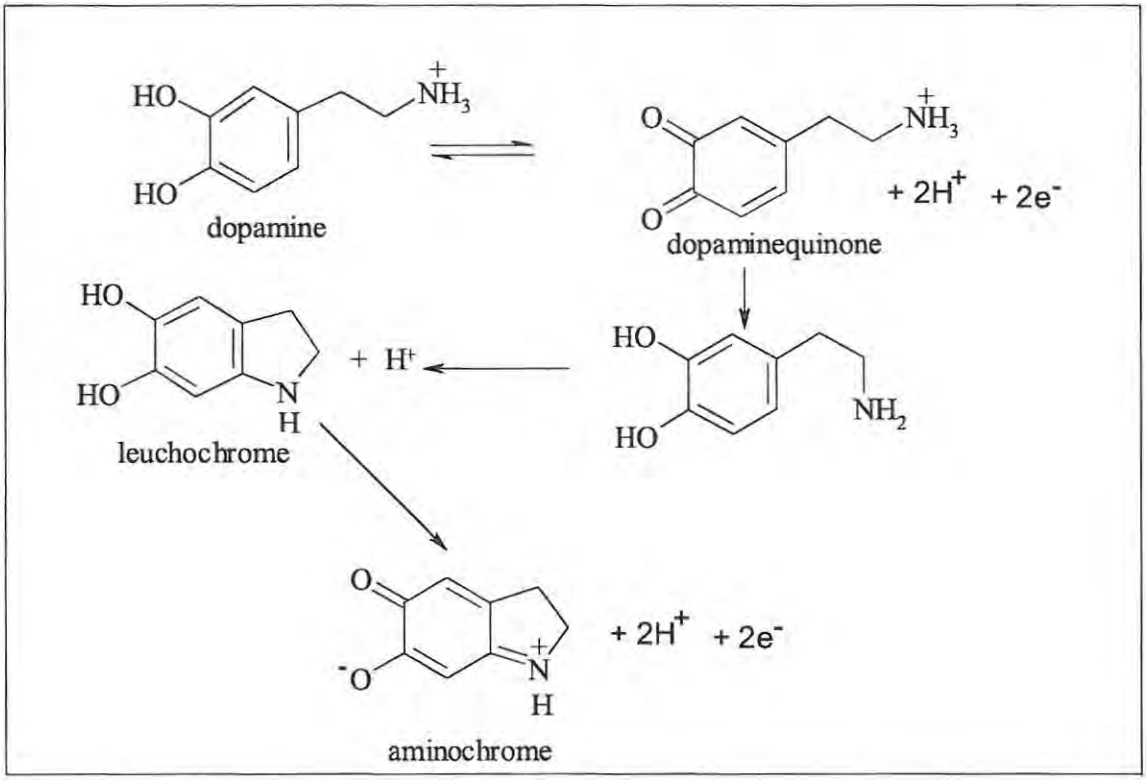

Scheme 4.2: Scheme of the oxidation of dopamine in alkaline media

4.2.1.1 Cyclic voltammetry of dopamine

Figure 4.3 shows the cyclic voltammogram of the same concentration of dopamine at an unmodified carbon paste electrode (CPE), curve a, and carbon paste electrode modified with iron (II) phthalocyanine (FePc-CPE), curve b, in pH 4 buffer. The anodic peak for dopamine was observed at about 0.4 V vs Ag*AgCl on unmodified CPE while the

cathodic peak was observed at 0.2V vs Ag|AgCl. With the FePc modified electrode, the anodic peak shifted to a less positive potential (0.32 V), Figure 4.3, curve b. The anodic currents were enhanced considerably in the presence of FePc. Since the cyclic voltammogram of the FePc-CPE in buffer alone did not show any significant peaks. The cyclic voltammetry changes observed in Figure 4.3 are due to the catalytic effects of FePc in the matrix of the electrode.

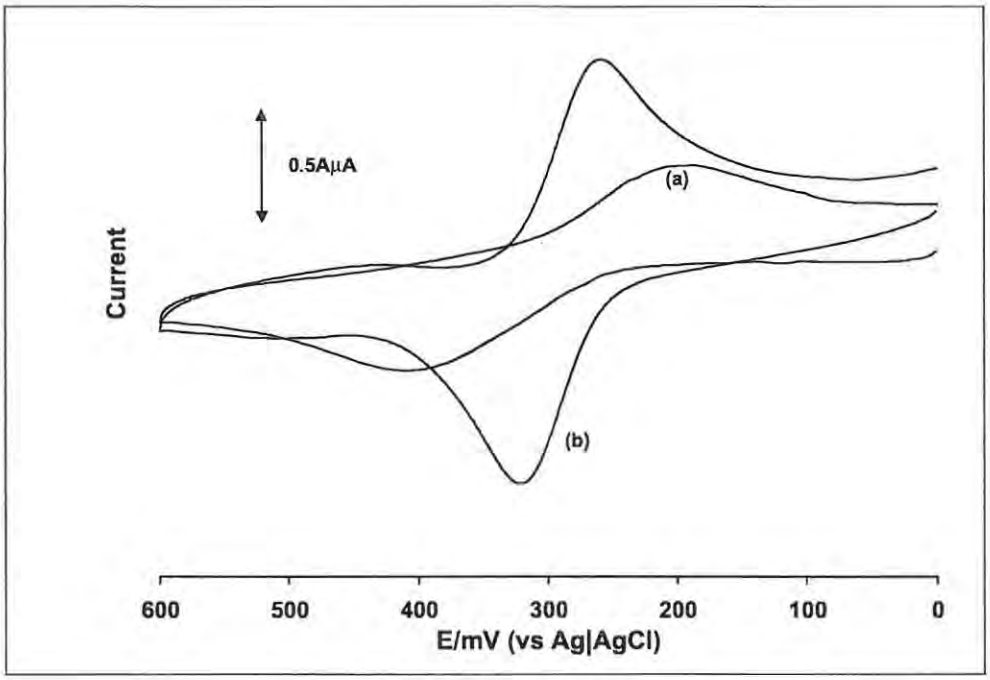

Figure 4.3: Cyclic voltammogram of $1.0x10^{-3}$ mol dm^{-3} DA at (a) CPE and (b) FePc-CPE, scan rate = 100 mV s^{-1}

The oxidation of dopamine is generally characterized by a high degree of irreversibility. Figure 4.3, curve b shows that modification of the CPE with FePc greatly improves the reversibility of the oxidation couple. The potential separation between the anodic and

cathodic peaks ()E_p) for dopamine at pH 4 was found to be 60 mV on FePc-CPE compared to 200 mV on unmodified CPE. This shows that the presence of FePc leads to a considerable improvement in the electrode kinetics. The CV of DA in pH 7.4 buffer is shown in Figure 4.4. A shift of the oxidation peak of DA to less positive potentials, by 100 mV, was observed, Figure 4.4, curve b. A)E_p of 80 mV was obtained, showing improvement in the reversibility of the couple.

Improved reversibility and a shift to less positive potentials, similar to Figures 4.3 and 4.4, were also observed when FeTSPc-CPE was employed for the detection of DA.

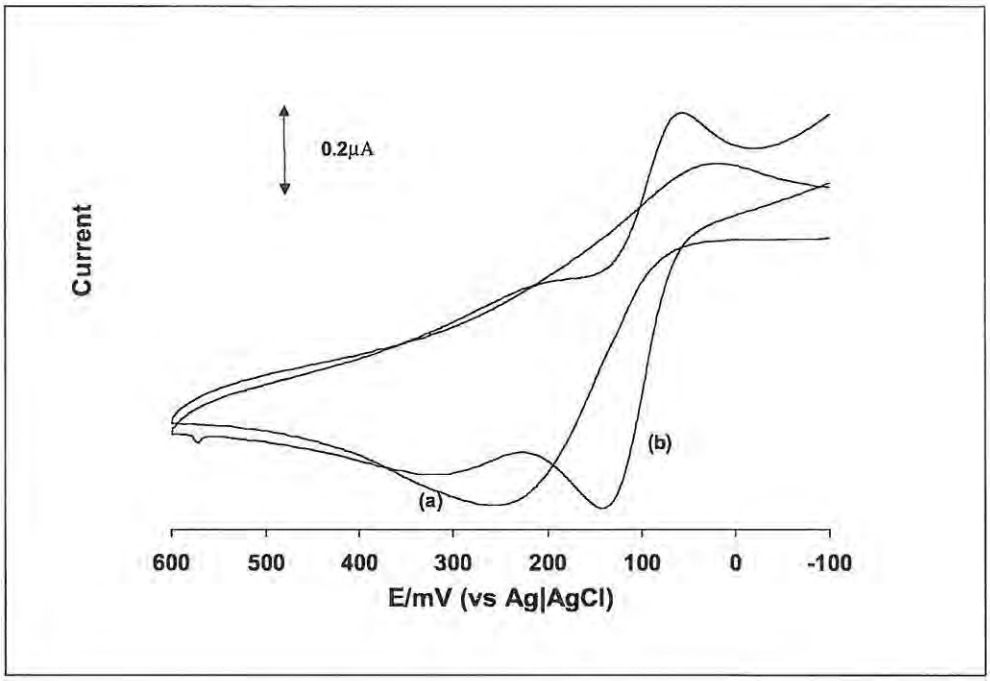

Figure 4.4: CV of $1.0x10^{-3}$ mol dm^{-3} DA in pH 7.4 buffer at (a) CPE (b) FePc-CPE. Scan rate = 100 mV s^{-1}

4.2.1.2 Osteryoung square wave voltammetry of dopamine

The charging current contribution to the background current limits the analytical determination of species using cyclic voltammetry to typical detection limits of 10^{-4} mol dm^{-3}. Thus Osteryoung square wave voltammetry (OSWV) was also employed.

The OSW voltammograms of $1.0x10^{-3}$ mol dm^{-3} DA in pH 7.4 buffer at CPE, curve a, and at FeTSPc-CPE, curve b, are shown in Figure 4.5. A large increase in the oxidation current of DA is observed on FeTSPc-CPE as well as a shift of the oxidation potential to less positive values. The large increase in current and the shift in oxidation potential are indicative of catalytic activity of $[FeTSPc]^{4-}$ towards the oxidation of DA. The same observation was made when FePc-CPE was employed for the oxidation of DA. The increase in current translates to a better sensitivity of the modified electrode towards the detection of DA.

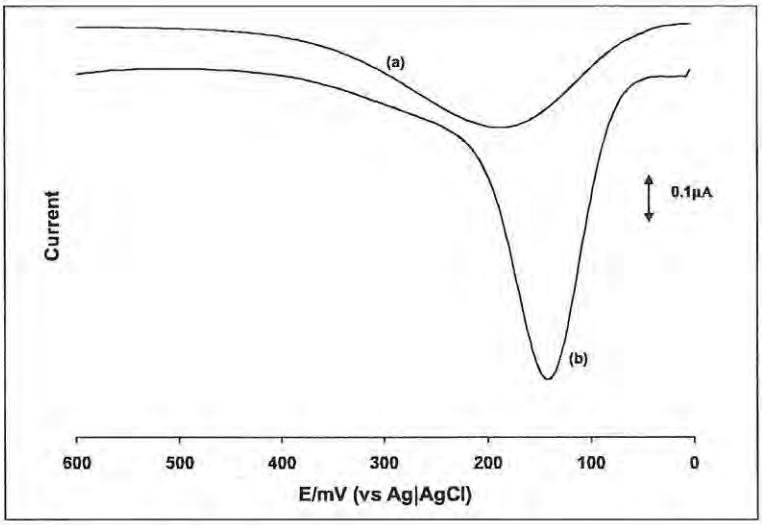

Figure 4.5: SWV of $1.0x10^{-3}$ mol dm^{-3} DA at (a) CPE (b) FeTSPc-CPE. Scan rate = 100 mV s^{-1}, pH 7.4

Both the FePc-CPE and FeTSPc-CPE were found to be stable towards the determination of DA since there was no significant decrease in anodic currents on consecutive scanning (20 scans) of the FePc-CPE or FeTSPc-CPE in DA. Also an increase in the peak current was obtained with an increase in scan rate as shown in Figure 4.6. A plot of the peak current versus the square root of scan rate was linear, the insert in Figure 4.6, showing that the oxidation of dopamine is a diffusion-controlled process at these electrodes.

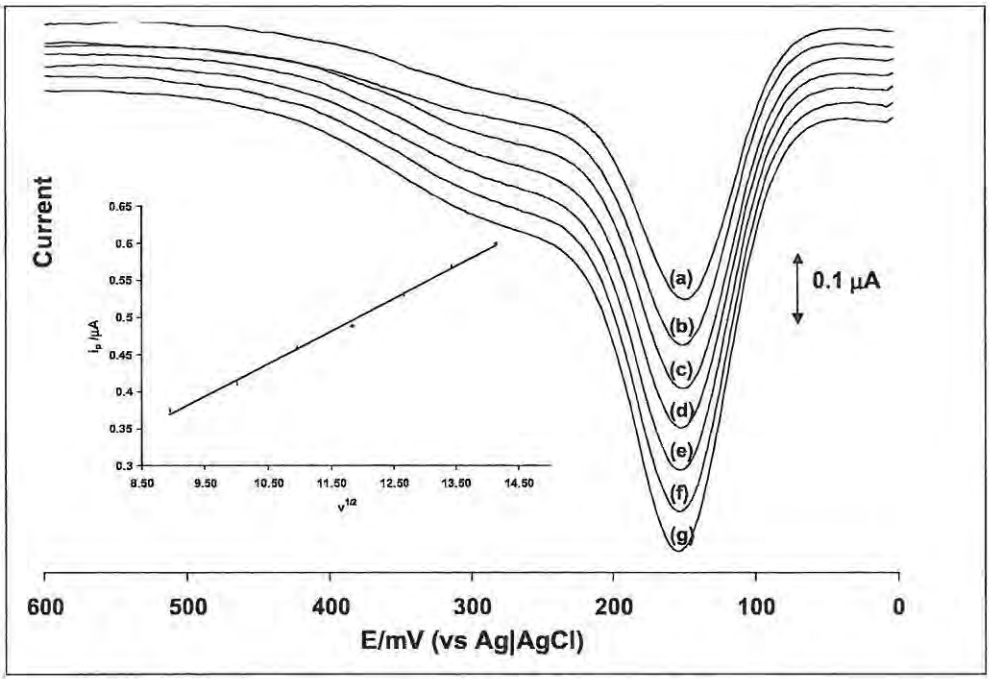

Figure 4.6: CVs of 1.0×10^{-4} mol dm^{-3} DA recorded at (a) 80 (b) 100 (c) 120 (d) 140 (e) 160 (f) 180 (g) 200 mV s^{-1} at FeTSPc-CPE. Insert is the plot of peak current against the square root of scan rate.

A linear increase in the oxidation current with an increase in the concentration of DA, Figure 4.7, was observed at these electrodes for concentrations ranging from $1x10^{-6}$ to $1.5x10^{-5}$ mol dm^{-3}. A regression equation of $y = 0.0111x + 1.3x10^{-8}$, where y is the peak height and x is the concentration of DA, and a correlation coefficient of 0.998 was obtained for the linear plot. A detection limit of 1.0×10^{-6} mol dm^{-3} was obtained at the modified electrode.

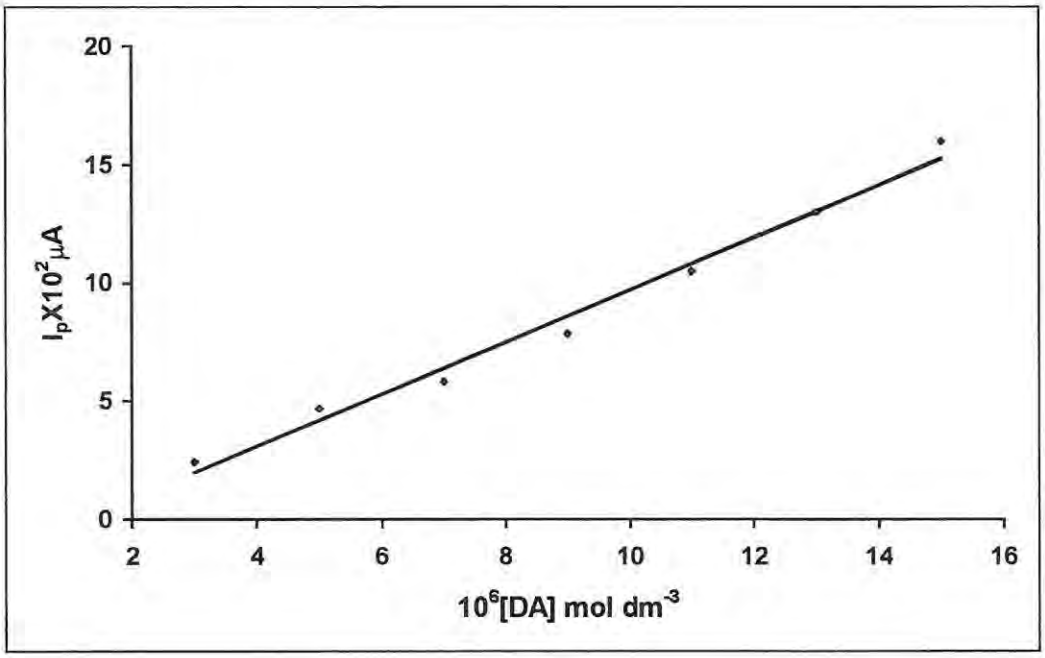

Figure 4.7: Plot of peak current with concentration of DA at FeTSPc-CPE

4.2.2 Serotonin

The OSW voltammogram of $1.0x10^{-3}$ mol dm^{-3} serotonin (5-HT) in pH 7.4 buffer at CPE showed a broad oxidation peak centered on 0.36V vs Ag|AgCl, Figure 4.8 curve a. When

FePc-CPE or FeTSPc-CPE was employed, Figure 4.8 curve b, the SWV was observed as a sharp and greatly enhanced peak at 0.32V.

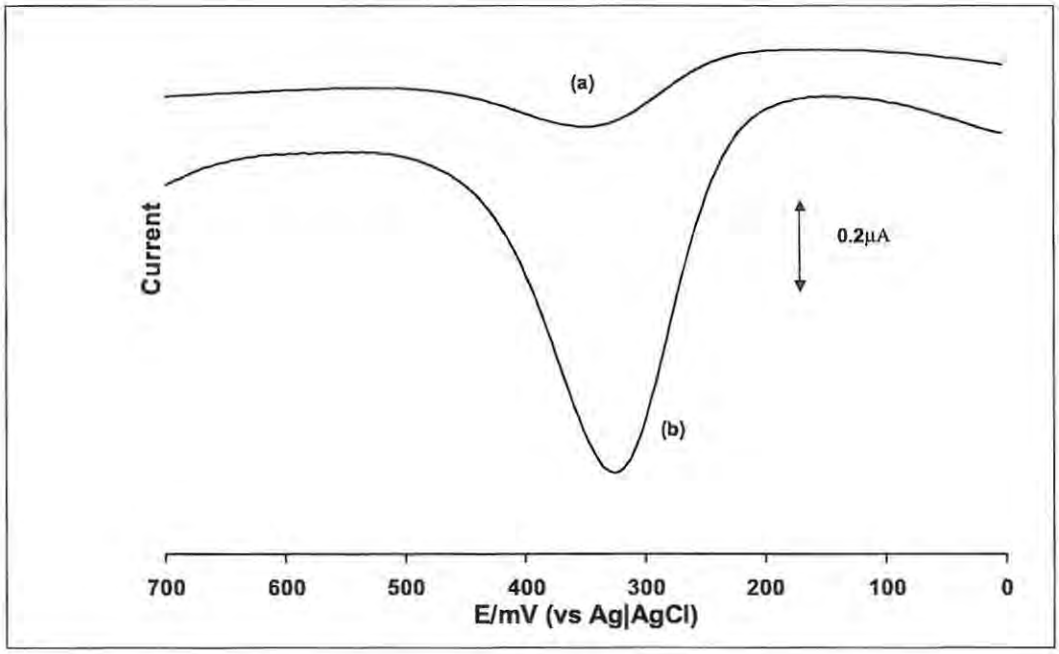

Figure 4.8: OSWV of $1.0x10^{-3}$ mol dm^{-3} 5-HT at (a) CPE and (b) FeTSPc-CPE. Scan rate = 100 mV, pH = 7.4.

The oxidation potential has shifted by 40mV to less positive values when compared to the unmodified CPE. The shift of the oxidation potential to less positive values and the large increase in oxidation current again signifies catalytic activity of the electrodes towards the determination of 5-HT, hence a better sensitivity of the modified electrode towards the detection of serotonin than the unmodified electrode.

As noted for DA above, the electrodes were found to be stable towards the determination of 5-HT since there was no significant decrease in anodic currents on consecutive scanning (20 scans) of the electrodes in 5-HT. Also plots of the peak currents versus the

square root of scan rate were linear showing that the oxidation of 5-HT is a diffusion-controlled process at these electrodes. A linear increase in the oxidation current with an increase in the concentration of 5-HT was also observed at the electrodes, Figure 4.9. A regression equation of $y = 0.0086x + 1.6x10^{-8}$ and a correlation coefficient of 0.998 were obtained for the linear plot. A detection limit of $1.8x10^{-6}$ mol dm^{-3} was obtained at the modified electrode.

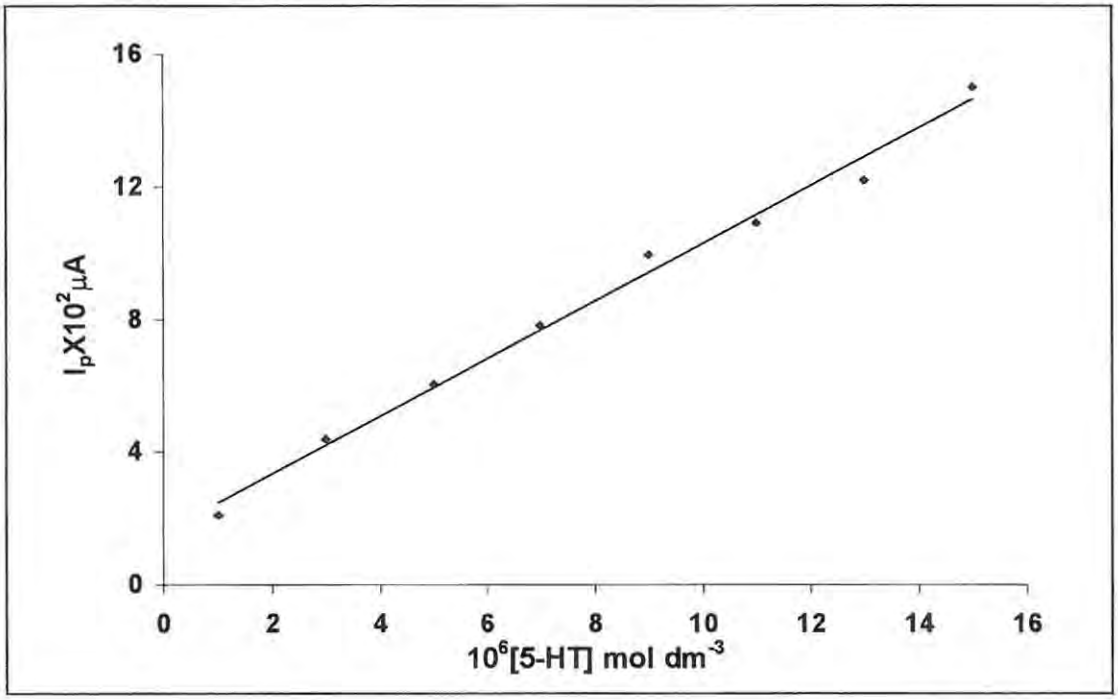

Figure 4.9: Plot of peak current with the concentration of 5-HT at FeTSPc-CPE

4.2.3 Histamine

There was no current observed for the oxidation of histamine at the FeTSPc-CPE. As discussed above, histamine is capable of oxidizing $[Fe^{II}TSPc]^{4-}$ forming $[Fe^{III}TSPc]^{3-}$ such that the regeneration of Fe^{II} species required for the catalytic cycle is prevented.

4.2.4 Mechanism of electrocatalytic activity

The accepted mechanism for the catalytic oxidation using MPc complexes is the oxidation of the MPc complex followed by electron transfer from the species to be catalysed to the oxidized MPc species. MPc complexes containing an electroactive central metal such as FePc or CoPc complexes generally show much better catalytic activity than MPc complexes with ring based redox processes such as NiPc and CuPc. In order to elucidate the mechanism of catalytic oxidation of DA and 5-HT, $[Fe^{II}TSPc]^{4-}$ was chemically oxidized (using nitrosonium tetrafluoroborate) to the $[Fe^{III}TSPc]^{3-}$ species and DA added to the solution. The spectral changes shown in Figure 4.10 were obtained.

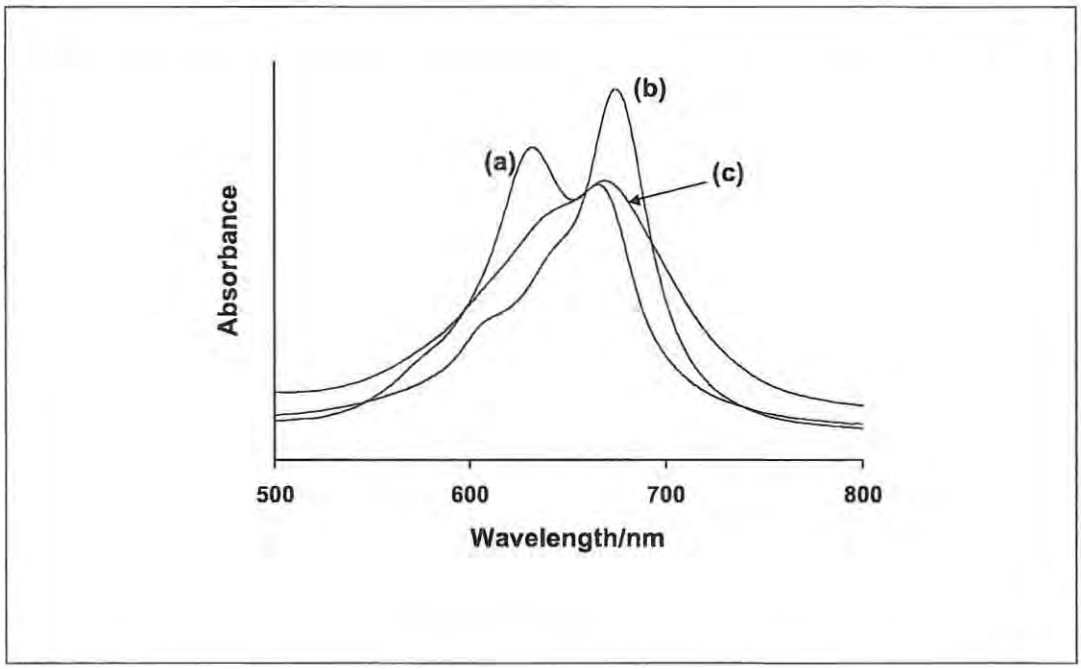

Figure 4.10: Electronic absorption spectra of (a) $[Fe^{II}TSPc]^{4-}$, (b) $[Fe^{III}TSPc]^{3-}$, (c) $[Fe^{III}TSPc]^{3-}$ following the addition of $5.6x10^{-4}$ mol dm^{-3} DA, pH = 7.4

The Q band region of $[Fe^{II}TSPc]^{4-}$ consists of two peaks due to the monomeric (665 nm) and dimeric (633 nm) species, as already discussed in Section 3.1.1. The spectra due to the $[Fe^{III}TSPc]^{3-}$ species consists of a single Q band at 673 nm, again similar to the change observed upon the electrochemical oxidation of $Fe^{II}TSPc$ in Section 3.1.4. The final spectrum obtained after addition of DA to $[Fe^{III}TSPc]^{3-}$ shows the regeneration of the spectrum consisting of the monomeric and dimeric peaks as observed for $[Fe^{II}TSPc]^{4-}$, Figure 4.10c, though the peaks due to the monomeric species is more pronounced than that due to the dimeric species. The spectral changes shown in Figure 4.10 thus suggest that the $[Fe^{III}TSPc]^{3-}$ species is reduced to the $[Fe^{II}TSPc]^{4-}$ species in the presence of DA. The proposed mechanism for $[FeTSPc]^{4-}$ catalysed oxidation of DA may thus be represented by equations 4.1 to 4.3:

$$[Fe^{II}TSPc]^{4-} + DA \quad [(DA)Fe^{II}TSPc]^{4-} \qquad \textbf{4.1}$$

$$[(DA)Fe^{II}TSPc]^{4-} \quad [(DA)Fe^{III}TSPc]^{3-} + e^{-} \qquad \textbf{4.2}$$

$$[(DA)Fe^{III}TSPc]^{3-} \quad DA^{+} + [\,Fe^{II}TSPc]^{4-} \qquad \textbf{4.3}$$

A similar mechanism represented by equation 4.4 to 4.6 is proposed for the oxidation of 5-HT at the modified electrode.

$$[Fe^{II}TSPc]^{4-} + 5\text{-}HT \rightarrow [(5\text{-}HT)Fe^{II}TSPc]^{4-} \qquad \textbf{4.4}$$

$$[(5\text{-}HT)Fe^{II}TSPc]^{4-} \rightarrow \quad [(5\text{-}HT)Fe^{III}TSPc]^{3-} + e^{-} \qquad \textbf{4.5}$$

$$[(5\text{-}HT)Fe^{III}TSPc]^{3-} \rightarrow \quad 5\text{-}HT^{+} + [Fe^{II}TSPc]^{4-} \qquad \textbf{4.6}$$

Also it would be expected that a similar mechanism occurs when FePc is employed as a catalyst. Equations 4.2 and 4.5 describe the electrochemical step, whereas equations 4.3

and 4.6 result from electron transfer from DA and 5-HT to the $Fe^{III}TSPc$ species respectively.

4.2.5 Detection of dopamine in the presence of serotonin

Since DA and 5-HT coexist *in vivo*, it is important that the modified electrode is capable of detecting them simultaneously, without significant interference. Figure 4.11 shows the OSW voltammogram of a mixture of DA and 5-HT on unmodified CPE and on FeTSPc-CPE, in pH 7.4 buffer.

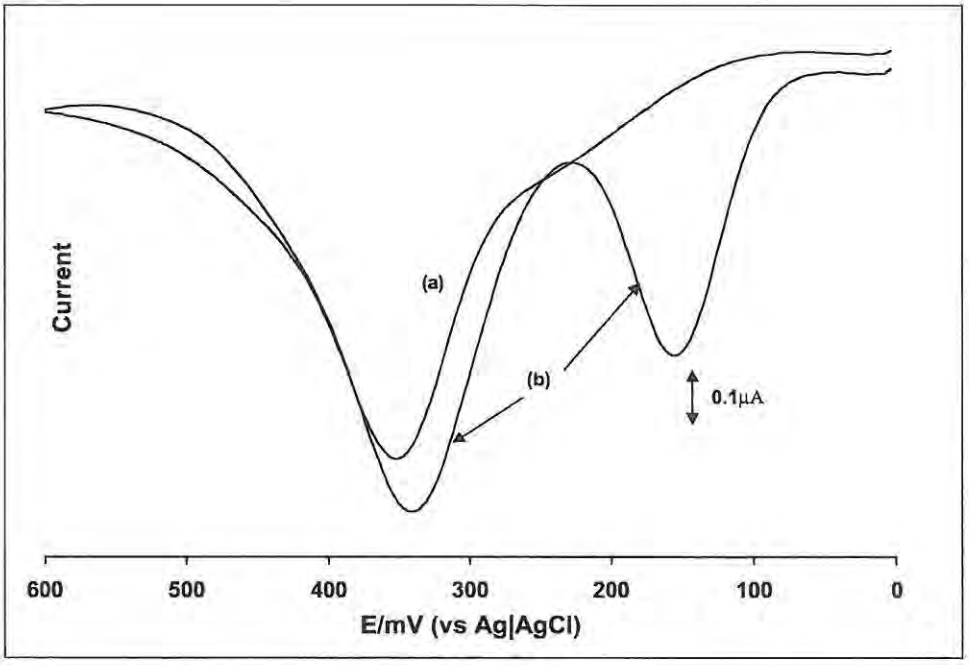

Figure 4.11: OSWV of a mixture of $4.0x10^{-6}$ mol dm^{-3} DA and $5.0x10^{-6}$ mol dm^{-3} 5-HT at (a) CPE and (b) FeTSPc-CPE. Scan rate = 100 mV s^{-1}, pH = 7.4

On the unmodified CPE only one peak is observed for the mixture of DA and 5-HT, which means that an overlap of the oxidation currents due to dopamine and serotonin

occurs at the unmodified electrode, Figure 4.11 curve a, but a separation of the peaks is observed on FeTSPc-CPE, Figure 4.11 curve b. This separation was also observed on FePc-CPE, but was not observed on CPE modified with NiPc, CoPc, CoTSPc or NiTSPc. The oxidation potentials of 5-HT and DA on FeTSPc-CPE do not change from those of the individual components showing that these species do not interfere with each other at the concentrations employed. A large increase in the oxidation currents for both DA and 5-HT was observed on FeTSPc-CPE when compared to unmodified CPE, Figure 4.11. The FeTSPc-CPE was found to be stable towards the determination of DA and 5-HT in that no significant decrease in the anodic currents on consecutive scanning (> 10 scans) of the FeTSPc-CPE in a mixture of DA and 5-HT. Also plots of peak currents versus the square root of scan rate were linear for both DA and 5-HT in the mixture, confirming diffusion-controlled process.

The oxidation currents of both DA and 5-HT increased with an increase in concentration, Figure 4.12. Calibration plots obtained for both DA and 5-HT from the data represented by Figure 4.12 are shown in Figure 4.13. The slope of the calibration curve of DA in the presence of 5-HT (or vise versa), Figure 4.13, was the same as that obtained for the species alone, confirming that no interaction occurs between 5-HT and DA.

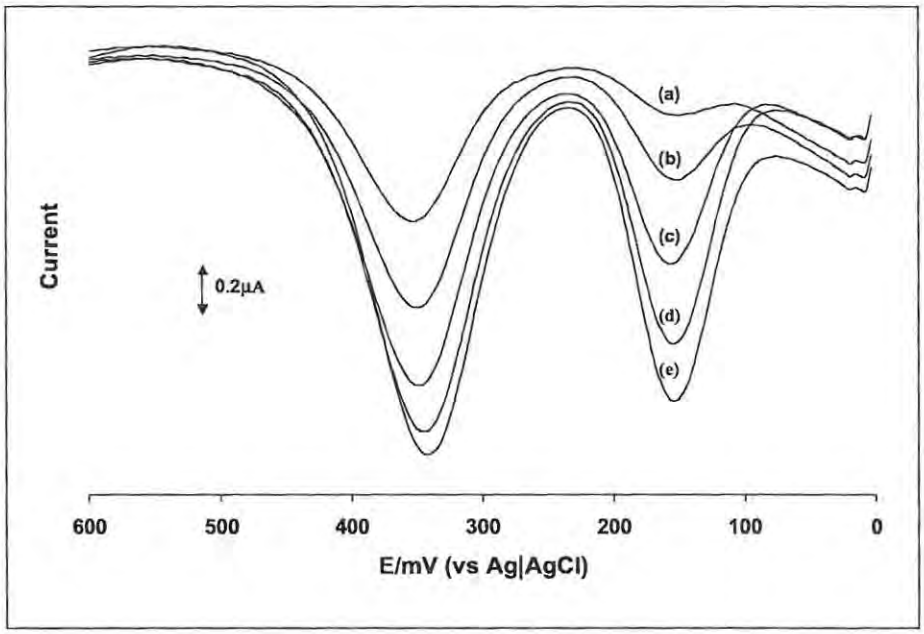

Figure 4.12: OSWV of a mixture of [DA] = [5-HT] = (a) $2.0x10^{-6}$ (b) $4.0x10^{-6}$ (c) $6.0x10^{-6}$ (d) $8.0x10^{-6}$ (e) $1.0x10^{-5}$ mol dm^{-3} at FeTSPc-CPE, pH = 7.4

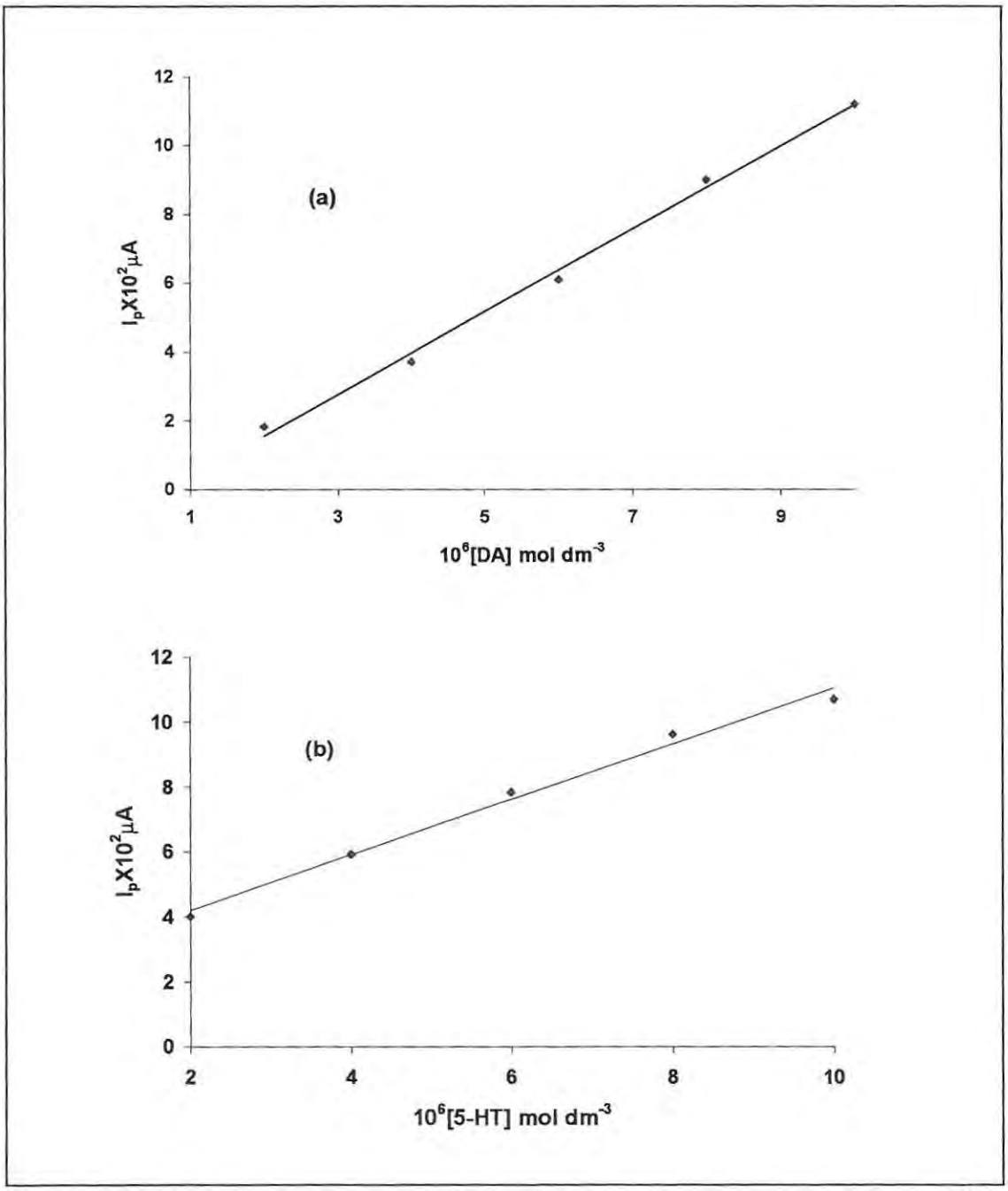

Figure 4.13: Calibration plots obtained for (a) DA and (b) 5-HT in a mixture at FeTSPc-CPE

4.2.6 Elimination of interference from ascorbic acid

As discussed in Section 1.4.4.2, the major problem associated with the use of electrochemical techniques for the analysis of neurotransmitters is the presence of easily oxidized molecules in the extracellular fluid (ECF) most especially ascorbic acid (AA). AA is present in concentrations 10^2-10^3 times higher than the neurotransmitters and gets oxidized at similar oxidation potentials[40,84,85,130,138] resulting in overlapped voltammetric response, thereby posing the problem of interference. The ability of the modified electrode to prevent the interference from AA is a desirable characteristic. Figure 4.14 shows the OSW voltammetry of ascorbic acid on unmodified CPE, curve a, FePc-CPE, curve b and FeTSPc-CPE, curve c.

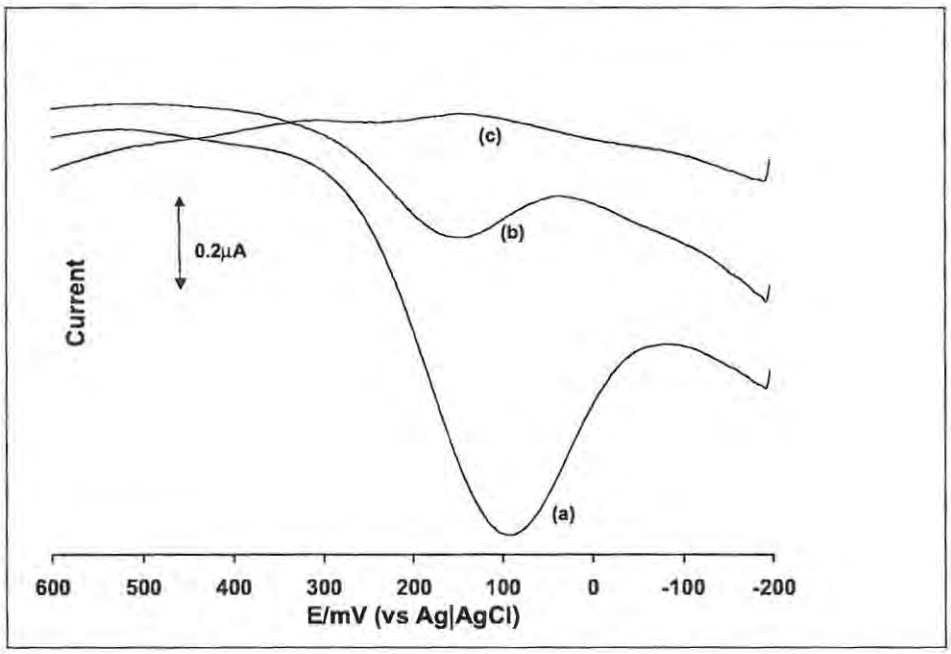

Figure 4.14: OSWV of $1.0x10^{-3}$ mol dm^{-3} AA at (a) CPE, (b) FePc-CPE and (c) FeTSPc-CPE, pH 7.4

FePc-CPE caused a displacement of the oxidation potential of ascorbic acid to more positive values (by 50 mV) and a large decrease in the oxidation currents showing that FePc decreases the ability of CPE to detect ascorbic acid, but does not completely deactivate the electrode towards the detection of AA. On the other hand no oxidation peak for AA was observed on FeTSPc-CPE, showing that this electrode is not sensitive to AA. There have been records of the use of carbon paste electrode modified with stearic acid for the determination of DA in the presence of a large excess of AA.[38] The negative charge imparted on the electrode by the stearate ions repelled the negatively charged ascorbate ions away from the electrode. In a similar manner, the observed deactivation of the CPE when modified with $[FeTSPc]^{4-}$ towards the detection of AA could be a result of the unfavourable interaction between the negatively charged AA and the negative charge on the FeTSPc-CPE. Similar disappearance in the AA oxidation peak was observed when negatively charged $[NiTSPc]^{4-}$ and $[CoTSPc]^{4-}$ were used to modified the CPE, but not when CoPc or NiPc were employed.

Analysis of DA in the presence of tenfold concentration of AA on FeTSPc-CPE gave an OSW voltammogram similar to that of DA alone, already shown in Figure 4.5 above. The slope of the calibration curve obtained for DA in the presence of AA was nearly the same as that obtained for DA alone. Similarly, AA had no effect on the analysis of 5-HT as evidenced by the fact no change in slope of the calibration curve for 5-HT was observed in the presence of a 10-fold excess of AA, showing that FeTSPc-CPE is capable of

eliminating the problem of interference posed by AA in the electrochemical analysis of DA and 5-HT.

4.2.7 Simultaneous determination of dopamine and serotonin in the presence of ascorbic acid

The OSW voltammogram of a mixture of DA and 5-HT in the presence of ten-fold AA on FeTSPc-CPE is shown in Figure 4.15. The oxidation peaks overlap on unmodified CPE, curve a, but the peaks separate for DA and 5-HT on FeTSPc-CPE, curve b.

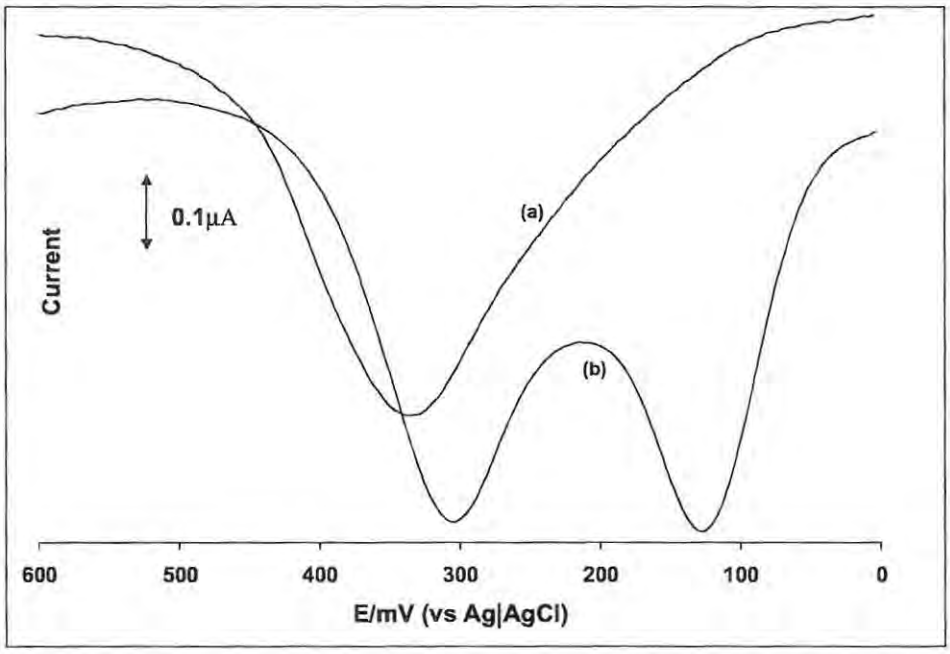

Figure 4.15: OSWV of [DA] = [5-HT] = 1.0×10^{-4} mol dm^{-4} [AA] = 1.0×10^{-3} mol dm^{-3} at (a) CPE (b) FeTSPc-CPE, pH = 7.4

The peak for AA would be very close to that of DA, but as discussed above (Section 4.2.6), this peak is excluded when the FeTSPc-CPE is employed. Potentials for DA and

5-HT in the presence of AA (Figure 4.15) are at the values obtained for DA and 5-HT individually, showing that AA does not affect the detection of these species. The oxidation currents for DA and 5-HT in the presence of a tenfold concentration of AA increased with increasing amounts of DA and 5-HT, as shown in Figure 4.16.

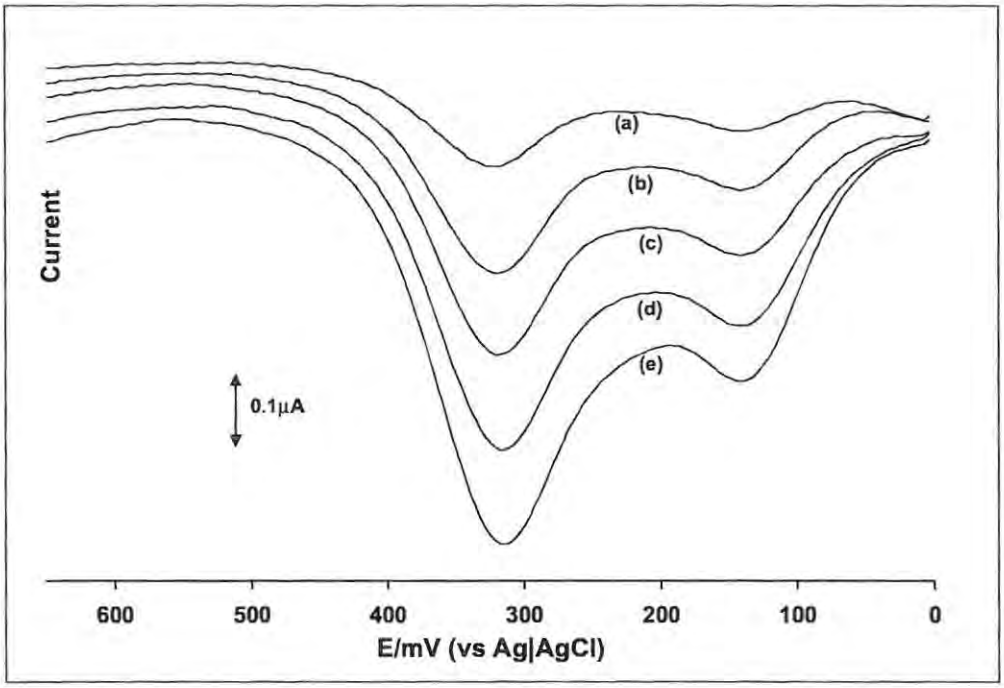

Figure 4.16: OSWV showing increase in peak current with increase in concentration of DA and 5-HT at FeTSPc-CPE in the presence of ten-fold AA. [DA] = [5-HT] = (a) $1.0x10^{-6}$ (b) $3.0x10^{-6}$ (c) $5.0x10^{-6}$ (d) $7.0x10^{-6}$ (e) $9.0x10^{-6}$ mol dm^{-3}, pH = 7.4

The calibration curves for DA and 5-HT in the mixture were linear, Figure 4.17, with slopes similar to those obtained for the individual DA and 5-HT, confirming that AA has no effect on the mixture of DA and 5-HT.

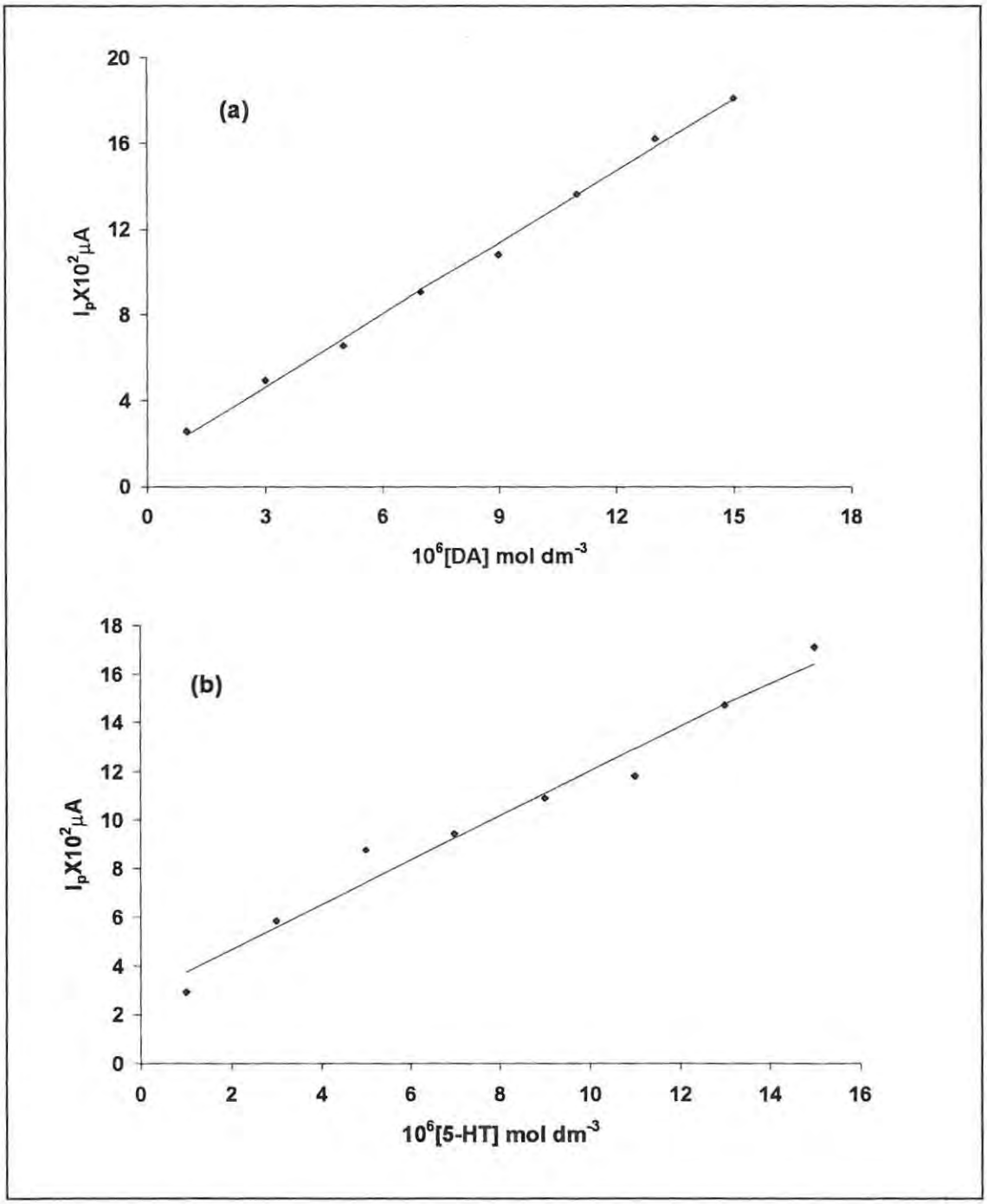

Figure 4.17: Calibration plots obtained for (a) DA and (b) 5-HT in a mixture in the presence of ten-fold excess of AA at FeTSPc-CPE

The ability to measure DA selectively in the presence of AA is still an important goal in biological and chemical research. As discussed in Section 1.4.4.2, one approach is to pre-coat the catalyst modified carbon electrodes with negatively charged polymers such as Nafion®[40] that repel the anionic ascorbic acid while attracting the positively charged ions. This approach suffers from some drawbacks such as non-uniform thickness of the film and poor reproducibility. Also the presence of high concentrations of other cations other than DA has been shown to affect the electrochemical measurement as they saturate the negative sites of the polymer.[149] The modification of the CPE by negatively charged catalysts reported in this work, avoids the use of Nafion® coating on the catalyst-modified electrode. The ability of the $[FeTSPc]^{4-}$ modified CPE to simultaneously detect both DA and 5-HT, while eliminating the interfering effects of ascorbic acid is an important observation since such electrodes have a potential to be employed in fast scan cyclic voltammetry (FSCV) systems without the need for prior separation of the neurotransmitters. A detection limit of the order of 10^{-6} mol dm^{-3} for both DA and 5-HT was obtained at the FeTSPc-CPE without significant interference in the presence of ten-fold excess ascorbic acid.

4.2.8 Electrocatalytic activity of other metallophthalocyanine complexes

Electrocatalytic activity (towards the oxidation of DA and 5-HT) of the metallophthalocyanine complexes of nickel (NiPc) and cobalt (CoPc) as well as other substituted FePc complexes was investigated. The report presented below discusses only the situation where the MPc complexes have been used to modify CPEs. GCEs were also modified with these MPc complexes by dip-dry, drop-dry and electrodeposition/electropolymerization methods but the results obtained were not promising.

4.2.8.1 Comparison of the catalytic activities of substituted iron phthalocyanine complexes

The electrocatalytic properties of MPcs are known to be affected by the presence of substituents in the axial and/or peripheral positions because of the electron withdrawing or donating properties of the substituents.[293] The effects of different axial and peripheral substituents on the electrocatalytic activity of FePc towards the detection of DA and 5-HT were studied. The substituted FePc complexes were used to modify CPEs.

Hexadecachloro iron (II) phthalocyanine [$FePc(Cl)_{16}$] modified CPE greatly increased the oxidation current of DA and 5-HT and shifted the oxidation potentials to less positive values as shown in Figure 4.18. However, the electrode was not stable for the detection of DA or 5-HT as the oxidation current decreased steadily with scan number. The decrease in oxidation current may be due to the irreversible binding of the oxidation product to the metal center.

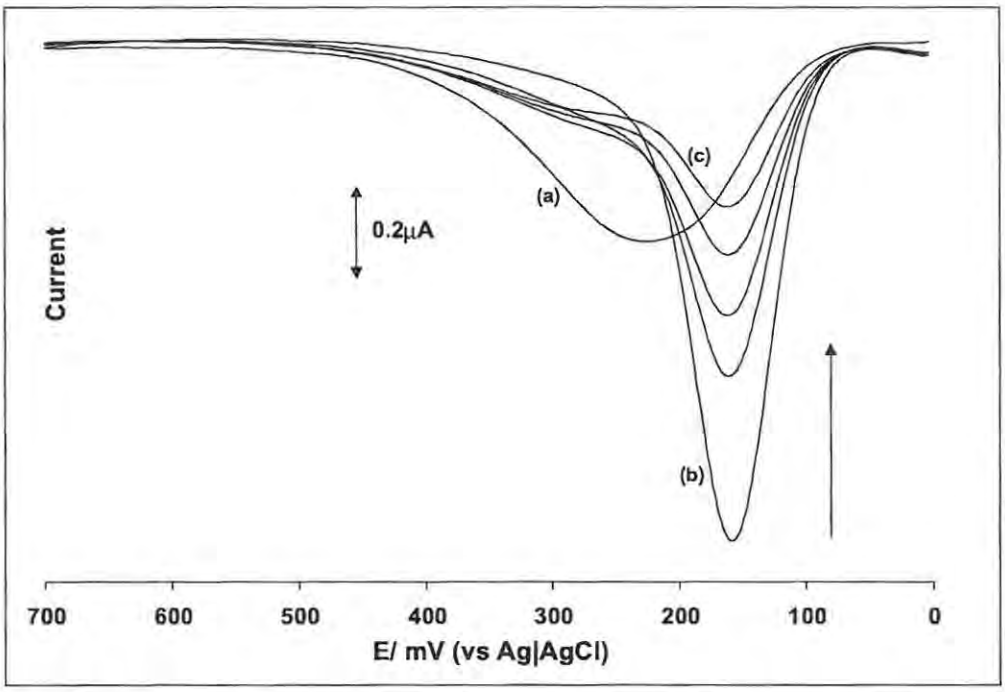

Figure 4.18: Decrease in peak current of $1x10^{-4}$ mol dm^{-3} DA with scan number at $FePc(Cl)_{16}$ modified CPE (a) CPE (b) $FePc(Cl)_{16}$-CPE, scan number 1, (c) scan number 5, pH = 7.4

Iron (II) tetranitrophthalocyanine ($FePc(NO_2)_4$) modified CPE did shift the oxidation potential of DA and 5-HT to less positive values but the oxidation current observed on this electrode was smaller than that of the unmodified electrode. The CPE modified with iron (II) tetraamino phthalocyanine ($FePc(NH_2)_4$) showed some catalytic activity towards the detection of DA and 5-HT by shifting the oxidation potential to less positive values and increasing the oxidation currents, shown in Figure 4.19, though high background currents were obtained.

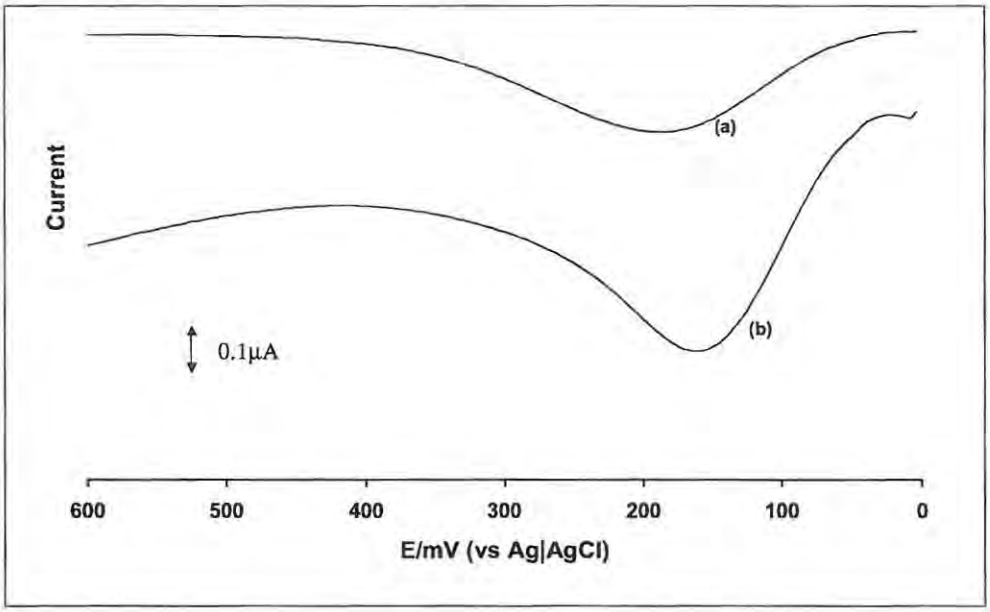

Figure 4.19: OSWV of $1.0x10^{-3}$ mol dm^{-3} DA at (a) CPE (b) $FePc(NH_2)_4$-CPE

The high background current is not desirable for the detection and quantification of substrates at low concentration levels, so this electrode was not considered for use any further.

Bis (axial) pyridine iron (II) phthalocyanine ($(py)_2FePc$) and bis (axial) cyano phthalocyanine ($(CN)_2FePc$) modified CPE caused a increase in the oxidation potential as well as a decrease in the oxidation current of DA compared to the current and the potential at unmodified electrodes. Whereas bis (axial) imidazole iron (II) phthalocyanine ($(im)_2FePc$) modified CPE caused both an increase in oxidation current and a decrease in oxidation potential (similar to Figure 4.18). The oxidation current however decreased

steadily with scan number. The smaller current observed on both $(py)_2FePc$ and $(CN)_2FePc$ modified electrodes may be explained by the fact that both cyanide and pyridine are more strongly coordinated to the active metal center than imidazole. There has been a report on the correlation between the electrocatalytic activity of the central metal atom of the MPc macrocycle and the ability to reversibly bind the substrate as an axial ligand.[294] The strong bonding between cyanide and pyridine and FePc may have prevented the DA or 5-HT from reversibly binding to the active Fe center, resulting in the smaller currents observed with electrodes modified with these complexes.

Modifying a CPE with iron (II) tetratertiarybutyl phthalocyanine ($FePc(t\text{-}Bu)_4$) prevented the flow of current through the electrode which precluded a comparison with the unmodified electrode. The bulky, non-conducting tertiary butyl group may be responsible for the loss of electrical contact in the electrodes modified with $FePc(t\text{-}Bu)_4$.

A summary of the observations recorded for the modification of CPE with some substituted FePc complexes is shown in Table 4.1.

Table 4.1: Summary of electrocatalytic activity observed at substituted FePc modified CPE

MPc	Observation	Limitations
$FePc(NH_2)_4$	decreases E_p, increased i_p,	high background current
$FePc(Cl)_{16}$	decreased E_p, increased i_p,	i_p decreased with scan number, unstable.
$FePc(NO_2)_4$	decreased E_p, decreased i_p	i_p decreased with scan number, unstable.
$(py)_2FePc$	increased E_p, decreased i_p	i_p decreased with scan number, unstable.
$(im)_2FePc$	decreased E_p, increased i_p	i_p decreased with scan number, unstable
$(CN)_2FePc$	increased E_p, decresed i_p	i_p decreased with scan number, unstable.
$FePc(t\text{-}Bu)_4$	no current flow	no current flow

4.2.8.2 Cobalt phthalocyanine complexes

The voltammograms obtained when CoPc was used to modify CPE had a very high background current compared to the unmodified electrode. Although the oxidation potential and the magnitude of the current remained the same as obtained with CPE, the increased background current is not desirable, as this will prevent detection at low concentrations. Also, as there was no improvement in the current densities or a shift of the oxidation potential to less positive values, the advantage of modifying the electrode with CoPc is not apparent. CPE modified with cobalt tetrasulfophthalocyanine $[CoTSPc]^{4-}$ gave voltammograms similar to the one obtained using CoPc. However, the electrode could suppress the current due to AA. Cobalt tetraamino phthalocyanine, $CoPc(NH_2)_4$, modified electrodes caused only a slight decrease in oxidation potential and an insignificant increase in oxidation current. A very large background current was observed at this electrode.

The lack of catalytic activity of the CoPc complexes towards the oxidation of DA and 5-HT, as evidenced by lack of increase in oxidation currents or lack of decrease in oxidation potential when compared to unmodified CPE is surprising. CoPc contains a redox active central metal and is expected to show similar behaviour as FePc. It is important however to note the observation of the $Co^{III}Pc/Co^{II}Pc$ couple is dependent on the nature of solvents, with donor solvents or the presence of ions in solution favouring the formation of $Co^{III}Pc$ species whereas non-donor solvents favour $Co^{II}Pc$, resulting in ring-based rather than metal-based oxidations.[214] Water is a relatively weak ligand for the stabilization of $Co^{III}Pc$ species.[280]

4.2.8.3 Nickel phthalocyanine complexes

CPEs modified with nickel phthalocyanine (NiPc), nickel tetrasulfophthalocyanine, $[NiTSPc]^{4-}$ or nickel tetraamino phthalocyanine, $NiPc(NH_2)_4$, did not produce significant increases in the oxidation currents of both DA and 5-HT. A general increase in background current was observed. The absence of catalytic activity is anticipated because NiPc complexes undergo only ring-based redox processes at potentials way out of the region where catalytic activity towards either DA or 5-HT is expected. The use of $Ni^{II}Pc(NH_2)_4$ electropolymerized onto GCE for the electrocatalytic oxidation of DA has been reported.[40] However, it was the polymeric form on the electrode surface that was electroactive towards the oxidation of DA, it was reported that the monomer did not show a catalytic activity.[40] This implies that the electrochemical property of the polymeric film is quite different from that of the monomeric species. It is the monomeric form of $Ni^{II}Pc(NH_2)_4$ that was used in this study, hence the absence of electrocatalytic activity.

4.3 Electrochemical studies of the interaction between histamine and iron (II) tetrasulfophthalocyanine

As explained above, $Fe^{II}TSPc$ could not catalyse the oxidation of histamine since it is oxidized to $Fe^{III}TSPc$ in the presence of histamine. The nature of the interaction of histamine and FeTSPc deserves a closer look electrochemically.

The addition of histamine to solution of $[Fe^{II}TSPc]^{4-}$ gave rise to changes in the cyclic voltammogram of $Fe^{II}TSPc$. This change in CV means that the species being electrolyzed is different from the original complex in solution. This confirms the coordination of histamine to $[Fe^{II}TSPc]^{4-}$ in solution. Figure 4.20 compares the cyclic voltammogram of $[Fe^{II}TSPc]^{4-}$, recorded at a GCE in pH 7.4 buffer, with that of the $[Fe^{III}TSPc]^{3-}$ - histamine complex. The oxidation of $Fe^{II}TSPc$ and the formation of $Fe^{III}TSPc$-histamine complex has been discussed above (Section 3.2.3)

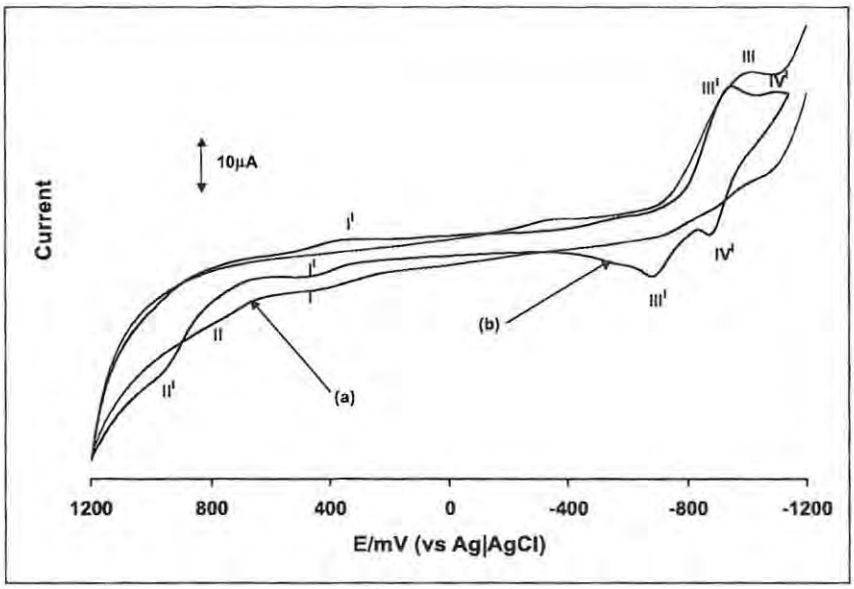

Figure 4.20: CV of (a) $[FeTSPc]^{4-}$ and (b) FeTSPc-histamine complex. Scan rate = 100 mV s^{-1}

The voltammograms were recorded following addition of two-fold excess histamine to the solution of $[Fe^{II}TSPc]^{4-}$ and allowing enough time for the complex to form, as judged by changes in the UV/vis spectra. There was a general enhancement of the currents for the $[Fe^{III}TSPc]^{3-}$ - histamine complex. The peak labelled **I** for $[Fe^{II}TSPc]^{4-}$ alone did not show a return peak in the absence of histamine but the $[Fe^{III}TSPc]^{3-}$ - histamine complex couple, $\mathbf{I^I}$, was found to be quasi-reversible. A relatively strong irreversible oxidation peak was observed for the $[Fe^{III}TSPc]^{3-}$ - histamine complex, process $\mathbf{II^I}$. Processes $\mathbf{I^I}$ and $\mathbf{II^I}$ were observed at $E_{½} = 0.40$ and $E_p = 0.95$ V vs Ag|AgCl. Two reduction couples were observed, and were more reversible than the reduction process in the absence of histamine. The reduction couples for the $[Fe^{III}TSPc]^{3-}$ - histamine complex were observed at –0.81 V and –0.98 V vs Ag|AgCl (labelled $\mathbf{III^I}$ and **IV** in Figure 4.20). No peaks were observed for histamine in this potential region, hence the observed cyclic voltammetry peaks are due to the $[Fe^{III}TSPc]^{3-}$ - histamine complex. No new peaks were observed on second and subsequent scans. The cyclic voltammogram for the $[Fe^{III}TSPc]^{3-}$ - histamine complex shows more intense peaks (Figure 4.20 curve b) than observed without histamine, Figure 4.20 curve a. This is due to increased solubility of the $[Fe^{III}TSPc]^{3-}$ - histamine complex compared to the $[Fe^{II}TSPc]^{4-}$ species. Also the $[Fe^{III}TSPc]^{3-}$ - histamine is monomeric. The observation of more reversible processes for the $[Fe^{III}TSPc]^{3-}$ - histamine complex when compared to the processes for $[Fe^{II}TSPc]^{4-}$ species in the absence of histamine, may be explained by the fact the oxidation of the latter occurs on the aggregated species, whereas it is the monomeric species which gets oxidized for the $[Fe^{III}TSPc]^{3-}$ - histamine complex.

The currents for all peaks increased with increase in the scan rate, Figure 4.21. A plot of the peak current against the square root of scan rate for data shown in Figure 4.21 was linear, confirming a diffusion-controlled process.

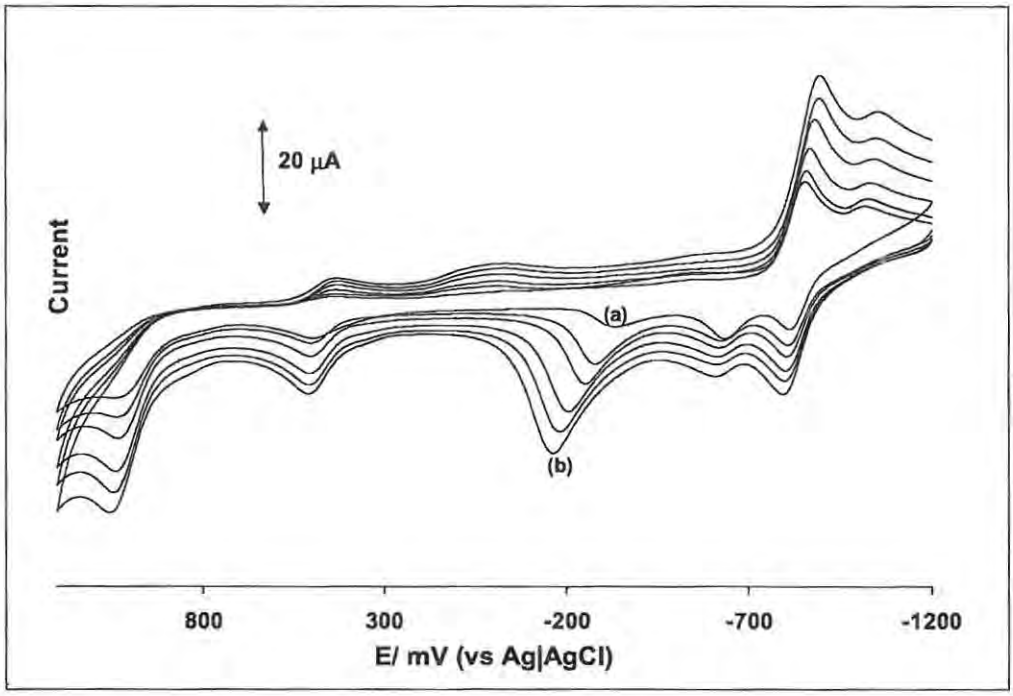

Figure 4.21: Variation of peak current of $Fe^{III}TSPc^{3-}$-histamine with scan rate. Scan rates = (a) 50 (b) 500, scan rates in between are 100, 200, 300 and 400 mV s^{-1}

In order to assign the cyclic voltammetry peaks for the $[Fe^{III}TSPc]^{3-}$ - histamine complex spectroelectrochemistry (OTTLE cell) was used. Electrolysis of a green $[Fe^{III}TSPc]^{3-}$ - histamine complex at potentials of the first couple $\mathbf{I}^{\mathbf{I}}$ (0.6V) resulted in the spectral changes shown in Figure 4.22, under pH 7.4 buffer conditions.

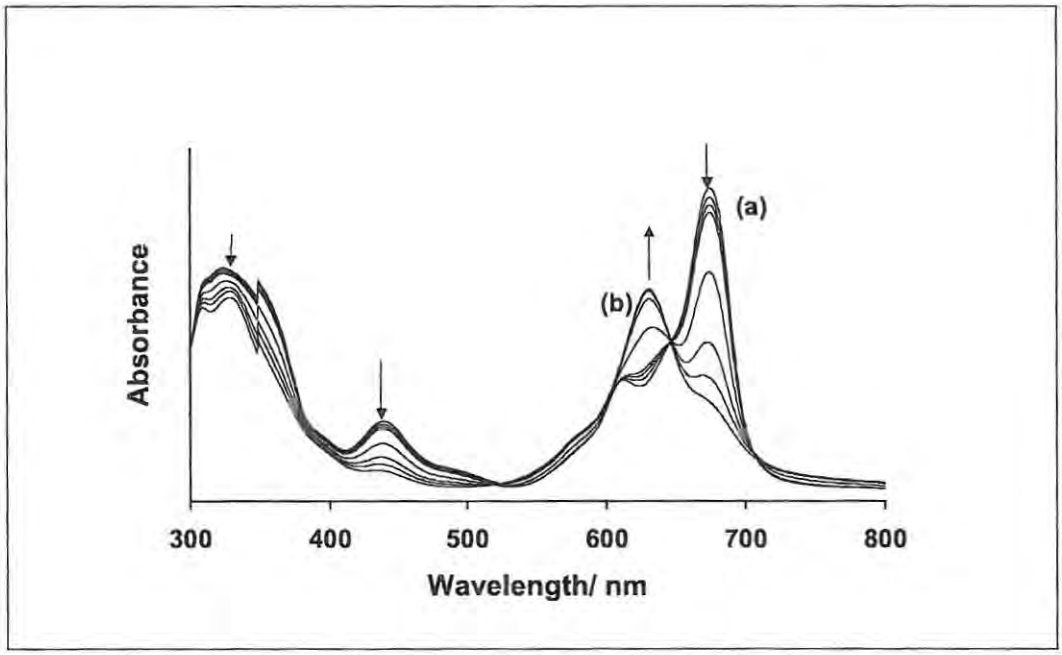

Figure 4.22: Electronic absorption spectral changes on electrolysis of $[Fe^{III}TSPc]^{3-}$ histamine complex at 0.6V vs Ag|AgCl in an OTTLE cell, pH = 7.4.

The UV/vis spectrum of the $[Fe^{III}TSPc]^{3-}$ -histamine complex, with a Q band centred at 673 nm, decreased in intensity and the peak at 632 nm increased in intensity. The peak at 438 nm decreased in intensity. Ring oxidation of the $[Fe^{III}TSPc]^{3-}$ complex to the $[Fe^{III}TSPc(-1)]^{3-}$ species has been reported.[280] The final spectrum following oxidation in Figure 4.22 is clearly not due to ring-based oxidation process.[288] The possibility of oxidation of $[Fe^{III}TSPc]^{3-}$ to Fe^{IV} phthalocyanine species under acid conditions has been discussed.[280] However, the spectra of the latter species are not known. The oxidation product could be reduced back electrochemically at 0 V to the $[Fe^{III}TSPc]^{3-}$ species. The number of moles of electrons transferred during the reduction was found to be near unity.

In order to confirm the nature of the species formed in Figure 4.22, chemical oxidation of $[Fe^{III}TSPc]^{3-}$ - histamine complex was undertaken. $[Fe^{III}TSPc]^{3-}$ - histamine complex was chemically oxidized using bromine and spectral changes shown in Figure 4.23 were observed. These consisted of the shifting of the Q band from 673 nm, curve a, to 636 nm, curve b, and further addition of bromine resulted in the shift of the spectra to 632 nm curve c.

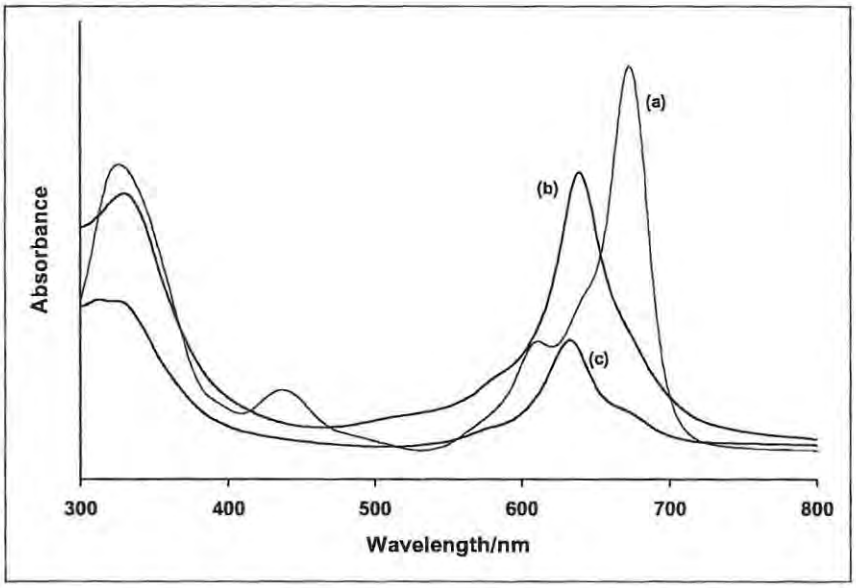

Figure 4.23: Electronic absorption spectra changes observed on bromine oxidation of $[Fe^{III}TSPc]^{3-}$ - histamine complex

The spectra of the $[FeTSPc]^{4-}$ in aqueous solution have been studied by Hadasch et.al.[278] The species with the Q band maxima at 632 nm has been assigned to the oxo-bridged $TSPcFe^{III}$–O– $Fe^{III}TSPc$. The oxo species is readily formed even by addition of NaOH to solutions of FeTSPc species. While the species with a Q band at 636 nm is associated with a stacked monomer, readily formed in the presence of axial ligands.[278] Thus it is

suggested that on chemical oxidation of the $[Fe^{III}TSPc]^{3-}$ - histamine complex, the first peak at 636 nm is due to the stacked monomer, which is converted to the oxo-bridged complex with a peak at 632 nm. Since oxidation is involved the most likely product is the $TSPcFe^{III}$–O– $Fe^{IV}TSPc$ mixed species or the $TSPcFe^{IV}$–O– $Fe^{IV}TSPc$. The $PcFe^{III}$-O-$Fe^{IV}Pc$ complexes have been reported.[214] In the absence of histamine, chemical oxidation of the starting $[Fe^{II}TSPc]^{4-}$ complex resulted in the spectral changes typical of metal oxidation to $[Fe^{III}TSPc]^{3-}$ followed by ring oxidation. The peaks at 636 and 632 nm were not observed. It does seem the presence of the histamine in axial position results in the generation of the stacked monomer.

Thus the last spectrum at 632 nm in Figure 4.22 is at the wavelength associated with the oxo-bridged complex.[278] The final species in Figure 4.22 is thus assigned the oxo-bridged complex, probably of the following nature: $TSPcFe^{III}$–O– $Fe^{IV}TSPc$ or $TSPcFe^{IV}$–O–$Fe^{IV}TSPc$. The fact that the original complex in Figure 4.22 could be regenerated on reduction suggested that the histamine ligands from the solution could coordinate to the $[Fe^{III}TSPc]^{3-}$ complex during the reduction. The irreversible peak for the $[Fe^{III}TSPc]^{3-}$ - histamine complex (process $\mathbf{II^I}$, in Figure 4.20 curve b) is then assigned to the phthalocyanine ring oxidation.

CHAPTER 5

DEVELOPMENT AND USE OF CARBON PASTE ULTRA MICRO ELECTRODES FOR THE DETECTION OF NEUROTRANSMITTERS*

* The following publication resulted from part of the research work presented in this chapter and it is not referenced further in this thesis: J. Oni, P. Westbroek, T. Nyokong, Electrochem. Commun., 2001, 3, 524.

5.1 Characterization of carbon paste ultra micro electrodes.

One of the most important characteristics an electrode must possess for application in direct electrochemical measurements in biological systems is a small size (ultra micro electrodes, UMEs), so that it can be placed in the extracellular fluid (ECF) with little or no damage to the surrounding tissue. The attainment of steady-state current that is time independent also makes UMEs the electrodes of choice for continuous measurements in biological systems. In order to extend the numerous benefits of UMEs to carbon paste-based electrodes, two types of electrodes were developed and characterized in this work. These are the carbon paste ultra micro disk electrode (CPUMDE) and the carbon paste ultra micro band electrode (CPUMBE). The electrodes were characterized using the redox couple of potassium ferrocyanide.

5.1.1 Parameters considered for ultra micro electrode fabrication

The carbon paste ultra micro electrodes employed in this work are novel and home-made. A number of parameters (listed below) were investigated in order to arrive at the optimum values suitable for the fabrication of this type of electrodes.

5.1.1.1 Graphite to Nujol® ratio

A very important parameter for consideration in the construction of the CPUMDE's and CPUMBE's is the optimum graphite to Nujol® composition of the carbon paste. It is well known that compared to the inert metals, carbon paste possesses a relatively large resistance, particularly wet carbon pastes. Pastes with different graphite to Nujol® ratios

were studied in order to find the optimum ratio for making pastes suitable for use in the fabrication of UMEs. The compositions studied in this work are summarized in Table 5.1.

The ratio of the oxidation current at half-wave potential, $E_{1/2}$, ($E_{1/2}$ is defined as the potential at which the current is half the limiting current in this chapter on microelectrodes) to $[Fe(CN)_6]^{4-}$ concentration was used to determine the appropriate graphite to Nujol® ratio for pastes used in UME fabrication. It can be seen from the ratio of the slope of the $[Fe(CN)_6]^{4-}$ oxidation current (determined at $E_{1/2}$ (0.33V) ± 50mV) and the $[Fe(CN)_6]^{4-}$ concentration (in A L V^{-1} mol^{-1}) that the most suitable compositions are between 1.9 and 2.2 g carbon per ml of mineral oil. For compositions less than these optimum values, the resistance of the carbon paste is too large, which results in ohmic drop effects. This effect is also responsible for the smaller value of the ratio given in Table 5.1. For compositions higher than 2.2 g carbon per ml of mineral oil the carbon paste becomes too dry resulting in a porous CPUMDE, while for CPUMBE the paste falls out of the grooves easily. This also results in an increase of the resistance of the electrode and finally to loss of electrical contact. As can be seen in Table 5.1, the ratio of the slope at $E_{1/2}$ ± 50mV and the $[Fe(CN)_6]^{4-}$ concentration should be at least 0.24. Approximately 20 % of the constructed electrodes (a set of 20 of each type of electrode) did not pass the elimination test and are not taken into account in this investigation.

Table 5.1: Summary of carbon paste composition and its suitability for use in the construction of ultra microelectrodes

Composition of carbon paste (g C / ml oil)	Ratio* of the slope of Fe(II) oxidation at $E_{1/2} \pm 50$mV and Fe(II) concentration (in A L V^{-1} mol^{-1})	Suitability for use in CPUMDE and CPUMBE
1.0	0.0110	Not good
1.3	0.0141	Not good
1.7	0.0185	Not good
1.8	0.0231	Not good
1.9	0.0258±0.0004	Good
2.0	0.0261±0.0003	Good
2.1	0.0263±0.0004	Good
2.2	0.0254±0.0004	Good
2.3	0.0239	Acceptable
2.7	0.0181	Not good
3.0	0.0149	Not good

* this value is an average calculated for each concentration of $[Fe(CN)_6]^{4-}$ in 0.5 mol dm^{-3} KNO_3.

5.1.1.2 Plastic holder for band electrodes

For CPUMBEs, it is also important to find the type of plastic that will be most suitable for use in the construction of the electrodes. The following types of plastic were used for this investigation: polypropylene (PP), polyvinylchloride (PVC), polycarbonate (Perspex®), polytetrafluoroethylene (PTFE) and polyethylene (PET).

It was found that for the optimum graphite to Nujol® ratio, polycarbonate was most suitable because it gave the most reproducible groove dimensions. Other plastics like PET suffered from splinters and uneven fibers along the grooves while softer plastics like PVC, PP and PTFE were too elastic, which resulted in continuous changes of the groove dimensions. Therefore only polycarbonate plastic was used for the fabrication of CPUMBEs.

From several preliminary tests it was found that grooves with widths smaller than 100 μm did not show good results, probably due to relatively large resistance of the thin carbon paste electrodes and difficulties in filling the grooves properly with carbon paste. Therefore a groove width between 100 and 150 μm was used, which is on the limit of ultra microelectrode dimensions. The length of each electrode in the band was 37 mm.

5.1.2 Carbon paste ultra micro disk electrode

Figure 5.1 shows current potential curves recorded at a CPUMDE. These were recorded as CV, but the return scans are not shown for clarity. All curves were obtained in a 0.5 mol dm^{-3} KNO_3 electrolyte solution as a function of increasing $[Fe(CN)_6]^{4-}$ concentration. An oxidation wave with $E_{1/2}$ = 0.33 V vs. Ag|AgCl is observed due to the oxidation of $[Fe(CN)_6]^{4-}$ and shows a limiting current plateau between 0.50 and 0.75 V vs. Ag|AgCl. The occurrence of a limiting current plateau indicates that a steady state condition (no changes in concentration profile as a function of time) is obtained.

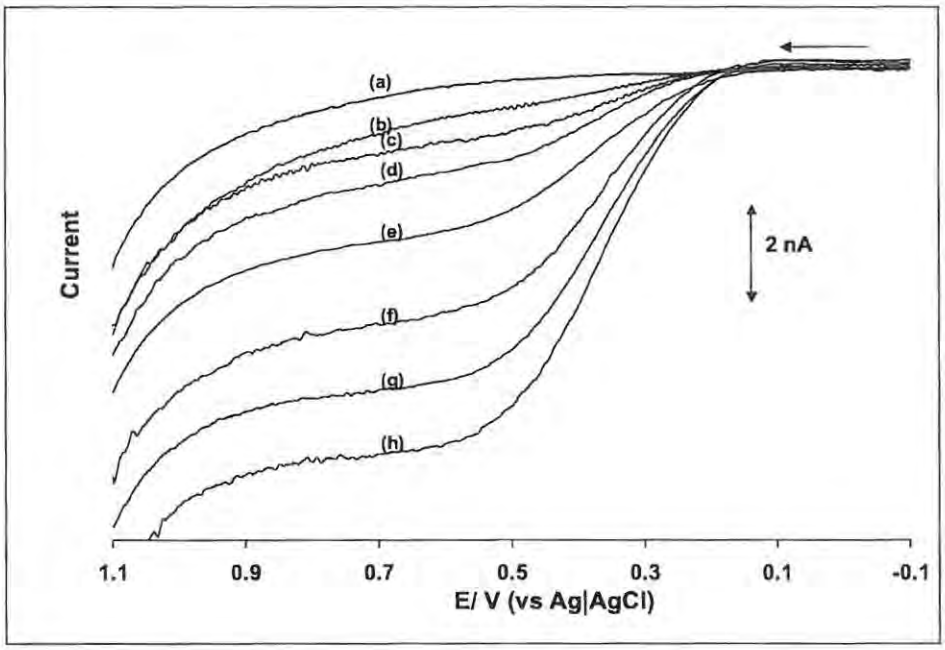

Figure 5.1: Current-potential curves obtained for the oxidation of (a) 0 (b) $1.49x10^{-5}$ (c) $2.97x10^{-5}$ (d) $5.88x10^{-5}$ (e) $1.15x10^{-4}$ (f) $1.7x10^{-4}$ (g) $2.22x10^{-4}$ (h) $2.73x10^{-4}$ mol dm^{-3} $[Fe(CN)_6]^{4-}$ at CPUMDE in 0.5 mol dm^{-3} KNO_3. Scan rate =100 mV s^{-1}

Plotting the limiting currents, taken at a potential of 0.6 V vs. Ag|AgCl obtained at CPUMDE's resulted in a linear curve with good reproducibility, Figure 5.2. A detection limit of 5.0×10^{-6} mol dm^{-3} was obtained, which is a large improvement compared to other steady state configurations like rotating disc electrodes and micro carbon paste electrodes with typical detection limits[295,296,297] of 10^{-4} mol dm^{-3}. The criterion used here for the determination of the detection limit is the concentration obtained at twice the value of the background current at 0.6 V.

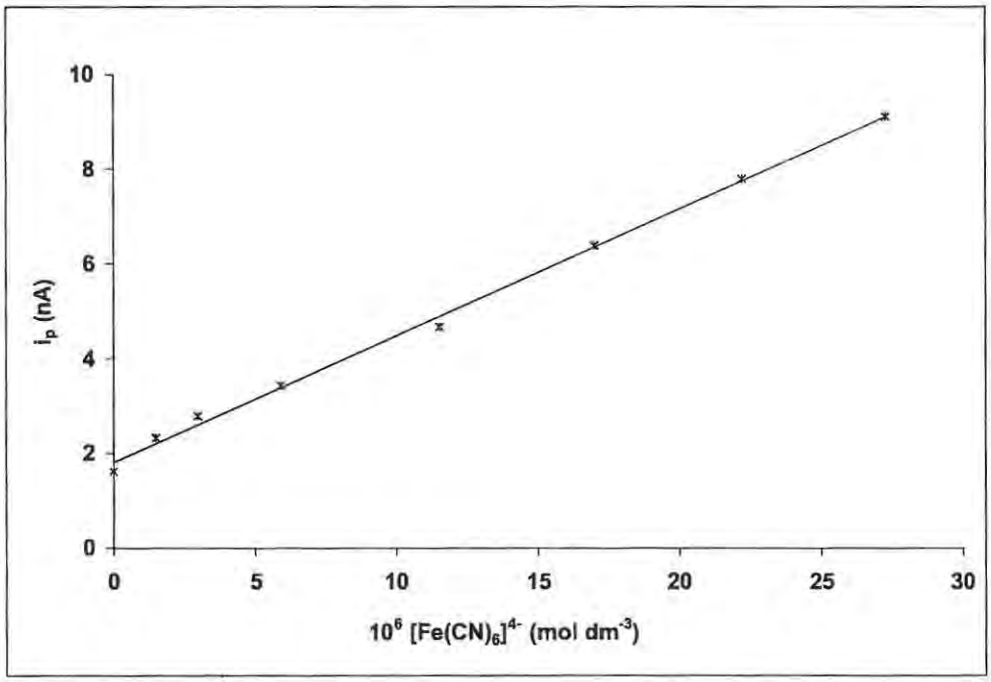

Figure 5.2: Calibration curve for the oxidation of $[Fe(CN)_6]^{4-}$ in 0.5 mol dm^{-3} KNO_3 at CPUMDE

5.1.3 Carbon paste ultra micro band electrode

The current potential curves recorded at an individual CPUMBE whose length and breadth were 37mm and 150 ± 10 μm respectively are shown in Figure 5.3. The curves were obtained in a 0.5 mol dm^{-3} KNO_3 electrolyte solution as a function of increasing $[Fe(CN)_6]^{4-}$ concentration.

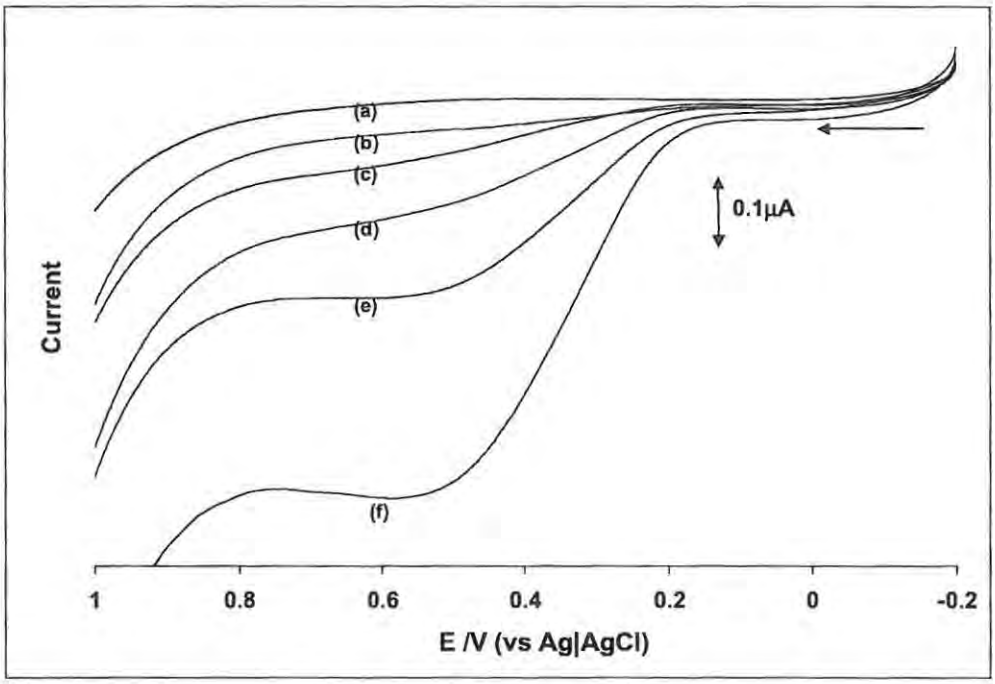

Figure 5.3: Current-potential curves obtained for the oxidation of (a) 0 (b) $5.1x10^{-6}$ (c) $1.02x10^{-5}$ (d) $2.03x10^{-5}$ (e) $4.04x10^{-5}$ (f) $8.05x10^{-5}$ $[Fe(CN)_6]^{4-}$ at CPUMBE, scan rate = 100 mV s^{-1}

An oxidation wave with $E_{1/2}$ = 0.33 V vs. Ag|AgCl was observed due to the oxidation of $[Fe(CN)_6]^{4-}$ and shows a limiting current plateau between 0.50 and 0.75 V vs. Ag|AgCl. The limiting current was obtained for concentrations of $[Fe(CN)_6]^{4-}$ lower than $6.50x10^{-5}$

mol dm^{-3}. The occurrence of a limiting current indicates that a steady state condition (no changes in concentration profile as a function of time) is obtained.

However, at concentrations of $[Fe(CN)_6]^{4-}$ higher than $6.50x10^{-5}$ mol dm^{-3}, a slight deviation from the steady-state condition is observed, which shows that the relatively large width of the electrode (about 150 μm) is indeed at the limit of ultra micro electrode dimensions. This means that a steady state condition is not attained totally. The diffusion layer thickness is still slightly dependent on time and increases very slowly, because of the relatively large dimensions of ultra microelectrode.

Another indication that the steady state condition is not attained totally is that only at small scan rates, (less than 10 mV s^{-1}) are time independent limiting currents obtained. For higher scan rates, a peak-shaped wave is observed as Figure 5.3 shows.

If the width of the CPUMBE electrode is made smaller than 150μm, the electrode develops a high resistance and at width dimensions greater than 150μm, the ultra microelectrode behaviour is completely lost and conventional peak-shaped voltammograms are obtained. These observations suggest that the optimum width for CPUME for true UME behaviour to be observed is 150μm.

A plot of the limiting currents, taken at a potential of 0.6 V vs. Ag|AgCl for the CPUMBE versus $[Fe(CN)_6]^{4-}$ concentration, resulted in linear curves with good reproducibility as shown in Figure 5.4. A close observation of Figure 5.3 shows that there are different background currents for different $[Fe(CN)_6]^{4-}$ concentrations. Therefore, the

limiting current shown in Figure 5.4 is the result of the difference between the experimental current at 0.6 V vs. Ag|AgCl and the background current at 0.1 V vs. Ag|AgCl. For the individual CPUMBE, a detection limit of 1.2×10^{-6} mol dm^{-3} was obtained, which is also a large improvement compared to other steady state configurations. Here, the criterion used for the determination of the detection limit is the concentration obtained at twice the value of the difference in background current at 0.6 V and 0.1 V vs. Ag|AgCl.

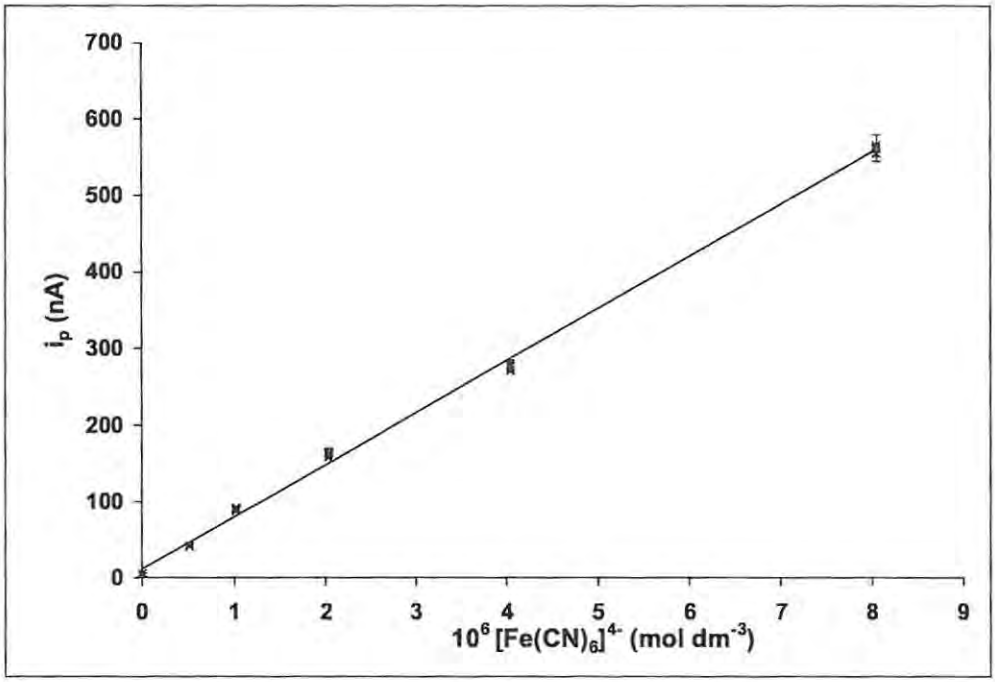

Figure 5.4: Calibration plot for the oxidation of $[Fe(CN)_6]^{4-}$ at CPUMBE

Although the width of the electrode is a fixed value, the length of the electrode in contact with the test solution is variable. Figure 5.5 shows cyclic voltammetric curves, recorded

in a 8.05×10^{-5} mol dm^{-3} $[Fe(CN)_6]^{4-}$ solution as a function of length of an individual CPUMBE. A linear relationship was found between the limiting current and the length (or the surface A) of the electrode. A plot of the limiting current against the area of the electrode is shown as an insert in Figure 5.5. This linear relationship is described by equation 5.1.

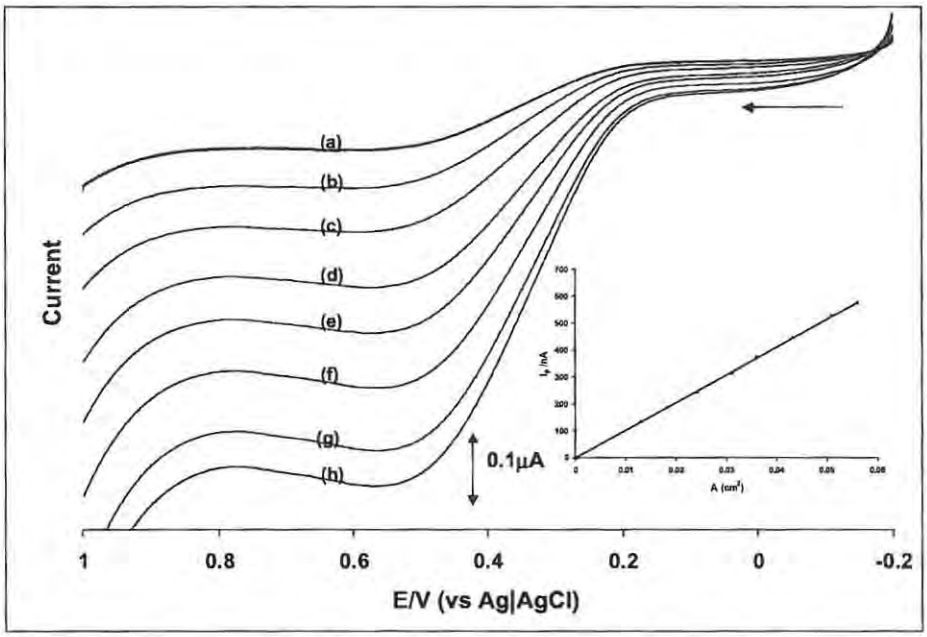

Figure 5.5: Current-potential curves of the oxidation of 8.05×10^{-5} mol dm^{-3} $[Fe(CN)_6]^{4-}$ at CPUMBE as a function of the length of the electrode in contact with the test solution. Length = (a) 0.4 (b) 0.8 (c) 1.2 (d) 1.6 (e) 2.0 (f) 2.4 (g) 2.4 (h) 3.2 cm

$$i_L = k A \qquad 5.1$$

where k is the slope of the plot of the limiting current against the area of the electrode.

But

$$k = n F k' c \qquad \textbf{5.2}$$

k' was found to be 1330 by substituting the value of the slope and the concentration of $[Fe(CN)_6)]^{4-}$ into equation 5.2 since k, n, F and c are known. Then

$$i_L = 1330\ n F A c \qquad \textbf{5.3}$$

with i_L the limiting current at 0.6 V vs. Ag|AgCl (nA), n the number of electrons, F the Faraday constant, A the surface of the electrode (cm^2) and c the concentration (mol dm^{-3}). With an increase in the length of the CPUMBE in contact with the test solution, higher current signals were obtained and as a consequence, the measurement of the signals is more accurate.

The surface of the CPUMBE's can be increased even more, by using ensembles of individual band electrodes. As was expected the faradaic signals obtained at ensembles of individual CPUMBE's are equal to the sum of the signals of the individual electrodes. Figure 5.6 shows the CV of 8.05×10^{-6} at ensembles of up to five electrodes. The oxidation signal obtained increased with the number of individual electrodes in the band employed.

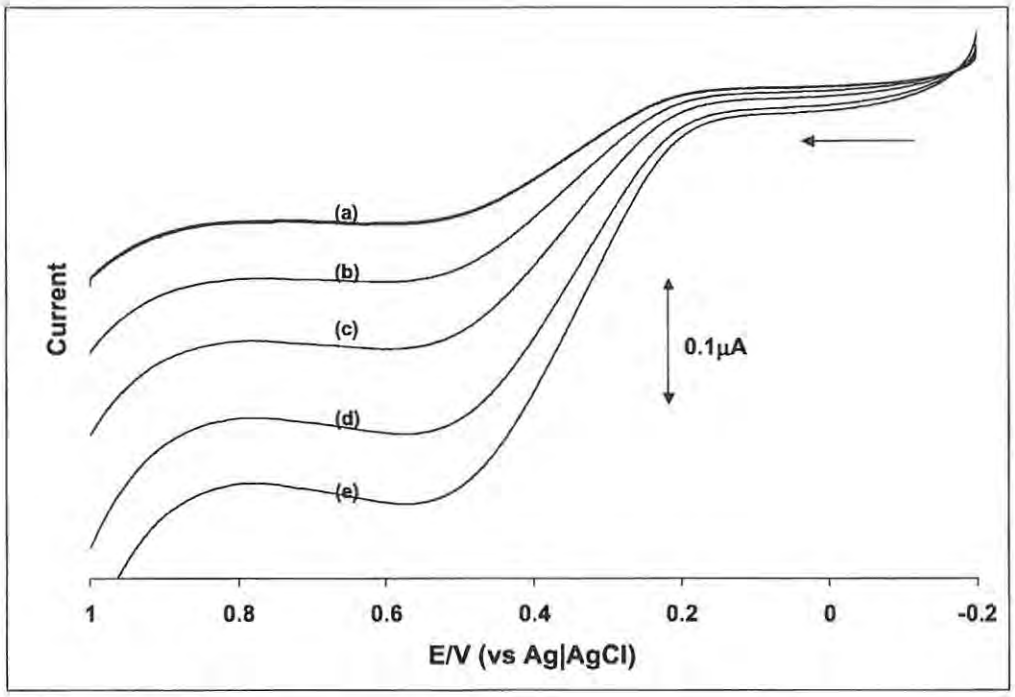

Figure 5.6: CV of 8.05×10^{-6} mol dm^{-3} $[Fe(CN)_6]^{4-}$ at (a) 1 (b) 2 (c) 3 (d) 4 (e) 5 electrodes in a band. Scan rate = 100 mV s^{-1}.

Care must be taken though while using an ensemble of electrodes. The individual electrodes should not be too close to their neighbours in order to avoid interdiffusion effects. In the CPUMBEs constructed, the individual electrodes were separated by a distance of 3mm based on the report of the work of Fletcher and Horne.[298] At this separation, interdiffusion effects are largely insignificant. When an array of electrodes was used, an improvement on the detection limit was obtained. Using an ensemble of three electrodes, a detection limit of 8.9×10^{-7} mol dm^{-3} was obtained. With a device of 5 individual electrodes a detection limit of 8.2×10^{-7} mol dm^{-3} was obtained.

It was observed that the detection limit of the CPUMBE is lower than the one for the CPUMDE. This can be explained by the fact that the background current of a band electrode can be measured more accurately making the estimation of the detection limit more accurate. Therefore the CPUMBEs become more interesting if their surface and as a consequence their current signal is increased without loosing the beneficial properties of UMEs.

5.1.4 Stability test of the electrodes

The stability of the CPUMDE's and CPUMBE's was tested by repetitive cycling in a 8.05×10^{-5} mol dm^{-3} $[Fe(CN)_6]^{4-}$ solution. Figure 5.7 shows the voltammograms obtained at an ensemble consisting of three individual CPUMBE's. It can be seen that the limiting current of the oxidation is almost independent of scan number, which means that good stability is obtained and that the possible occurrence of creep of the test solution between the plastic body and the carbon paste is absent. Similarly, stable currents were obtained for the CPUMDEs in a solution of 8.05×10^{-5} mol dm^{-3} $[Fe(CN)_6]^{4-}$.

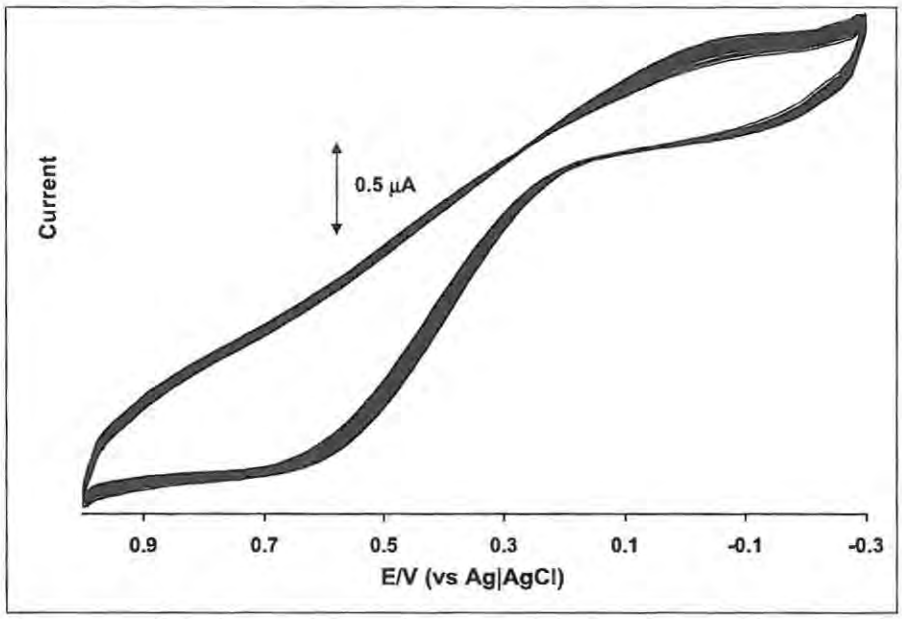

Figure 5.7: Cyclic voltammogram showing 56 scans recorded using a CPUMBE consisting of three individual electrodes in a solution of 8.05×10^{-5} mol dm^{-3} $[Fe(CN)_6]^{4-}$ in 0.5 mol dm^{-3} KNO_3.

Both the CPUMDE and CPUMBE have promising results concerning ultra microelectrode behavior, but the resistance of the electrodes even for the optimal paste composition, is relatively high. This was confirmed by variation of the polarization rate of the electrode. At higher polarization rates (> 200 mV s^{-1}) the background current increases remarkably due to capacitive current. This means that high polarization rate, which is one of the benefits of ultra microelectrodes, cannot not be achieved in this case.

The designed CPUMDEs and CPUMBEs show promising properties from electroanalytical, technical and commercial point of view because of their ease of fabrication and the very cheap materials involved in the fabrication process. Relatively small detection limits were obtained, which probably can still be improved depending on

the analyte, the electrochemical method used (like potential step methods) and/or by increase of the amount of individual electrodes in an array of CPUMDEs and CPUMBEs. Despite the fact that carbon paste electrodes are frequently used in electro analytical applications, the beneficial attribute of UMES have almost not been extended to carbon paste-based electrodes up to now. With the electrodes described in this work, existing applications for carbon paste can be improved because of better detection limits and probably new applications for this type of electrode will be introduced in the light of the good stability of the electrodes.

5.2 Detection of neurotransmitters at iron (II) tetrasulfophthalocyanine modified ultra micro electrodes

Since UMEs showed lower detection limits than the millimetric-sized electrodes, CPUMDE was used for the analysis of neurotransmitters in order to improve on the detection limits obtained at the millimetric-sized electrode.

CPUMDEs modified with iron (II) tetrasulfophthalocyanine (FeTSPc-CPUMDE) were prepared and used for the detection of DA and 5-HT. DA was also detected in the presence of AA. The electroanalytical technique used was cyclic voltammetry. As explained above, only the anodic waves are shown in all the Figures for clarity where FeTSPc-CPUMDEs were employed as working electrodes.

5.2.1 Dopamine

The cyclic voltammetry of DA in pH 7.4 Tris buffer at a FeTSPc-CPUMDE is shown in Figure 5.8. The oxidation wave was observed at 122mV vs Ag|AgCl. A steady state current condition evidenced by the presence of a current plateau was observed suggesting a true UME behaviour of the modified electrode towards the oxidation of DA. The electrode was found to be stable towards the detection of DA as the fouling of the electrode did not occur after numerous scans in a solution of DA. An increase in oxidation current was obtained with an increase in the concentration of DA, Figure 5.8.

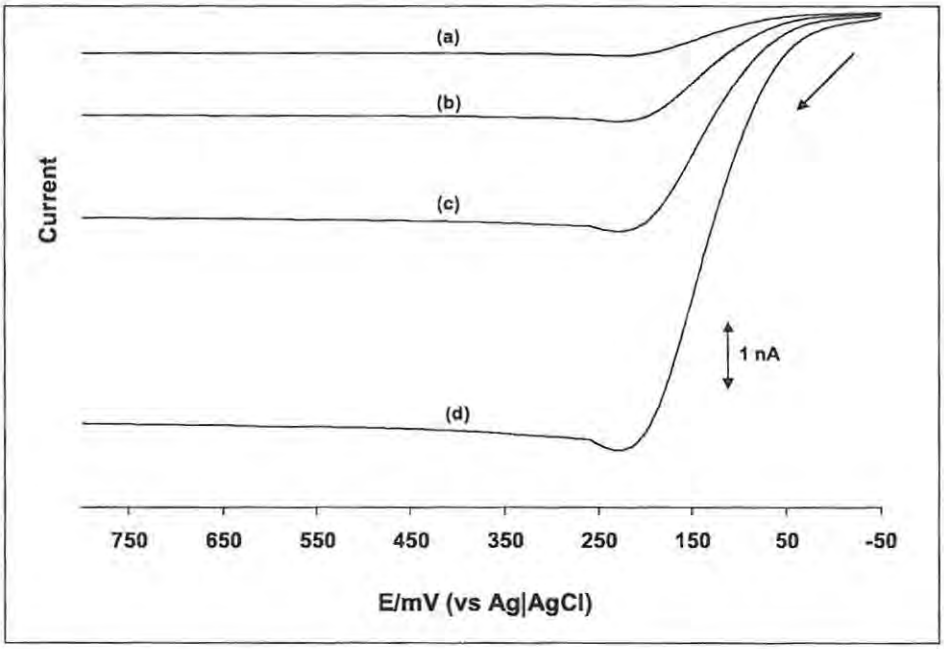

Figure 5.8: CV of (a) $3.05x10^{-6}$ (b) $6.03x10^{-6}$ (c) $1.20x10^{-5}$ (d) $2.38x10^{-5}$ mol dm^{-3} DA recorded at FeTSPc-CPUMDE. Scan rate = 100 mV s^{-1}, pH = 7.4

Plotting the oxidation current obtained at the modified electrode against the concentration of DA gave a linear plot, shown in Figure 5.9, with a regression equation $i_p = 2.73x10^{-8}$ [x] + $1.23x10^{-3}$ where i_p is the current and [x] is the concentration of DA. A detection limit of $4.4 \pm 0.2x10^{-7}$ was obtained at the modified electrode.

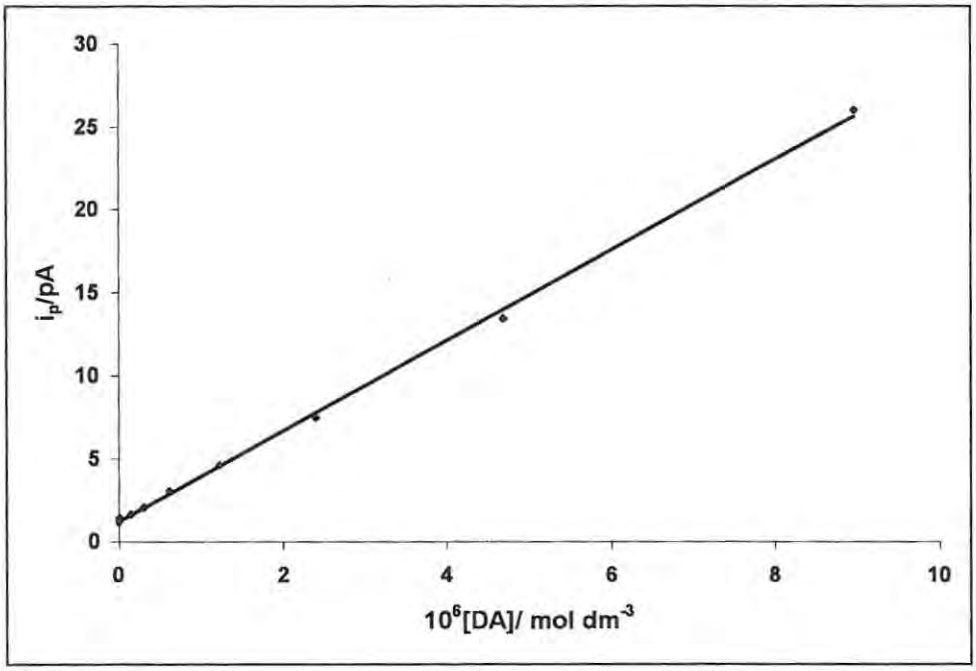

Figure 5.9: Plot of peak current vs concentration of DA at FeTSPc-CPUMDE in pH 7.4 buffer

The FeTSPc-CPUMDE can thus be used for the detection of DA under steady state conditions, which is desirable for measurements *in vivo* in that a potential value within the region where a current plateau was obtained could be applied to the electrode and the concentration of DA monitored continuously with time.

5.2.2 Serotonin

The forward scan of the CV of 6.30×10^{-6} mol dm^{-3} 5-HT in pH 7.4 Tris buffer at FeTSPc-CPUMDE is shown in Figure 5.10 curve b, curve a is the background recorded in the absence of 5-HT.The oxidation wave was observed at 285mV.

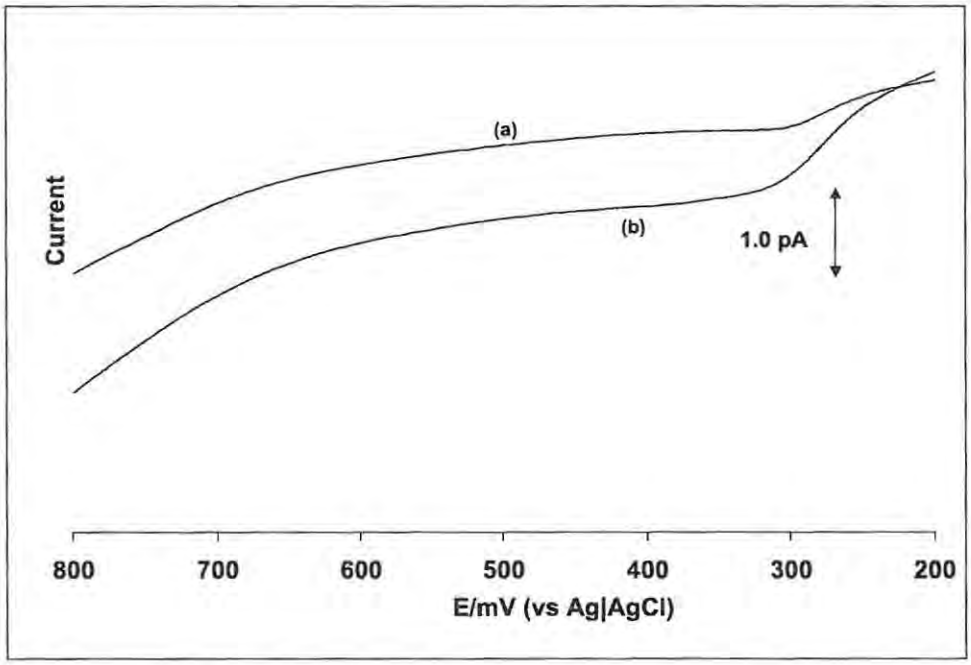

Figure 5.10: Cyclic voltammogram of (a) 0 and (b) 6.30×10^{-6} mol dm^{-3} 5-HT at FeTSPc-CPUMDE. Scan rate = 100 mV s^{-1}, pH = 7.4

As observed for DA, a steady state current condition was obtained for the oxidation of 5-HT at the modified electrode. As opposed to the case with DA, the current response obtained at the electrode in a solution of constant 5-HT concentration decreases with scan number.

This may be due to the poisoning of the electrode surface or the depletion of 5-HT in the vicinity of the electrode. It is well known that 5-HT gets oxidized irreversibly[139] and that the electrode reaction products do not diffuse away considerably from the vicinity of UMEs. Thus the decrease in the oxidation current of 5-HT may be due to the accumulation of the non-electroactive oxidation product in the vicinity of the electrode. However, if the electrode is removed from the test solution and rinsed with water before each run, a reproducible current response was obtained. This observation suggests that the oxidation product could be loosely attached to the electrode surface and gets rinsed off easily or simply removing the electrode from the solution is sufficient to generate enough turbulence to cause the oxidation product to disperse in the bulk of the solution and thus present a "fresh" 5-HT layer to the electrode surface when it is replaced in the test solution.

5.2.3 Ascorbic acid

Figure 5.11 shows the current-potential curves (forward scan of CV) recorded for the oxidation of AA at FeTSPc-CPUMDE. An increase in the oxidation current with an increase in the concentration of AA was observed. The detection of the oxidation current of AA at the modified electrode is totally unexpected bearing in mind the results obtained in Section 4.2.6 where a millimetric-sized carbon paste electrode modified with $[FeTSPc]^{4-}$ prevented the oxidation of AA at the electrode.

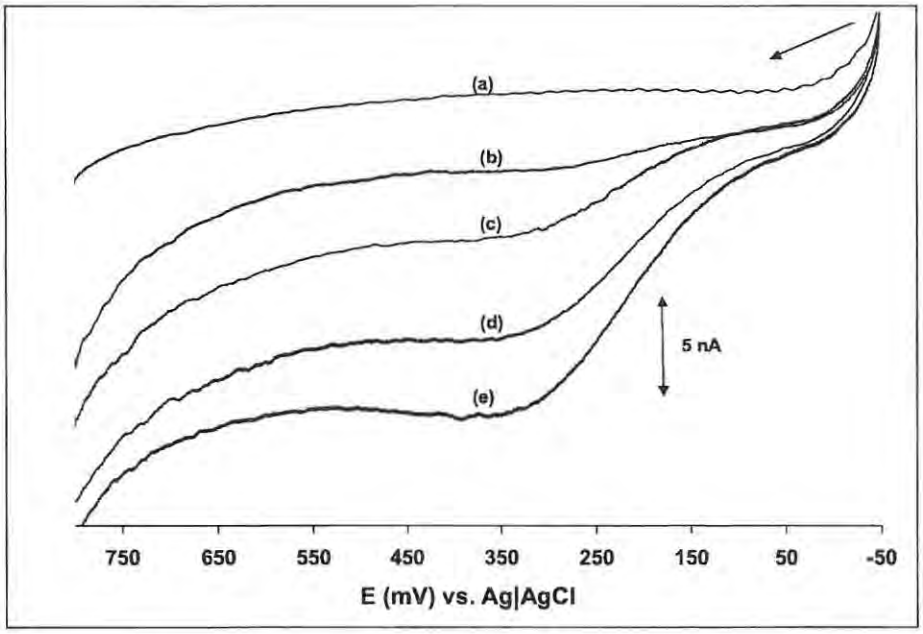

Figure 5.11: Forward scan of the cyclic voltammogram of (a) 0 (b) $1.66x10^{-6}$ (c) $3.32x10^{-6}$ (d) $5.80x10^{-6}$ (e) $8.26x10^{-6}$ AA at FeTSPc-CPUMDE. Scan rate = 100mV s^{-1}

It is important to note that at millimetric-sized electrodes, the absence of the oxidation current of AA is observed only up to certain concentration limits.[147,148,152] This was also observed for FeTSPc-CPE for very high concentrations of AA, though no currents due to the oxidation of AA were observed up to a concentration of $2.0x10^{-3}$ mol dm^{-3} AA. This means that the capacity of the negatively charged modifier to repel ascorbic acid is also limited and depends on the ratio of the amount of negative charge at the electrode (Q_{el}) to the amount of charges approaching the electrode by spherical diffusion (Q_{dif}). However, at ultra micro electrodes Q_{el}/Q_{dif} is much smaller than the one at common electrodes, where diffusion is linear. The smaller ratio of Q_{el}/Q_{diff} may be responsible for the

detection of the signal of ascorbic acid at the ultra micro electrode. A plot of the peak current against the concentration of AA gave a linear curve, shown in Figure 5.12, with a regression equation $i_p = 1.66x10^{-8}$ [x]+ $1.26x10^{-3}$, where [x] is the concentration of AA. A detection limit of $7.5x10^{-7}$ mol dm^{-3} was obtained at the electrode.

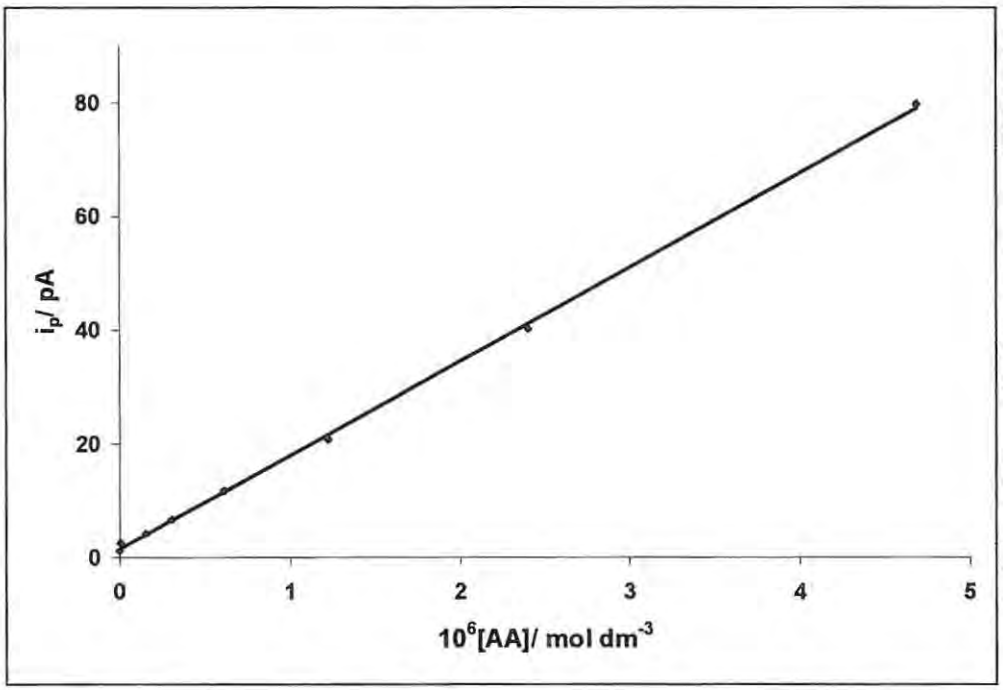

Figure 5.12: Calibration plot for the oxidation of AA at FeTSPc-CPE in pH 7.4 buffer

Both DA and AA exchange two electrons at the electrode but a substantial difference was noticed in the slopes of their calibration curves, $2.73x10^{-8}$ and $1.66x10^{-8}$ respectively. The slopes are proportional to the number of electrons and the square root of their diffusion coefficients. The value of the diffusion coefficient of DA^{299} (D_{DA}) = $1.5\pm0.5x10^{-5}$ cm^2 s^{-1} and that of AA^{300} (D_{AA}) = $5.37\pm0.3x10^{-6}$ cm^{-2} s^{-1}. The ratio of $(D_{DA}^{1/2})/(D_{AA}^{1/2})$ = 1.6.

This is about the same value obtained for the ratio of the slopes of the calibration plot of DA and AA.

5.2.4 Simultaneous detection of dopamine and ascorbic acid in a mixture

The oxidation waves of DA and AA were observed with $E_{1/2}$ of 122 and 212 mV respectively at the FeTSPc-CPUMDE. Despite the wide separation in the oxidation potentials, a separation of the oxidation currents into two separate plateaux was not observed for a mixture containing DA and AA; instead an overlap of the oxidation waves of both DA and AA was observed at the electrode.

In this work, an attempt is made to resolve the resultant current obtained from the oxidation of a mixture of DA and AA into the individual contributions from DA and AA. Using these values, their concentrations can be calculated.

Most of the attempts aimed at eliminating the interference posed by AA in the determination of DA are focused on preventing the oxidation current of AA from being observed or shifting its oxidation potentials to more positive values. This results in a loss of equally important information on the concentration of ascorbic acid. Moreover, shifting the oxidation potential to more positive values moves the problem of interference to the potential window where ascorbic acid can still interfere with the oxidation waves of other neurotransmitter substances. In none of the previous studies was attention given

to obtaining the concentrations of ascorbic acid and dopamine from the single resultant peak obtained from the oxidation of a mixture containing these species.

Figure 5.13 shows the forward scan of the CV curves obtained for increasing concentration of DA added to $1x10^{-4}$ mol dm^{-3} AA. On a close observation of Figure 5.13, it is seen that the $E_{1/2}$ shifts from the initial value of AA's towards that of DA as the concentration of DA (c_{DA}) increases. This shift is complete when c_{DA} is 33% of the concentration of AA (c_{AA}) in the mixture.

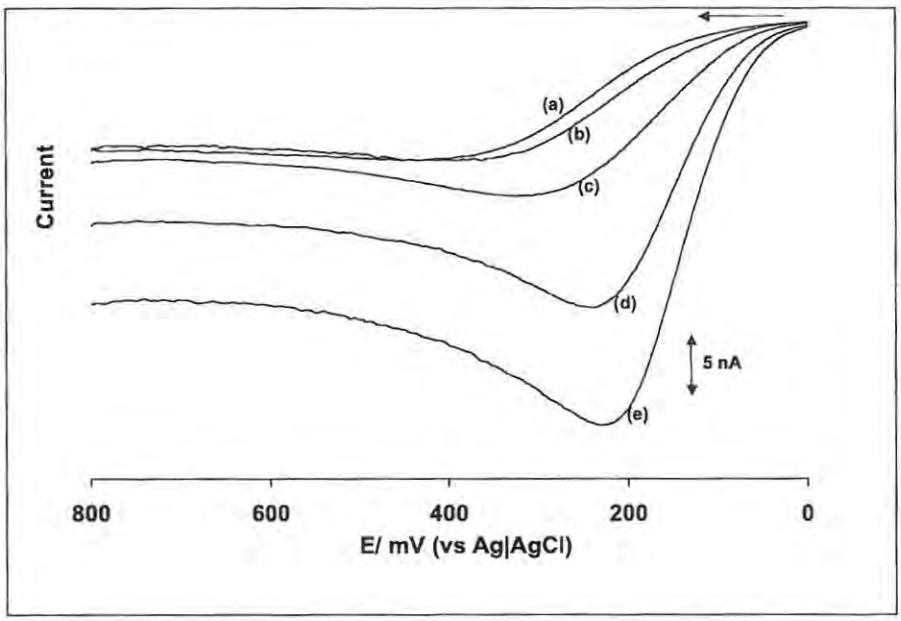

Figure 5.13: CV of (a) 0 (b) $1.54x10^{-6}$ (c) $9.20x10^{-6}$ (d) $3.98x10^{-5}$ (e) $8.56x10^{-5}$ DA added to $1.0x10^{-4}$ mol dm^{-3} AA at FeTSPc-CPUMDE. Scan rate = 100 mV s^{-1}, pH = 7.4

A plot of the shift in $E_{1/2}$ as a function of the ratio of the concentrations of DA and AA in the mixture is shown in Figure 5.14. From this plot, the ratio of c_{DA}/c_{AA} in a mixture could be obtained if the half-wave potential is known.

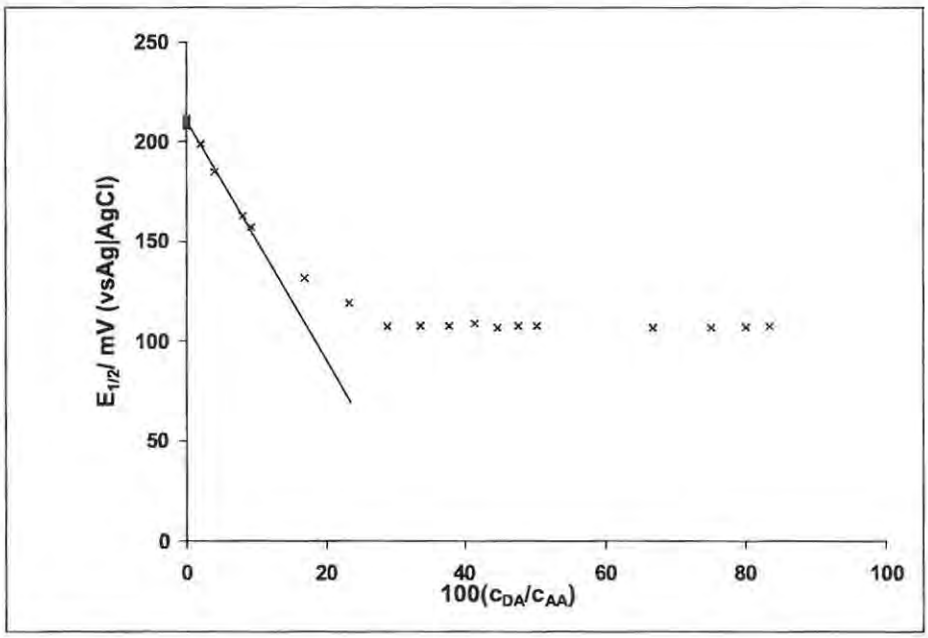

Figure 5.14: Plot of variation of $E_{1/2}$ as a function of the ratio c_{DA} to c_{AA}

Apart from the shift in $E_{1/2}$, there was no return wave obtained for DA at $c_{DA} < c_{AA}$, a reverse wave for DA was only obtained when c_{DA} was more than c_{AA}. The absence of a reverse wave suggests that the oxidation product of DA is immediately reduced back to DA in solution by AA as represented by equations 5.4 and 5.5

$$DA_R \equiv DA_O + 2e^- + 2H^+ \qquad \textbf{5.4}$$

$$DA_O + AA_R \equiv DA_R + AA_O \qquad \textbf{5.5}$$

O and R indicate the oxidized and reduced form of DA and AA.

The oxidation of AA at the electrode can also be represented as equation 5.6

$$AA_R \equiv AA_O + 2e^- + 2H^+ \qquad \textbf{5.6}$$

The shift of half-wave potential (Figure 5.13) shows that for an increasing dopamine concentration reaction 5.4 becomes more important and the rate of reaction 5.6 decreases because of competition with reaction 5.5 to consume ascorbic acid.

UV spectroscopic evidence was sought to confirm the above mechanism represented by equations 5.4 to 5.6. DA was chemically oxidized using bromine and AA was added to the solution of DA_O produced to prove reaction 5.5. The changes in spectral features are shown in Figure 5.15.

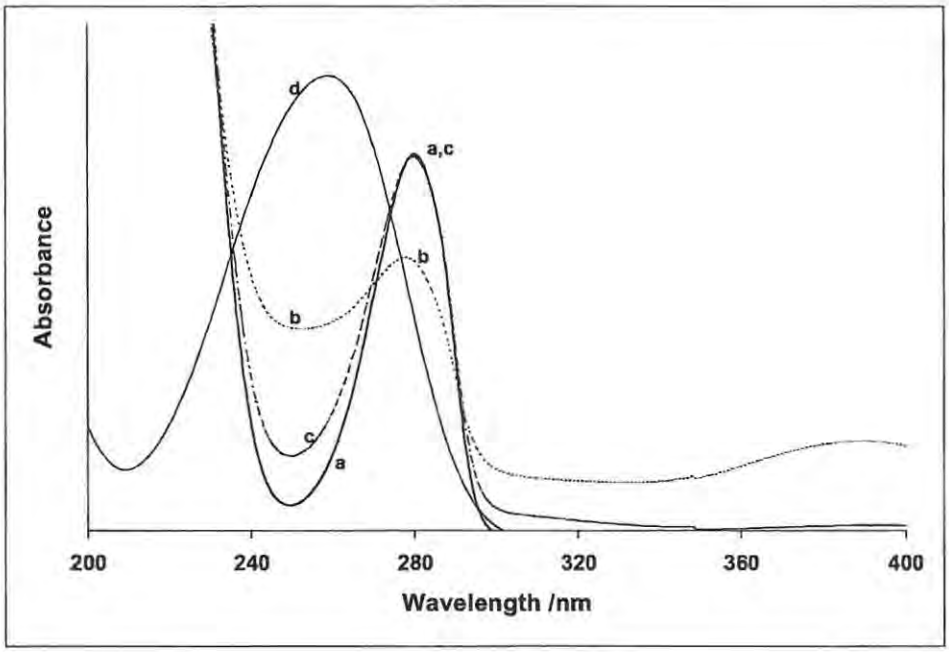

Figure 5.15: Changes in spectral features observed for the oxidation of DA in the presence of AA in pH 7.4 buffer (a) $2.0x10^{-3}$ mol dm^{-3} DA (b) $2.0x10^{-3}$ mol dm^{-3} DA + Br_2 (c) DA + Br_2 + AA (d) $1.5x10^{-3}$ AA

DA absorbs at 284 nm, trace a. Upon oxidation with bromine, the intensity of the absorption peak decreased without a significant shift in wavelength, trace b. When AA was added, the initial DA peak was regenerated; trace c. Trace d is the UV spectrum of the same concentration of AA added to the solution of trace b. The absence of a significant absorption by trace c in the region of AA absorption (trace d) suggests that the added AA was used up in regenerating DA.

An expression is derived below for the determination of the concentration of DA, which incorporates the ratio of the diffusion coefficients of DA and AA, the ratio of the

oxidation currents and the shift in $E_{1/2}$ induced by increasing the concentration of DA in a solution of AA.

In order to obtain the concentration of dopamine and ascorbic acid in a mixture, the oxidation wave of the mixture was recorded and the peak current and half-wave potential determined. From the half-wave potential, the ratio of c_{DA}/c_{AA} was obtained using Figure 5.14 for a concentration ratio up to 0.33. This means that for this approach to measure dopamine concentrations accurately its concentration must be less than 33% of the ascorbic acid concentration. This is more like the situation present in biological samples. Frequently the ratio is less than 0.1. The linear portion of the plot in Figure 5.14 up to $c_{DA}/c_{AA} = 0.1$ was used to derive the expressions below.

To convert the concentration ratio to current ratio, a correction factor (1.6) to offset the difference in diffusion coefficients was introduced. This factor is the ratio of the diffusion coefficients of DA and AA. The current ratios were thus converted to concentration ratios using equation 5.7.

$$\frac{i_{DA}}{i_{AA}} = 1.6\left(\frac{c_{DA}}{c_{AA}}\right) \qquad \textbf{5.7}$$

where i_{DA} and i_{AA} are the currents of DA and AA respectively.

For values of c_{DA}/c_{AA} up to 0.1, the relationship between the concentration ratio and the shift in $E_{1/2}$ potential is found to be linear, with slope of –582 and intercept of 210 mV, given by equation 5.8.

$$E_{1/2} = -582\left(\frac{c_{DA}}{c_{AA}}\right) + 210 \qquad \textbf{5.8}$$

Substituting equation 5.8 into equation 5.7 gives equation 5.9

$$\frac{i_{DA}}{i_{AA}} = 1.6\left(\frac{E_{1/2} - 210}{-582}\right) \qquad \textbf{5.9}$$

Bearing in mind that the peak current observed (i_p) is a combination of the background current (i_{bg}) and the current due to the oxidation of both DA and AA, an expression for the total current can then be written as equation 5.10.

$$i_p = i_{DA} + i_{AA} + i_{bg} \qquad \textbf{5.10}$$

Rearranging equation 5.10 gives

$$i_{DA} = i_p - i_{AA} - i_{bg} \qquad \textbf{5.11}$$

Substituting equation 5.11 into equation 5.9 and simplifying gives equation 5.12

$$i_p - i_{bg} = i_{AA}\left[1 + 1.6\left(\frac{E_{1/2} - 210}{-582}\right)\right] \qquad \textbf{5.12}$$

From the regression equation of the calibration plot of AA

$$i_{AA} = 1.66x10^{-8} c_{AA} + 1.26x10^{-3} \qquad \textbf{5.13}$$

Substituting equation 5.13 into equation 5.12 and rearranging gives equation 5.14

$$c_{AA} = \left[\frac{-582(i_p - 2i_{bg})}{k(1.66E_{1/2} - 918)} \right] \qquad \textbf{5.14}$$

k is the slope of the calibration plot for AA ($1.66x10^{-8}$).

Calibration plots were developed for DA in the presence of varying concentrations of AA, shown in Figure 5.16.

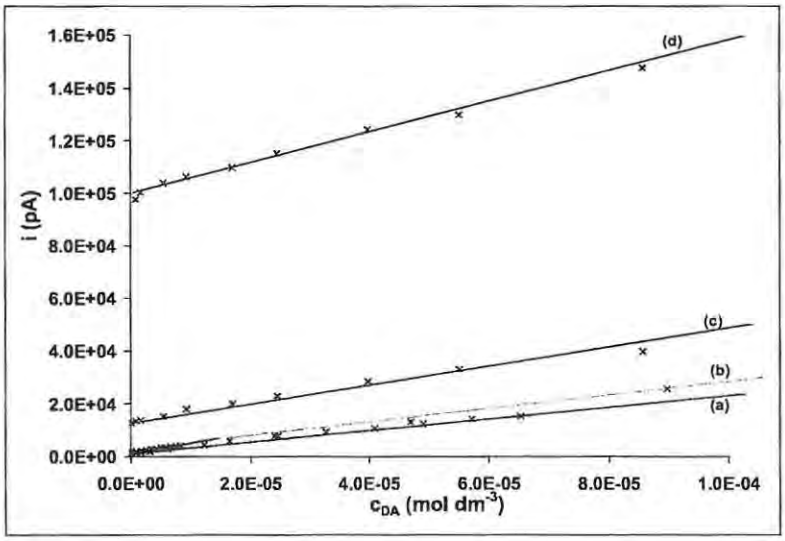

Figure 5.16: Calibration plots for DA in (a) 0 (b) $8.2x10^{-6}$ (c) $7.7x10^{-5}$ (d) $7.6x10^{-4}$ mol dm^{-3} AA at FeTSPc-CPUMDE, pH = 7.4

The slopes (k') of these calibration plots were found to increase linearly as the concentration of AA increases. A logarithmic plot of the slopes of the calibration plot against the concentration of AA, Figure 5.17, was linear.

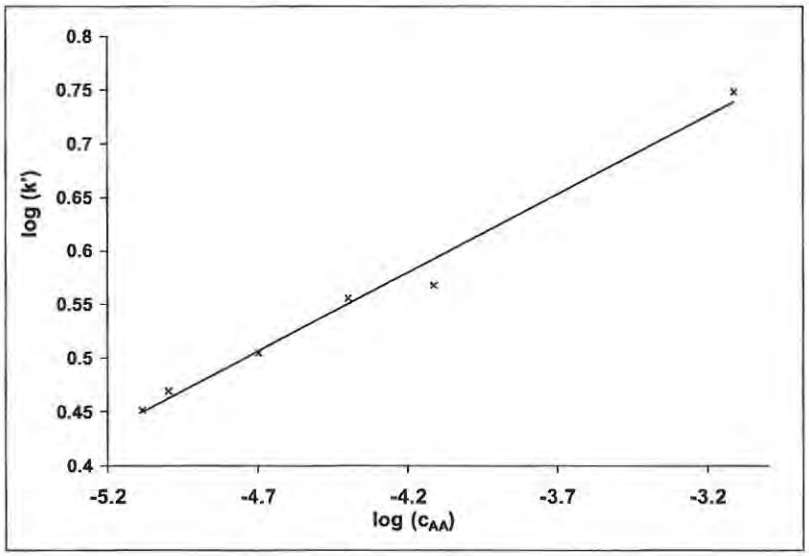

Figure 5.17: Logarithmic plot of the slope of calibration plot of DA against the concentration of AA

When the concentration of AA has been determined from equation 5.14, Figure 5.17 could be used to obtain the corresponding slope (k') of the calibration plot of DA at the AA concentration. The concentration of DA will then be the product of the slope and the current due to DA as shown in equation 5.15

$$c_{DA} = k' i_{DA} \qquad \textbf{5.15}$$

But i_{DA} is given by equation 5.11. Combining equation 5.11 and 5.15 gives equation 5.16

$$c_{DA} = k'(i_p - i_{AA} - i_{bg}) \qquad \textbf{5.16}$$

In order to obtain the concentration of DA and AA in a mixture of known concentration, the cyclic voltammogram of the mixture was recorded and the peak current and half-wave potential noted. These values were substituted into equations 5.14 and 5.16 from which the concentrations of AA and DA were calculated. The calculated concentrations were compared with the values obtained from measurements carried out with standard solutions of DA and AA separately. Quite good correlation was obtained as shown in Figure 5.18. The values obtained for DA is shown as the main plot while that of AA is shown as an insert.

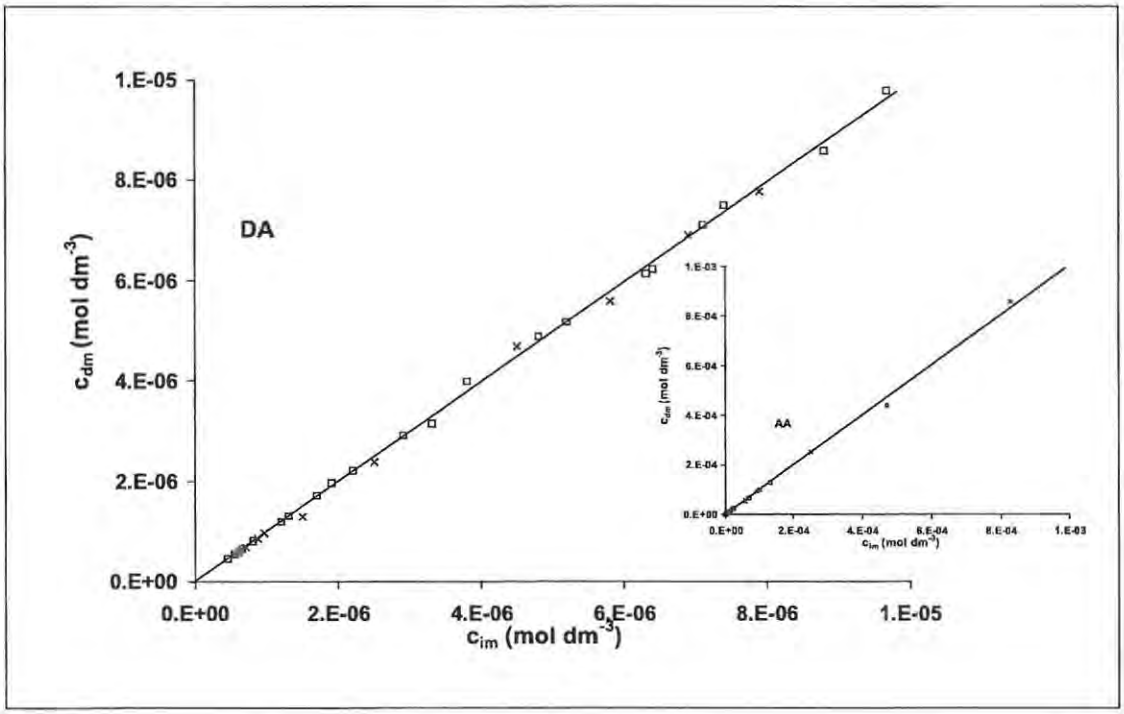

Figure 5.18: Plot showing correlation between the experimental ( ) and standard (x) concentration values obtained at the modified electrode

The method described is capable of detecting both dopamine and ascorbic acid in the same sample by electrocatalytic oxidation of these compounds at a Fe(II)TSPc modified carbon paste ultra micro electrode without peak separation and/or inhibition of oxidation reactions. A detection limit of 4.4×10^{-7} was obtained for DA in the region of c_{DA}/c_{AA} from 0.01 to 0.10. This translates to detecting DA in the presence of up to a hundred-fold concentration of AA. When the ratio was smaller than 0.01, the error in the detection limit becomes higher because of the small shift of the half-wave potential.

CHAPTER 6

VOLTAMMETRIC DETECTION OF VITAMIN B_1 AND ITS DETERMINATION IN TABLETS

6.1 Detection of vitamin B_1 at unmodified carbon paste electrode

The cyclic voltammogram of vitamin B_1 recorded at unmodified CPE in pH 10.0 Tris buffer is shown in Figure 6.1.

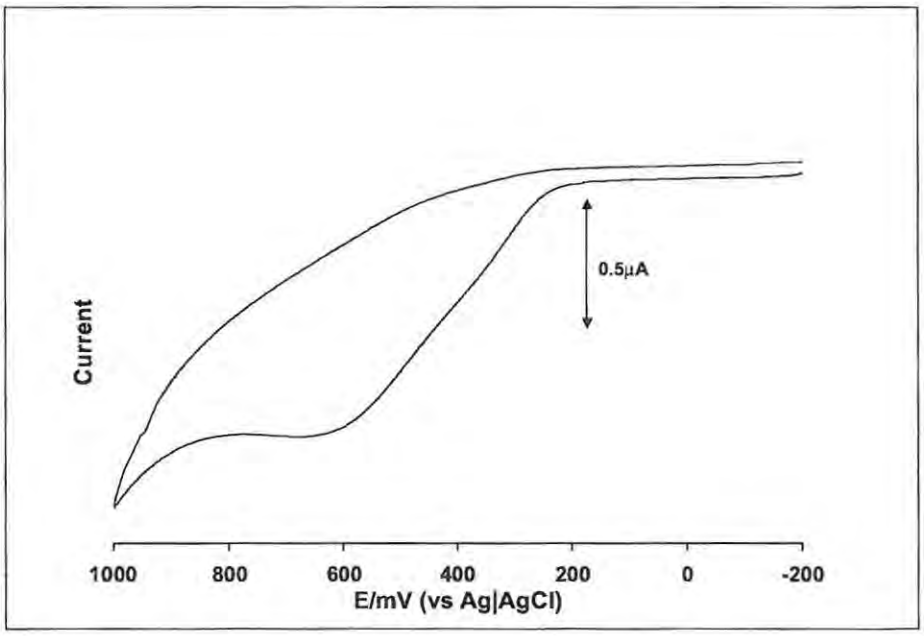

Figure 6.1: Cyclic voltammogram of $1x10^{-3}$ mol dm^{-3} vitamin B_1 in pH 10.0 Tris buffer at an unmodified carbon paste electrode. Scan rate = 100 mV s^{-1}

The oxidation of vitamin B_1 is well known[160,301,302] in alkaline medium and it is a two-electron, two-proton process forming thiochrome as the oxidation product as shown by equation 6.1.

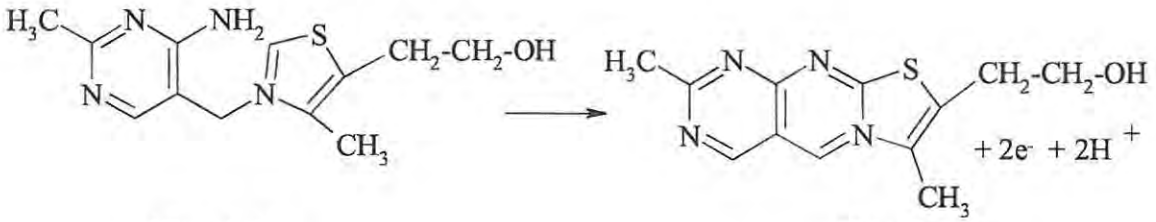

Vitamin B_1 Thiochrome

6.1

Osteryoung square wave voltammetry at the unmodified carbon paste electrode, Figure 6.2, consisted of two distinct peaks for vitamin B_1 of about the same height at 400 and 600 mV vs. Ag|AgCl. Thus the CV in Figure 6.1 is an envelope of two peaks. The presence of two peaks indicates that a relatively stable intermediate product is formed after the release of one electron. At higher potentials a second electron is released, resulting in the formation of thiochrome.

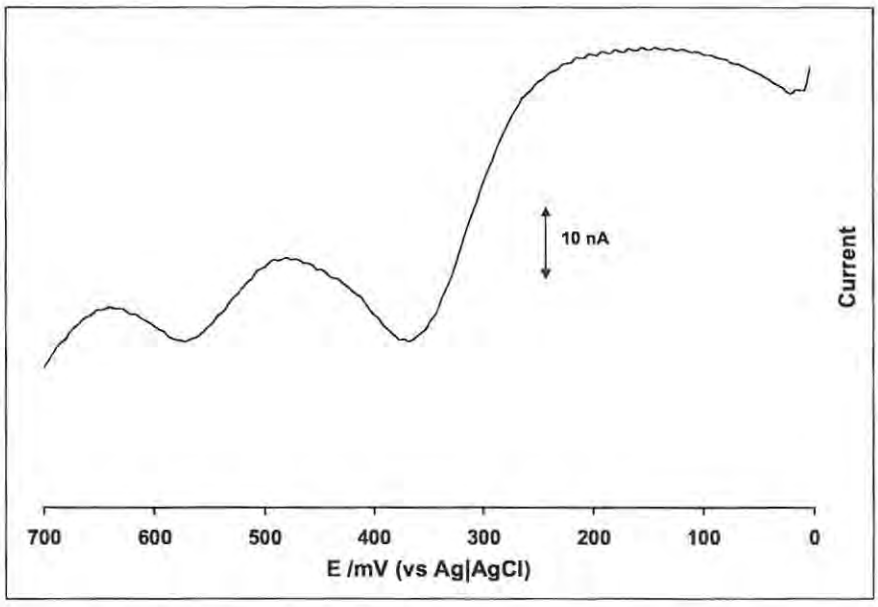

Figure 6.2: OSWV of $1x10^{-3}$ mol dm^{-3} vitamin B_1 in pH 10.0 Tris buffer at an unmodified carbon paste electrode. Scan rate = 60 mV s^{-1}

Repeating the experiment in pH 4.0 and 7.0 did not show any faradaic current. This can probably be attributed to the electro-inactivity of the protonated form of vitamin B_1.

Besides the slow kinetics of electron transfer between the electrode and vitamin B_1 in solution, the oxidation product of vitamin B_1 did not diffuse away from the unmodified CPE surface such that the electrode gets poisoned to the extent that no current due to oxidation of vitamin B_1 could be detected anymore after a few scans as shown in Figure 6.3.

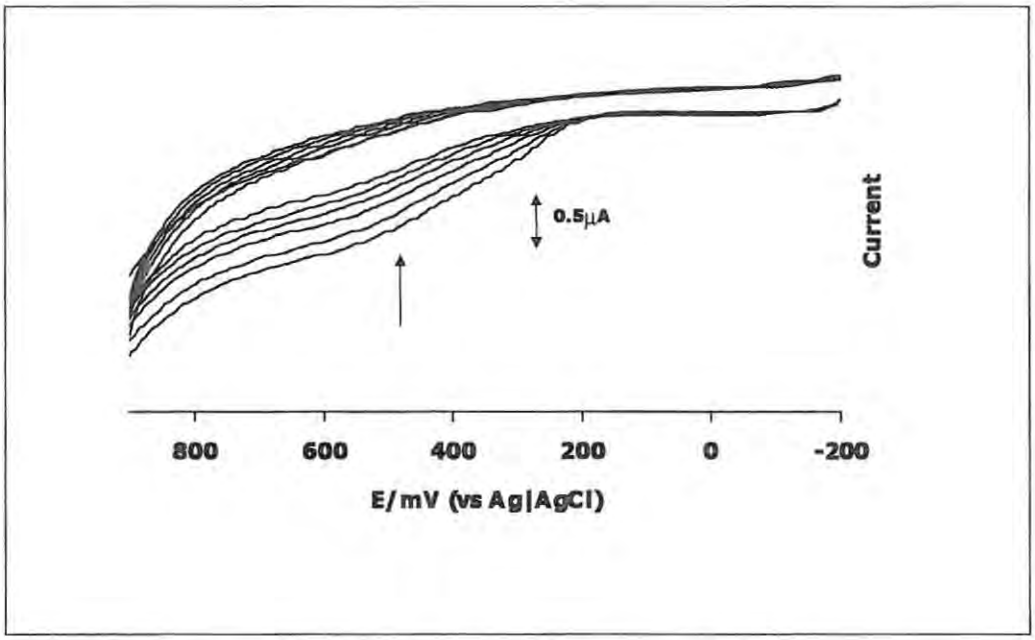

Figure 6.3: Cyclic voltammogram of $1.0x10^{-3}$ mol dm^{-3} vitamin B_1 showing decrease in oxidation current with scan number as a result of the poisoning of the electrode surface. Scan rate = 100 mV s^{-1} pH = 10.0

The poisoning of the electrode by the reaction products at the electrode surface is one of the factors that place a limitation on the use of electroanalytical techniques for the detection and determination of pharmaceutical preparations in general. The use of modified electrodes can however, dramatically improve the stability of the electrode as well as its sensitivity and selectivity. Metallophthalocyanines have been used to modify electrode surfaces in order to improve their stability and reproducibility in cases where the products of the electrode process poison the electrode surface.[55,58,237] Besides, there is the added advantage of the ease of regeneration of a fresh surface on a carbon paste electrode by simply cutting off the poisoned surface with the edge of smooth paper.

Thus carbon paste electrode modified with manganese phthalocyanine was prepared and used for the detection and determination of vitamin B_1.

6.2 Detection of vitamin B_1 at manganese phthalocyanine modified carbon paste electrode

The cyclic voltammogram of the MnPc-CPE was recorded in buffer solutions of pH 4.0, 7.0 and 10.0. No oxidation or reduction peaks were detected for the electrode alone at the different pH values investigated.

The voltammogram obtained when the carbon paste electrode modified with MnPc was employed for the detection of vitamin B_1 is shown in Figure 6.4, curve b. It is overlaid with the voltammogram obtained at an unmodified CPE, curve a, for comparison.

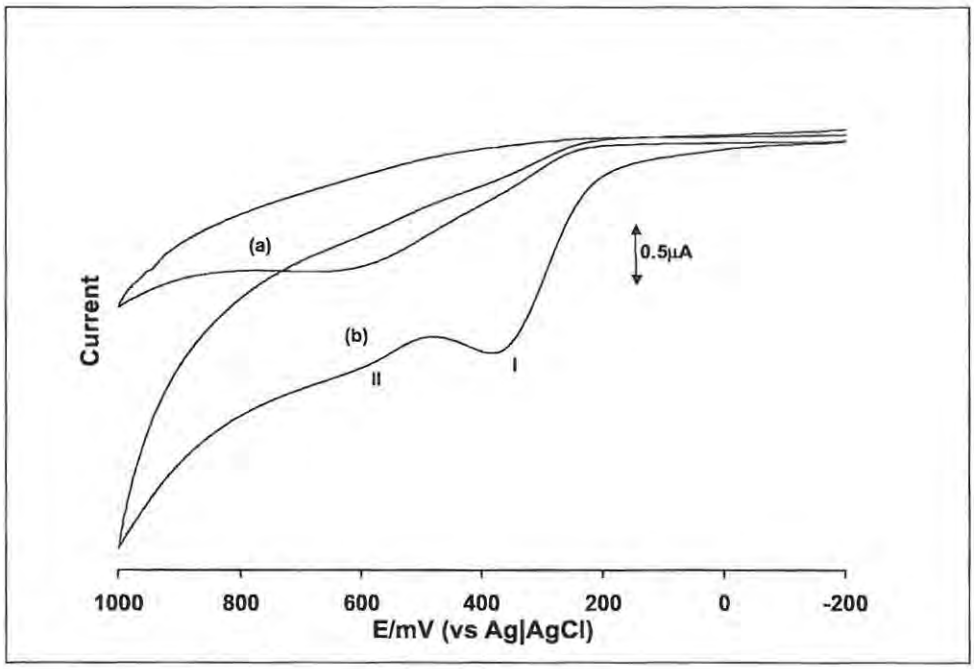

Figure 6.4: Cyclic voltammogram of $1.0x10^{-3}$ mol dm^{-3} vitamin B_1 in pH 10.0 Tris buffer at (a) CPE and (b) MnPc-CPE. Scan tare = 100 mV s^{-1} (I) 1st oxidation step (II) 2nd oxidation step.

The voltammogram obtained at MnPc-CPE showed a large increase in oxidation current obtained in the region of the potential of the first wave. The enhanced oxidation current is indicative of the catalytic activity of the MnPc modified CPE towards the first step (I in Figure 6.4) in the oxidation of vitamin B_1. There was no catalytic activity observed in the potential region of the second step (II) of the oxidation process.

Not only does modifying carbon paste electrode with MnPc produce a catalytic effect on the oxidation of vitamin B_1, it also causes the electrode to be stable towards the oxidation process by preventing the poisoning of the surface in that there was no considerable decrease in the current response after twenty scans. Figure 6.5 shows a plot of the oxidation current of vitamin B_1 against scan number when MnPc-CPE was employed. A

relatively stable current response was obtained showing that a reproducible current response was obtained for the oxidation process at the modified electrode. This indicates that the adsorption characteristics of the poisoning species are changed in such a way that irreversible adsorption on the unmodified CPE is inhibited at the modified CPE.

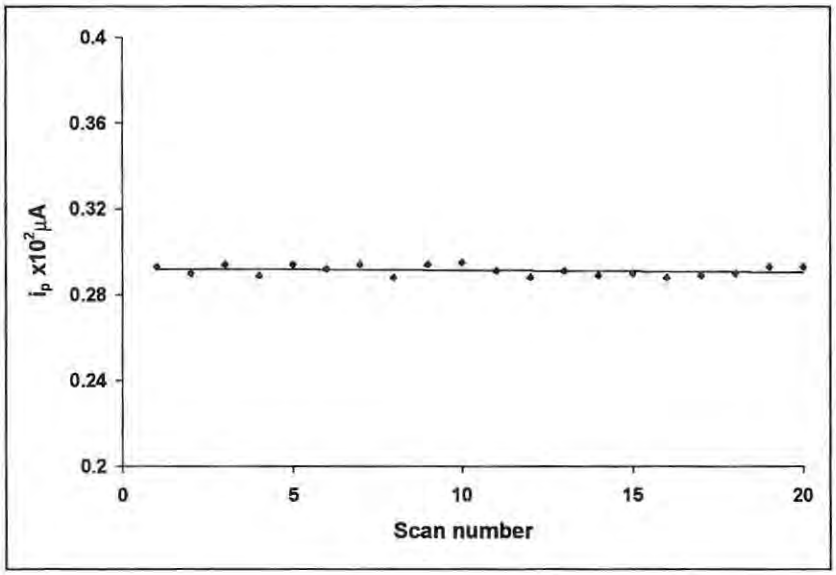

Figure 6.5: Variation of oxidation current of 2.0×10^{-5} mol dm^{-3} vitamin B_1 with scan number at MnPc-CPE. Scan rate = 100 mV s^{-1}, pH = 10.0

A plot of the peak current at 400 mV vs. Ag|AgCl versus the square root of the scan rate was linear, which indicates that the rate of the first oxidation step of vitamin B_1 is diffusion controlled.

6.3 Mechanism of electrocatalytic oxidation of vitamin B_1 at manganese phthalocyanine modified electrode

Electrocatalytic activities by metallophthalocyanine complexes usually involve the oxidation of the MPc complex followed by electron transfer from the species to be catalysed to the oxidized MPc.[229] $Mn^{II}Pc$ is known to be capable of oxidation to $Mn^{III}Pc$,[303,304] which makes the oxidized MnPc on the electrode capable of accepting an electron from vitamin B_1, hence the catalytic activity. The following mechanism, equations 6.2 to 6.4, is therefore proposed for the electrocatalytic oxidation of vitamin B_1 at the MnPc modified electrode :

$$Mn(II)Pc \equiv Mn(III)Pc + e^- \qquad \textbf{6.2}$$

$$Mn(III)Pc + C_{12}H_{17}N_4OS \equiv Mn(II)Pc + [C_{12}H_{16}N_4OS]^{\bullet} + H^+ \qquad \textbf{6.3}$$

$$[C_{12}H_{16}N_4OS]^{\bullet} \equiv C_{12}H_{15}N_4OS + H^+ + e^- \qquad \textbf{6.4}$$

Equation 6.4, corresponding to the wave at 600 mV vs. Ag|AgCl, is not electrocatalysed.

CPEs modified with metallophthalocyanine complexes of iron (FePc), cobalt (CoPc) and nickel (NiPc) were also prepared and used for the detection of vitamin B_1 but no catalytic activity was observed at these electrodes. The lack of catalytic activity particularly by FePc and CoPc is surprising since they are expected to show catalytic activities similar to

MnPc. NiPc is redox inactive at the metal center, this may explain the absence of catalytic activity at the NiPc modified CPE.

As shown is Figure 6.5, the modified electrode was found to be stable for the determination of vitamin B_1. Figure 6.6 shows the cyclic voltammograms obtained at the MnPc-CPE as a function of increasing concentration of vitamin B_1. It was observed that an increase in the concentration of vitamin B_1 was accompanied by a corresponding increase in the oxidation current.

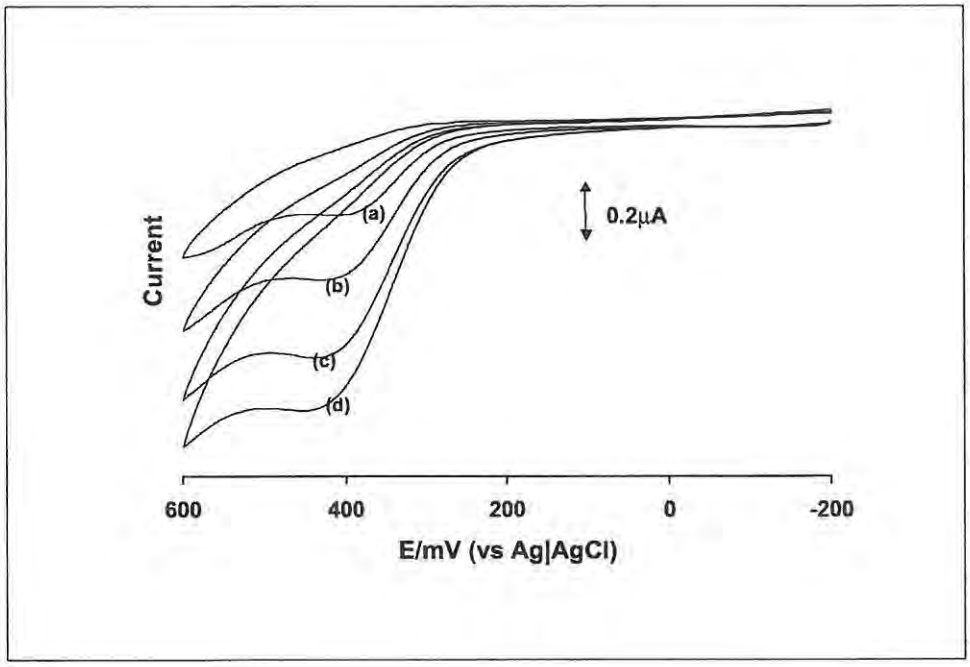

Figure 6.6: CV of (a) $2.0x10^{-5}$ (b) $4.0x10^{-5}$ (c) $6.0x10^{-5}$ (d) $8.0x10^{-5}$ mol dm^{-3} vitamin B_1 obtained at MnPc-CPE. Scan rate = 100 mV s^{-1}, pH = 10.0.

A linear curve was obtained for the plot of the oxidation current against the concentration of vitamin B_1, Figure 6.7, with a regression equation of $i_p = 0.00885[x] + 1.3x10^{-7}$, where

i_p is the peak current in Amps and [x] is the vitamin B_1 concentration in mol dm $^{-3}$. This equation was obtained from 15 series of experiments, carried out at three batches of independently constructed MnPc-CPE electrodes. From Figure 6.7, it can be seen that a detection limit of 1.46 ± 0.04x10^{-5} mol dm^{-3} is obtained, using the condition that the detection limit corresponds to twice the background current. This detection limit obtained at the modified electrode is within the appropriate region required for the determination of vitamin B_1 in the dosage form.

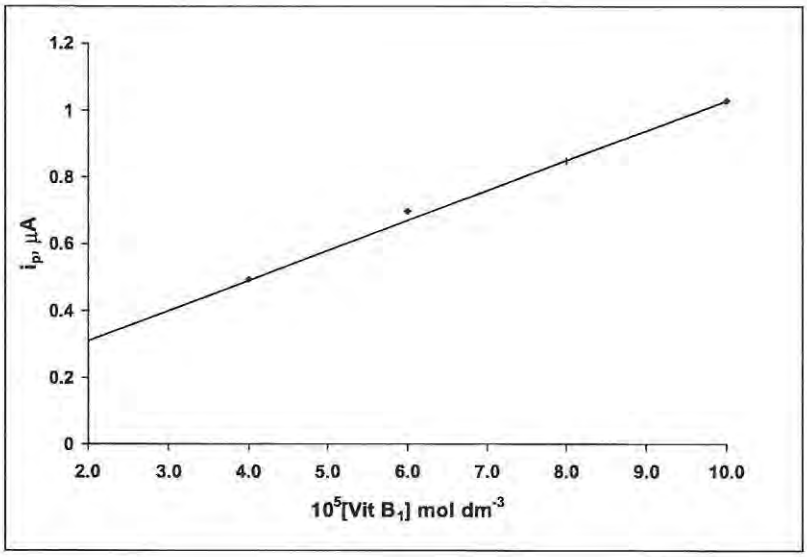

Figure 6.7: Plot of oxidation current obtained at MnPc-CPE against concentration of vitamin B_1

Vitamin B_1 was also determined by using square wave voltammetry, despite the better shape of the peaks, no remarkable improvement was obtained on the detection limit. This

is expected since vitamin B_1 gets oxidized irreversibly. An improvement in detection limit is possible only with reversible systems when SWV is employed.

6.4 Analysis of vitamin B_1 tablets

The modified electrode was used to determine the amount of vitamin B_1 in tablets using the standard addition method. For the purpose of quantifying the vitamin B_1 content of the tablets, containing 100 mg vitamin B_1 according to the manufacturer, they were prepared for analysis as described in the experimental section (Section 2.6). A summary of the results obtained by measuring the peak current at 400mV vs Ag|AgCl and calculating the concentration using the calibration plot shown in Figure 6.7 for the analysis of 125 tablets is provided in Table 6.1. These data were obtained by using five different electrodes at five tablets per electrode. Each measurement was repeated five times. A vitamin B_1 content of 99.79 ± 0.10 mg was obtained, in close agreement with the 100mg/tablet quoted by the manufacturer.

Table 6.1: Vitamin B_1 content of analysed tablets

Electrode batch number	Vitamin B_1 content (mg) obtained with 5 electrodes and 5 measurements per electrode
1	99.82 ± 0.08
2	99.77 ± 0.11
3	99.70 ± 0.09

4	99.80 ± 0.12
5	99.84 ± 0.10
Average	99.79 ± 0.10

This work demonstrates the possibility of the use of voltammetric method for the direct determination of vitamin B_1 in tablets at an MnPc modified carbon paste electrode. The modified electrode was found to be stable towards the determination of vitamin B_1 because it was not poisoned during the oxidation of vitamin B_1 as opposed to the unmodified electrode that gets poisoned quickly. The method is sensitive, rapid, reliable, easy to perform and very suitable for the analysis of vitamin B_1 in tablets.

CONCLUSION

Some metallophthalocyanine complexes have been synthesized and investigated as potential electrocatalysts for the detection and analysis of dopamine, serotonin and histamine. Apart from studying the possible interactions that could take place between the metallophthalocyanines and these transmitters substances as a necessary step towards understanding the mechanism of the electrocatalytic process, the study of the interaction is of biological importance because metallophthalocyanines are important models for biological systems due to their close structural relationship with the porphyrins.

Dopamine, serotonin and histamine formed complexes with iron (II) tetrasulfophthalocyanine. In the complexes formed, both dopamine and serotonin were oxidized and iron was reduced from the +2 oxidation state to +1 in FeTSPc. The complexes formed with dopamine and serotonin were designated as $[(DA^{+})Fe^{I}TSPc]^{4-}$ and $[(5\text{-}HT^{+})Fe^{I}TSPc]^{4-}$ respectively. Histamine showed a very different pattern from that observed for dopamine and serotonin when it formed a complex with iron (II) tetrasulfophthalocyanine. Coordination of histamine resulted in the oxidation of iron from the +2 oxidation state to +3. The complex formed was designated as $[(His)Fe^{III}TSPc]^{3-}$. The rate and equilibrium constants obtained for the coordination were in the range of values reported in the literature for axial ligand exchange reactions of iron phthalocyanine complexes.

Iron (II) tetrasulfophthalocyanine modified millimetric-sized carbon paste electrodes exhibited good electrocatalytic activity towards the oxidation of both dopamine and serotonin by considerably increasing their oxidation currents and shifting their oxidation potentials to less positive values compared to the unmodified electrode. A detection limit of the order of 10^{-6} mol dm^{-3} was obtained at the modified electrodes for the determination of dopamine and serotonin. Not only did the modified electrodes show electrocatalytic activity towards the determination of both dopamine and serotonin, the electrodes were able to prevent the oxidation currents due to ascorbic acid from being observed. This is a very important development in that the major interfering molecule in the electroanalysis of neurotransmitters in biological or physiological samples is ascorbic acid. The modified electrodes were very stable for the analysis of both dopamine and serotonin either individually or in a mixture, and in the presence of ascorbic acid.

The electrocatalytic activity and stability of iron (II) tetrasulfophthalocyanine modified electrodes was compared with activity and stability of other electrodes modified with various substituted iron phthalocyanine complexes and the phthalocyanine complexes of cobalt and nickel. Iron (II) tetrasulfophthalocyanine gave the best catalytic activity.

Ultra micro carbon paste disc and band electrodes were prepared and characterized using the redox couple of potassium ferrocyanide. Steady state current conditions were observed at the electrodes signifying true ultra micro lectrode behaviour. Carbon paste ultra micro disc electrodes modified with iron (II) tetrasulfophthalocyanine were used for

the determination of dopamine and ascorbic acid in a mixture. Although the modified ultra micro electrode could not discriminate against the oxidation of ascorbic acid because of the smaller negative charge available at the electrode surface relative to the charge of ascorbic acid in solution, an expression was derived for the determination of dopamine in a mixture with ascorbic acid. A detection limit of 4.2×10^{-7} mol dm^{-3} was obtained for dopamine at the modified ultra micro electrode in the presence of ascorbic acid.

There is still the need to optimize the ultra micro electrode fabrication and modification procedure as this electrode holds great potential for the direct *in vivo* detection and quantification of neurotransmitters because of the lower detection limit which, of course, could still be improved upon.

Manganese phthalocyanine modified carbon paste electrodes were found to exhibit good electrocatalytic activity towards the oxidation of vitamin B_1. Modifying the electrode also prevented the fouling observed at unmodified electrodes showing that the modified electrode approach is capable of solving the problem of surface passivation by the products of the electrode reaction process. This surface passivation is the main reason for the general neglect of electroanalytical techniques in the analysis of pharmaceutical products despite the many advantages these techniques offer. The modified electrodes were employed for the determination of vitamin B_1 in tablets using the standard addition method.

References

1 J. Wang, Analytical Electrochemistry, VCH Publishers Inc., New York, 1994.

2 P.T. Kissinger, C.R. Preddy, R.E. Shoup, W.R. Heineman in Laboratory Techniques in Electroanalytical Chemistry, 2nd ed., Eds. P.T. Kissinger, W. R. Heineman, Marcel Dekker Inc., New York, 1996.

3 A.J. Bard, L.R. Faulkner, Electrochemical Methods; Fundamentals and Application, John Wiley and Sons, New York, 1980.

4 C.M.A. Brett, A.M.O. Brett, Electrochemistry, Principles, Methods and Applications, Oxford University Press, Oxford, 1993.

5 P.T. Kissinger, in Laboratory Techniques in Electroanalytical Chemistry, 2nd ed., Eds. P.T. Kissinger, W.R. Heineman, Marcel Dekker Inc., New York, 1996.

6 F.M. Hawkridge, in Laboratory Techniques in Electroanalytical Chemistry, 2nd ed, Eds. P.T. Kissinger, W.R. Heineman, Marcel Dekker Inc., New York, 1996.

7 R.L. McCreery, K.K. Cline, Laboratory Techniques in Electroanalytical Chemistry, 2nd edition, Eds. P.T. Kissinger, W.R. Heineman, Marcel and Dekker Inc. 1996.

8 R.N. Adams, Anal. Chem., 1958, 30, 1576.

9 G. Dryhurst, D.L. McAllister, Laboratory Techniques in Electroanalytical Chemistry, 1st edition, Eds. P.T. Kissinger, W.R. Heineman, Marcel and Dekker Inc. 1984.

10 K. Kalcher, J-M. Kauffmann, J. Wang, I. Svancara, K. Vytras, C. Neuhold, Z. Yang, Electroanalysis, 1995, 7, 5.

11 E.D. Kingsley, D.I. Curran, Anal. Chim. Acta, 1988, 206, 385.

12 J. Wang, B.K. Deshmukh, M.A. Targove, J. Electroanal. Chem., 1985, 194, 339.

13 N.D. Danielson, I. Wanga, M.A. Targove, Anal. Chem., 1989, 61, 2585

14 J. Lindquist, Anal. Chem., 1973, 45, 1006.

15 N.A. Ulakhovich, E.P. Medyantseva, G.K. Budnikov, Zhur. Anal. Khim., 1993, 48, 690. Translated by Kazan State University.

16 K. Kalcher, Electroanalysis, 1990, 2, 419.

17 M.E. Rice, Z. Galus, R.N. Adams, J. Electroanal. Chem., 1983, 143, 89.

18 F.I. Cheng, C.K. Martin, Anal. Chem., 1988, 249, 339.

19 H. Monien, H. Specker, K. Zinke, Z. Fresenius, Anal. Chem. 1967, 225, 342.

20 N.E. Zoulis, D.P. Nikolelis, C.E. Efstathiou, Analyst, 1990, 115, 291.

21 I. Svancara, K. Kalcher, W. Diewald, K. Vytras, Electroanalysis, 1996, 8, 336.

22 P.D. Lyne, R.D. O'Neil, Anal. Chem., 1990, 62, 2347.

23 I. Svancara, K. Vytras, Anal. Chim. Acta, 1988, 206, 385.

24 W.R. Heineman, P.T. Kissinger, in Laboratory Techniques in Electroanalytical Techniques, 2nd ed., Eds. P.T. Kissinger, W.R. Heineman, Marcel Dekker Inc., New York, 1996.

25 G.C. Barker, I.L. Jenkins, Analyst, 1952, 77, 685

26 J. Osteryoung, R.A. Osteryoung, Anal. Chem., 1985, 57, 101A.

27 L.M. Moretto, P.Ugo, R. Lacasse, G.Y. Champagne, J. Chevalet, J. Electroanal. Chem., 1999, 467, 193.

28 L.M. Moretto, B. Brunetti, J. Chavalet, P. Ugo, Electrochem. Commun., 2000, 2, 175.

29 W.R. Heineman, Anal. Chem., 1978, 50, 390A.

30 R. Cieslinski, N.R. Armstrong, Anal. Chem., 1979, 51, 565.

31 IUPAC recommendations, 1997, Pure and Appl. Chem., 1997, 69, 1317.

32 R.F. Lane, A.T. Hubbard, J. Phys. Chem., 1973, 77, 1401.

33 C.M. Elliot, R.W. Murray, Anal. Chem., 1976, 48, 1247.

34 C.R. Martin, C.A. Foss Jr., in Laboratory Techniques in Electroanalytical Chemistry, 2nd ed.,Eds. P.T. Kissinger, W.R. Heineman, Marcel Dekker Inc., New York, 1996.

35 A.J. Bard, J. Chem., Ed., 1983, 60, 303.

36 K. Ozoemena, P. Westbroek, T. Nyokong, Electrochem. Commun., 2001, 3, 529.

37 J. Wang, T. Golden, K. Varughese, I. El-Rayes, Anal. Chem., 1989, 61, 509.

38 M.B. Gilbert, D.J. Curran, Anal. Chem., 1986, 58, 1028.

39 T.J. Mafatle, T. Nyokong, J. Electroanal. Chem. 1996, 408, 213.

40 T-F. Kang, G-L. Shen, R-Q, Yu, Anal. Chim. Acta, 1997, 356, 245.

41 S. Griveau, G. Pavez, J.H. Zagal, F. Bedioui, J. Electroanal. Chem., 2001, 497, 75.

42 M.A. Ruiz, M.G. Blazquez, J.M. Pingarron, Anal. Chim. Acta, 1995, 305, 49.

43 B.F. Watkins, J.R. Behling, E. Kariv, L.L. Miller, J. Am. Chem. Soc., 1975, 97, 3549.

44 L. Netzer, J. Sagiv, J. Am. Chem. Soc., 1983, 105, 674.

45 J-M. Zen, W-M. Wang, G. Ilangovan, Anal. Chim. Acta, 1998, 372, 315.

46 C.A. Goss, C.J. Miller, M. Majda, J. Phys. Chem., 1991, 300, 337.

47 N. Winograd, T. Kuwana, Electroanal. Chem., 1974, 7, 1.

48 K. Ashley, F. Weinert, M.G. Samant, H. Seki, M.R. Philpott, J. Phys. Chem., 1991, 95, 7409.

49 R.W. Collins, Y-T. Kim, Anal. Chem., 1990, 62, 887A.

50 T. Ikeshoji, T. Iwasaki, Inorg. Chem., 1988, 27, 1123.

51 F.F Fan, A.J. Bard, J. Electrochem. Soc,. 1989, 136, 3216.

52 J.H. Schott, C.P. Araña, H.D. Abruña, H.H. Petach, C.M. Elliot, H.S. White, J. Phys. Chem., 1992, 96, 5222.

53 P.T. Varineau, B.A. Buttry, J. Phys. Chem., 1987, 91, 1292.

54 S. Dong, Y. Wang, Electroanalysis, 1989, 1, 99.

55 N. Grootboom, T. Nyokong, Anal. Chim. Acta, 2001, 432, 49.

56 L.R. Sharma, G. Singh, A. Sharma, B. Electrochem., 1988, 4, 679.

57 T. Ruzgas, J. Emnèus, L. Gorton, G. Marco-Varga, Anal. Chim. Acta, 1995, 311, 425.

58 T. Mafatle, T. Nyokong, Anal. Chim. Acta, 1997, 354, 307.

59 J.P. Collman, P. Danisevich, Y. Jonai, M. Marrocco, C. Koval, F.C. Anson, J. Am. Chem. Soc., 1980, 192, 6027.

60 C. Shi, F.C. Anson, Inorg. Chem., 1995, 34, 4554.

61 B.A. Moyer, M.S. Thompson, T.J. Meyer, J. Am. Chem. Soc., 1980, 102, 2310.

62 S.L. Vikalazi, T. Nyokong, Polyhedron, 1998, 17, 4415.

63 S.L. Vilakazi, T. Nyokong, Polyhedron, 2000, 19, 229.

64 Q-Y. Peng, T.F. Guarr, Electrochimica Acta, 1994, 39, 2629.

65 A.C. Michael, R.M. Wightman, Laboratory Techniques in Electroanalytical Chemistry, 2nd ed., Eds P.T. Kissinger and W.R. Heineman, Marcel Dekker Inc., New York, 1996.

66 C. Amatore, in Physical Electrochemistry, Principles, Methods and Applications, ed I. Rubinstein, Marcel Dekker Inc., New York, 1995.

67 J.O. Howell, J. Goncalves, C. Amatore, L. Klasinc, J. Kochi, R.M. Wightman, J. Am. Chem. Soc., 1984, 106, 3968.

68 D.O. Wipf, K.R. Wehmeyer, R.M. Wightman, J. Org. Chem., 1986, 51, 4760.

69 A. Fitch, D.H. Evans, J. Electroanal. Chem., 1986, 202, 83.

70 M.I. Montenegro, D. Pletcher, J. Electroanal. Chem., 1986, 200, 371.

71 C.P. Andrieux, P. Hapiot, J.M. Saveant, Electroanalysis, 1990, 2, 183.

72 R. Wehmeyer, M.R. Deakin, R.M. Wightman, Anal. Chem., 1985, 57, 1913.

73 W.F. Berry, S.G. Weber, J. Electroanal. Chem., 1986, 208, 77.

74 A.G. Ewing, M.A. Dayton, R.M. Wightman, Anal. Chem., 1981, 53, 1842.

75 A.S. Baranski, J. Electrochem. Soc., 1986, 133, 93.

76 M.A. Dayton, J.C. Brown, K.J. Stutts, R.M. Wightman, Anal. Chem., 1980, 52, 496.

77 T. Hepel, W. Plot, J. Osteryoung, J. Phys. Chem., 1983, 87, 1278.

78 T. Hepel, J.Osteryoung, J. Phys. Chem., 1982, 86, 1406.

79 A.J. White, J.W. Jorgenson, Anal. Chem., 1986, 58, 2992.

80 R.C. Engstrom, C.N. Pharr, Anal. Chem., 1989, 61, 1099A.

81 A.J. Bard, F. Fan, D.T. Pierce, P.R. Unwin, D.O. Wipf, F. Zhou, Science, 1991, 254, 68.

82 J.B. Chien, R.A. Wallingford, A.G. Ewing, J. Neurochem, 1990, 54, 633.

83 R.N. Adams, Prog. Neurobiol., 1990, 35, 297.

84 R.M. Wightman, L.J. May, A.C. Michael, Anal. Chem., 1988, 60, 769A.

85 J.A. Stamford, J.B. Justice, Anal. Chem., 1996, 359A.

86 G.I. Stevenson, R. Baker, Edu. in Chem., 1996, 124.

87 I. Dox, B.J. Melloni, G.F. Eisner, Melloni's illustrated medical dictionary. The William and Wilkins Company, Baltimore, 1979.

88 G. Siegel, B. Agranoff, B.R.W Albers, P. Molinoff, Basic neurochemistry, 4th edition, Ravens press, New York, 1989.

89 A. Veca, J.H. Dreisbach, J. Chem. Edu., 1988, 65, 108.

90 H. Dale, Proc. R. Soc. Med., 1935, 28, 319.

91 H.F. Bradford., Chemical Neurobiology, An Introduction to Neurochemistry, W.H. Freeman and Company, New York, 1986, p155.

92 Z.L. Kruk, C.J. Pycock, Neurotransmitters and Drugs, Croom Helm, London, 1979 p9.

93 O. Hornykiewicz, in Movement Disorders, eds C.D. Marsden and S. Fahn, Butterworth Scientific, London, 1982, p41-58.

94 E.D. Bird, L.L. Iversen, Brain Res. 1974, 97, 457.

95 L.L. Iversen, S.P.R. Rose, Eds Biochemistry and Mental Illness, The Biochemical Society, London, 1973.

96 A.R. Green, D.W. Costain, in Pharmacology of Affective Disorders, Eds E.S. Paykel, A. Coppen, Oxford, 1979, p14.

97 R.J. Bridges, J.W. Geddes, D.T. Monaghan, C.W. Cotman, Excitatory amino acids in health and disease, Ed. D. Lodge, John Wiley and sons, 1988, p321

98 M.N. Rossor, C. Stevendsen, P. Hunt, C.Q. Mountjoy, M. Roth, L.L. Iversen, Neurosci. Lett., 1981, 28, 217

99 G.E. Figg, A.C. Foster, Neuroscience, 1983, 9, 701.

100 T.W. Stone, M.J. Jarid, Brain Res., 1983, 264, 165.

101 J.W. Olney, Excitatory amino acids in health and disease, Ed. D. Lodge, John Wiley and sons, 1988, p31.

102 G.N. Woodruff, A.C. Foster, E.F.H. Wong, R. Cull, J.A. Kemp, L.L. Iversen, Excitatory amino acids in health and disease, Ed. D. Logde, John Wiley and sons, 1988, p379.

103 R.N. Adams, Anal. Chem., 1976, 48, 1128A

104 P. Waldmeir, L. Maitre, Anal. Biochem., 1973, 51, 474.

105 S. Undenfriend, J. Biol. Chem., 1955, 215, 337.

106 P.T. Waalkes, J. Lab. Clin. Med., 1959, 53, 824.

107 K.M. Taylor, Neurobiol. Dopamine, 1979, 31.

108 K.Imai, J. Chromatogr., 1975, 105, 135.

109 N. Ben-Jonathan, J.C. Porter, Endocrinology, 1976, 98, 1497.

110 Z.Yi, P.R.Brown, Biomed. Chromatogr., 1991, 5, 101.

111 E.Gelpi, Advanced Chromatogr., 1987, 26, 231.

112 R.G. Wiegand, E. Scherfling, J. Neurochem., 1962, 9, 113.

113 F. Karoum, Anal. Biochem., 1972, 47, 550.

114 H. Svendsen, T. Greibrokk, J. Chromatogr., 1981, 213, 429.

115 D.D. Clarke, J. Gas Chromatogr., 1969, 5, 307.

116 M. Morris, Anal. Lett., 1976, 95, 467.

117 C. Zhang, J. Huang, Z. Zhang, M. Aizawa, Anal. Chim. Acta, 1998, 374, 105.

118 L. Zhang, N. Teshima, T. Hasebe, M. Kurihara, T. Kawashima, Talanta, 1999, 50(3), 677.

119 K. Mori, Life Sciences, 1987, 41, 901.

120 S.H. Koslow, F.Cattabeni, E. Costa, Science, 1972, 176, 177.

121 K.F. Faull, Life Sciences, 1987, 41, 889.

122 N.Kaneda, J. Chromatogr., 1986, 360, 211.

123 I.N. Mefford, Life Sciences, 1987, 41, 893.

124 P.T. Kissinger, G.C. Davis, R.E. Shoup, Anal. Chem., 53,1981, 156.

125 F.C. Cheng, Y.Shih, Y-J. Liang, C-S. Yang, J. Chromatogr. B, 1996, 682, 195.

126 S. Ikeyona, Chem. Pharm. Bull., 1978, 26, 3530.

127 C.T. Duda, Tech. Behav. Neural Sci., 1993, 11, 41.

128 F.G. Gonon, F. Navarre, M.J. Buda, Anal. Chem., 1984, 56, 575

129 R.M.Wightman, D.J. Wiedemann, L.J. May, E.W. Kristensen, J.E. Baur, Anal. Chem., 1988, 60, 1268.

130 C. Hsueh, R. Bravo, A.J. Jaramilo, A. Brajter-Toth, Anal. Chim. Acta, 1997, 349, 67.

131 B.P. Jackson, S.M.Dietz, R.M. Wightman, Anal. Chem., 1995, 67, 1115.

132 A. Domenech, M.T. Domenech-Carbo, H. Garcia, M.S. Galletero, Chem. Commun., 1999, 2173.

133 K. Miyazaki, G. Matsumoto, M. Yamada, S. Yasui, H. Kanako, Electrochim. Acta, 1999, 44, 3809.

134 B. Duong, R. Arachabaleta, N.J. Tao, J. Electroanal. Chem., 1998, 447, 63.

135 Z.Gao, H. Huang, Chem. Commun., 1998, 2107.

136 A. Fujishima, T.N. Rao, E. Popa, B.V. Sarada, I. Yagi, D.A.Tryk, J. Electroanal. Chem., 1999, 473, 179.

137 J-M. Zen, I-L. Cheng, Y. Shih, Anal. Chim. Acta, 1998, 369, 103.

138 Z. Gao, D. Yap, Y. Zhang, Anal. Sci., 1998, 4, 1059.

139 B.V. Sarada, T.N. Rao, D.A. Tryk, A. Fujishima, Anal. Chem., 2000, 72, 1632.

140 A. Ciszewski, G. Milczarek, Anal. Chem., 1999, 71, 1055.

141 J.X.Feng, M. Brazell, K.Renner, R. Kasser, R.N. Adams, Anal. Chem. 1987, 59, 1863.

142 F.G. Gonon, C.M. Fombarlet, M.J. Buda, J.F. Pujol, Anal. Chem., 1981, 53, 1386.

143 F.G. Gonon, M. Buda, R. Cespuglio, M. Jouvet, J.F. Pujol, Nature, 1980, 286, 902.

144 L. Falat, H-Y. Heng, Anal. Chem., 1982, 54, 2108.

145 M. Poon, R.L. McCreery, Anal. Chem., 1986, 58, 2745.

146 D.T. Fagan, I.F. Hu, T. Kuwana, Anal. Chem., 1985, 57, 2759.

147 R.M. Wightman, T.K. Kwagoe, Talanta, 1994, 41, 865.

148 G. Nagy, G.A. Gerherdt, A.F. Oke, M.E. Rice, R.N.Adams, R.B.Moore, M.N. Szentirmay, C.R. Martin, J. Electroanal. Chem., 1983, 188, 85.

149 J-M. Zen, I-L. Chen, Electroanal., 1997, 9, 537.

150 D-M. Zhou, H-X. Ju, H-Y. Chen, J. Electroanal. Chem., 1996, 408, 219.

151 X-T. Xu, F. Kitamura, T. Ohsaka, K. Tokuda, Anal. Sci., 1994, 10, 399.

152 G. Edogdu, H.B. Mark Jr, E. Karagozler, Anal. Lett., 1996, 29, 221.

153 N.Larsson, T. Ruzgas, L. Gorton, M. Kokaia, P. Kissinger, E.CsÖregi, Electrochim. Acta, 1998, 43, 3541.

154 E.S. Forzani, G.A. Rivas, V.M. Solis, J. Electroanal. Chem., 1997, 435, 77.

155 J. Wang, M.S. Lin, Anal., Chem., 1988, 60, 1545.

156 D. Michael, E.R. Travis, R.M. Wightman, Anal. Chem., 1998, 586A.

157 P.S.Cahill, D. Walker, J.M. Finnegan, G.E.Michelson, E.R. Travis, R.M. Wightman, Anal. Chem., 1996, 68, 3180.

158 R.M. Wightman, J.D. Michael, J. Pharm. Biomed. Anal., 1999, 19, 33.

159 J.R.A. Pollock, R. Stevens, Dictionary of Organic Compounds, Eyre & Spottiswoode Publishers, 1965, vol.1, p 238.

160 A. Korolkovas, Essentials of medicinal chemistry, John Wiley and sons, 2nd ed, 1988, p100.

161 F.A. Robinson, The Vitamin B complex, John Wiley and sons, 1951, p 57.

162 J.P. Hart, M.D. Norman, S. Tsang, Analyst, 1995, 120, 1059.

163 S. Albalahurtado, M.T. Vecianano gnes, M. Izquierdopulido, M. Marinefront, J. Chromatogr. *A.*, 1997, 778, 247.

164 R.E. Echols, H.H. Miller, L. Thompson, J. Chromatogr., 1985, 347, 89.

165 F.A. Elesi, A.Z. Abuzuhri, S.I. Alkhalil, M.S. Abdelatif, Talanta, 1997, 44, 2051

166 C.G. Benito, T.G. Sancho, J.M. Calatayud, Anal. Chim. Acta, 1993, 279, 293.

167 N.Q. Jie, D.L. Yang, Q.N. Zhang, J.H. Yang, Z.Q. Song, Anal. Chim. Acta,

1998, 359, 87.

168 Q. Chen, D. Li, H. Yang, Q. Zhu, H. Zheng, J. Xu, Analyst, 1999, 124, 771.

169 N. Grekas, A.C. Calokerinos, Talanta, 1990, 37, 1043.

170 M.A. Ryan, J.D. Ingle, Anal Chem., 1980, 52, 2177.

171 United States Pharmacopeia, National formulary XIX, 2000, 1639.

172 British Pharmacopoeia, HM Stationery Office, London, 1993, 2, 1129.

173 G.H. Zhang, T. Imato, Y. Asano, T. Sonoda, H. Kobayashi, N. Ishibashi, Anal. Chem., 1990, 62, 1644.

174 A. Ciszweski, J. Wang, Analyst, 1992, 117, 985.

175 R.P. Linstead, J. Chem. Soc. 1934, 1016

176 R.P. Linstead, J. Chem., Soc., 1936, 1195

177 E. Ough, T. Nyokong, K.A.M. Creber, M.J. Stillman, Inorg. Chem., 1988, 27, 2725.

178 A.B.P. Lever, S.R. Pickens, P.C. Minor, L. Licoccia,B.S. Ramaswamy, K. Magnell, J. Am. Chem. Soc., 1981, 103, 6800.

179 H. Sugimoto, T. Higashi, M. Mori, Chem., Lett., 1982, 801

180 P. Sayer, M. Gouterman, C.R. Connell, Acc. Chem. Res., 1982, 15, 73.

181 N.B. McKeown, Chem. & Ind., 1999, 92

182 A.B.P. Lever, Adv. Inorg. Radiochem., 1965, 7, 28.

183 P. Gregory, J. Porphyrins and Phthalocyanines, 1999, 3, 468.

184 R.P. Linstead, A.R. Lowe, J. Chem. Soc., 1934, 1022.

185 A. Shaabani, J. Chem. Res. (S), 1998, 672.

186 D.M. Maree, T. Nyokong, J. Chem. Res. (S), 2001, 68.

187 C.C. Leznoff, S.M. Marcuccio, S. Greenberg, A.P.B. Lever, K.B. Tomer, Can. J. Chem., 1985, 63, 133.

188 M. Hanack, P. Haisch, H. Lehman, Synthesis, 1993, 387.

189 J.H. Weber, D.H. Busch, Inorg. Chem., 1965, 4, 469.

190 J. Metz, O. Schneider, M. Hanack, Inorg. Chem., 1984, 23, 1065.

191 T. Nyokong, J. Chem. Soc., Dalton Trans., 1993, 3601.

192 L. Boucher, Coordination Chemistry of Macrocyclic compounds, Ed. G.A. Melson, Plenium Press, 1979, 461.

193 T. Nyokong, M.J. Stillman in Phthalocyanine: Properties and Applications, Eds. A.P.B. Lever, C.C. Leznoff, vol. 1, VCH Publishers, New York, 1993.

194 M. Gouterman, in The Porphyrins, vol. III, part A, Physical Chemistry, Ed. D. Dolphin, Academic Press, New York, 1978.

195 R. Taube, Pure Appl. Chem., 1974, 38, 427.

196 J.R. Platt, H.C. Longuett-Higgins, C.W. Rector, J. Chem. Phys., 1950, 18, 1174.

197 B.R. Hellebone, M.J. Stillman, J. Chem. Soc., Faraday Trans. II, 1978, 74, 2107.

198 Y. Iyeshida, K. Yakushi, H. Kuroda, Chem. Phys., 1984, 87, 101.

199 L. Edwards, M. Gouterman, C.B. Rose, J. Am. Chem. Soc., 1976, 98, 7638.

200 W.A. Nevin, W. Liu, S. Greenberg, M.R. Hempstead, S.M. Maruccio, M.M. Melnik, C.C. Leznoff, A.B.P. Lever, Inorg. Chem., 1987, 26, 291.

201 A.B.P. Lever, M.R. Hempstead, C.C. Leznoff, W. Liu, M. Melnik, W.A. Nevin, P. Seymour, Pure Appl. Chem., 1986, 58, 1467.

202 N. Nensala, T. Nyokong, Polyhedron, 1998, 17, 3467.

203 K. Kasuga, M. Tsutsui, Coord. Chem. Rev., 1980, 32, 67.

204 N. Nensala, T. Nyokong, Polyhedron, 1996, 15, 867.

205 O.T.E. Sielcken, M.M. van Tilborg, M.F.M. Rocks, R. Hendricks, W. Drenth,

R.J.M. Nolte, J. Am. Chem. Soc., 1987, 109, 4261.

206 N. Chebotareva, T. Nyokong, J. Coord. Chem., 1999, 46, 433.

207 M. Sekota, T. Nyokong, Polyhedron, 1997, 16, 3279.

208 J.F. Myers, R.G.W. Canham, A.B.P. Lever, Inorg. Chem., 1975, 14, 461.

209 D.W. Clack, J.R. Yandle, Inorg. Chem., 1972, 11,1739.

210 D.W. Clack, N.S. Hush, I.S. Woosley, Inorg. Chim. Acta, 1976, 19, 129.

211 L.D. Rollman, R.T. Iwamoto, J. Am. Chem. Soc., 1968, 90, 1455.

212 D.W. Clack, N.S. Hush, J.Am. Chem. Soc., 1965, 87, 4238.

213 R.H. Felton, H. Linschitz, J. Am. Chem., Soc., 1966, 88, 1113.

214 A.B.P. Lever, E.R. Milaeva, G. Speier, in The Phthalocyanines; Properties and Applications, Vol. III, Eds. C.C. Lenznoff, A.B.P. Lever, VCH Publishers, New York, 1993

215 R.O Loufty, C. Chang, J. Chem., Phys., 1980, 73, 2902.

216 A. Louati, M.El. Meray, J.J. Andre, J. Smith, K.M. Kadish, M. Cross, A. Giraudeau, Inorg. Chem., 1985, 24, 1175.

217 A.B.P. Lever, J.P. Wilshire, Can. J. Chem., 1976, 54, 2514.

218 A. Giraudeau, A. Louati, M. Cross, J.J. Andre, J. Simon, C.H. Su, K.M. Kadish, J. Am. Chem. Soc., 1983, 105, 2917.

219 G. Fu, Y-S. Fu, K. Kayaraj, A.B.P. Lever, Inorg. Chem., 1990, 29, 4090.

220 T. Nyokong, Z. Gasyna, M.J. Stillman, Inorg. Chem., 1987, 26, 1087.

221 T. Nyokong, Z. Gasyna, M.J. Stillman, Inorg. Chem., 1987, 26, 548.

222 T. Nyokong, Synth. Met., 1994, 66, 107.

223 A.B.P. Lever, S. Liccoccia, B.S. Ramaswamy, S.A. Kandil, D.V. Stynes, Inorg. Chim. Acta, 1981, 51, 169.

224 R.H. Campbell, G.A. Heath, G.T. Hefter, R.C. McQeen, J. Chem. Soc. Chem. Commun., 1983, 1128.

225 H. Li, T.F. Guarr, J. Chem. Soc. Chem. Commun., 1989, 832.

226 C.C. Leznoff, S. Greenberg, S.M. Marcuccio, P.C. Minor, P. Seymour, A.B.P. Lever, Inorg. Chim. Acta, 1984, 89, L35.

227 R.J. Blagrove, Austr. J. Chem., 1973, 26, 472.

228 W. Liu, M.R. Hempstead, W.A. Nevin, M. Melnik, A.B.P. Lever, C.C. Leznoff, J. Chem. Soc. Dalton Trans., 1987, 2511.

229 J.H. Zagal, coord. Chem. Rev. 1992, 119, 89.

230 C.A. Melendres, X. Feng, J. Electrochem. Soc., 1983, 130, 811.

231 H. Nalwa, J.S. Shirk, in Phthalocyanines: Properties and Applications, Eds. A.B.P. Lever, C.C. Leznoff, vol.4, VCH Publishers, New York, 1993.

232 R.K. Pandey, J. Porphyrins and Phthalocyanines, 2000, 4, 368.

233 I. Rosenthal, in Phthalocyanines: Properties and Applications, Eds. A.B.P. Lever, C.C. Leznoff, vol. 4, VCH Publishers, New York, 1993.

234 H. Ali, J.E. van Lier, in Phthalocyanines: Properties and Applications, Eds. A.B.P. Lever, C.C. Leznoff, vol. 4, VCH Publishers, New York, 1993.

235 A.B.P. Lever, J. Porphyrins and Phthalocyanines, 1999, 3, 488.

236 P. Vasuvedan, N. Poughat, A.K. Shuklat, Appl. Organomet. Chem., 1996, 591.

237 S. Maree, T. Nyokong, J. Electroanal. Chem., 2000, 492, 120.

238 J. Zagal, M. Paez, C. Fierro, Proc. Electrochem. Soc., 1987, 87, 198.

239 M. Thamae, T. Nyokong, J. Electroanal. Chem., 1999, 470, 126.

240 N. Kobayashi, W.A. Nevin, Appl. Organomet. Chem., 1996, 10, 579.

241 J. Limson, T. Nyokong, Electroanalysis, 1997, 9, 255.

242 M. Sekota, T. Nyokong, Electroanalysis, 1997, 9, 1257

243 F. Bedioui, S. Trevin, J. Devynck, Biosens. Bioelecron., 1997, 12, 205.

244 T. Mafatle, T. Nyokong, J. Electroanal. Chem., 1996, 408, 213.

245 E.T.W. Schipper, J.P.A Heuts, P. Piet, T.P.M. Beelen, A.L. German, J. Mol. Catal. 1994, 87, 161.

246 E. Karmann, D. Schlettwein, N.I. Jaeger, J. Electroanal. Chem.,1996, 405, 149.

247 J.H. Zagal, S. Lira, S. Ureta-Zanartu, J. Electroanal. Chem., 1986, 210, 95.

248 L.M. Santos, R.P. Baldwin, Anal. Chem. 1987, 59, 1766.

249 T. Abe, Y. Yoshida, T. Tokita, F. Taguchi, H. Imaya, M.L. Kaneko, J. Electroanal. Chem., 1996, 412, 125.

250 C.M. Lieber, N.S. Lewis, J. Am. Chem. Soc., 1984, 106, 5033.

251 J. Zagal, P. Bindra, E. Yeager, J. Electrochem. Soc., 1980, 127, 1056.

252 M.A.T. Gilmartin, R.J. Ewen, J.P. Hart, J. Electroanal. Chem., 1996, 401, 127.

253 J.P. Hart, A.K. Abass, Anal. Chim. Acta, 1997, 342, 199.

254 J. Zagal, P. Herrera, K. Brink, Z.S. Ureta, Proc. Electrochem. Soc., 1984, 84, 602.

255 K. Ogura, S. Yamasaki, J. Appl. Electrochem., 1985, 15, 279.

256 N. Doddapaneni, Proc. Electrochem. Soc., 1984, 84, 630.

257 J. Yamaki, A. Yamaji, J. Electrochem. Soc., 1982, 129, 5.

258 L.Mao, Talanta, 1998, 46, 1547.

259 J. Jin, Talanta, 1999, 48, 1005.

260 L. Agnes, C.M.N. Azvedo, K. Araki, H.E. Toma, Anal. Chim. Acta, 1996, 329, 91.

261 P. Ascenzi, M. Brunori, G. Pessesi, C. Ercolani, F. Monacelli, J. Chem., Soc., Dalton Trans., 1987, 369.

262 P. Ascenzi, R. Fruttero, C. Ercolani, F. Monacelli, Analusis, 1996, 24, 316.

263 I. Zilberman, J. Hayon, T. Katchalski, O. Raveh, J. Rishpon, A. Shames, A. Bettelheim, J. Electrochem. Soc., 1997, 144, L228.

264 G. Pennesi, C. Ercolani, G. Rossi, P. Ascenzi, M. Brunori, F. Monacelli, J. Chem. Soc., Dalton Trans., 1990, 105.

265 H. Hoshino, L. Laverman, P.C. Ford, Coord. Chem. Rev., 1999, 187, 75.

266 M.A. Brooks, E.W. Tsai, in Laboratory Techniques in Electroanalytical Chemistry 2nd ed., Eds. P.T. Kissinger, W.R. Heineman, Marcel Dekker Inc, New York, 1996.

267 Q.-Y. Chen, D.-H. Li, H.-H. Yang, Q.-Z. Zhu, H. Zheng, J.-G. Xu, Analyst, 1999, 124, 771.

268 M.N. Golovin, P. Seymour, K. Jayaraj, Y. Fu, A.B.P. Lever, Inorg. Chem., 1990, 29, 1719.

269 B.N. Achar, G.M. Fohlen, J.A. Parker, J. Keshavayya, Polyhedron, 1987, 6, 1463.

270 E.H. Huntress, R.L. Shriner, Org. Synth. Coll., 1943, 2, 459.

271 N. Kobayashi, H. Lam, W.A. Nevin, C.C. Leznoff, H. Shirai, J. Am. Chem. Soc., 1994, 116, 879.

272 R. Behnish, M. Hanack, Synth. Met., 1990, 36, 397.

273 F. Hartl, K.M. Den k, J. electroanal. Chem. 1991, 317, 179.

274 L.C. Gruen, R.J. Blagrove, Aust. J. Chem., 1973, 26, 319.

275 E.W. Abel, J.M. Pratt, R. Whelan, J. Chem Soc., Dalton Trans., 1976, 509.

276 Z.A. Schelly, D.J. Havard, P. Hemes, E.M. Eyring, J. Phys. Chem., 1970, 74, 3040.

277 W.A. Nevin, W. Liu, M. Melník, A.B.P. Lever, J. Electroanal. Chem., 1986, 213, 217.

278 A. Hadasch, A. Sorokin, A. Robion, L. Fraisse, B. Meunier, New J. Chem., 1998, 45.

279 M.J. Stillman, in Phthalocyanines: Properties and Applications, Eds. C.C. Leznoff, A.B.P. Lever, Vol. 1, VCH Publishers, New York, 1989.

280 S. Zecevic, B. Simic-Glavaski, E. Yeager, A.B.P. Lever, P.C. Minor, J. Electroanal. Chem., 1985, 196, 339

281 N.A. Davies, M.T. Wilson, E. Slade, S.P. Fricker, B.A. Murrer, N.A. Powell, G.R. Henderson, Chem. Commun., 1997, 47.

282 U. El-Uyaan, E. Herlinger, R.F. Jameson, W. Linert, J. Chem. Soc., Dalton Trans., 1997, 2813.

283 K.J. Paeng, D.H. Shin, I.R. Paeng, Inorg. Chem., 1997, 36, 2901.

284 L.J. Boucher, P. Rivera, Inorg. Chem., 1980, 19, 1816.

285 N. Kobel, H. Hanack, Inorg. Chem., 1986, 25, 103.

286 R.J. Sunberg, R.B. Martin, Chem. Rev. 1974, 74, 496.

287 J.H. Weber, D.H. Busch, Inorg. Chem., 1965, 4, 472.

288 R.J. Sunberg, R.B. Martin, Chem. Rev., 1974, 74, 508.

289 T. Nyokong, Polyhedron, 1995, 14, 2325.

290 T.Nyokong, Polyhedron, 1995, 14, 643.

291 M.D. Hawley, S.V. Tatawawadi, S. Pieraski, R.N. Adams, J. Am. Chem. Soc., 1967, 89, 447.

292 C.J. Grol, in The Neurobiology of Dopamine, Eds. A.S. Horn, J. Korf, B.H.C. Westerink, Academy Press, London, 1977.

293 F. Zhao, J. Zhang, T. Abe, D. Wöhrle, M. Kaneko, J. Mol. Catal., A: Chemical, 1999, 145, 245.

294 J.H. Zagal, Electrochim. Acta, 1985, 30, 449.

295 P. Westbroek, B. Van Haute, E. Temmerman, Fres. J. Anal. Chem., 1996, 354, 405.

296 F. Govaert, E. Tammerman, P. Westbroek, Anal. Commun., 1998, 35, 153.

297 P. Westbroek, E. Temmmerman, J. Electroanal. Chem., 2000, 482, 40.

298 S. Fletcher, M.D. Horne, Electrochem. Commun., 1999, 1, 502.

299 A. Hiratsuka, H. Muquruma, R. Nagata, N. Nakamura, K. Sato, S. Uckiyama, I. Karube, J. Membrane Sci., 2000, 175, 25.

300 I.O. Marion, R. Snadulescu, N. Boncicat, J. Pharm. Biomed. Anal. 2000, 23, 227.

301 J. Marks, A guide to the vitamins, their role in heath and disease, Medical and Technical Publishing Ltd., 1975, p74.

302 A. White, P. Handler, E. L. Smith, Principles of Biochemistry, McGraw-Hill book company, 5th edition, , 1973, p1153.

303 P.C. Minor, A.B.P. Lever, Inorg. Chem., 1983, 22, 826.

304 H. Campbell, G.A. Heath, G.T. Hefter, R.C.S. McQueen, J. Chem., Soc., Chem. Commun.,1983, 1123.